

I

High Dimensional Surface Electromyography and Low Dimensional Muscle Synergy in Lower Limb Amputees During Transient- and Steady-State Gait

by

Pouyan Mehryar

**Submitted in accordance with the requirements
for the degree of Doctor of Philosophy**

**The University of Leeds
School of Mechanical Engineering**

May 2018

The candidate confirms that the work submitted is his own and that appropriate credit has been given where reference has been made to the work of others.

This copy has been supplied on the understanding that it is copyright material and that no quotation from the thesis may be published without proper acknowledgement.

The candidate confirms that the work submitted is his own, except where the work that has formed part of jointly-authored publications has been included. The contribution of the candidate and the other authors to this work has been explicitly indicated. The candidate confirms that appropriate credit has been given within the thesis where reference has been made to the work of others.

This copy has been supplied on the understanding that it is a copyright material and that no quotation from the thesis may be published without proper acknowledgement.

The candidate performed the major tasks of the work presented in these published papers, such as the development of algorithm, experimental procedures, data analysis, and the results. The co-authors reviewed and guided the candidate and provided valuable feedback.

The right of Pouyan Mehryar to be identified as Author of this work has been asserted by him in accordance with the Copyright, Designs and Patents Act 1988.

Abstract

The prevalence of lower limb amputation has been rising rapidly with the primary causes associated with dysvascular disease and traumatic injuries. The knowledge of muscle coordination during walking could help in the rehabilitation of individuals with limb loss. The goal of this research was to investigate the neuromuscular differences between healthy subjects (HS) and lower limb amputees during the walking task at different states and speeds using different statistical approaches.

High dimensional (HD) electromyography (EMG) data for ten muscles were collected from thirteen healthy subjects' (HS) dominant leg and eleven transfemoral amputees' (TFA) intact leg (IL) during transient-state walking at three self-selected speeds (slow, normal, and fast). This data were analyzed at two levels from two different approaches: the HD EMG/muscle activation pattern and low dimensional muscle synergy/modular motor control which were obtained using the linear envelope of EMG signals and concatenated non-negative matrix factorization (CNMF), respectively, from biomechanics and robotic control approach.

While the biomechanics approach considers the covariance between the HD muscle activities and low dimensional temporal components of muscle synergy, robotic control accounts for individual muscle activities and temporal components of muscle synergy using statistical parametric mapping (SPM).

HD EMG data for ten muscles were also collected from four HS and one transtibial amputee's (TTA) IL and prosthetic leg (PL) during steady-state walking at a self-selected speed. The muscle synergy was analyzed using the developed CNMF algorithm among legs in pairwise comparisons.

The effect of speeds on both HS and TFA muscle activities from biomechanics and robotic control perspectives showed statistically significant differences, suggesting neuromuscular adaptation mechanism in both groups to satisfy the kinematic and kinetic demands of increasing transient-state walking speed. Some differences in HD muscle activities related to the plantarflexors could be observed among the groups, indicating compensatory adjustment of TFA IL for the lack of push off from the PL.

The effect of speeds on HS muscle synergy vectors showed reasonable correlations as opposed to those of TFA synergy vectors during transient-state walking. The high correlation suggests that the central nervous system (CNS) activates the same group of muscles synergistically.

In comparison among HS dominant leg, TTA IL and TTA PL, the primary muscle(s) had a significant impact on the level of muscle synergy vectors correlation.

The activation coefficient profiles suggested that amputees' IL and PL were significantly different when compared together and to the HS.

The same number of synergy groups (=4) found in HS, TFA and TTA indicate analogous complexity implemented by the CNS which does not depend on the state of the gait cycle (transient vs. steady), speed (slow, normal and fast), and level of amputation (below knee vs. above knee). These results have important clinical and robotic control implications. It could provide useful information to therapists to tailor rehabilitation strategy to focus on the muscles and the timing where significant differences occur in the gait cycle. As a result, this could decrease the risk of secondary physical conditions (e.g., osteoarthritis) and increase gait efficiency. The information may also be useful for the prosthetic manufacturers to design prostheses that incorporate information from the IL and/or PL to improve the myoelectric prostheses and develop synergy-based control frame.

*To my parents who have been supportive throughout the completion of this thesis.
Also, to my brother, Peiman for his endless support.*

ACKNOWLEDGMENTS

I would like to express my gratitude to my supervisors *Professor Abbas Dehghani-Sanij* and *Professor Rory O'Connor* for their continuous support, patience, encouragement, and enthusiasm for the subject area throughout my PhD. None of my work would have been possible without their kind supervisions.

I am grateful to *Dr. Mohammad Sharif Shourijeh* for his immense amount of knowledge he has given me in the field of engineering and helped me to develop the critical thinking skills which certainly enabled me to understand and achieve my goal.

I offer my sincerest gratitude to *Mrs. Tahmineh Rezaeian*, *Mr. Amin Reza Khandan*, *Dr. James Brown*, *Dr. Neil Messenger* and *Dr. Farzam Farahmand* for the support and resources they provided at the University of Leeds and Sharif University of Technology throughout the course of my research.

None of my work would have been possible if it had not been for the massive effort of friends and colleagues behind this project leading by *Mrs. Tahmineh Rezaeian* working to collect the data at the Motion Laboratory at “Djavad Mowafaghian Research Centre of Intelligent Neuro-Rehabilitation Technologies”; the Sharif University of Technology in Tehran-Iran.

I would like to also thanks all the participants from family and friends to all the amputees who volunteered and devoted their valuable time to make this research possible.

I am also grateful for the opportunities to collaborate with the Sharif University of Technology in Iran, to travel to the University of Aalborg in Denmark and the University of Leuven in Belgium for training courses, as well as to attend several conferences in the UK, Spain, and the USA to further my research area.

Last but not least, I would like to express my special thanks to my beloved family for their moral support, inspiration, and encouragement during the ups and downs of my PhD. If it had not been for them, I would not be where I am today.

List of Contents

List of Contents	VII
List of Figures.....	XIV
List of Tables	XXVIII
List of Abbreviations	XXXI
List of Publications Directly Related to This Research.....	XXXV
Chapter 1 INTRODUCTION.....	1
1.1 Background.....	1
1.1.1 Prevalence of Amputation	1
1.1.2 Use of Prosthesis in Rehabilitation	1
1.1.3 HD EMG Studies in Lower Limb Amputees	3
1.1.4 Muscle Synergy Studies in HS and Pathological Group	3
1.2 Motivation.....	4
1.3 Aims and Objectives	5
1.3.1 Aims.....	5
1.3.2 Objectives	5
1.4 Scope of this Research	6
1.5 Contribution of this Research	10
1.6 Thesis Outline	11
Chapter 2 LITERATURE REVIEW.....	13
2.1 Introduction	13
2.2 Lower Limb Biomechanics	13
2.2.1 Basic Anatomy	13
2.2.2 Types of Movements and Muscles	14
2.2.3 Human Gait.....	14
2.2.3.1 Phases of Gait Cycle.....	15
2.2.3.2 States of the Gait Cycle	17
2.2.4 Kinematics and Kinetics	18
2.2.5 Gait Measurement Devices	18
2.3 Surface EMG for Studying Muscle Coordination.....	19
2.3.1 Detection of EMG Signal	19
2.3.2 EMG Profiles.....	20
2.3.2.1 Level of Muscle Activity.....	21

VIII

2.3.2.2	Duration of Muscle Activity.....	21
2.3.2.3	Factors Influencing Surface EMG.....	22
2.3.3	Muscle Synergy/Modular Motor Control	24
2.3.3.1	Muscle Synergy Methodological Consideration	25
2.3.4	Statistical Parametric Mapping (SPM)	30
2.3.4.1	Multivariate 1D SPM Test (Paired Hotelling's T^2)	31
2.3.4.2	Multivariate 1D SPM Test (Hotelling's T^2).....	31
2.3.4.3	Univariate 1D Test (Two-Sample t-test)	32
2.4	Neuromuscular Aspects of Human Motion	33
2.4.1	Able-bodies Gait Biomechanics.....	33
2.4.1.1	Functional Tasks of the Gait Cycle.....	33
2.4.1.2	Gait Initiation and Transient-State Walking in HS.....	38
2.4.1.3	Muscle Activity in HS during steady-state walking.....	38
2.4.1.4	Muscle Activity in HS with Increased Walking Speeds	39
2.4.1.5	Muscle Synergy in HS.....	40
2.4.2	Lower Limb Amputee Gait Biomechanics	42
2.4.2.1	Types and Prevalence of Amputation.....	42
2.4.2.2	Walking Speed in Lower Limb Amputees	43
2.4.2.3	Kinematic, Kinetic and Power Studies in Lower Limb Amputees	44
2.4.2.4	GRF Studies in Lower Limb Amputees	46
2.4.2.5	Gait Deficiencies in Lower Limb Amputees	46
2.4.2.6	Consequences of Gait Deficiencies.....	48
2.4.2.7	Changes of EMG in Transfemoral Amputees	48
2.4.2.8	Changes of EMG in Transtibial Amputees.....	49
2.4.2.9	Muscle Synergy in Pathological Population.....	49
2.4.2.10	Muscle Synergy in Lower Limb Amputees.....	49
2.5	Lower Limb Prostheses.....	50
2.5.1	Knee Assembly	51
2.5.2	Mechanically Passive Prostheses	52
2.5.3	Microprocessor Knee	53
2.5.4	Motorised Knee/Power Knee.....	53
2.5.5	Semi-Active Prosthetic Devices.....	54
2.5.6	Transtibial Prostheses.....	54
2.6	Control Strategies in Lower Limb Prostheses.....	55
2.7	Gap of Knowledge.....	56

2.8	Summary.....	56
Chapter 3 HIGH DIMENSIONAL MUSCLE ACTIVATION PATTERNS IN TRANSFEMORAL AMPUTEES DURING TRANSIENT-STATE WALKING 57		
3.1	Introduction	57
3.2	Experimental Protocol	57
3.2.1	Methodology	57
3.2.2	Surface EMG Signal Processing	60
3.2.2.1	Raw Surface EMG	60
3.2.2.2	Filtration Technique.....	61
3.2.2.3	Linear Envelope	61
3.2.3	Statistical Parametric Mapping (High Dimensional EMG)	61
3.2.3.1	Within-Subject Hypotheses	63
3.2.3.2	Between-Subject Hypotheses	64
3.2.4	Justification for Separating Group and Speed Factors for Statistical Analysis.....	65
3.3	Results.....	65
3.3.1	Muscle Activation Patterns and Magnitudes Description	68
3.3.1.1	Slow Transient-State Walking	68
3.3.1.2	Normal Transient-State Walking.....	69
3.3.1.3	Fast Transient-State Walking	71
3.3.2	Statistical Parametric Mapping	76
3.3.2.1	Within-Subject (Biomechanics Perspective)	76
3.3.2.2	Within-Subject (Robotic Control Perspective).....	89
3.3.2.3	Between-Subject (Biomechanics Perspective)	108
3.3.2.4	Between-Subject (Robotic Control Perspective).....	118
3.4	Discussion.....	122
3.4.1	Statistical Analyses (HD Muscle Activation Patterns)	122
3.4.1.1	Within-Subject (Biomechanics Perspective)	122
3.4.1.2	Within-Subject (Robotic Control Perspective).....	125
3.4.1.3	Between-Subject (Biomechanics Perspective)	128
3.4.1.4	Between-Subject (Robotic Control Perspective).....	129
3.4.1.5	Comparing Individual Muscle Activities to the Literature.....	131
3.5	Summary.....	133
3.6	Conclusion	133
Chapter 4 MODULAR MOTOR CONTROL IN TRANSFEMORAL AMPUTEES DURING TRANSIENT-STATE WALKING135		
4.1	Introduction	135

4.2	Experimental Protocol	136
4.2.1	Methodology	136
4.3	Algorithm Description	136
4.3.1	Signal Processing	136
4.3.2	Non-Negative Matrix Factorization (NMF)	136
4.3.3	NMF Frameworks.....	137
4.3.4	Concatenated Non-Negative Matrix Factorization (CNMF) Frameworks	137
4.3.5	Justification for not Using Other Factorization Techniques	137
4.3.6	Justification for Using CNMF Factorization Techniques over NMF	138
4.3.7	CNMF MATLAB Implementation	138
4.3.8	Variance Accounted For (VAF).....	138
4.3.9	Synergy Output Normalization.....	139
4.3.10	Functional Sorting	139
4.3.11	Correlation Analysis	140
4.3.12	Statistical Parametric Mapping	140
4.3.12.1	Within-Subject Hypotheses	141
4.3.12.2	Between-Subject Hypotheses	141
4.4	Results.....	143
4.4.1	Analysis of Dimensionality.....	143
4.4.1.1	Within-Subject.....	143
4.4.1.2	Between-Subject.....	144
4.4.2	Correlation Analysis Using R^2 (Individual-Muscle Criterion)	145
4.4.2.1	Within-Subject.....	145
4.4.2.2	Between-Subject.....	146
4.4.3	Correlation Analysis Using ICC	147
4.4.3.1	Within-Subject.....	148
4.4.3.2	Between-Subject.....	149
4.4.4	CNMF Activation Coefficient Profile Repeatability	150
4.4.4.1	Within-Subject.....	150
4.4.5	Muscle Synergy Analysis Description.....	151
4.4.5.1	Within-Subject.....	151
4.4.5.2	Between-Subject.....	156
4.4.6	Module Contribution	162
4.4.7	Statistical Analyses (Spatially Fixed Muscle Synergies)	163

4.4.7.1	Within-Subject.....	163
4.4.7.2	Between-Subject (Muscle Synergy Vector)	164
4.4.8	Statistical Analyses (Activation Coefficient Profile)	165
4.4.8.1	Within-Subject (Biomechanics Perspective)	165
4.4.8.2	Within-Subject (Robotic Control Perspective).....	166
4.4.8.3	Between-Subject (Biomechanics Perspective)	177
4.4.8.4	Between-Subject (Control Perspective).....	181
4.5	Discussions.....	185
4.5.1	Analysis of dimensionality (VAF)	185
4.5.2	Correlation Analysis (Individual-Muscle Criterion)	185
4.5.3	CNMF Activation Coefficient Profile Repeatability	185
4.5.4	Module Contribution	186
4.5.5	Within-Subject (Synergy/Module Comparison)	186
4.5.6	Between-Subject (Synergy/Module Comparison)	187
4.5.6.1	Motor Modules Comparison with Literature	187
4.5.7	Statistical Analyses (Activation Coefficient Profile)	188
4.5.7.1	Within-Subject (Biomechanics Perspective)	188
4.5.7.2	Within-Subject (Robotic Control Perspective).....	189
4.5.7.3	Comparison of Activation Coefficient Profile with Literature.	191
4.5.7.4	Between-Subject (Biomechanics Perspective)	191
4.5.7.5	Between-Subject (Robotic Control Perspective).....	192
4.6	Summary.....	193
4.7	Conclusion	194
Chapter 5 MODULAR MOTOR CONTROL IN TRANSTIBIAL AMPUTEE DURING STEADY-STATE WALKING		196
5.1	Introduction	196
5.2	Experimental Protocol	196
5.2.1	Methodology	196
5.3	Algorithm Description for Muscle Synergy Analysis.....	200
5.3.1	Signal Processing	200
5.3.2	Concatenated Non-Negative Matrix Factorization (CNMF)	200
5.3.3	CNMF Frameworks	200
5.3.4	Variance Accounted For (VAF).....	200
5.3.5	Functional Sorting	201
5.3.6	Correlation Analysis	201
5.3.7	Statistical Parametric Mapping (SPM)	201

5.4	Results.....	202
5.4.1	Variance Accounted For (VAF).....	202
5.4.2	Intra-class Correlation (ICC).....	202
5.4.3	Muscle Synergy Analysis Description.....	203
5.4.4	TTA Muscle Synergy Comparison with TFA.....	206
5.4.5	Statistical Analyses (Spatially Fixed Muscle Synergies).....	208
5.4.5.1	Correlation Analysis using R^2	208
5.4.6	Statistical Analyses (Activation Coefficient Profile).....	208
5.5	Discussion.....	211
5.6	Summary.....	213
5.7	Conclusion.....	213
Chapter 6	COMMON DISCUSSIONS.....	215
6.1	Introduction.....	215
6.2	Comparison Between HD Sensorimotor Modules and HS Low Dimensional Temporal Component of Muscle Synergy.....	215
6.2.1	HS HD Sensorimotor Modules vs. HS Low Dimensional Activation Coefficient Profiles (Within-Subject).....	215
6.2.2	TFA HD Sensorimotor Modules vs. TFA Low Dimensional Activation Coefficient Profiles (Within-Subject).....	216
6.3	Motor Modules Comparison between TTA and TFA.....	218
6.4	Applicability of This Study.....	219
6.4.1	Clinical Implications.....	219
6.4.2	Robotic Control Implications.....	220
6.4.2.1	Clinical State of the Art (Direct Control).....	220
6.4.2.2	Model-free Approaches.....	220
6.4.2.3	Neuro-mechanical Modeling (Model-based Approach).....	222
6.4.2.4	Mid-level Control.....	223
6.4.2.5	Mimicking Healthy Subjects Control.....	223
6.5	Summary.....	223
6.6	Conclusion.....	223
Chapter 7	SUMMARY, CONCLUSIONS, LIMITATIONS AND FUTURE WORK.....	225
7.1	Summary and Assessment of Research Objectives.....	225
7.2	Conclusions.....	229
7.3	Limitations.....	232
7.4	Future Work.....	233

REFERENCES	236
APPENDICES	256
Appendix A Literature Review Supplements	257
Appendix B Chapter 3 Supplements	275
Appendix C Chapter 5 Supplements	282
Appendix D Ethical Approval.....	283
Appendix E List of Publications and Awards	288
E.1 Publications from this Thesis (P. Mehryar, main author).....	288
E.2 Related Publications (P. Mehryar, co-author)	288
E.3 Awards.....	289

List of Figures

Figure 1.1: Flowchart of study 1; neuromuscular analysis in terms of HD muscle activation and muscle synergy of HS dominant leg and TFA IL during transient-state walking at different speeds considering biomechanics and robotic control perspective.....	8
Figure 1.2: Flowchart of study 2; neuromuscular analysis in terms of muscle synergy between HS, TTA IL and TTA PL during steady-state walking; Abbreviation: upper knee (UKN).....	9
Figure 1.3: Flowchart of the thesis organization	11
Figure 2.1: Lower limb muscles and bones. (A) superficial lower limb muscles [97] and (B) main lower limb bones [98].....	14
Figure 2.2: Gait cycle diagram; break down of single support and double support (adapted from [103])	16
Figure 2.3: Gait phases and events in the gait cycle, Initiation of gait starts with the right leg (grey) (modified from [104]).	16
Figure 2.4: Gait initiation (A and B) and transient-state gait (C and D) of leading and trailing limb, respectively (Adapted from [52]).	18
Figure 2.5: Schematic of muscle synergy/modular motor control; C1-C3 are activation coefficient profiles, W1-W3 are muscle synergy vectors, and m1-m5 are original muscle activations (adapted from [176]).....	25
Figure 2.6: Lower limb joint angles for the hip, knee, and ankle during normal steady-state walking in the sagittal plane (adapted from [104]).	36
Figure 2.7: GRF components during the stance phase of steady-state walking (adapted from [234]).....	36
Figure 2.8: (A) Average joint moments and (B) average joint powers for hip, knee, and ankle of able-bodied, transfemoral and transtibial intact limb during stance phase when walking at normal steady-state speed. Bold line, dashed line and the thin dashed line indicates able-bodied, transfemoral and transtibial IL, respectively (adapted from [235]).....	37
Figure 2.9: Lower limb major muscle group activities during normal steady-state walking (adapted from [100]).	37
Figure 2.10: Different level of amputation (adapted from [250])	42
Figure 2.11: Distribution of the phases in the GC for HS and TFA; stance (grey) and swing (white) (adapted from [255])	44
Figure 2.12: (A) joints kinematic patterns and (B) power comparison in HS and TFA. A: ankle, B: knee, and C: hip (adapted from [256]). HS (solid line), TFA IL (dotted dash) and TFA PL (dotted)	45
Figure 2.13 Transfemoral amputees gait deficiencies (adapted from [105])....	47
Figure 2.14: Components of the transfemoral prosthesis (adapted from [105])	50
Figure 3.1: EMG attachments on TFA (A) front IL, (B) back IL, and (C) side PL.	60

- Figure 3.2: HS EMG ensemble averages of individual muscle over all trials at slow, normal, and fast speeds. The thick line and shaded area indicate mean EMG and \pm one standard deviation, respectively.66**
- Figure 3.3: TFA EMG ensemble averages of individual muscle over all trials at slow, normal, and fast speeds. The thick line and shaded area indicate mean EMG and \pm one standard deviation, respectively.67**
- Figure 3.4: EMG ensemble averages of HS and TFA (averaged over all trials) for each muscle at slow speed. The thick line and shaded area indicate mean EMG and \pm one standard deviation. The vertical dashed line indicates TO.73**
- Figure 3.5: EMG ensemble averages of HS and TFA (averaged over all trials) for each muscle at normal speed. The thick line and shaded area indicate mean EMG and \pm one standard deviation. The vertical dashed line indicates TO.74**
- Figure 3.6: EMG ensemble averages of HS and TFA (averaged over all trials) for each muscle at fast speed. The thick line and shaded area indicate mean EMG and \pm one standard deviation. The vertical dashed line indicates TO.75**
- Figure 3.7: HS M1 non-parametric post hoc SPM vector field results (paired Hotelling's T2 test) depicting significant differences between speeds. The red dashed lines indicate critical thresholds of $T2^* = 41.443, 40.591$ and 31.575 for (A), (B), and (C), respectively. Suprathreshold clusters are shown in grey where $p < 0.02$77**
- Figure 3.8: HS M2 non-parametric post hoc SPM vector field results (paired Hotelling's T2 test) depicting significant differences between speeds. The red dashed lines indicate critical thresholds of $T2^* = 40.389, 37.189$ and 43.900 for (A), (B), and (C), respectively. Suprathreshold clusters are shown in grey where $p < 0.02$78**
- Figure 3.9: HS M3 non-parametric post hoc SPM vector field results (paired Hotelling's T2 test) depicting significant differences between speeds. The red dashed lines indicate critical thresholds of $T2^* = 30.117, 23.659$ and 24.881 for (A), (B), and (C), respectively. Suprathreshold clusters are shown in grey where $p < 0.02$79**
- Figure 3.10: HS M4 non-parametric post hoc SPM vector field results (paired Hotelling's T2 test) depicting significant differences between speeds. The red dashed lines indicate critical thresholds of $T2^* = 28.181, 25.618$ and 22.417 for (A), (B), and (C), respectively. Suprathreshold clusters are shown in grey where $p < 0.02$80**
- Figure 3.11: HS ankle co-contraction non-parametric post hoc SPM vector field results (paired Hotelling's T2 test) depicting significant differences between speeds. The red dashed lines indicate critical thresholds of $T2^* = 73.966, 57.406$ and 62.223 for (A), (B), and (C), respectively. Suprathreshold clusters are shown in grey where $p < 0.02$81**

- Figure 3.12: HS knee co-contraction non-parametric post hoc SPM vector field results (paired Hotelling's T2 test) depicting significant differences between speeds. The red dashed lines indicate critical thresholds of $T2^* = 111.957, 93.062$ and 102.976 for (A), (B), and (C), respectively. Suprathreshold clusters are shown in grey where $p < 0.02$82**
- Figure 3.13: TFA M1 non-parametric post hoc SPM vector field results (paired Hotelling's T2 test) depicting significant differences between speeds. The red dashed lines indicate critical thresholds of $T2^* = 58.666, 53.322$ and 59.779 for (A), (B), and (C), respectively. Suprathreshold clusters are shown in grey where $p < 0.02$83**
- Figure 3.14: TFA M2 non-parametric post hoc SPM vector field results (paired Hotelling's T2 test) depicting significant differences between speeds. The red dashed lines indicate critical thresholds of $T2^* = 75.525, 42.075$ and 54.108 for (A), (B), and (C), respectively. Suprathreshold clusters are shown in grey where $p < 0.02$84**
- Figure 3.15: TFA M3 non-parametric post hoc SPM vector field results (paired Hotelling's T2 test) depicting significant differences between speeds. The red dashed lines indicate critical thresholds of $T2^* = 30.186, 31.389$ and 26.218 for (A), (B), and (C), respectively. Suprathreshold clusters are shown in grey where $p < 0.02$85**
- Figure 3.16: TFA M4 non-parametric post hoc SPM vector field results (paired Hotelling's T2 test) depicting significant differences between speeds. The red dashed lines indicate critical thresholds of $T2^* = 34.853, 29.822$ and 34.865 for (A), (B), and (C), respectively. Suprathreshold clusters are shown in grey where $p < 0.02$86**
- Figure 3.17: TFA ankle co-contraction non-parametric post hoc SPM vector field results (paired Hotelling's T2 test) depicting significant differences between speeds. The red dashed lines indicate critical thresholds of $T2^* = 144.184, 109.896$ and 88.846 for (A), (B), and (C), respectively. Suprathreshold clusters are shown in grey where $p < 0.02$87**
- Figure 3.18: TFA knee co-contraction non-parametric post hoc SPM vector field results (paired Hotelling's T2 test) depicting significant differences between speeds. The red dashed lines indicate critical thresholds of $T2^* = 204.491, 203.579$ and 286.709 for (A), (B), and (C), respectively. Suprathreshold clusters are shown in grey where $p < 0.02$88**
- Figure 3.19: HS RF parametric RM ANOVA within- and between-subjects, depicting significant differences between speeds. The horizontal red dotted line indicates the critical threshold of 7.908 . Suprathreshold clusters are shown in grey where $p < 0.05$90**
- Figure 3.20: HS RF within-subject post hoc paired t statistic between speeds. The red dashed lines indicate critical thresholds of $t^* = 4.77, 4.78$ and 4.69 for (A), (B), and (C), respectively. Suprathreshold clusters are shown in grey where $p < 0.02$90**
- Figure 3.21: HS VM parametric RM ANOVA within- and between-subjects, depicting significant differences between speeds. The horizontal red dotted line indicates the critical threshold of 7.502 . Suprathreshold clusters are shown in grey where $p < 0.05$91**

- Figure 3.22: HS VM within-subject post hoc paired t statistic between speeds.**
The red dashed lines indicate critical thresholds of $t^* = 4.65, 4.54$ and 4.48 for (A), (B), and (C), respectively. Suprathreshold clusters are shown in grey where $p < 0.02$91
- Figure 3.23: HS VL parametric RM ANOVA within- and between-subjects,**
depicting significant differences between speeds. The horizontal red dotted line indicates the critical threshold of 7.750 . Suprathreshold clusters are shown in grey where $p < 0.05$92
- Figure 3.24: HS VL within-subject post hoc paired t statistic between speeds.**
The red dashed lines indicate critical thresholds of $t^* = 4.71, 4.55$ and 4.68 for (A), (B), and (C), respectively. Suprathreshold clusters are shown in grey where $p < 0.02$92
- Figure 3.25: HS BFLH parametric RM ANOVA within- and between-subjects,**
depicting significant differences between speeds. The horizontal red dotted line indicates the critical threshold of 7.487 . Suprathreshold clusters are shown in grey where $p < 0.05$93
- Figure 3.26: HS BFLH within-subject post hoc paired t statistic between speeds.**
The red dashed lines indicate critical thresholds of $t^* = 4.79, 4.65$ and 4.71 for (A), (B), and (C), respectively. Suprathreshold clusters are shown in grey where $p < 0.02$93
- Figure 3.27: HS SEM parametric RM ANOVA within- and between-subjects,**
depicting significant differences between speeds. The horizontal red dotted line indicates the critical threshold of 7.423 . Suprathreshold clusters are shown in grey where $p < 0.05$94
- Figure 3.28: HS SEM within-subject post hoc paired t statistic between speeds.**
The red dashed lines indicate critical thresholds of $t^* = 4.68, 4.62$ and 4.55 for (A), (B), and (C), respectively. Suprathreshold clusters are shown in grey where $p < 0.02$94
- Figure 3.29: HS TFL parametric RM ANOVA within- and between-subjects,**
depicting significant differences between speeds. The horizontal red dotted line indicates the critical threshold of 7.850 . Suprathreshold clusters are shown in grey where $p < 0.05$95
- Figure 3.30: HS TFL within-subject post hoc paired t statistic between speeds.**
The red dashed lines indicate critical thresholds of $t^* = 4.87, 4.65$ and 4.75 for (A), (B), and (C), respectively. Suprathreshold clusters are shown in grey where $p < 0.02$95
- Figure 3.31: HS TA parametric RM ANOVA within- and between-subjects,**
depicting significant differences between speeds. The horizontal red dotted line indicates the critical threshold of 7.265 . Suprathreshold clusters are shown in grey where $p < 0.05$96
- Figure 3.32: HS TA within-subject post hoc paired t statistic between speeds.**
The red dashed lines indicate critical thresholds of $t^* = 4.60, 4.51$ and 4.69 for (A), (B), and (C), respectively. Suprathreshold clusters are shown in grey where $p < 0.02$96

- Figure 3.33: HS GM parametric RM ANOVA within- and between-subjects, depicting significant differences between speeds. The horizontal red dotted line indicates the critical threshold of 7.810. Suprathreshold clusters are shown in grey where $p < 0.05$97**
- Figure 3.34: HS GM within-subject post hoc paired t statistic between speeds. The red dashed lines indicate critical thresholds of $t^* = 4.84, 4.66$ and 4.68 for (A), (B), and (C), respectively. Suprathreshold clusters are shown in grey where $p < 0.02$97**
- Figure 3.35: HS GL parametric RM ANOVA within- and between-subjects, depicting significant differences between speeds. The horizontal red dotted line indicates the critical threshold of 7.556. Suprathreshold clusters are shown in grey where $p < 0.05$98**
- Figure 3.36: HS GL within-subject post hoc paired t statistic between speeds. The red dashed lines indicate critical thresholds of $t^* = 4.69, 4.62$ and 4.60 for (A), (B), and (C), respectively. Suprathreshold clusters are shown in grey where $p < 0.02$98**
- Figure 3.37: HS SOL parametric RM ANOVA within- and between-subjects, depicting significant differences between speeds. The horizontal red dotted line indicates the critical threshold of 7.615. Suprathreshold clusters are shown in grey where $p < 0.05$99**
- Figure 3.38: HS SOL within-subject post hoc paired t statistic between speeds. The red dashed lines indicate critical thresholds of $t^* = 4.64, 4.67$ and 4.67 for (A), (B), and (C), respectively. Suprathreshold clusters are shown in grey where $p < 0.02$99**
- Figure 3.39: TFA RF parametric RM ANOVA within- and between-subjects, depicting significant differences between speeds. The horizontal red dotted line indicates the critical threshold of 8.217. Suprathreshold clusters are shown in grey where $p < 0.05$100**
- Figure 3.40: TFA RF within-subject post hoc paired t statistic between speeds. The red dashed lines indicate critical thresholds of $t^* = 5.09, 4.96$ and 4.99 for (A), (B), and (C), respectively. Suprathreshold clusters are shown in grey where $p < 0.02$100**
- Figure 3.41: TFA VM parametric RM ANOVA within- and between-subjects, depicting significant differences between speeds. The horizontal red dotted line indicates the critical threshold of 8.478. Suprathreshold clusters are shown in grey where $p < 0.05$101**
- Figure 3.42: TFA VM within-subject post hoc paired t statistic between speeds. The red dashed lines indicate critical thresholds of $t^* = 5.39, 4.25$ and 5.18 for (A), (B), and (C), respectively. Suprathreshold clusters are shown in grey where $p < 0.02$101**
- Figure 3.43: TFA VL parametric RM ANOVA within- and between-subjects, depicting significant differences between speeds. The horizontal red dotted line indicates the critical threshold of 8.003. Suprathreshold clusters are shown in grey where $p < 0.05$102**

- Figure 3.44: TFA VL within-subject post hoc paired t statistic between speeds.**
The red dashed lines indicate critical thresholds of $t^* = 4.75, 4.71$ and 5.07 for (A), (B), and (C), respectively. Suprathreshold clusters are shown in grey where $p < 0.02$102
- Figure 3.45: TFA BFLH parametric RM ANOVA within- and between-subjects,**
depicting significant differences between speeds. The horizontal red dotted line indicates the critical threshold of 8.637 . Suprathreshold clusters are shown in grey where $p < 0.05$103
- Figure 3.46: TFA BFLH within-subject post hoc paired t statistic between speeds.**
The red dashed lines indicate critical thresholds of $t^* = 4.953, 5.167$ and 5.153 for (A), (B), and (C), respectively. Suprathreshold clusters are shown in grey where $p < 0.02$103
- Figure 3.47: TFA TA parametric RM ANOVA within- and between-subjects,**
depicting significant differences between speeds. The horizontal red dotted line indicates the critical threshold of 8.381 . Suprathreshold clusters are shown in grey where $p < 0.05$104
- Figure 3.48: TFA TA within-subject post hoc paired t statistic between speeds.**
The red dashed lines indicate critical thresholds of $t^* = 5.31, 5.20$ and 5.15 for (A), (B), and (C), respectively. Suprathreshold clusters are shown in grey where $p < 0.02$104
- Figure 3.49: TFA GM parametric RM ANOVA within- and between-subjects,**
depicting significant differences between speeds. The horizontal red dotted line indicates the critical threshold of 7.365 . Suprathreshold clusters are shown in grey where $p < 0.05$105
- Figure 3.50: TFA GM within-subject post hoc paired t statistic between speeds.**
The red dashed lines indicate critical thresholds of $t^* = 5.21, 5.04$ and 4.24 for (A), (B), and (C), respectively. Suprathreshold clusters are shown in grey where $p < 0.02$105
- Figure 3.51: TFA GL parametric RM ANOVA within- and between-subjects,**
depicting significant differences between speeds. The horizontal red dotted line indicates the critical threshold of 7.897 . Suprathreshold clusters are shown in grey where $p < 0.05$106
- Figure 3.52: TFA GL within-subject post hoc paired t statistic between speeds.**
The red dashed lines indicate critical thresholds of $t^* = 5.21, 4.89$ and 5.13 for (A), (B), and (C), respectively. Suprathreshold clusters are shown in grey where $p < 0.02$106
- Figure 3.53: TFA SEM parametric RM ANOVA within- and between-subjects,**
depicting significant differences between speeds. The horizontal red dotted line indicates the critical threshold of 8.497 . Suprathreshold clusters are shown in grey where $p < 0.05$107
- Figure 3.54: TFA TFL parametric RM ANOVA within- and between-subjects,**
depicting significant differences between speeds. The horizontal red dotted line indicates the critical threshold of 8.291 . Suprathreshold clusters are shown in grey where $p < 0.05$107

- Figure 3.55: TFA SOL parametric RM ANOVA within- and between-subjects, depicting significant differences between speeds. The horizontal red dotted line indicates the critical threshold of 8.081. Suprathreshold clusters are shown in grey where $p < 0.05$108
- Figure 3.56: HD M1 SPM vector field result (Hotelling's T^2) depicting HS vs. TFA differences at slow speed. The red dashed line indicates critical threshold of $T^2 = 22.255$. Suprathreshold clusters are shown in grey where $p < 0.05$109
- Figure 3.57: HD M2 SPM vector field result (Hotelling's T^2) depicting HS vs. TFA differences at slow speed. The red dashed line indicates critical threshold of $T^2 = 21.933$. Suprathreshold clusters are shown in grey where $p < 0.05$109
- Figure 3.58: HD M3 SPM vector field result (Hotelling's T^2) depicting HS vs. TFA differences at slow speed. The red dashed line indicates critical threshold of $T^2 = 16.906$. Suprathreshold clusters are shown in grey where $p < 0.05$110
- Figure 3.59: HD M4 SPM vector field result (Hotelling's T^2) depicting HS vs. TFA differences at slow speed. The red dashed line indicates critical threshold of $T^2 = 17.073$. Suprathreshold clusters are shown in grey where $p < 0.05$110
- Figure 3.60: Ankle SPM vector field result (Hotelling's T^2) depicting HS vs. TFA differences at slow speed. The red dashed line indicates critical threshold of $T^2 = 28.134$. Suprathreshold clusters are shown in grey where $p < 0.05$111
- Figure 3.61: Knee SPM vector field result (Hotelling's T^2) depicting HS vs. TFA differences at slow speed. The red dashed line indicates critical threshold of $T^2 = 35.649$. Suprathreshold clusters are shown in grey where $p < 0.05$111
- Figure 3.62: HD M1 SPM vector field result (Hotelling's T^2) depicting HS vs. TFA differences at normal speed. The red dashed line indicates critical threshold of $T^2 = 22.875$. Suprathreshold clusters are shown in grey where $p < 0.05$112
- Figure 3.63: HD M2 SPM vector field result (Hotelling's T^2) depicting HS vs. TFA differences at normal speed. The red dashed line indicates critical threshold of $T^2 = 22.351$. Suprathreshold clusters are shown in grey where $p < 0.05$112
- Figure 3.64: HD M3 SPM vector field result (Hotelling's T^2) depicting HS vs. TFA differences at normal speed. The red dashed line indicates critical threshold of $T^2 = 17.296$. Suprathreshold clusters are shown in grey where $p < 0.05$113
- Figure 3.65: HD M4 SPM vector field result (Hotelling's T^2) depicting HS vs. TFA differences at normal speed. The red dashed line indicates critical threshold of $T^2 = 16.573$. Suprathreshold clusters are shown in grey where $p < 0.05$113

- Figure 3.66: Ankle SPM vector field result (Hotelling's T^2) depicting HS vs. TFA differences at normal speed. The red dashed line indicates critical threshold of $T^2=28.565$. Suprathreshold clusters are shown in grey where $p<0.05$114**
- Figure 3.67: Knee SPM vector field result (Hotelling's T^2) depicting HS vs. TFA differences at normal speed. The red dashed line indicates critical threshold of $T^2=35.814$. Suprathreshold clusters are shown in grey where $p<0.05$114**
- Figure 3.68: HD M1 SPM vector field result (Hotelling's T^2) depicting HS vs. TFA differences at fast speed. The red dashed line indicates critical threshold of $T^2=22.591$. Suprathreshold clusters are shown in grey where $p<0.05$115**
- Figure 3.69: HD M2 SPM vector field result (Hotelling's T^2) depicting HS vs. TFA differences at fast speed. The red dashed line indicates critical threshold of $T^2=22.290$. Suprathreshold clusters are shown in grey where $p<0.05$115**
- Figure 3.70: HD M3 SPM vector field result (Hotelling's T^2) depicting HS vs. TFA differences at fast speed. The red dashed line indicates critical threshold of $T^2=16.686$. Suprathreshold clusters are shown in grey where $p<0.05$116**
- Figure 3.71: HD M4 SPM vector field result (Hotelling's T^2) depicting HS vs. TFA differences at fast speed. The red dashed line indicates critical threshold of $T^2=16.709$. Suprathreshold clusters are shown in grey where $p<0.05$116**
- Figure 3.72: Ankle SPM vector field result (Hotelling's T^2) depicting HS vs. TFA differences at fast speed. The red dashed line indicates critical threshold of $T^2=28.333$. Suprathreshold clusters are shown in grey where $p<0.05$117**
- Figure 3.73: Knee SPM vector field result (Hotelling's T^2) depicting HS vs. TFA differences at fast speed. The red dashed line indicates critical threshold of $T^2=35.681$. Suprathreshold clusters are shown in grey where $p<0.05$117**
- Figure 3.74: A statistical inference curve indicating a significant relationship between HS and TFA muscles at slow speed. Red dashed line indicates critical threshold ($t^*RF=3.076$, $t^*VM=3.071$, $t^*VL=3.122$, $t^*BFLH=3.096$, $t^*SEM=3.160$, $t^*TFL=.154$, $t^*TA=3.094$, $t^*GM=3.143$, $t^*GL=3.108$, $t^*SOL=3.087$). Suprathreshold clusters are shown in grey where $p<0.05$119**
- Figure 3.75: A statistical inference curve indicating a significant relationship between HS and TFA muscles at normal speed. Red dashed line indicates critical threshold ($t^*RF=3.140$, $t^*VM=3.117$, $t^*VL=3.075$, $t^*BFLH=3.075$, $t^*SEM=3.093$, $t^*TFL=3.130$, $t^*TA=3.085$, $t^*GM=3.120$, $t^*GL=3.108$, $t^*SOL=3.096$). Suprathreshold clusters are shown in grey where $p<0.05$120**

Figure 3.76: A statistical inference curve indicating a significant relationship between HS and TFA muscles at fast speed. Red dashed line indicates critical threshold ($t^*RF=3.079$, $t^*VM=3.077$, $t^*VL=3.069$, $t^*BFLH=3.069$, $t^*SEM=3.063$, $t^*TFL=3.096$, $t^*TA=3.025$, $t^*GM=3.113$, $t^*GL=3.041$, $t^*SOL=3.063$). Suprathreshold clusters are shown in grey where $p<0.05$	121
Figure 4.1: VAF comparison as a function of the number of synergies in HS at slow, normal and fast speeds.	143
Figure 4.2: VAF comparison as a function of the number of synergies in TFA at slow, normal and fast speeds.	143
Figure 4.3: VAF comparison as a function of the number of synergy groups in HS and TFA at slow speed.	144
Figure 4.4: VAF comparison as a function of the number of synergy groups in HS and TFA at normal speed.	144
Figure 4.5: VAF comparison as a function of the number of synergy groups in HS and TFA at fast speed.	145
Figure 4.6 HS R^2 between the reconstructed and original muscle signal when four synergy groups were selected during slow, normal and fast speeds. Standard error bars indicate \pm one.	145
Figure 4.7: TFA R^2 between the reconstructed and original muscle signal when four synergy groups were selected during slow, normal and fast speeds. Standard error bars indicate \pm one.	146
Figure 4.8: HS R^2 between the reconstructed and original muscle signal when four synergy groups were selected at slow speed. Standard error bars indicate \pm one.	146
Figure 4.9: HS R^2 between the reconstructed and original muscle signal when four synergy groups were selected at normal speed. Standard error bars indicate \pm one.	147
Figure 4.10: HS R^2 between the reconstructed and original muscle signal when four synergy groups were selected at fast speed. Standard error bars indicate \pm one.	147
Figure 4.11: HS ICC between the reconstructed and original muscle signal when four synergy groups were selected during slow, normal and fast speeds. Standard error bars indicate \pm one.	148
Figure 4.12: TFA ICC between the reconstructed and original muscle signal when four synergy groups were selected during slow, normal and fast speeds. Standard error bars indicate \pm one.	148
Figure 4.13: HS ICC between the reconstructed and original muscle signal when four synergy groups were selected at slow speed. Standard error bars indicate \pm one.	149
Figure 4.14: HS ICC between the reconstructed and original muscle signal when four synergy groups were selected at normal speed. Standard error bars indicate \pm one.	149

- Figure 4.15: HS ICC between the reconstructed and original muscle signal when four synergy groups were selected at fast speed. Standard error bars indicate \pm one.150**
- Figure 4.16: HS (A) muscle synergy vectors (S1-S4) and (B) activation coefficient profiles (C1-C4) during slow, normal and fast speeds. In (A), the bars represent muscle weightings within each synergy group. In (B), the thick lines represent the mean trajectory of activation coefficient profiles and the shaded area \pm one standard deviation from the mean.....152**
- Figure 4.17: TFA (A) muscle synergy vectors (S1-S4) and (B) activation coefficient profiles (C1-C4) during slow, normal and fast speeds. In (A), the bars represent muscle weightings within each synergy group. In (B), the thick lines represent the mean trajectory of activation coefficient profiles and the shaded area \pm one standard deviation from the mean.....154**
- Figure 4.18: (A) muscle synergy vectors (S1-S4) and (B) activation coefficient profiles (C1-C4) for HS and TFA groups during slow speed. In (A), bars represent weighting of each muscle within each synergy group. In (B), thick lines represent the mean trajectory of the activation coefficient profiles and the shaded area \pm one standard deviation from the mean.157**
- Figure 4.19: (A) muscle synergy vectors (S1-S4) and (B) activation coefficient profiles (C1-C4) for HS and TFA groups during normal speed. In (A), bars represent weighting of each muscle within each synergy group. In (B), thick lines represent the mean trajectory of the activation coefficient profiles and the shaded area \pm one standard deviation from the mean.159**
- Figure 4.20: (A) muscle synergy vectors (S1-S4) and (B) activation coefficient profiles (C1-C4) for HS and TFA groups during fast speed. In (A), bars represent weighting of each muscle within each synergy group. In (B), thick lines represent the mean trajectory of the activation coefficient profiles and the shaded area \pm one standard deviation from the mean.161**
- Figure 4.21: Individual synergy group contribution with respect to the total contribution between HS and TFA at (A) slow, (B) normal and (C) fast.162**
- Figure 4.22: HS post hoc SPM vector field results (paired Hotelling's T2 test) depicting significant differences between speeds. The red dashed lines indicate critical thresholds of $T2^* = 83.273, 80.709$ and 81.242 for (A), (B), and (C), respectively. Suprathreshold clusters are shown in grey where $p < 0.02$165**
- Figure 4.23: TFA post hoc SPM vector field results (paired Hotelling's T2 test) depicting significant differences between speeds. The red dashed lines indicate critical thresholds of $T2^* = 130.348, 127.465$ and 137.54 for (A), (B), and (C), respectively. Suprathreshold clusters are shown in grey where $p < 0.02$166**
- Figure 4.24: HS C1 parametric RM ANOVA within- and between-subjects, depicting significant differences between speeds. The horizontal red dotted line indicates the critical threshold of 7.46. Suprathreshold clusters are shown in grey where $p < 0.05$168**

- Figure 4.25: HS C1 within-subject post hoc paired t statistic between pairs of walking speeds. The red dashed lines indicate critical thresholds of $t^* = 4.53, 4.44$ and 4.43 for (A), (B), and (C), respectively. Suprathreshold clusters are shown in grey where $p < 0.02$168
- Figure 4.26: HS C2 parametric RM ANOVA within- and between-subjects, depicting significant differences between speeds. The horizontal red dotted line indicates the critical RFT threshold of 7.81 . Suprathreshold clusters are shown in grey where $p < 0.05$169
- Figure 4.27: HS C2 within-subject post hoc paired t statistic between pairs of walking speeds. The red dashed lines indicate critical thresholds of $t^* = 4.67, 4.70$ and 4.66 for (A), (B) and (C), respectively. Suprathreshold clusters are shown in grey where $p < 0.02$169
- Figure 4.28: HS C3 parametric RM ANOVA within- and between-subjects, depicting significant differences between speeds. The horizontal red dotted line indicates the critical threshold of 7.82 . Suprathreshold clusters are shown in grey where $p < 0.05$170
- Figure 4.29: HS C3 within-subject post hoc paired t statistic between pairs of walking speeds. The red dashed lines indicate critical thresholds of $t^* = 4.61, 4.53$ and 4.67 for (A), (B), and (C), respectively. Suprathreshold clusters are shown in grey where $p < 0.02$170
- Figure 4.30: HS C4 parametric RM ANOVA within- and between-subjects, depicting significant differences between speeds. The horizontal red dotted line indicates the critical threshold of 7.4 . Suprathreshold clusters are shown in grey where $p < 0.05$171
- Figure 4.31: HS C4 within-subject post hoc paired t statistic between pairs of walking speeds. The red dashed lines indicate critical thresholds of $t^* = 4.61, 4.52$ and 4.49 for (A), (B), and (C), respectively. Suprathreshold clusters are shown in grey where $p < 0.02$171
- Figure 4.32: TFA C1 parametric RM ANOVA within- and between-subjects, depicting significant differences between speeds. The horizontal red dotted line indicates the critical threshold of 8.02 . Suprathreshold clusters are shown in grey where $p < 0.05$173
- Figure 4.33: TFA C1 within-subject post hoc paired t statistic between pairs of walking speeds. The red dashed lines indicate critical thresholds of $t^* = 4.79, 5.01$ and 4.9 for (A), (B), and (C), respectively. Suprathreshold clusters are shown in grey where $p < 0.02$173
- Figure 4.34: TFA C2 parametric RM ANOVA within- and between-subjects, depicting significant differences between speeds. The horizontal red dotted line indicates the critical threshold of 7.89 . Suprathreshold clusters are shown in grey where $p < 0.05$174
- Figure 4.35: TFA C2 within-subject post hoc paired t statistic between pairs of walking speeds. The red dashed lines indicate critical thresholds of $t^* = 5.04, 5.02$ and 5.14 for (A), (B), and (C), respectively. Suprathreshold clusters are shown in grey where $p < 0.02$174

- Figure 4.36: TFA C3 parametric RM ANOVA within- and between-subjects, depicting significant differences between speeds. The horizontal red dotted line indicates the critical threshold of 8.12. Suprathreshold clusters are shown in grey where $p < 0.05$175
- Figure 4.37: TFA C4 parametric RM ANOVA within- and between-subjects, depicting significant differences between speeds. The horizontal red dotted line indicates the critical threshold of 8.32. Suprathreshold clusters are shown in grey where $p < 0.05$176
- Figure 4.38: TFA C4 within-subject post hoc paired t statistic between pairs of walking speeds. The red dashed lines indicate critical thresholds of $t^* = 5.03, 5.14$ and 5.12 for (A), (B), and (C), respectively. Suprathreshold clusters are shown in grey where $p < 0.02$176
- Figure 4.39: SPM vector field result (Hotelling's T^2) depicting HS vs. TFA differences at slow speed. The red dashed line indicates critical threshold of $T2^* = 27.738$. Suprathreshold clusters are shown in grey where $p < 0.05$178
- Figure 4.40: Post hoc two sample SPM t-test results comparing HS versus TFA at slow speeds for individual C. Red dashed line indicates critical threshold ((A): $t^*C1 = 3.895$, (B): $t^*C2 = 3.938$, (C): $t^*C3 = 3.996$, and (D): $t^*C4 = 3.964$). Suprathreshold clusters are shown in grey where $p < 0.01$.178
- Figure 4.41: SPM vector field result (Hotelling's T^2) depicting HS vs. TFA differences at normal speed. The red dashed line indicates critical threshold of $T2^* = 28.256$. Suprathreshold clusters are shown in grey where $p < 0.05$179
- Figure 4.42: Post hoc two sample SPM t-test results comparing HS versus TFA at normal speeds for individual C. Red dashed line indicates critical threshold ((A): $t^*C1 = 3.945$, (B): $t^*C2 = 3.986$, (C): $t^*C3 = 3.998$, and (D): $t^*C4 = 4.006$). Suprathreshold clusters are shown in grey where $p < 0.01$.179
- Figure 4.43: SPM vector field result (Hotelling's T^2) depicting HS vs. TFA differences at fast speed. The red dashed line indicates critical threshold of $T2^* = 28.244$. Suprathreshold clusters are shown in grey where $p < 0.05$180
- Figure 4.44: Post hoc two sample SPM t-test results comparing HS versus TFA at fast speeds for individual C. Red dashed line indicates critical threshold ((A): $t^*C1 = 3.993$, (B): $t^*C2 = 3.982$, (C): $t^*C3 = 4.016$, and (D): $t^*C4 = 3.942$). Suprathreshold clusters are shown in grey where $p < 0.01$180
- Figure 4.45: A statistical inference curve indicating a significant relationship between HS C and TFA C at slow speed. Red dashed line indicates critical threshold ((A): $t^*C1 = 3.019$, (B): $t^*C2 = 3.097$, (C): $t^*C3 = 3.083$, and (D): $t^*C4 = 3.115$). The period where the critical threshold is exceeded depicted as grey ($p < 0.05$).182
- Figure 4.46: A statistical inference curve indicating a significant relationship between HS C and TFA C at normal speed. Red dashed line indicates critical threshold ((A): $t^*C1 = 3.063$, (B): $t^*C2 = 3.095$, (C): $t^*C3 = 3.081$, and (D): $t^*C4 = 3.094$). The period where the critical threshold is exceeded depicted as grey ($p < 0.05$).183

Figure 4.47: A statistical inference curve indicating a significant relationship between HS C and TFA C at fast speed. Red dashed line indicates critical threshold ((A): $t^*C1=3.045$, (B): $t^*C2=3.085$, (C): $t^*C3=3.081$, and (D): $t^*C4=3.049$). The period where the critical threshold is exceeded depicted as grey ($p<0.05$).....	184
Figure 5.1: Experimental setup: (A) surface EMG, (B) foot switches location; 1: Heel; 2 & 3: 1 st & 5 th Metatarsal; 4: Toe, (C) ultrasound scanner, and (D) muscle view using ultrasound	197
Figure 5.2 EMG and reflective markers attachments on HS. (A) front dominant leg, (B) back dominant leg, (C) side dominant leg, (D) side non-dominant leg.	198
Figure 5.3: EMG and reflective markers attachments on TTA IL and PL. (A) front IL, (B) posterior IL, (C) side IL, (D) front PL, (E) posterior PL and (F) side PL.....	198
Figure 5.4: (A) HS and (B) TTA walking (length: 10 m; Inclination: 0° pathway)	199
Figure 5.5: VAF comparison as a function of the number of synergies in cases 1-4.	202
Figure 5.6: ICC of reconstructed signals compared to the original signal for each muscle in cases 1-4.	203
Figure 5.7: (A) Muscle weighting within each synergy and (B) activation coefficient profiles of cases 1-4.....	204
Figure 5.8: Comparison between muscle synergies of TTA and TFA.	207
Figure 5.9: A statistical inference curve indicating a significant relationship between HS C and TTA IL C (case 1) at normal speed. Red dashed line indicates critical threshold ((A): $t^*C1=3.362$, (B): $t^*C2=3.341$, (C): $t^*C3=3.408$, (D): $t^*C4=3.433$). The period where the critical threshold is exceeded depicted as grey ($p<0.05$).	209
Figure 5.10: A statistical inference curve indicating a significant relationship between HS UKN C and TTA UKN IL C (case 2) at normal speed. Red dashed line indicates critical threshold ((A): $t^*C1=3.360$, (B): $t^*C2=3.473$, (C): $t^*C3=3.384$). The period where the critical threshold is exceeded depicted as grey ($p<0.05$).	209
Figure 5.11: A statistical inference curve indicating a significant relationship between HS UKN C and TTA UKN PL C (case 3) at normal speed. Red dashed line indicates critical threshold ((A): $t^*C1=3.379$, (B): $t^*C2=3.511$, (C): $t^*C3=3.421$). The period where the critical threshold is exceeded depicted as grey ($p<0.05$).	210
Figure 5.12: A statistical inference curve indicating a significant relationship between TTA UKN IL C and TTA UKN PL C (case 4) at normal speed. Red dashed line indicates critical threshold ((A): $t^*C1=4.633$, (B): $t^*C2=4.578$, (C): $t^*C3=4.395$). The period where the critical threshold is exceeded depicted as grey ($p<0.05$).	210

Figure A.1: (A) Ensemble average EMG profiles of neonates, toddlers, preschoolers and adults for both legs during the GC. (B) Activation coefficient profiles extracted from the ensemble EMG average (adapted from [224]).	269
Figure A.2: Examples of mechanically passive lower limb prostheses (adapted from [275, 280]).	269
Figure A.3: Examples of Mechanically passive prostheses. (A) Single-axis knee with hydraulic cylinder [351], and (B) KX06: Polycentric prosthetic knee with hydraulic [352].	270
Figure A.4: Examples of microprocessor lower limb prostheses (adapted from [353]).	270
Figure A.5: Commercially available power knee prostheses (adapted from [354]).	270
Figure A.6: Semi-active lower limb prosthetic device. (A) Adapted from [286] (B) University of Leeds prosthetic device (adapted from [8]).	271
Figure A.7: Prosthetic foot examples (adapted from [355]).	272
Figure B.1: EMG and reflective markers attachments on one of the HS. (A) front dominant leg, (B) back dominant leg, and (C) side non-dominant leg.	277
Figure B.2: An example of HS EMG data process during one trial. The first, second, third and fourth rows show raw, bandpass filter (4th order Butterworth HPF 20Hz, LPF 500Hz), rectified and linear envelope (2nd order Butterworth LPF with the cut of frequency of 6 Hz) data during transient-state gait, respectively.	278

List of Tables

Table 3.1: Participants' walking speed; mean \pm standard deviation (m/s).....	58
Table 3.2: Muscles corresponded to each HD Module which is associated with the biomechanical subtasks are considered for biomechanics hypotheses.....	63
Table 3.3: HS and TFA major and minor bursts (peaks) muscle activities during transient-state walking at each speed. The approximate peak values available from the muscles in the literature review are included for HS [9, 96] and TFA [36, 47]. NF indicates not found.	72
Table 4.1: HS activation coefficient profile repeatability between trials/subjects using ICC.....	150
Table 4.2: TFA activation coefficient profile repeatability between trials/subjects using ICC.....	150
Table 4.3: HS muscle weightings contribution and corresponding activation timing profile of S1 across speeds. Early, mid and terminal stance represent ES, MS, and TS; initial, mid and terminal swing represents ISW, MSW, and TSW; the whole stance and swing phase represents SP and SW respectively.	153
Table 4.4: HS muscle weightings contribution and corresponding activation timing profile of S2 across speeds.	153
Table 4.5: HS muscle weightings contribution and corresponding activation timing profile of S3 across speeds.	153
Table 4.6: HS muscle weightings contribution and corresponding activation timing profile of S4 across speeds.	153
Table 4.7: TFA muscle weightings contribution and corresponding activation timing profile of S1 across speeds.	155
Table 4.8: TFA muscle weightings contribution and corresponding activation timing profile of S2 across speeds.	155
Table 4.9: TFA muscle weightings contribution and corresponding activation timing profile of S3 across speeds.	155
Table 4.10: TFA muscle weightings contribution and corresponding activation timing profile of S4 across speeds.	155
Table 4.11: HS muscle weightings contribution and activation timing profile within each corresponding module during slow speed.	156
Table 4.12: TFA muscle weightings contribution and activation timing profile within each corresponding module during slow speed.	156
Table 4.13: HS muscle weightings contribution and activation timing profile within each corresponding module during normal speed.	158
Table 4.14: TFA muscle weightings contribution and activation timing profile within each corresponding module during normal speed.	158
Table 4.15: HS muscle weightings contribution and activation timing profile within each corresponding module during fast speed.....	160

Table 4.16: TFA muscle weightings contribution and activation timing profile within each corresponding module during fast speed.....	160
Table 4.17: Highest and lowest muscle synergy group contribution and corresponding muscle group association.	162
Table 4.18: R² values for four muscle synergies in HS at different speeds; The module average obtained column wise represents the average correlation of each module with respect to all paired-wise speed comparison. The overall average value obtained row-wise represents the average correlation of all muscle synergies with respect to each pair-wise speed comparison.	163
Table 4.19: R² values for four muscle synergies in TFA at different speeds; Refer to Table 4.18 for the meaning of the module average and the overall average.	164
Table 4.20: The comparison between HS and TFA at each speed by means of R².....	164
Table 4.21: Summary of the suprathreshold clusters obtained from the main test (SPM Hotelling's T2) and post hoc test (SPM two-sample t-test) between HS and TFA at each speed category (biomechanics perspective).....	177
Table 4.22: Summary of the suprathreshold clusters obtained from the SPM two-sample t-test between HS and TFA at each speed category (control perspective).....	181
Table 5.1: Muscle weightings contribution and activation timing profile within each corresponding module (case 1: HS dominant leg).	205
Table 5.2: Muscle weightings contribution and activation timing profile within each corresponding module (case 1: TTA IL).	205
Table 5.3: Muscle weightings contribution and activation timing profile within each corresponding module (case 2 & 3: HS UKN).	205
Table 5.4: Muscle weightings contribution and activation timing profile within each corresponding module (case 2 & 4: TTA UKN IL).	206
Table 5.5: Muscle weightings contribution and activation timing profile within each corresponding module (case 3: TTA UKN PL).	206
Table 5.6: Muscle weightings contribution and activation timing profile within each corresponding module (case 4: TTA UKN PL).	206
Table 5.7: Muscle synergy comparison in case 1-4 using R². NA indicates not applicable.	208
Table 5.8: Summary of the suprathreshold clusters of case 1-4 occurred during the GC. Early, mid and terminal stance represent ES, MS, and TS; initial, mid and terminal swing represents ISW, MSW, and TSW, respectively.	211
Table A.1: Ankle muscles and corresponding movements (adapted from [99]).	257
Table A.2: Knee muscles and corresponding movements (adapted from [99]).	257
Table A.3: Hip muscles and corresponding movements (adapted from [99]).	258

Table A.4: Ambulatory measurement devices. Compiled from [9, 104, 110, 117, 346].	259
Table A.5: Comparison between gait analysis systems. Compiled from [110, 346, 347].	260
Table A.6: Summary of the studies on lower limb surface EMG, filtration techniques used on HS and TFA during ADLs.	260
Table A.7: Factors impact surface EMG. Compiled from [111, 155, 157].	261
Table A.8: Literature review on muscle synergies during ADLs.	262
Table A.9: Key statistical output variables	268
Table A.10 Some of the most commercially available prostheses.	271
Table A.11: Summary of the EMG signals and classifiers implemented for predicting intended control output in lower limb prostheses.	273
Table B.1: Demographic data of HS.	275
Table B.2: Demographic data of TFA.	276
Table B.3: Details of TFA.	277
Table C.1: Demographic data of HS during steady-state walking	282
Table C.2: Demographic data of TTA during steady-state walking	282
Table C.3: Details of TTA.	282

List of Abbreviations

1D	One-dimensional
AD	Anterior Deltoid
ADDL	Adductor Longus
ADM	Adductor Magnus
ANOVA	Analysis of Variance
BB	Biceps Brachii
BFLH	Biceps Femoris Long Head
BFSH	Biceps Femoris Short Head
C	Activation Coefficient Profile
C1	Activation Coefficient Profile 1
C2	Activation Coefficient Profile 2
C3	Activation Coefficient Profile 3
C4	Activation Coefficient Profile 4
CF	Conventional Feet
CO	Crossover
E	Error
EC	End Contact
EDB	Extensor Digitorum Brevis
EHB	Extensor Hallucis Brevis
EHL	Extensor Hallucis Longus
EO	External Oblique
ERE	Erector Spinae
ES	Early Stance
ESR	Energy Storing-and-Returning
Eval	Eigenvalue
F/E	Flexion/Extension
FA	Feet Adjacent
FC	Foot Contact
FDB	Flexor Digitorum Brevis
FDL	Flexor Digitorum Longus
FES	Functional Electrical Stimulation
FHL	Flexor Hallucis Longus
FIR	Finite Impulse Response
FO	Foot-off
FSR	Force Sensitive Resistor

GL	Gastrocnemius Lateralis
GM	Gastrocnemius Medialis
GMAX	Gluteus Maximus
GMED	Gluteus Medius
GR	Gracilis
HAM	Hamstrings
HC	Heel Contact
HPF	High Pass Filter
HR	Heel-rise
HS	Healthy Subjects
HST	Heel Strike
Hz	Hertz
IC	Initial Contact
ICA	Independent Component Analysis
ICC	Intra-class Correlation
IL	Intact Leg
IMU	Inertial Measurement Unit
IMVC	Isometric Maximal Voluntary Contraction
IO	Internal Oblique
IP	Iliopsoas
ISCIs	Incomplete Spinal Cord Injuries
ISW	Initial Swing
JMP	Jumping
LD	Latissimus Dorsi
LDA	Linear Discriminant Analysis
LGW	Level Ground Walking
LPF	Low Pass Filter
LR	Loading Response
M1	High Dimensional Sensorimotor Module 1
M2	High Dimensional Sensorimotor Module 2
M3	High Dimensional Sensorimotor Module 3
M4	High Dimensional Sensorimotor Module 4
MANOVA	Multivariate ANOVA
MS	Mid-stance
MSW	Mid-swing
NA	Not Applicable
NF	Not Found
NM	Not Mentioned

NMF	Non-negative Matrix Factorization
OA	Osteoarthritis
OI	Opposite Initial Contact
OT	Opposite Toe Off
PCA	Principal Component Analysis
PERB	Peroneus Brevis
PERL	Peroneus Longus
PF/DF	Plantarflexion/Dorsiflexion
PL	Prosthetic Leg
PSW	Pre-swing
QDA	Quadratic Discriminant Analysis
QUAD	Quadriceps
R2	Coefficient of Determination
RA	Ramp Ascending
RAB	Rectus Abdominis
RAS	Rectus Abdominis Superior Portion
RD	Ramp Descending
Rehab	Rehabilitation
RF	Rectus Femoris
RFT	Random Field Theory
RM	Repeated-measures
RMS	Root Mean Square
RN	Running
S	Muscle Synergy Vector
S1	Muscle Synergy Vector 1
S2	Muscle Synergy Vector 2
S3	Muscle Synergy Vector 3
S4	Muscle Synergy Vector 4
SA	Stair Ascending
SACH	Solid Ankle Cushioned Heel
SAR	Sartorius
SD	Stair Descending
SEM	Semitendinosus
SEMIM	Semimembranosus
SENIAM	Non-Invasive Assessment of Muscles
SIP	Stepping in Place
SOL	Soleus
SP	Stance Phase

SPL	Splenius Capitis
SPM	Statistical Parametric Mapping
SS	Sidestepping
ST	Sternocleidomastoideus
STD	Standing
STG	Sitting
SVM	Support Vector Machine
TA	Tibialis Anterior
TB	Triceps Brachii
TC	Terminal Contact
TFA	Transfemoral Amputees
TFL	Tensor Fasciae Latae
TO	Toe-off
TS	Terminal Stance
TSW	Terminal Swing
TTA	Transtibial Amputees
TV	Tibia Vertical
UKN	Upper Knee
UT	Upper Trapezius
VAF	Variance Accounted For
VE	Vastus Externus
VI	Vastus Internus
VL	Vastus Lateralis
VM	Vastus Medialis
WB	Walking Backward
WF	Walking Forward
WL	Walking Leftward
WR	Walking Rightward

List of Publications Directly Related to This Research

Section 4.3 and 5.3 are based on jointly-authored publications:

1. **Mehryar, P.**, Shourijeh, M.S., Maqbool, H.F., Torabi, M. and Dehghani-Sanij, A.A., 2016, August. Muscle synergy analysis in transtibial amputee during ramp ascending activity. In *Engineering in Medicine and Biology Society (EMBC), 2016 IEEE 38th Annual International Conference of the* (pp. 1676-1679). IEEE.
2. **Mehryar, P.**, Shourijeh, M.S., and Dehghani-Sanij, A.A., 2016, October. Muscle synergy analysis in transtibial amputee during ramp descending activity. In *International Conference on neurorehabilitation 2016. Segovia, Spain: Springer*.

The entire chapter 5 is based on the following publication:

1. **Mehryar, P.**, Shourijeh, M.S., Rezaeian, T., Iqbal, N., Messenger, N., and Dehghani-Sanij, A.A., 2017, August. Changes in synergy of transtibial amputee during gait: A pilot study. In *Engineering in Medicine and Biology Society (EMBC), 2017 IEEE BHI-2017 International Conference on Biomedical and Health Informatics*. IEEE.

Chapter 1

INTRODUCTION

1.1 Background

1.1.1 Prevalence of Amputation

The incidence of lower limb amputation is increasing drastically in the world. The three leading causes of this type of amputation are the vascular disease, war injuries and motor vehicle and road accidents [1, 2]. There are more than 32 million amputees all around the world in which 75% accounts for lower limb, and 17% accounts for bilateral amputees [3, 4]. In the UK, approximately 34,109 persons underwent lower limb amputations in 151 hospitals from 2007 to 2010 [5], which is over 11000 amputations per year. In the US, about 185,000 amputations are carried out every year, and It is estimated that this number will double by 2050 and reach a total of 3.6 million [6].

1.1.2 Use of Prosthesis in Rehabilitation

Following amputation, successful rehabilitation is very crucial as patients require extensive training to compensate for the loss of muscle function and lack of somatosensory feedback as well as to achieve natural and efficient gait when using a prosthesis. The gait efficiency is a crucial factor which helps the patients to reduce exhaustion or harm when using the prosthesis while performing locomotive tasks. The use of the prosthetic device is one of the most important interventions to improve the amputees' quality of life. There have been significant advances in prostheses to overcome complications such as high energy consumption, gait deficiency or low mobility. However, there is still need for improvement of the lower limb prostheses to achieve superior ambulation in amputees, especially in the case of high degree amputations (e.g., transfemoral).

The commercially available prostheses related to lower limb extremity are divided into three types: mechanically passive devices, microprocessor-controlled passive devices (actively controlled) and powered devices. In addition, there are three categories of foot prosthesis including Conventional Feet (CF), Energy Storing-and-Returning (ESR) Feet and bionic feet. Mechanically passive knee prosthetic devices and CF (Solid Ankle Cushioned Heel (SACH)) are the most commonly used prostheses for amputees [7]. Passive devices, including both mechanically passive and microprocessor-controlled, are capable of dissipating energy at the joints. However; they cannot produce net power like a healthy joint in a human during normal locomotion. In addition, they

require a significantly larger volitional effort from amputees and complex activities such as ascending ramps and stairs cannot be performed very smoothly. However, the powered devices may overcome these issues by implementing the control system which provides positive power. One of the main hurdles of the powered devices is the high-power consumption due to their continuous activation. This is opposed to the gait strategy of human muscles which become activated and deactivated at different parts of the gait cycle (GC) [8]. For instance, in level ground walking, high activity of lower limb muscles is observed during the stance phase (SP) as compared to the swing phase [9]. Lastly, an increased cognitive load of amputees is required using multi-joint powered devices [10].

Hence, the need for better controlling lower limb prostheses which could mimic the human muscle activations has brought the idea of using information from the muscles. One of the major sources of biological signals in neural control is surface electromyography (EMG). This signal can be detected from the muscles of lower extremities using surface EMG electrodes to control lower limb prostheses. Early application of surface EMG for control was mostly based on the amplitude-based threshold (onset and offset control strategy) to lock/unlock the prosthetic knee joint during some activities [11, 12]. EMG signals also have been implemented for direct proportional control of different joints of lower limb prosthetics including knee [13] and ankle joints [14]. Other studies investigated EMG pattern recognition to identify the user intent in different activities and to control the prosthetic device smoothly, intuitively and naturally in different terrains [15-19].

Regardless of the type of prostheses and control systems being used, unilateral lower limb amputees tend to overload the intact leg (IL) subconsciously or deliberately which seems to play an important role in developing secondary physical conditions including osteoarthritis (OA), osteopenia, osteoporosis, and back pain [20, 21]. The most common sites of OA are the knee and hip joints of IL [21-23]. Esposito et al. [24] reported the increase rate of Knee OA in TFA IL is ten times more than transtibial amputees (TTA) and non-amputees. Kellgren et al. [22] found the increased incidence rate of hip OA of PL and IL as compared to the non-amputees. Consequently, this may have an impact on muscle activation patterns as patients load their muscles differently to perform the same task as compared to the non-amputees [25].

Therefore, the activation patterns of lower limb amputees' muscles spanning the IL and PL joints could provide an understanding of neuromuscular compensation strategies in amputees. This can be studied at two levels namely high dimensional (HD) EMG/muscle activation pattern and low dimensional muscle synergy/modular motor

control from biomechanics and robotic control perspectives as explained in subsequent sections.

1.1.3 HD EMG Studies in Lower Limb Amputees

Prior studies investigated muscle electrical signal characteristics of lower limb amputees' PL to evaluate biomechanical differences (i.e., muscle coordination and moments) [26-40] as well as to develop new robotic control paradigms for controlling prosthetic devices during activities of daily livings (ADLs) [11, 12, 14-16, 35, 41-45]. In addition, others have focused on the IL muscle activations of transtibial [26-28, 32, 38] and transfemoral [35, 36, 46-50] amputees from biomechanics and robotic control perspectives.

In most of the gait-related studies investigated steady-state walking, however, it is crucial to understand the other aspects of gait in amputees. This includes the transition from standing to walking (gait initiation), transition from gait initiation to steady-state (transient-state), steady-state walking and transition from steady-state to upright standing (gait termination) [51, 52]. Changing states requires complex interaction between nervous, muscular and skeletal systems which may result in falls in people with a poor score in clinical tests [53, 54] and people with limb loss [55-57] especially when changing states (gait initiation and transient-state) [58, 59]. In previous studies, gait initiation was examined in healthy subjects (HS) in terms of kinematics and kinetics [52, 60-68] and muscle activations of lower limbs [52, 53, 61-66, 68]. Other researchers investigated gait initiation in lower limb amputees accounting for different biomechanical parameters including temporal variables, ground reaction forces, the center of mass and center of pressure [51, 67, 69-72] and muscle activations of IL and PL [35, 73]. However, none of the prior literature accounts for the characteristics of inter-muscle covariance (i.e., inter-muscle co-activation and multi-muscle synergy) and time dependence (i.e., whole time-series) in the lower limb amputees' muscle activations. In addition, little attention has been devoted to the first stride after gait initiation (i.e., transient-state) in which it is believed that the gait has not yet reached to its consistent natural pattern (i.e., steady-state) [52, 62, 66].

To the author's knowledge, no study was found to compare the high dimensional muscle activation patterns in HS and TFA during transient-state walking at different speeds which accounts for inter-muscle covariance and time dependence.

1.1.4 Muscle Synergy Studies in HS and Pathological Group

The complicated HD muscle activation patterns can be decomposed, using a mathematical technique i.e., non-negative matrix factorization (NMF), into low-dimensional subsets namely an independent spatially fixed matrix of weights (known as muscle synergies, muscle synergy vectors or motor modules), which represents the

relative weighting of each muscle within each synergy group and time-varying activation (known as activation coefficient profile), which represents the relative activation of the motor modules during the GC [74-77]. Muscle synergy analyses have been proven to simplify the construction of motor behaviors [78-81].

Several authors reported muscle synergies in normal steady-state walking, walking at different speeds, backward walking, perturbed walking, inclined locomotion, running and sidestepping, the transition from walking to running and vice-versa [82-87]. In addition, there have been studies focusing on pathological populations which showed the number of muscle synergy groups was lower in people with Parkinson disease, cerebral palsy, stroke and spinal cord injuries than the HS [88-91]. The same number of muscle synergies were found between HS and lower limb amputees during ADLs, indicating analogous complexity implemented by the CNS which does not depend on the level of amputation. These studies found activation coefficient was significantly different in some regions of the GC [92-95]. However, two main limitations of these studies were the low sample size, and they only accounted for the steady-state walking.

To the author's knowledge, modular motor control in HS and lower limb amputees during transient-state walking at different speeds have not yet been studied in the literature.

1.2 Motivation

It is clear that there is a real need to understand the neuromuscular behavior of the lower limb amputees prior to developing neurorehabilitation program and designing robotic-aided myoelectric prosthesis. Due to the richness of neural information and non-invasiveness of surface EMG, extracting muscle information would be a viable and safe way to investigate the adjustment strategy of the neuromuscular system in an individual with amputation. It is undoubtedly challenging to realize the ideal performance of the PL due to the loss of muscles and somatosensory feedback. Thus, the muscle coordination of the IL could be used to provide clinically valuable information from biomechanics and robotic control perspectives.

To the best of the author's knowledge, there is no study in the literature that evaluated the neuromuscular coordination in HS and lower limb amputees during gait at two levels (i.e., HD EMG and low dimensional muscle synergy) accounting for two approaches (i.e., biomechanics and robotic control), at different walking states (transient-state and steady-state) and different speeds (slow, normal, and fast).

Biomechanics approach could contribute in the field of rehabilitation, providing valuable information on the functional outcomes of muscle activation, neural structure underlying the motor behaviors, and how they alter in pathologies and after rehabilitation.

Robotic control approach could be implemented in the next generation of prosthetic devices to provide a new paradigm for controlling artificial limbs and create a better solution for replacing natural motor function in an individual with amputation.

1.3 Aims and Objectives

1.3.1 Aims

The aims of this research are:

- To examine the neuromuscular coordination behavior of HS and TFA across transient-state walking speeds to identify the adjustment and compensatory strategies in HS dominant leg and TFA IL from biomechanics and robotic control perspectives;
- To examine low dimensional modular motor control of HS and TTA during steady-state walking to identify neuromuscular changes in TTA IL and PL.

1.3.2 Objectives

The objectives of this project are as follows:

- To investigate the differences in temporal characteristics of HD sensorimotor Modules and all muscles that contribute to the co-contraction of ankle and knee joints (biomechanics perspective) as well as individual muscle activations (robotic control perspective) for both HS and TFA in response to increasing transient-state walking speeds (within-subject HD EMG).
- To investigate the differences in temporal characteristics of HD sensorimotor Modules and all muscles that contribute to the co-contraction of ankle and knee joints (biomechanics perspective) as well as individual muscle activations (robotic control perspective) between HS and TFA during transient-state walking at different speeds (slow, normal and fast) (between-subject HD EMG).
- To develop a reliable and robust algorithm for muscle synergy analysis which accounts for the whole population rather than an individual subject.
- To examine the changes in complexity of control strategy implemented by the CNS of HS and TFA with increasing transient-state walking speed.
- To assess whether the muscle recruitment of spatially fixed muscle synergy vectors changes in HS and TFA with increases in transient-state walking speeds.

- To assess whether muscle synergies change between HS and TFA at each speed.
- To investigate the differences in low dimensional temporal components of muscle synergy (i.e., activation coefficient profiles) of HS and TFA from biomechanics and robotic control perspectives in response to increasing transient-state walking speeds (within-subject activation coefficient profile).
- To investigate the differences in low dimensional temporal components of muscle synergy (i.e., activation coefficient profiles) between HS and TFA from biomechanics and robotic control perspectives during transient-state walking at each speed category (between-subject activation coefficient profile).
- To compare the changes in complexity of control strategy implemented by the CNS between HS and TTA during steady-state walking. To determine whether muscle synergy complexity changes with respect to the number of recorded muscles.
- To determine whether muscle synergy complexity changes with respect to the number of recorded muscles.
- To assess whether muscle recruitment of spatially fixed muscle synergies changes among HS dominant leg, TTA IL, and TTA PL.
- To investigate the differences in low dimensional temporal components of muscle synergy (i.e., activation coefficient profiles among HS dominant leg, TTA IL, and TTA PL (case1-4) during normal steady-state walking (between-subject activation coefficient profile).
- To assess commonalities/differences in the statistically significant differences between HD sensorimotor Modules and low dimensional activation coefficient profiles of HS and TFA across speeds.
- To assess the commonalities/differences between TTA and TFA muscle synergies.

1.4 Scope of this Research

This research presents a methodology 1) to understand the neuromuscular adjustment strategy in HS dominant leg and TFA IL during transient-state walking (within-subject analysis) 2) to understand the compensatory mechanism deployed by the TFA IL as compared to the HS dominant leg with regard to HD muscle activations and low dimensional modular motor control during transient-state walking (between-subject analysis) and 3) to investigate modular motor control differences in TTA IL and PL as compared to the HS during steady-state walking (between-subject analysis). In this line of work, two main studies were conducted as shown in Figure 1.1 and Figure 1.2.

Study one focuses on the neuromuscular coordination of HS and TFA at two levels: 1) HD EMG or muscle activation pattern and 2) low dimensional muscle synergy or modular motor control. While HD muscle activation provides information about the activation timing, shape and level of muscle activity, muscle synergy can be used to measure the neuromuscular complexity and provide relevant details on the motor performance (Figure 1.1). Study two focuses on the neuromuscular coordination of HS and TTA from the low dimensional level only (Figure 1.2).

Study one was regarded as exploratory thereby two approaches were considered namely biomechanics and robotic control to investigate a *priori* hypotheses using statistical parametric mapping (SPM). The biomechanics hypotheses of HD muscle activation and low dimensional muscle synergy consider the inter-muscle dependence and inter-activation coefficient profile dependence, respectively whereas the robotic control hypotheses take individual muscle activations and individual activation coefficient profiles into account (Figure 1.1). Study two explores the robotic control approach by considering individual activation coefficient profiles only (Figure 1.2).

The findings from these studies could be useful at two levels. On the one hand, this allows therapists to focus on the part of the GC in which the significant differences occur as compared to the HS in order to improve the muscles performance and better control progression and stability during walking. On the other hand, this could be used by the prosthetic companies to develop a new control paradigm to compensate for the deficiency, and mimic the activity performed by a healthy HD EMG activity or low dimensional activation coefficient profile.

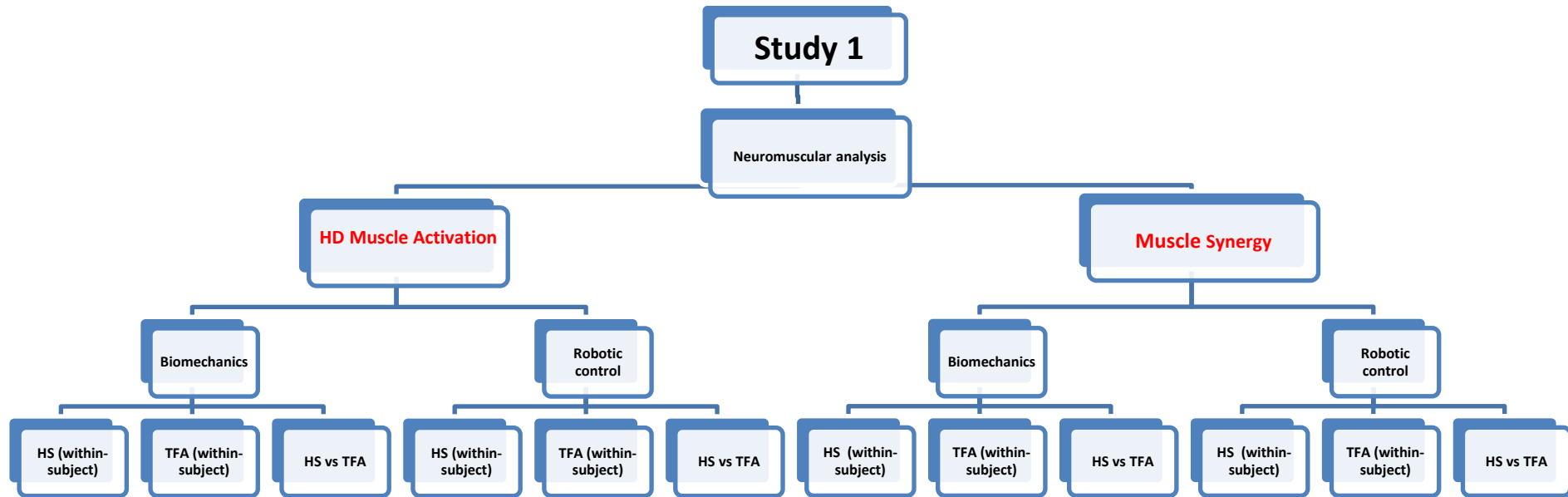


Figure 1.1: Flowchart of study 1; neuromuscular analysis in terms of HD muscle activation and muscle synergy of HS dominant leg and TFA IL during transient-state walking at different speeds considering biomechanics and robotic control perspective.

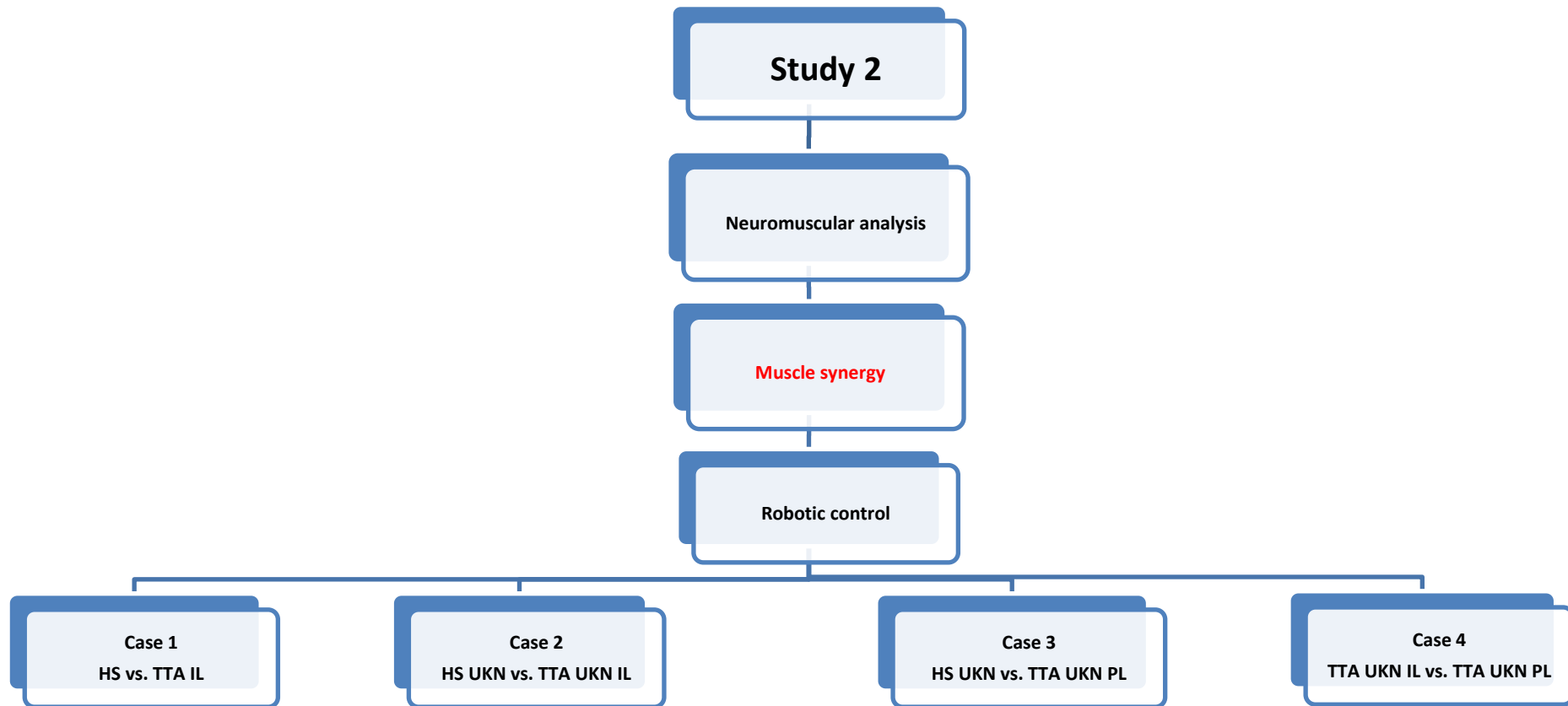


Figure 1.2: Flowchart of study 2; neuromuscular analysis in terms of muscle synergy between HS, TTA IL and TTA PL during steady-state walking; Abbreviation: upper knee (UKN).

1.5 Contribution of this Research

The biomechanics and robotic control approach proposed in this thesis contribute to the healthcare-related applications with the focus on the lower limb amputees and to the body of knowledge.

Major contributions of this research are as follows:

1. Identifying the differences in muscle activation patterns of HS dominant leg and TFA IL during transient-state walking across speeds considering the characteristics of inter-muscle dependence (biomechanics perspective), and individual muscles (robotic control) as well as time dependence in EMG time-series within- and between-subject.
2. Developing a reliable and robust algorithm to decompose the HD EMG signals into low dimensional subsets which accounts for the whole population rather than an individual subject.
3. Identifying the complexity of the neuromuscular system in controlling the HS dominant leg and TFA IL during transient-state walking across speeds.
4. Assessing the correlation of spatially fixed muscle synergies in HS and TFA within- and between-subject.
5. Investigating the differences in the temporal component of muscle synergy (i.e., activation coefficient profile) of HS dominant leg and TFA IL during transient-state walking across different speeds considering the covariance between activation coefficient profiles (biomechanics perspective), and individual activation coefficient profiles (robotic control perspective) as well as the whole time-series.
6. Identifying the complexity of the neuromuscular system in controlling the HS dominant leg, TTA IL, and PL during steady-state walking.
7. Assessing the correlation of spatially fixed muscle synergy vector HS and TTA during steady-state walking.
8. Identifying the differences in activation coefficient profile between HS and TTA during normal steady-state walking considering individual activation coefficient profiles and the whole time-series.

1.6 Thesis Outline

The thesis is presented in seven chapters as shown in Figure 1.3:

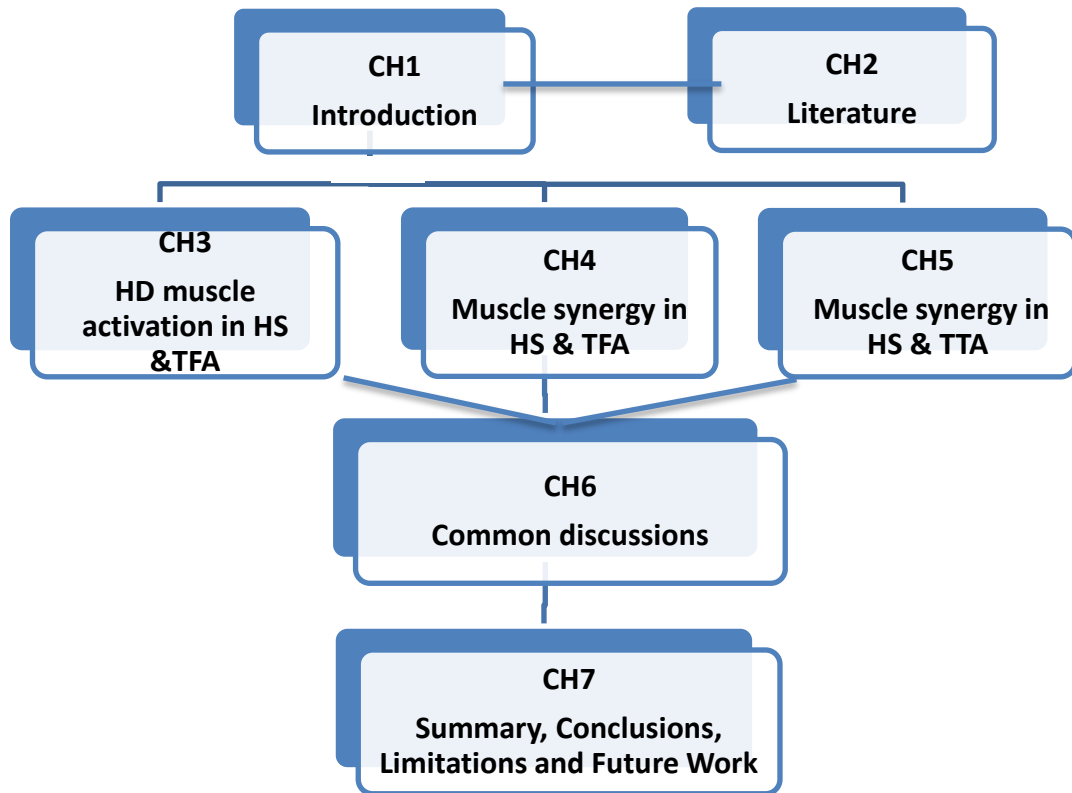


Figure 1.3: Flowchart of the thesis organization

Chapter 1 presents the background, motivation, aims, and objectives for investigating the neuromuscular differences in HS and lower limb amputees. Furthermore, it describes the contributions of this research.

Chapter 2 presents an overview of lower limb biomechanics including muscles and associated movements as well as the biomechanics terminologies of gait, kinematics, kinetics. In addition, different means of gait measurement devices is studied.

The use of surface EMG at two levels are studied namely HD EMG/muscle activation patterns and muscle synergy/modular motor control. Furthermore, the drawbacks intrinsic to surface EMG and different methodological concerns using surface EMG in muscle synergies are investigated. Comprehensive research is conducted on neuromuscular aspects of human motion including the biomechanics variables kinematics, and kinetics as well as HD EMG profile and muscle synergies in healthy subjects and lower limb amputees during walking. The gait deficiency in lower limb amputees and the major secondary complications after amputation are discussed.

Various lower limb prostheses are studied including knee and ankle joints, focusing on the types and control strategies implemented for movement of lower limb amputees.

Chapter 3 forms the first of two neuromuscular studies in this thesis (Figure 1.1 HD muscle activation). In this chapter, HD EMG is recorded from HS dominant leg and TFA IL during transient-state walking with increases in speed (slow, normal and fast). HD muscle activation patterns are compared in HS and TFA intra- and inter-subjectively. The chapter closes by discussing the differences in muscle activations of HS and TFA from biomechanics and robotic control perspectives.

Chapter 4 forms another aspect of the first of two neuromuscular studies in this thesis (Figure 1.1 muscle synergy). In this chapter, a mathematical technique known as concatenated non-negative matrix factorization is developed to investigate the components of muscle synergies in HS dominant leg and TFA IL while performing transient-state walking with increases in speed. The results highlight the correlation of spatially fixed muscles synergies intra- and inter-subjectively. In addition, the temporal components of muscle synergy (i.e., activation coefficient profiles) are compared from biomechanics and robotic control perspectives intra- and inter-subjectively. The chapter closes by discussing the possible adaptation strategies and compensatory adjustment implemented by TFA.

Chapter 5 forms the second of two neuromuscular studies in this thesis (Figure 1.2 muscle synergy), focusing on modular motor control differences between HS and TTA during normal steady-state walking. In this chapter, concatenated non-negative matrix factorization which was developed in the previous chapter is implemented to investigate the components of muscle synergies in HS dominant leg, TTA IL and TTA PL at a different state of walking (steady-state). The results highlight the correlation of spatially fixed muscles synergies between HS and TTA legs. In addition, individual temporal components of muscle synergy (i.e., activation coefficient profiles) are compared inter-subjectively between two groups as well as intra-subjectively between TTA IL and PL. The chapter closes by discussing the possible adaptation strategies and compensatory adjustment implemented by TTA.

Chapter 6 presents the commonalities/differences between the significant differences of HD sensorimotor Modules and low dimensional activation coefficient profiles of HS and TFA across speeds. In addition, commonalities/differences between TTA and TFA synergy vectors are discussed. The justifications are presented for the selection of methodological analyses from the choice of HD and low dimensional activation to statistical analysis and choice of the decomposition algorithm. Consequently, the possibilities of using the findings of this research in clinics and neurorehabilitation robotic-aided prostheses are presented.

Chapter 7 presents the summary of the research work, highlights the main achievements and contributions, limitations and offers the recommendation for future work.

Chapter 2

LITERATURE REVIEW

2.1 Introduction

This chapter is divided into three main sections. The first section provides general information on muscles anatomy and their association with the movements during gait. The biomechanics terminologies namely human gait, kinematic and kinetic are described; and various gait measurement devices are studied. The second section is conducted on the use of surface electromyography for studying muscle coordination, focusing on the high dimensional EMG signal and muscle synergies/modular motor control. Furthermore, the drawbacks intrinsic to surface EMG and different methodological concerns in muscle synergies are investigated. Consequently, this section aims at carrying out comprehensive research on the neuromuscular aspects of human motion from biomechanics perspectives to high dimensional electromyography and muscle synergies/modular motor control in healthy subjects and pathological populations during ADLs. In addition, the gait deficiency in lower limb amputees and the major secondary complications after amputation are discussed. Lastly, different types of prostheses (i.e., knee and ankle) and control strategies (i.e., echo and pattern recognition) are briefly studied. In addition, previous studies on the control strategies that have used EMG from lower limb muscles to control prostheses are investigated. Finally, the gap of knowledge in high dimensional EMG and muscle synergies are discussed.

2.2 Lower Limb Biomechanics

2.2.1 Basic Anatomy

The muscles of the lower limb are divided into two categories: The above/upper knee muscles and below knee muscles. The two major groups in the above knee muscles are hamstrings and quadriceps. The hamstrings muscles namely semimembranosus (SEMIM), semitendinosus (SEM) and biceps femoris long head (BFLH) are located at the posterior section of the leg and responsible for knee flexion and hip extension. The quadriceps muscles are a group of four muscles including rectus femoris (RF), vastus medialis (VM), vastus lateralis (VL), and vastus intermedius (VI) which are located at the anterior section of the leg and responsible for the extension of the knee and the shank segment. The main two bones of the lower limb are femur and tibia. The femur interacts with tibia to move the knee. Another significant bone in the below knee is fibula which

connects with the tibia and helps for the movement of the foot. There are around 50 muscles in the lower limb [96]. The ankle and the foot consist of 26 bones and 33 joints. The ankle not only helps to maintain stability but also perform different movements such as plantarflexion and dorsiflexion. The main plantarflexor muscles are gastrocnemius medialis (GM), gastrocnemius lateralis (GL), and soleus (SOL) which are responsible for propelling the body forward by generating push off during walking. Achilles tendon is the most important structure in the lower leg responsible for storing the elastic energy required for ADLs. It connects three muscles of the calf (gastrocnemius), plantaris, and soleus to the heel bone. Lower limb muscles and bones are shown in Figure 2.1 (A) and (B), respectively.

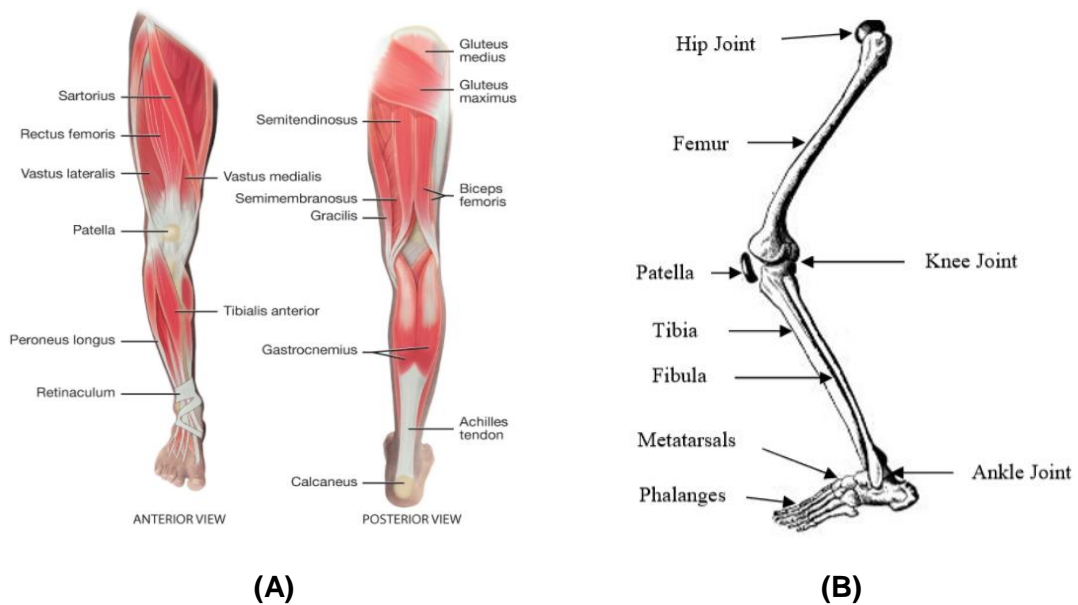


Figure 2.1: Lower limb muscles and bones. (A) superficial lower limb muscles [97] and (B) main lower limb bones [98].

2.2.2 Types of Movements and Muscles

The muscles can be categorized into different groups based on the movement performed. Each movement has its own counter movement (antagonist) in which moves in the opposite of the original movement. [99]. The role of the ankle, knee and hip muscles have been shown in Appendix A, Table A.1 to Table A.3 in which the agonist and antagonist movements corresponding to each muscle group is determined.

2.2.3 Human Gait

Human gait is the most common form of physical activities in daily life which comprised of the integrated activity of muscles acting across many joints. Rowe et al. [100] defines walking process as “a form of a bipedal progression in which the repetitive movements of the lower limbs include periods of double support, when both feet are in contact with the ground, followed by periods of time when only one foot is supporting the body (single support) while the

other is being moved above the ground (swing)". Bernstein [101] showed different combinations of muscle patterns quite possibly achieve the same movement because of the synergistic and antagonistic nature of many of these muscles. It has been shown that healthy/able-bodied patterns of motion at the ankle, knee, and hip could remain the same as opposed to the drastic changes in muscle activities or moment of force [96].

2.2.3.1 Phases of Gait Cycle

The gait cycle is defined as the time between two successive step occurrences and often begins with the heel touching the ground (known as initial contact) [102]. The gait cycle is divided into two major components, the stance phase, and the swing phase. Stance phase occurs when the foot is in contact with the ground whereas the swing phase occurs when the foot is in the air for forward progression. Generally, at a normal speed, stance phase, and swing phase consists of 60% and 40% of a gait cycle, respectively. Each stance comprised of two double support phases (each accounting for 10% of gait cycle) (Figure 2.2).

The stance phase is divided into four sub-phases:

1. **Loading response (LR):** Time period from after immediate initial contact to the toe-off of the contralateral extremity from the ground. This is when the first period of double support occurs.
2. **Mid-stance (MS):** It starts with contralateral toe-off and ends when both ankles are aligned in the frontal plane.
3. **Terminal stance (TS):** Period from ankle alignment in the frontal plane to just about the contralateral foot contacts the ground.
4. **Pre-swing (PSW):** Time intervals from contralateral initial contact to prior toe-off of the ipsilateral extremity from the ground.

Swing phase is divided into 3 sub-phases:

1. **Initial swing (ISW):** begins with a lift of the limb and continues until maximum flexion occurs (60 degrees).
2. **Mid-swing (MSW):** is the period of maximum knee flexion until vertical positioning of the tibia.
3. **Terminal swing (TSW):** Following when the tibia is vertically positioned to just prior to IC.

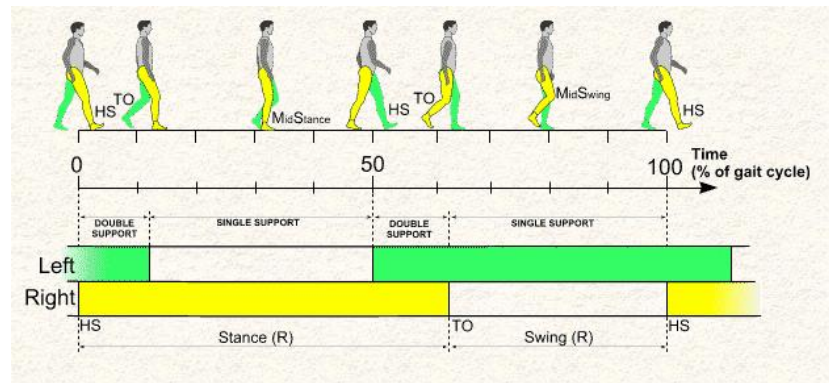


Figure 2.2: Gait cycle diagram; break down of single support and double support (adapted from [103])

Figure 2.3 shows the gait cycle events namely initial contact (IC), opposite toe off (OT), heel-rise (HR), opposite initial contact (OI), toe-off (TO), feet adjacent (FA) and tibia vertical (TV). In the literature, the event IC is also known as heel contact (HC), heel strike (HST) or foot contact (FC). TO event is also termed as a foot-off (FO), end contact (EC) and terminal contact (TC).

The distribution contribution of each sub-phase to the GC is as follows: LR (0–10% of the gait cycle), MS (10–30%), TS (30–50%), PSW (50–60%), ISW (60–73%), MSW (73–87%) and TSW (87–100%) [9].

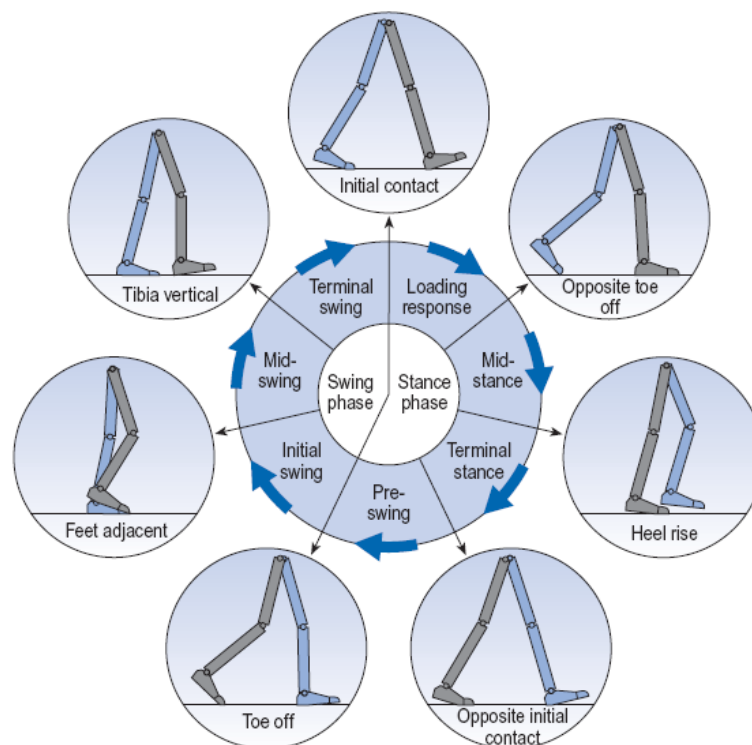


Figure 2.3: Gait phases and events in the gait cycle, Initiation of gait starts with the right leg (grey) (modified from [104]).

One stride is also known as a gait cycle. Moreover, stride is the linear distance between corresponding successive points of contact of the heel of the same foot (e.g., HS of right

foot to next HS of the same foot). However, step is the linear distance in the plane of progression between corresponding successive contact points of opposite feet [105].

2.2.3.2 States of the Gait Cycle

Gait cycle can be performed in different ways depending on the previous state of the human position. This includes the transition from standing to walking (gait initiation), transition from gait initiation to steady-state (transient-state), steady-state walking and transition from steady-state to upright standing (gait termination) [51, 52].

Gait initiation involves complex interactions between nervous, muscular and skeletal systems that serve to move the body from a quasi-static (standing) to a movement-state (walking). Gait initiation is split up into different phases. The first limb which initiates the movement is known as the leading limb (swinging limb), and the contralateral leg which follows the leading limb is known as the trailing limb. Figure 2.4 shows the gait patterns in four gait periods. A represents the interval from the leading limb onset of the gait initiation until the IC, and C is the next gait cycle of the ipsilateral limb (transient-state). On the other hand, B is the interval of the trailing limb onset of the gait initiation until IC, and D represents the next gait cycle of the trailing limb (transient-state).

There is little agreement in the previous research regarding the number of steps required to reach the steady-state walking. Researchers focused on different biomechanical parameters to define this. Mann et al. [66] analyzed the joint angles and force plate data to conclude that steady-state can be reached in three steps. Nissan and Whittle [106] investigated where the largest acceleration occurs in the first two steps. Breniere and Do [107] concluded that the steady-state was attained after one step based on the force plate data by calculating the body center of mass velocity. Miller et al. [108] studied the mechanical energy analysis of gait initiation and showed that steady-state was reached by the end of three full steps. Other researchers who conducted kinematics of initial walking assumed at least three steps were required to reach the steady-state [52, 54, 60, 62]. Kibushi et al. [109] suggested for the EMG data at least 10 strides are required to reach the steady-state.

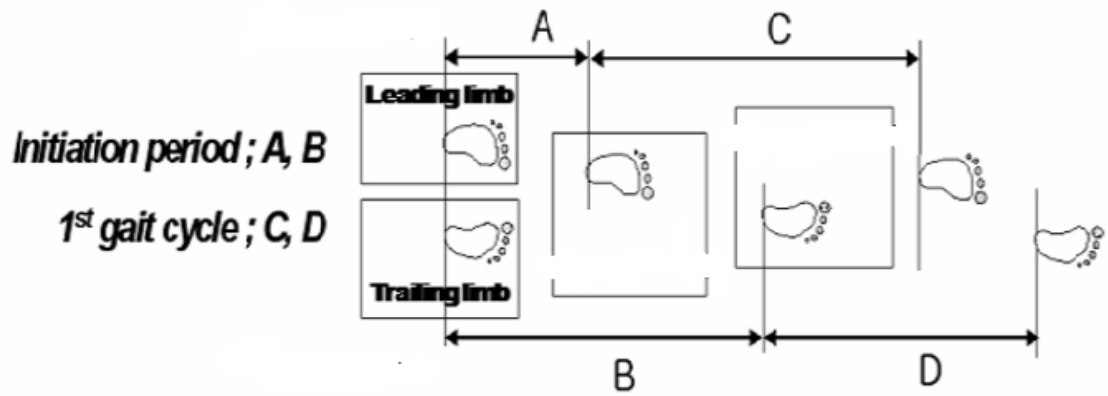


Figure 2.4: Gait initiation (A and B) and transient-state gait (C and D) of leading and trailing limb, respectively (Adapted from [52]).

2.2.4 Kinematics and Kinetics

Kinematic variables are associated with the movement of joints and segments independent of the forces such as linear and angular displacements, velocities and accelerations. Kinetic variables are associated with the movement as a result of both internal (movement of muscles, ligaments, or due to friction between joints) and external (ground or external loads) forces.

2.2.5 Gait Measurement Devices

A wide variety of measurement systems have been developed to record information of temporal, kinematic, kinetic and muscle parameters during locomotive tasks. These measurement devices consist of stationary and ambulatory systems. The former is confined to limited space (e.g., laboratories) whereas the latter can be attached at various location of the human body and be used outdoors. Laboratory equipment consists of devices such as motion capture system (Vicon camera system), force plates (e.g., Kistler), pressure mapping insoles (Noraxon insoles) which measure the kinematic parameters, GRF and center of pressure, respectively. These devices are more precise, have no restriction on power consumption, provide better reproducibility and repeatability however they are generally limited to the indoor spaces, more expensive, heavy and large in size. On the contrary, the ambulatory system includes wearable sensors such as surface EMG (e.g., Myon), inertial measurement unit (e.g., Shimmer) and foot switches (e.g., Noraxon) are small in size, cheap, light and portable, however, they are prone to outside noise and inferences, limited battery duration and a fewer gait parameters can be recorded [110]. Appendix A, Table A.4 shows the list of most used stationary and ambulatory measurement devices. Appendix A, Table A.5 shows the advantages and disadvantages of stationary and ambulatory devices. A detailed review was conducted on gait measurement devices by [110].

2.3 Surface EMG for Studying Muscle Coordination

Surface EMG is the electrical signal associated with the muscle contraction which is essentially the sum of the action potential made by the active motor units [111]. EMG is the primary signal to describe the neural output from the spinal cord [76]. It provides information regarding the duration, shape, and level of muscle activity [9]. Mean EMG activity level of the whole time-series is the simplest way to report muscle activation. However, important information would be lost only focusing on this parameter. Therefore, EMG profiles and the activation-deactivation of the muscle contraction are most commonly reported to identify the changes in muscle coordination [9, 76].

2.3.1 Detection of EMG Signal

In order to detect EMG signals, two approaches are used: surface or non-invasive EMG and intramuscular or invasive EMG.

The former type consists of electrodes which are in contact with the skin. The electrodes can be directly connected to the sensors or indirectly connected through a cable. The electrode is a bridge between the skin and the sensor to convey electrical impulses. The differential amplifiers sensor rejects the common electrical activity from both sites and amplifies the difference. Therefore, the common mode between the pairs is allowed to be rejected. The current wireless EMG electrodes consist of 2 active and 1 reference electrodes which convey the information to the receiver. Prior to the conversion of the analog to digital signals by the encoder, the EMG signals are amplified and filtered by the sensors. Finally, the digital signal is processed, displayed and recorded by relevant software [99].

The latter type consists of the needle which is inserted into muscle via skin. Several needles may be required to obtain sufficient EMG. Non-invasive EMG is preferred over the invasive because 1) the needle could irritate the skin and muscle as well as results in pain during dynamic movement 2) the needle is very small as compared to the volume of the muscles thereby the information may not be reflective of the total muscle mass involved in the activity [112] 3) the needle placement requires trained and specialized medical personnel [76].

The use of EMG can be perceived in applications such as physical rehabilitation (physiotherapy), urology (treatment of incontinence), and biomechanics (sports training, and motion analysis). Moreover, it plays an important role in the diagnosis of neuromuscular diseases such as muscular dystrophy, pinched nerve or peripheral nerve damage [113].

2.3.2 EMG Profiles

The raw EMG signals are noisy and stochastic, however, they have been reported by many researchers previously [96, 114-116] to identify the onset and offset. The problems arise from the unprocessed EMG are the difficulty in interpreting the amplitude and shape of the signals as well as investigating the variation among the recorded cycles. Therefore, processing of the raw EMG is required to report muscle activity profiles.

The signals can break into many electrical firings which occur at different rates and the overall signal in the time domain is comprised of these frequencies. The frequency is the number of events in which firing occurs per second, and it is measured in Hertz (Hz). According to several studies, the common frequency of EMG signals lies between 20 and 500Hz [46, 99]. Therefore, filtration is performed by applying a bandpass filter to the raw data which removes the unnecessary high and low frequency.

Following the filtration, several techniques have been reported in the literature as a means of signal processing to obtain muscle activity namely 1) Full wave rectification (i.e., absolute value) 2) linear envelope (rectified and low pass filter) 3) integration of the full wave rectification over the whole time-series 4) integration of the full wave rectification for a fixed period of time, reset to zero, then integration cycle repeated 5) integration of the full wave rectification to a preset level, reset to zero, then integration repeated [117]. The most common technique to report EMG profile is a linear envelope [76, 96, 117-121]. Several researchers have used different filtration order and cut-off frequency to obtain linear envelope for various applications.

Appendix A, Table A.6 provides information about the muscles recorded and filtering techniques used on healthy subjects and transfemoral amputees.

In order to make a meaningful conclusion, several normalization methods have been implemented based on a reference point. This depends on the application, however the most common ones include 1) maximum voluntary contraction (MVC) 2) peak measured amplitude over all trials. The former one is performed against static resistance, and the latter is based on the peak value obtained from the dynamic activities of all trials.

The original time domain (mili-seconds) is converted to a percentage by interpolating the data to 100-400 data points depending on the locomotive task and speed [76, 122, 123].

The ensemble average EMG provides the mean curve and a standard deviation band (range of plus/minus 1 standard deviation) of the stride to stride variability of the linear envelope which improves the signal-to-noise ratio [124].

Depending on the application, a different number of cycles have been used in the literature ranging from 3 to 40 cycles [84, 86, 120, 125, 126].

Regardless of the signal processing techniques used, many researchers found linear relationships between EMG amplitudes and muscle tension [127-131]. Other studies showed non-linearity in some of the muscles during the high tension activities [127-129].

2.3.2.1 Level of Muscle Activity

In order to compare the muscle activity level between muscles and/or subjects, the degree of muscle activation becomes an important parameter. In this context, normalization is performed based on the isometric maximal voluntary contraction (IMVC) or sub-maximal isometric contraction [132]. These types of normalizations are dependent on the arbitrary angle in which the maximum effort is performed. However, they can be misinterpreted when applied to the dynamic activities [133].

It has been reported that there is no consensus on the best normalization method to be used [134]. Therefore, accurate information about the level of muscle activity (exact value expressed as a percentage of the maximum neural drive) during a certain activity cannot be obtained from EMG measurements [76]. That is to say, only approximate degree of muscle activity and major muscles involved in the tasks can be determined by means of MVC. Notwithstanding, despite the lack of precision, it facilitates the comparison between muscle and/or subjects as compared to the raw EMG activity [135]. It is worth mentioning that the study of muscle coordination does not necessarily require information about the amplitude of muscle activation. Many studies focused on the onset and offset or shape of the EMG pattern, deployed normalization based on the peak measured amplitude over all trials [90, 91, 136, 137] or mean measured amplitude over all trials [118]

2.3.2.2 Duration of Muscle Activity

The analysis of EMG often involves identifying rapid transient changes in the muscle activation during locomotive tasks. The most common approach for determination of the motor-related events from the EMG signal is a visual inspection by a trained person [138-140]. It has been reported; higher precision is obtained by the expert using visual inspection due to the details of the signals can be investigated by the experts' experience and skills [141]. However, others questioned the reliability of the visual inspections and reported low reproducibility [142, 143]. The limitations of visual inspections are dependency on subjective criteria, time-consuming, offline analysis and based on the skills and experience of the inspector [144]. To overcome these issues, computerized methods for event detections have been implemented.

The onset and offset of EMG activity are identified using a defined threshold based on the decision criteria. Single threshold methods calculate the mean power of the background noise on the rectified raw EMG [145]. Other techniques involve an amplitude threshold based on the noise related to the linear envelope of EMG [146]. In the literature, several EMG threshold values have been proposed including 1st, 2nd, or 3rd standard deviations plus the mean of baseline activity, 15–25% of the peak EMG [147], and minimum EMG plus half a range of EMG [126]. Some researchers improved upon the accuracy within the Single threshold methods such that the threshold is based on the weighted average of N consecutive samples [148, 149] or two adjacent windows [143] rather than on its instantaneous value. More advanced methods have been proposed using two thresholds with the possibility of correct detection and of setting the probabilities false positive occurrence [150]. Other researchers proposed thresholds developed based on the abrupt changes of the variance of the EMG signal by implementing cumulative sum [144], approximated generalized likelihood ratio [151], and approximated cumulative sum [152] using no windowing, a sliding window, and two adjacent sliding windows, respectively. The more advanced threshold is in accordance with the continuous wavelet transform due to the changes in frequency content on the EMG signal at the onset of muscular activation [153]. Staude and Wolf [144] proposed a threshold which accounts for the dynamic parameter profile. A parameter such as signal-to-noise ratio, onset rise time, and background noise level have impacts on detection of muscle activity [147]. Li and Aruin [154] used the Teager-Kaiser energy operator to reduce the background noise level while accounts for the amplitude and frequency of the EMG. Superior precision has been observed in this approach as compared to the classical approach particularly when the raw EMG signal has a low signal-to-noise ratio.

As explained above various onset detection algorithm have been proposed in which many of the thresholds rely on the indicator extracted from the EMG signal with a threshold. However, they are significantly different from the structure and the individual parameter setting implemented for activity [144]. Therefore, the accuracy and reliability of the threshold value can be impacted by the detection algorithm. Furthermore, various methodologies lead to different representations of the muscle activation. It is important to choose a detection algorithm which may provide reliable results for a particular application regardless of being subjective.

2.3.2.3 Factors Influencing Surface EMG

There are several factors influencing the surface EMG including the detection systems, geometrical, physical, physiological fiber membrane properties, non-physiological anatomic and motor unit properties (more details are presented in Appendix A, Table

A.7) [155]. The subsequent items are the most important factors affecting surface EMG which can be avoided during and after data acquisition.

Cross Talk

Crosstalk refers to the signal recorded over one muscle that is contaminated from the EMG signal by a nearby muscle and conducted through the intervening volume to the EMG electrodes [156]. This is one of the most crucial sources of error in surface EMG interpretation [76]. Several authors reported the crosstalk could be due to the extinction of the action potentials at the ends of the tendon and differences in the sources of the non-propagating and propagating signals [155, 157, 158]. Campanini et al. [159] showed the higher variability in tibialis anterior muscle activity could be due to electrode placement. In addition, a second epoch of activity was observed when the electrodes are located towards the peroneus longus which was not shown in other places. The extent that the cross talk interfere with the muscle activation is not easy to detect by means of surface EMG. Some proposed different ways to reduce the effect of crosstalk using cross-correlation [160]. On the other hand, Lowery et al. [161] showed that cross-correlation is not an appropriate statistical quantity for quantifying crosstalk. In addition, the results obtained from the electrical muscle stimulation would not provide accurate information regarding the crosstalk due to the differences in motor unit recruitment strategy between voluntary and electrically-provoked contractions [161]. It has been reported that the double-differential electrodes [162], reducing the electrode distance, and placing the electrodes on the muscle bellies [163] would decrease cross-talk [76].

Amplitude Cancellation

Amplitude cancellation of positive and negative phases of motor unit action potentials can result from the surface EMG underestimating the excitation signal that was sent from the spinal cord to the muscle [155, 164]. Algebraic summation of motor-unit action-potential trains in cats showed a non-linear increase of EMG magnitude [164]. Another study confirmed the result by means of computation models, indicating the interpretation of changes in the amplitude of the activation signal is confounded by the amplitude cancellation [165]. Although the amplitude cancellation has only been observed in animals and computational models, its interference with the EMG activity level with respect to increased neural drive at a high degree of excitation is known. Additionally, the reduction in muscle fiber conduction velocity, due to fatigue, increases the duration of motor unit action potentials which increases amplitude cancellations [165]. It is worth mentioning; amplitude normalization would reduce the amplitude cancellation. Importantly, the studies whose focus are on muscle coordination (i.e., high dimensional

EMG pattern and/or modular motor control) are not affected by the amplitude cancellation [76].

Spatial Variability of Muscle Activity

Inhomogeneities in muscle activation have been shown in animals [166, 167] and humans [167]. Other factors such as muscle fiber and mechanical heterogeneity may result in different muscle activity level [166]. Two main limitations may lead to wrong interpretation of muscle activity namely 1) variability in the location of the electrodes placed in different subjects and 2) relative movement of the detection system with respect to the muscle. The former can be resolved by selecting the same location on the muscle for attachment of the electrode inter-subjectively (e.g., muscle belly). In the literature, the optimal detection configuration has been selected by means of a multi-channel method to estimate the site of innervation zone. The electrodes must be placed on one side and over the innervation zone for the entire duration of the dynamic task [76, 168]. The latter limitation can be avoided using a two-dimensional high-density surface EMG which covers a larger surface area [169]. The relative movement of the electrodes with respect to the muscle during a dynamic task is estimated using a high-density recording by identifying the tendons and innervation zones. However, the main limitations of this technique are the number of electrodes for processing and the number of muscles that can be recorded during one recording. Due to the difference in morphology inter-subjectively, it is a great challenge to place all the electrodes at the same location on the muscle for all the subjects [169]. Therefore, the recording must be done cautiously using this approach.

2.3.3 Muscle Synergy/Modular Motor Control

Human movement stems from the complex interaction between the nervous, muscular, and skeletal systems [96]. The musculoskeletal system has redundant degrees of freedom because the human body is comprised of many muscles. The lower limb has more than 50 muscles and at least half of them contribute to the movement of the leg during gait in the sagittal plane [96]. In order to solve the redundancy problem, the CNS simplifies the control of muscles by the concept of muscle synergy. That is, the main features of muscle activity patterns could be explained by a few underlying components which have been proven to simplify the construction of motor behaviors [78-81, 170-172].

Therefore, the complicated high dimensional muscle activation patterns can be decomposed, using a mathematical technique (i.e., NMF), into low-dimensional subsets namely an independent spatially fixed matrix of weights (known as muscle synergies, motor modules, modules, synergy vectors or weighting coefficients) which represents the relative weighting of each muscle within each synergy group and time-varying

activation (known as activation coefficient profiles, activation coefficient, coefficients, neural commands, temporal components, motor primitives) represents the relative activation of the motor modules during gait cycle. Collectively, one synergy vector and its corresponding activation coefficient profile can be termed a synergy or module [78] (Figure 2.5). Muscle synergies are considered to be the fundamental control signals responsible for producing the HD repertoire of muscle activation required for performing specific locomotion [80, 173-175].

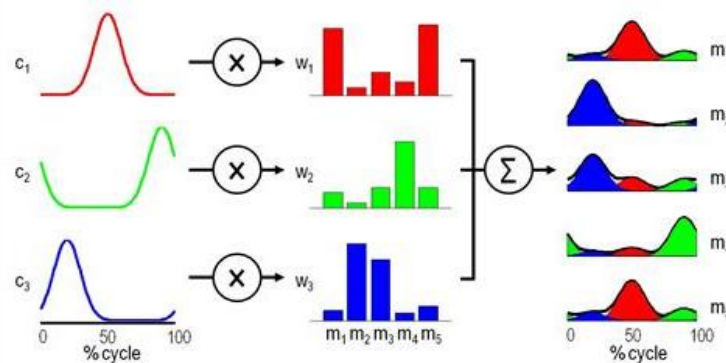


Figure 2.5: Schematic of muscle synergy/modular motor control; C1-C3 are activation coefficient profiles, W1-W3 are muscle synergy vectors, and m1-m5 are original muscle activations (adapted from [176]).

Muscle synergy analysis has been implemented in animal models [80, 174, 177], intact human [176, 178], individuals with neurological problems [91, 179-183] and other pathologies [92-95, 126].

2.3.3.1 Muscle Synergy Methodological Consideration

There are several *a priori* assumptions regarding muscle synergy analysis that may influence the results and interpretation of outcomes. Some of these are including decomposition algorithm, signal processing approach, EMG normalization method, analysis of dimensionality, data structure, which muscle synergy components remain constant and which can vary between trials/subjects, muscle synergy components normalization method and means of comparison of muscle synergy components. Therefore, great care is needed to understand the consequences of these assumptions when comparing the results of studies together.

Decomposition Algorithm

Previous studies have proposed several decomposition techniques including principal component analysis (PCA), independent component analysis (ICA), and NMF. PCA is a factor analysis technique that finds a set of orthogonal components known as principal components that represent the covariance of the original dataset [184, 185]. ICA is a non-linear blind-source separation technique that identifies the statistically independent

components (factors) that can be reconstructed to generate a mixed set of signals [186, 187]. NMF is a parts-based representation of the original signal using its non-negativity constraints [74, 188]. Tresch et al. [75] compared a range of different factorization algorithms and found similar results to one another despite different sets of assumption used in each algorithm. Another study aimed at comparing variations of the NMF algorithm to decrease the cost functions between the original matrix and reconstructed components [189].

Signal Processing Approach

After decomposition analysis method is selected, several methodological assumptions are required throughout the muscle synergy analysis. The typical signal processing procedures involve high pass filtering (HPF) before rectification, low pass filtering (LPF) after rectification (i.e., linear envelope), amplitude normalization, time normalization.

Several studies have been conducted with regard to the various filtering types and order as well as amplitude normalization strategies [190-192].

Filtering Type and Order

No study has been found in the literature that aims to investigate the effect of filter type and filter order on muscle synergy analysis. However, Devaprakash et al. [193] studied the difference in EMG processing using a 2nd order Butterworth filter and 2nd order critically damped filter with a consistent cut off frequency and reported only small differences in the EMG data which did not impact clinical interpretation. De Luca et al. [194] found that the minimal difference on the spectral shapes between the 2nd and 3rd order (>1% difference in root mean square between EMG profiles). Therefore, the outcomes of these studies suggest the filter type and filter order may not significantly impact the muscle synergy results.

High Pass Filtering Before Rectification

Prior research showed a range of HPFs applied before rectification of the EMG signals including: 40Hz [91, 195, 196], 35Hz [197, 198], and 20Hz [192, 199]. Merletti and Torino [200] recommended an HPF from 5 to 10 which is currently endorsed by the International Society of Electrophysiology and Kinesiology (ISEK). De Luca et al. [194] reported that a 20 Hz HPF provides the best compromise between retaining EMG desired informational content and eliminating movement artifacts. Generally, an HPF is applied to reduce non-physiological signals (i.e., motion artifacts) [201]. Therefore, it is expected that the HPF does not have an impact on muscle synergy analysis. However, this remains to be studied thoroughly for future research.

Low Pass Filtering After Rectification

A wide variety of LPFs have been implemented in the prior synergy literature from 1 [202], 3 [83], 4 [91], 6 [92-95, 136], 10 [90], 15 [58], 20 [203], 30 [204], 35 Hz [198] to 40 Hz [197]. Hug et al. [192] noted that the number of synergy groups varied in healthy subjects during cycling between three different cut-off frequencies (i.e., 4, 10 and 15 Hz). It was shown that higher low-pass cut-off frequency would lead to higher number of synergies. However, the impact on the muscle synergy components has not been shown. Shuman et al. [201] reported the sensitivity of the number of synergy groups to LPF, ranging from 4 to 40 Hz in typically-developing children and children with cerebral palsy. They found the number of synergy groups increased for both populations with an increase in low pass cut-off frequency.

EMG Normalization Method

With regards to the amplitude normalization, several methods were implemented in scaling the EMG data for muscle synergy analysis including MVC [87, 126, 205], peak measured amplitude over all trials [90, 91, 136] peak measured amplitude per trial [179, 206], median trial maximum [207], unit magnitude per trial [123], unit variance over all trials [208, 209] and unit variance per trial [123]

Unit variance prevents the large representations of high variance muscles in muscle weightings of muscle synergy analysis [203]. Shuman et al. [201] reported small changes in total variance accounted for in scaling the data using peak amplitude and unit variance prior to the muscle synergy analysis. Banks et al. [123] have shown less sensitivity of activation coefficient profiles to EMG normalization method as opposed to the synergy vectors which showed the clearest variability using unit magnitude per trial EMG.

Time Normalization

Due to the differences in duration of the gait cycle between trials, interpolation of each trial is performed to have an equal number of points for obtaining the ensemble average. Depending on the locomotion task and speed, the trials are interpolated to 100-400 points [122]. Time-normalization is an important task to obtain representative EMG envelope to compare intra- and inter-subject analysis such that scalar point or whole time-series can be considered for statistical analyses.

Therefore, in order to compare between trials/subjects/groups, the cycle is linearly converted from the experimentally recorded time units (milliseconds), corresponding to the cycle (i.e., heel strike to the heel strike of the ipsilateral leg), to a representing cycle percentage [118, 210]. Most gait-related synergy studies interpolated

the data to 101 points per gait cycle [85, 91, 211]. However, it is noteworthy that the intra- and inter-subject kinematics variability is neglected thus, a certain region of the gait cycle might not represent the corresponding phase for all subjects [118].

Analysis of Synergy Dimensionality

The number of muscle synergies to be selected to reconstruct the original signal stems from the percentage of variance accounted for (VAF) by a combination of synergies. The VAF describes how much of the variability in the linear envelope of the original input data is accounted for by the output reconstructed components from the synergy vectors and their recruitment activation coefficient profiles [198].

Some literature proposed a minimum threshold by means of VAF, the coefficient of determination (R^2) [208, 211], while others add another criterion such as the addition of the next synergy group will not increase VAF by a certain amount [78, 126, 212]. Additionally, as a local criterion to determine the number of muscle synergies, some researchers account for the reconstruction quality of each muscle by means of the coefficient of determination [204] and intra-class correlation (ICC) [92-95, 213].

The VAF threshold ranges from 80% [136, 179, 214] to 95% [123, 201], and including intermediate values including 85% [83, 176, 215] and 90% [76, 82, 84-87, 91, 109, 126, 198, 216-218].

The threshold for each muscle reconstruction quality is determined by either $R^2 > 0.6$ [204], $ICC > 0.5$ [92-95, 213] or $VAF > 0.75$ [87] and 0.8 [204]. Other researchers studied the changes in the slope of the VAF or R^2 and by adding a synergy up until a considerable change in either of these parameters is perceived [79, 179, 219].

Comprehensive research has been conducted on muscle synergy analysis of the HS and different pathological populations, investigating different parameters including activity, muscle, filtration type and order, cut off frequency, VAF threshold and number of synergy groups (Appendix A, Table A.8).

Data Structure

Oliveira et al. [84] illustrated the number of trials as well as the data structure (i.e., individual, averaged, or concatenated into one matrix) has no significant effect on the number of muscle synergy groups extracted. However, they reported reconstruction quality has decreased when ensemble average and concatenation of small data sets are used.

Types of Synergy Vectors

The muscle synergy vector calculation approaches either hold the synergy vector constant across all trials [91-95] or allow it to vary from trial to trial [185, 190]. Banks et al. [123] revealed using varying synergy vectors lead to great differences in trial-to-trial activation coefficient profiles by means of cosine similarities.

Sorting Method

Due to the local minima issue, the functional sorting was implemented to rearrange the indices of synergy and coefficient of one trial/subject/group based on the other trial/subject/group. An arbitrary reference was chosen to sort muscle synergy based on the similarity of synergy vectors and/or activation coefficient profiles values by means of maximum coefficient of determination [81, 84]. Other researchers implemented maximal cosine similarity to ensure that each synergy was similar across trials within each subject [109, 191, 220, 221]. However, other quantities such as intra-class correlation can be implemented which accounts for the patterns and consider multiple inputs [213, 222]. Investigators provided little to no details regarding sorting method which makes a comparison of results a challenge.

Muscle Synergy Components Normalization Methods

To facilitate the comparison of the muscle synergy components, the muscle synergy vectors and activation coefficient profile are typically normalized in some fashion [123, 136]. The most common output normalization approaches include synergy vectors by unit magnitude [123], synergy vector by maximum value [85, 88, 223], and activation coefficient profile by maximum value [83, 190]. If synergy vectors were normalized, then activation coefficient profiles were normalized by the inverse of the normalization synergy vector, so their products remain the same and vice versa [92-95].

Banks et al. [123] studied the effect of different synergies output normalization to differentiate between responder and non-responder post-stroke patients with intrinsic physiologic differences based on muscle synergy analysis results. They reported no significant influence on results.

Means of Comparison of Muscle Synergy Components

Similarities between subjects/population are investigated for muscle synergy vectors and activation coefficient profiles by means of coefficient of correlation [58, 82, 85, 88, 126, 185, 190, 195, 201, 209, 211, 215, 217, 221, 224], coefficient of determination [92-95, 136], cross correlation [83, 86, 91, 123, 170, 179, 218], normalized scalar product [80, 81, 202, 216], cosine similarities [109, 123, 221], SPM [92-95]. SPM is a promising statistical tool which facilitates the analysis of biomechanical variables by considering a

priori assumptions. The following section presents the SPM in more details and its advantages over the traditional/classical statistical analyses.

2.3.4 Statistical Parametric Mapping (SPM)

Biomechanical variables are often manifested as one-dimensional scalar trajectories in which they are used in either directed or non-directed null hypotheses. In case of directed hypothesis, the statistical analysis pertains to the specific biomechanical variables in particular points (e.g., 30% gait cycle) or windows (e.g., 20-30% gait cycle). Testing other time points or windows than the original *a priori* hypothesis would constitute bias because the number of tests increases the risk of incorrectly not accepting the null hypothesis. This bias is known as post hoc regional focus. That is, traditionally, in biomechanics, discrete points such as maximum value or the time that the maximum occurs is considered. However, if there is no *a priori* hypothesis, the whole trajectory needs to be considered. In case of non-directed hypothesis which pertains to the specific biomechanical variable (e.g., moments), it would be biased only to investigate one plane of motion (e.g., sagittal) thus decreasing the number of null hypotheses. Another potential bias is considering the components of the biomechanical variables as an independent component. If a *priori* hypothesis does not pertain to the individual component, it would introduce a source of bias known as inter-component covariance. Both post hoc regional focus bias and inter-component covariance bias have shown to impact the outcomes of statistical analysis if a *priori* hypothesis does not pertain to particular time point or windows and independent biomechanical component, respectively [225, 226]. Statistical parametric mapping is a vector field statistical test for continuous-level statistical analysis which mitigates both biased sources [225]. The SPM technique was first implemented in three dimensional functional Brain Images research [227] and was extended into biomechanics field [225, 226, 228]. The multi-component vector which is represented in 1D time or space uses random field theory (RFT) [225, 229] to calculate the probability that observed vector field changes resulted from chance vector field fluctuations [225]. For a detailed explanation and mathematical implementation of SPM refer to [225]. Important key statistical variables and their description were stated in Appendix A, Table A.9.

To account for inter-component covariance, SPM paired Hotelling's T^2 and Hotelling's T^2 statistics (i.e., multivariate one-dimensional (1D) SPM) are used within- and between-subject, respectively. In addition, 1D analysis of variance (ANOVA) repeated-measures (RM) and two-sample t-test (univariate 1D SPM) are implemented for the null hypothesis which pertains to independent-component (variable) analysis within- and between-subject, respectively.

In this thesis, the multivariate and univariate 1D SPM tests are considered for the null hypotheses pertains to the biomechanics and robotic control approaches, respectively.

2.3.4.1 Multivariate 1D SPM Test (Paired Hotelling's T^2)

There are different techniques that can be used in SPM. Paired Hotelling's T^2 is similar to the paired t-test, which is given by the one-sample T^2 statistics (Equation 2.1). SPM calculates the test statistic, critical t threshold, and p-values by considering vector covariance, field smoothness, and random field behavior, respectively [225, 226].

$$\text{SPM}\{T^2\} \equiv T^2(q) = J \bar{\mathbf{y}}(q)^\top \mathbf{W}(q)^{-1} \bar{\mathbf{y}}(q) \quad (2.1)$$

Where J , $\mathbf{y}(q)$ and \mathbf{W} are the number of vector fields, the mean vector field, and the $(l \times l)$ sample covariance matrix, respectively. Equation 2.2 shows pooled variance matrix.

$$\mathbf{W}(q) = \frac{1}{J-1} \left(\sum_{j=1}^J \left(\mathbf{y}_j(q) - \bar{\mathbf{y}}(q) \right) \left(\mathbf{y}_j(q) - \bar{\mathbf{y}}(q) \right)^\top \right) \quad (2.2)$$

\mathbf{W} indicates the variances within and correlations between vector components across the J responses.

2.3.4.2 Multivariate 1D SPM Test (Hotelling's T^2)

Another statistical analysis is Hotelling's T^2 which is conceptually similar to the scalar two-sample t-test, but it is equivalent to vector fields of scalar values (Equation 2.3).

$$\text{SPM}\{T^2\} \equiv T^2(q) = \frac{J_1 J_2}{J_1 + J_2} \left(\bar{\mathbf{y}}_1(q) - \bar{\mathbf{y}}_2(q) \right)^\top \mathbf{W}(q)^{-1} \left(\bar{\mathbf{y}}_1(q) - \bar{\mathbf{y}}_2(q) \right) \quad (2.3)$$

where J is the number of vector fields, $\mathbf{y}(q)$ is the mean vector field, $\Delta \mathbf{y}(q)$ is the vector field difference, \mathbf{W} is the pooled variance matrix (Equation 2.4) and subscripts "1" and "2" refers to case 1 (group 1) and case 2 (group 2), respectively [225].

$$\mathbf{W} = \frac{1}{J_1 + J_2 - 2} \left(\sum_{j=1}^{J_1} (\mathbf{y}_{1j} - \bar{\mathbf{y}}_1)(\mathbf{y}_{1j} - \bar{\mathbf{y}}_1)^\top + \sum_{j=1}^{J_2} (\mathbf{y}_{2j} - \bar{\mathbf{y}}_2)(\mathbf{y}_{2j} - \bar{\mathbf{y}}_2)^\top \right) \quad (2.4)$$

representing the variances-within and correlations-between vector components across the J responses [225]. The probability that the suprathreshold cluster (i.e., statistically significant difference) occurred by chance is calculated based on the random field behavior of the vector to maintain the error rate of $\alpha=0.05$.

2.3.4.3 Univariate 1D Test (Two-Sample t-test)

t value continuum (Equation 2.5) (t value trajectory, t value waveform or t value) is:

$$t = (\text{Mean Difference}) / (\text{Normalized Variance}) \quad (2.5)$$

case 1 > case 2 (below $t = 0$) and case 1 < case 2 (above $t = 0$) indicate a greater and lower mean difference in case 1 as compared to case 2 during the time-registered period (e.g., GC), respectively. In addition, t-values above the upper threshold (t-critical) suggest significantly greater case 2 values, and t values below the lower threshold suggest significantly greater case 1 values [92, 93, 95, 230]. For regions of the SPM (t) which fail to cross the threshold, the interpretation is the same as in all classical hypothesis tests: insufficient evidence to reject the null hypothesis. More simply, in areas which do not cross the threshold the mean difference is not large relative to the variance [225, 226].

2.4 Neuromuscular Aspects of Human Motion

2.4.1 Able-bodied Gait Biomechanics

2.4.1.1 Functional Tasks of the Gait Cycle

Task1: Weight Acceptance/Loading Response

The lower limb joint angles and muscle activation during walking can be described in reference to the functional tasks namely weighting acceptance, single limb support and limb advancement (acceleration and deceleration).

Weighting acceptance begins with the IC or heel strike. This coincides with the first double support phase in which the body weight transferred to the supporting limb. At this moment the contralateral limb is preparing for TO. In the sagittal plane, the ankle and knee begin to plantarflex (10-15°) and flex (15-20°) for shock absorption after IC, respectively. During this time, hip is in flexion (30°) and remain constant (Figure 2.6).

During the IC, the kinetic information reveals increase vertical ground reaction force (GRF) reaching 100% of body weight. Anterior-posterior reaction force reaches a peak during the LR (13% body weight). The medio-lateral ground reaction force occurs in the middle of LR which is small and highly variable (5% body weight) (Figure 2.7).

During the IC, the vertical GRF is located behind the ankle joint and in front of the knee and hip joints. The ankle dorsiflexor is caused by eccentric contraction of tibialis anterior to control the lowering of the foot and prevent from slapping, the extension of the knee is allowed by eccentric contraction of quadriceps to counteract the flexion moment and stabilize the knee, flexion is caused by a contraction of hamstrings, and the flexion of hip is caused by the contraction of rectus femoris. This would lead to ankle dorsiflexor, knee flexor and hip extensor moments at the IC (Figure 2.8 (A)) [56].

The internal ankle moment becomes plantarflexor as the vertical GRF moves anteriorly. Knee and hip moments become extensor during this time. The knee extensor muscles serve to control the amount of knee flexion (K1 - power absorption at the knee in loading). Hip extensor muscles (hamstrings) contract concentrically to extend the femur and pull the body forward over the stance leg during weighting acceptance (H1 - power generation at the hip in loading) (Figure 2.8 (B)) [118].

Task 2: Single Limb Support

Single limb support begins when the contralateral limb is in swing phase. The stance limb supports the entire body mass during foot flat and late stance and ensures the safe progression of the swinging limb.

As the shank advances over the stance foot, ankle moves into plantarflexion, and the knee and hip are in extension during mid-stance (10-30% GC). Both quadriceps and hip extensors contract concentrically (Figure 2.9). Plantarflexor muscles are activated to stabilize the knee. At this moment the body begins to move from force absorption at impact to force propulsion forward. At the end of the MS, hip extensor or flexor muscle activity is not presented (Figure 2.9) and the hip flexion moment is eliminated (Figure 2.8 (A)).

Terminal stance (30-50% GC) begins with the heel rise and ends when the contralateral touches the ground. At the start of heel rise, ankle dorsiflexion decelerates, and hip begins to extend, putting the support limb into trailing limb position.

The vertical GRF moves anteriorly and passes the ankle which leads to the contraction of plantarflexor muscles to stabilize the ankle joint and create a peak ankle plantarflexor moment of 1.5-2 Nm/Kg during the TS (Figure 2.8 (A)). The knee joint approach zero and then become flexor as the vertical GRF passes behind, through and in front of the joint (Figure 2.8 (A)). The power is positive meaning power generation in mid-stance (K2). According to Winter [118, 231], this represents 10-15% of the power generation during gait. During mid-stance to terminal stance, the vertical GRF passes through the joint and then behind the hip joint which produces relatively small moment and flexor in orientation (Figure 2.8 (A)). Power absorption is observed as the thigh begins to rotate backward and the hip flexors contract eccentrically (H2 – power absorption at the hip in stance) (Figure 2.8 (B)) [118, 231].

The changes in GRF components are as follows: vertical GRF hit the trough approximately 0.6-0.9 N/kg, the anterior-posterior GRF changes anteriorly and the medial-lateral become medial in direction during normal steady-state walking speed (Figure 2.7).

Task 3 Limb Advancement (Acceleration and Deceleration)

Limb advancement begins with PSW phase or second double support (50-60% GC) where the trailing limb is preparing the body for leg swing and provide adequate foot clearance during swing phase. The main role of the double support phase is the weight transition from the trail, supporting onto the lead, swinging limb.

During the PSW phase (50-60%), plantarflexor muscles concentrically contracting cause the foot to actively plantarflex (A2 – power burst at the ankle in SPW) and ankle joint rapidly plantarflexes to approximately 20° (Figure 2.6). The muscles create enough push off to advance swing limb, causes the flexion in the knee (35-40°), and providing adequate foot clearance in swing phase. The vertical GRF passes behind the knee and hip joints create small knee extensor to decelerate the backward swinging

leg and foot (K3 – power burst at the knee in PSW) and hip flexor moments to pull the leading limb forward (H3 – power generation at the hip in PSW), respectively (Figure 2.8 (A) and (B)) [96, 231].

During the ISW phase (60-73%), due to the increase in knee and hip flexion, the foot is lifted off the ground. The low level of plantarflexor activity remains during the swing to provide adequate knee flexion which co-contracts against the rectus femoris and vasti during this time. Ankle changes from 20° plantarflex to dorsiflex position due to the contraction of tibialis anterior. Because of the absence of vertical GRF and negligible inertial properties of the foot, the ankle moment is reduced. To avoid trips and ensure the foot clearance, the peak knee flexion of 50-60° (Figure 2.6) is required which is allowed by the concentric contraction of the hamstrings (Figure 2.9). The hip first extends to 10° and then flexes to 20° (Figure 2.6) due to concentric contraction of the hip flexors (iliopsoas) (Figure 2.9).

During the MSW phase (73-87% GC), the swinging limb is parallel to the stance limb until it is forward and the shank is vertical. Ankle dorsiflexor muscles contract to ensure foot clearance as the stance limb is in single support phase. The knee flexes to 60° but then extends approximately 30° (Figure 2.6) because of the sartorius muscle contraction. The hip flexes to 30° (Figure 2.6) by contraction of hip adductors [232, 233].

During the TSW phase (87-100% GC), the deceleration of the limb occurs in order to control the foot during the IC. The ankle angle approaches neutral position through the TSW (Figure 2.6). The foot is prepared for IC by the pretibial muscle concentrically contracting during this time (Figure 2.9). The quadriceps contract concentrically to extend the knee (Figure 2.9), while hip flexion of 25-30° remains constant (Figure 2.6). The hamstring muscles act as mainly as a knee flexor to decelerate the limb (K4 – power absorption at the knee in TSW) (Figure 2.8 (B)). The quadriceps and hamstrings concentrically co-contract to position the femur for IC.

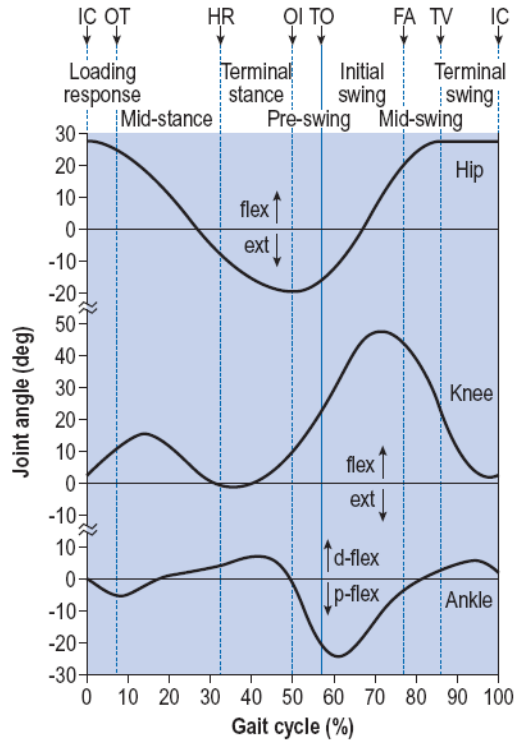


Figure 2.6: Lower limb joint angles for the hip, knee, and ankle during normal steady-state walking in the sagittal plane (adapted from [104]).

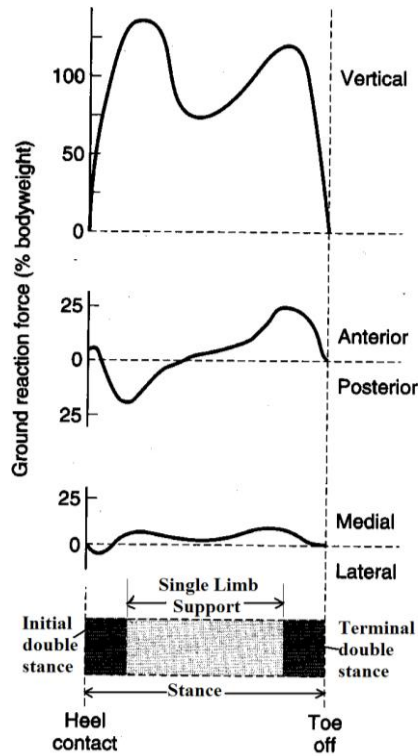


Figure 2.7: GRF components during the stance phase of steady-state walking (adapted from [234]).

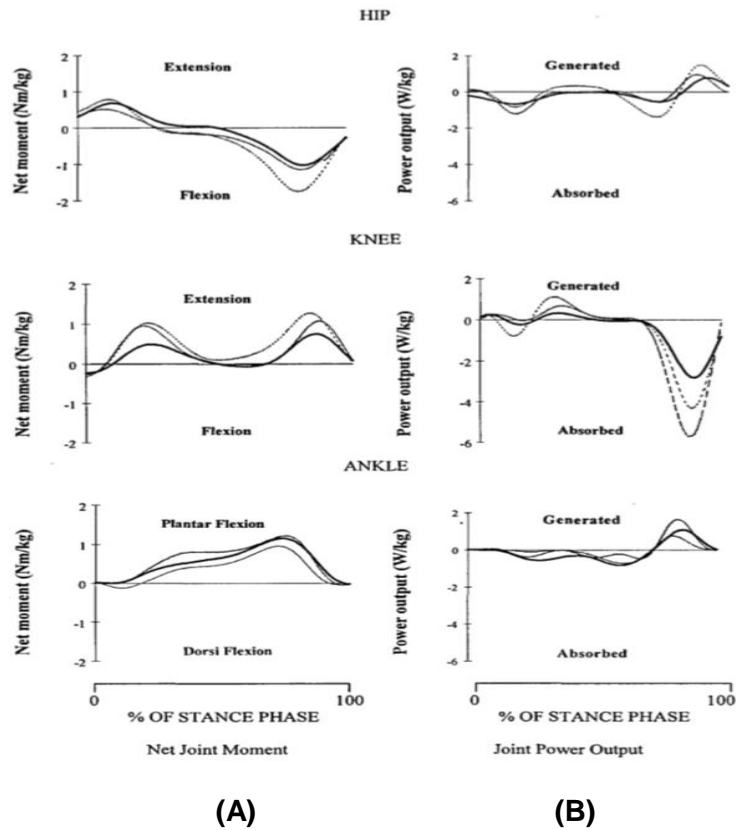


Figure 2.8: (A) Average joint moments and (B) average joint powers for hip, knee, and ankle of able-bodied, transfemoral and transtibial intact limb during stance phase when walking at normal steady-state speed. Bold line, dashed line and the thin dashed line indicates able-bodied, transfemoral and transtibial IL, respectively (adapted from [235]).

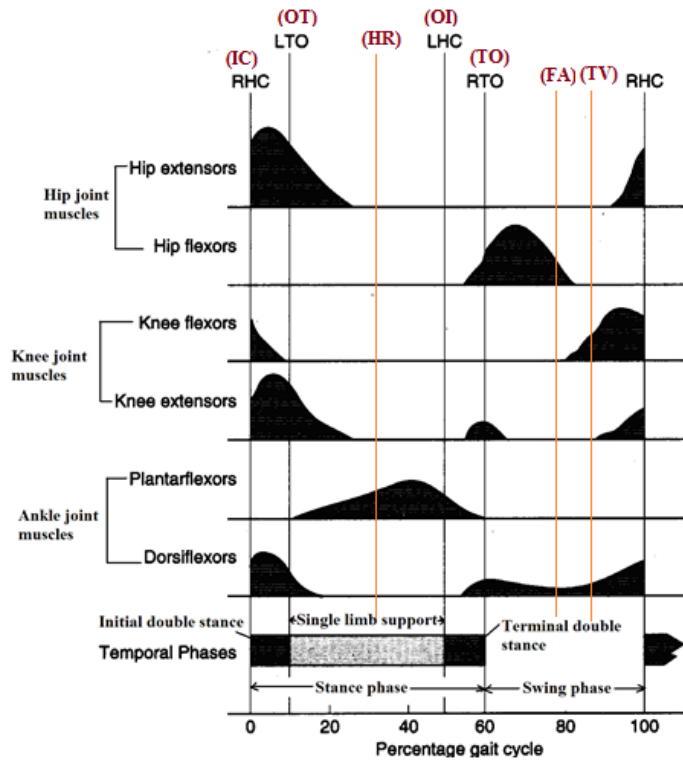


Figure 2.9: Lower limb major muscle group activities during normal steady-state walking (adapted from [100]).

2.4.1.2 Gait Initiation and Transient-State Walking in HS

Gait initiation is a complex process which involves the neuromusculoskeletal systems to control the body against a perturbed situation [52, 66, 68, 117]. Several studies reported falls in people with a poor scores in clinical tests [53, 54] and people with limb loss [55-57], particularly when changing states (i.e., a transfer from standing to walking and transient-state) [58, 59]. In previous studies, gait initiation was examined in HS in terms of kinematics and kinetics [52, 60-68].

Studies on muscle activation of the HS showed a contraction of the RF, BFLH, and GMED in upright standing position prior to movement initiation [52, 64]. After gait initiation, GL and TA are contracted. However, BFLH and GMED are relaxed. To lift the leading limb TA and RF become activated, but BFLH and GMED stay relaxed. The GMED of trailing limb deactivated and TA of the leading limb activated while RF and GMED of the leading limb activated. The leading limb knee flexion at the heel off is caused by the contraction of RF and TA and deactivation of the GL and BFLH. The activation of TA and the deactivation of RF continued during swing phase. At the terminal swing, the BFLH was activated to prepare the leg for the IC. TA continued to be activated until the mid-stance during the next gait cycle after gait initiation. While activation of BFLH and GL during the trailing limb heel off cause the extension of the knee and propelling the body forward, the GMED of the trailing limb deactivated and RF of the leading limb activated prior to the IC of the leading limb. RF and BFLH of leading limb stay contracted until the TO of the trailing limb.

It has been reported that TA and GL activities are in opposite phase from each other during gait initiation [52, 64]. Two studies reported contradictory results regarding activation of TA in response to increased walking speeds from upright standing which one stated increased activation [62] and the other no change in activation [52].

2.4.1.3 Muscle Activity in HS during steady-state walking

It has been shown in the literature than steady-state walking can be achieved after three to five steps [52, 54, 60, 62]. Muscle activities have shown to be more consistent during steady-state walking as compared to the gait-initiation and transient-state [28, 52, 109].

The movement of each joint is the result of a group of muscles activation and contribution to the different phases of the GC. Perry [9] and winter [96] investigated the muscle activation patterns of the HS during steady-state walking. The following paragraph is the summary of major muscle groups activation and the epochs where the major and minor peaks occur (Figure 2.9).

Ankle dorsiflexors (TA and hallicus longus) activity begins at the end of swing phase and continues into weight acceptance, peaking at (~5% GC). The second burst occurs at around TO (Figure 2.9). Ankle plantarflexors (triceps surae) activity commences after weight acceptance phase and rises during stance reaching a peak at TS (~45% GC) (Figure 2.9). Knee extensors (quadriceps) major activity begins at terminal swing when tibia vertical (TV) event occurs (~90% GC) and continues into weight acceptance phase, peaking at ~10% GC. The second minor activity occurs prior to the TO (~60) (Figure 2.9) [96]. The knee flexors (hamstrings) muscle group is primarily active in the latter half of the swing phase peaking at ~95% GC. However, BFLH major activity occurs at ~4% GC (Figure 2.9) [96]. In some cases, the second minor activity occurs during ISW peaking at ~70% GC. The hip extensor (gluteus muscles) activity starts in the late swing and continues into weight acceptance where the major peak occurs at ~10%. The second minor burst occurs in ISW in some individuals (Figure 2.9) [96]. The hip flexors (Iliopsoas and RF) major activity commences during ISW (Figure 2.9).

2.4.1.4 Muscle Activity in HS with Increased Walking Speeds

The ability to modulate muscle recruitment at different speeds and grades is an essential part of the human motor control. In general, muscle activity in the able-bodied has shown a similar pattern, and duration, however, with heightened amplitude in response to increasing steady-state walking speeds [125, 236-240]. In addition, the contribution of muscles for achieving walking subtasks is dependent on the walking speed.

The triceps surae was activated during the late stance and increased in amplitude with changes in walking speeds [236, 241]. However, ankle plantarflexor showed to be insensitive to increased speed during the weighting acceptance of the GC. It has been shown that the mechanical work of GM and SOL, contributed toward forward propulsion during the PSW, and is larger than all the other muscles work together [242].

TA activity was reported to be insensitive to the increase walking speeds during the early swing (first burst) however; the activity was heightened during the early stance (second burst) [236]. While the first burst contributed to foot clearance, the second burst represented an anticipatory response to the loading during the IC which increased in amplitude with respect to the change of speeds [236]. Den Otter et al. [236] reported the epoch where the second burst occurred was disappeared at slower speeds.

Non-linear change of muscle activities is observed with increased walking speeds in previous studies [125, 236, 243, 244]. An additional BFLH activity was found during the late stance to ISW at a very slow speed (0.28 ms^{-1}) which may be related to the external rotation of the lower leg [236, 243, 244]. The peak burst of gluteus medius has

shown to increase in amplitude during MS to TS at slow walking speeds as compared to the fast walking speeds [125]. Additionally, at extremely slow walking speeds, the peak amplitude of hip extensor muscle activity is heightened during the MS as compared to the normal speeds [236]. This suggests, the large contribution of the muscle activity in single-leg support phase at slow walking speeds.

The RF activity has been reported in prior research to increase during the PSW to ISW as it contributes to advancing the leg forward and decelerating the shank during the ISW. An extra epoch of RF activity was observed during the TSW at very slow speed ($<0.28 \text{ ms}^{-1}$) walking which provides hip flexion to forward the leg [9, 236, 243-245].

Murray et al. [125] showed the highest variability in hip abductor amplitude between able-bodied with respect to the change of speeds. This was evident during slow walking in which high variability was observed in side to side displacement of the pelvis. In addition, walking speed influences the peak activation timing. For example, gastrocnemius activity occurred earlier during the propulsion phase at fast walking speeds as compared to the slow walking speeds. Therefore, the neuromuscular activation changes non-linearly in response to the increase and decrease speeds [109].

2.4.1.5 Muscle Synergy in HS

Several authors reported muscle synergies in normal steady-state walking, walking at different speeds, backward walking, perturbed walking, inclined locomotion, running and sidestepping, the transition from walking to running and vice-versa [82-87]. These studies found the number of muscle synergy groups during walking is between 4 and 6.

Although systematic correlations have been shown between the timing of the activation coefficient profiles and occurrence of specific biomechanical events of the locomotion tasks [170, 185], the specific modulation of muscle synergy components may vary across gait cycles. This variability accounts for the observed variability in high dimensional EMG patterns from cycle to cycle [246].

The activation coefficient profiles of neonate have been shown to share similarities to the pattern of adults' temporal component muscle synergies (no. 2 and no. 4) however, longer in duration. In adults, no. 2 contributed to the body support during the stance phase and no. 4 acted to propel the body forward during swing phase. In the neonate, no particular activation was found during touch-down and lift-off. In toddlers (around 1-year-old), in addition to the two activation coefficient profiles similar to the neonate, two new profiles were found which contributed to the touch-down (no. 1) and lift-off (no. 3). These events contributed to the deceleration and acceleration of the body which is similar to the adults' profile no.1 and no.3. In preschoolers (2–4years), the four profiles illustrated transitional patterns, intermediate average peak timing between

toddlers and adults. The older child's profile became closer to the adult suggesting the continuous development of the modular motor control (Appendix A, Figure A.1).

Neptune et al. [77] showed five muscle activation modules was sufficient to generate forward dynamics simulation of gait and their associations with biomechanical subtasks of walking. They reported, knee and hip extensors contribute to body support in early stance while acting to decelerate forward motion (Module 1), plantarflexors contribute to loading and propulsion in late stance (Module 2), dorsiflexor and hip flexor contribute to foot lift-off and deceleration of the leg in early and late swing as well as trunk stabilization throughout swing phase (Module 3), knee flexors decelerates leg in late swing (Module 4) and hip flexors contribute to acceleration of the leg forward in pre- and early swing (Module 5).

Gui et al. [218]. investigated the relationship of muscle synergies and biomechanical subtasks in response to increasing walking speeds. They concluded the muscle synergies are shared as walking speed changes. Furthermore, the four muscle synergies and biomechanical subtasks stay invariant with increased walking speeds.

Clark et al. found the complexity and variability of muscle activity could be accounted for by four activation coefficient profiles during steady-state walking with various speeds.

Haigo et al. [221] studied the muscle synergies in gait transition from walking to running and vice versa. At the spontaneous walk to run transition, the peak activation coefficient profiles phases, mainly related to the activation of triceps surae, were shifted to an earlier phase. The gradual shift in activation coefficient profile may associate with the afferent information whereas the voluntary gait transition can be regulated by modulating only the descending neural input to the muscle synergies.

Monaco et al. [58] noted muscle synergy components did not seem to be considerably impacted by aging during walking despite the changes in HD muscle activation patterns.

Several studies showed that the muscle synergies are shared, and basic activation coefficient profiles held stable and consistent during steady-state walking over the wide range of speeds [83, 91, 218]. That is to say, the CNS implements the same groups of muscle synergies, proportionally increase the intensity of the activation coefficient profiles to satisfy the kinematic and kinetic demands of increased steady-state walking speed. In addition, other studies showed the shape and pattern of the four to six activation coefficient profiles have been impacted very little to changes in walking direction [247], locomotion mode [82, 83, 185, 221, 247], loading and unloading of the body [170, 248]. The similarity of the average activation coefficient profiles suggests

each temporal component is shaped with respect to the total duration of the stride so that the resulting muscle activation has a long duration at low speeds and a short duration at high speed [176].

However, some studies showed the muscle synergies dependency on locomotion mode and speed. Kibushi et al. [109] concluded the activation coefficient is flexibly controlled by the CNS in the regulation of walking speed. Yokoyama et al. [249] reported different sets of muscle synergies were extracted depending on the task and speed. Other researcher reported the timing and the weighting of the patterns might significantly differ with changes in walking direction, speed and loading and unloading of the body [170, 248].

2.4.2 Lower Limb Amputee Gait Biomechanics

2.4.2.1 Types and Prevalence of Amputation

One of the most physically and mentally devastating events that can occur to a person is limb loss. There are two types of amputations: upper extremity and lower extremity. The lower limb amputation can be above the knee (transfemoral) and below the knee (transtibial) in which surgical procedures are carried out to remove the lower limb above and below the knee joint, respectively. There are other types of amputations depending on the proximity to the joint of the body (i.e., hip disarticulation and knee disarticulation) as shown in Figure 2.10.

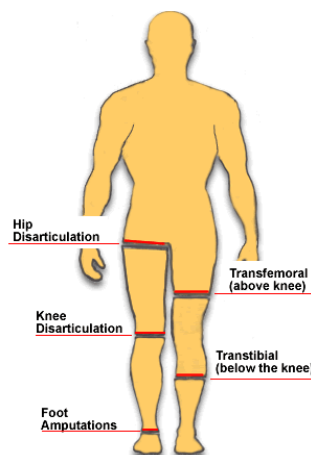


Figure 2.10: Different level of amputation (adapted from [250])

The main cause of limb amputation is a loss of blood supply to a limb. This is the most common reason for lower limb amputation which can be due to vascular diseases, chronic kidney diseases, diabetes and cerebrovascular diseases (approximately 70%) [1]. The second main cause of amputation is associated with the war injuries. In the UK, war injuries had left 41,000 and 9,000 major limb injuries in World War I and World War II, respectively [2]. Other wars such as the Korean, Afghanistan and Iraq War also added

to the amputees' population. More recently, in spite of several military's preventive programs, Iraq war had led to approximately 3500 traumatic amputations due to landmine and shrapnel injuries [2]. The third main cause of amputation is due to motor vehicle and road accidents.

There are more than 32 million amputees all around the world in which 75% are for lower limb, and 17% are bilateral amputees [3, 4].

In the United Kingdom (UK), approximately 34,109 lower limb amputations were performed in 151 hospitals from 2007 to 2010 [5]. According to the UK National Amputee Statistical Database (NASDAB), the number of referrals for lower limb amputees was considerably higher, approximately 92% of all referred amputees, than upper limb amputees between April 2006 and March 2007. Among these amputees, 70% were reported due to dysvascular disease and approximately 33% comprised of amputees who had diabetes. More than 50% of referrals were above 65 years, with 75 years and over accounting for more than a quarter of all referrals. Based on the Information Services Division NHS Scotland 2009, the two most common type of amputations were transtibial and transfemoral, which accounted for 53% and 39% of all referrals, respectively. It is worth mentioning that these statistics do not include other organizations such as primary care trusts intermediate care services, social services and private providers [251]. In addition, it was reported that during the period of 2007-2010, approximately 34,109 persons underwent lower limb amputations in 151 hospitals in the UK [5].

In the United States (US), the total number of amputees was approximately 1.9 million in 2012. The number of upper and lower amputations is estimated to be 185,000 persons each year. By 2030, it is expected that the new lower limb amputation will increase to 58,000 annually. Additionally, It is estimated that this number will double by 2050 and reach a total of 3.6 million [6]. In the US, the etiology of limb loss in lower extremities is due to dysvascular disease, including diabetes (54%), trauma (45%) and cancer (less than 2%). Elderly patients are most prone to dysvascular disease-related amputation whereas younger people are more at risk of trauma-related amputations [252]. From the above statistics, one could conclude amputation is a major public health issue.

2.4.2.2 Walking Speed in Lower Limb Amputees

Unilateral amputees would adopt asymmetrical gait patterns due to the missing functionality of the prosthetic limb. It has been shown in TFA IL that double support and stance phase is longer and swing phase is shorter than those of HS (Figure 2.11). TTA shorter stance phase and longer steps of PL have been observed as compared to the

HS [253, 254]. Previous studies reported slower walking speeds in transtibial and transfemoral amputees than age-matched normal subjects [37, 235, 255-257]. Kelly et al. [258] suggested the increase in transtibial amputees' intact leg pain with increased walking velocities could be due to the significant loading on the intact limb at higher speed. The loading asymmetry increases and temporal asymmetry decreases as walking speed increased in amputees.

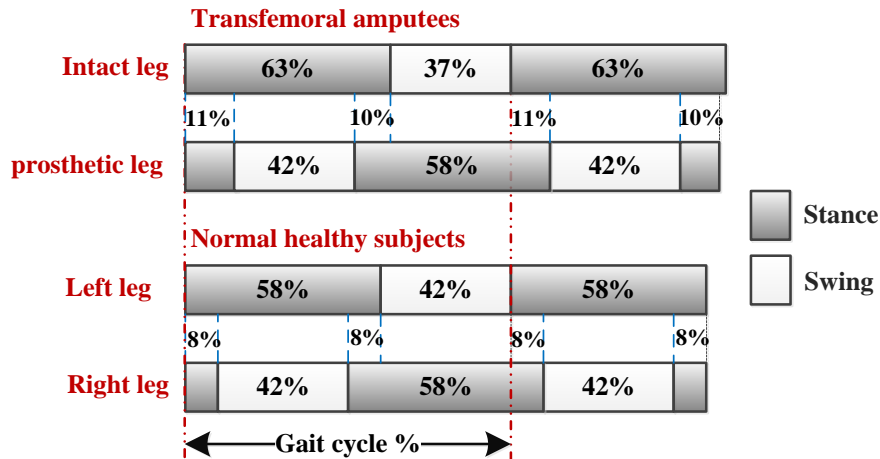


Figure 2.11: Distribution of the phases in the GC for HS and TFA; stance (grey) and swing (white) (adapted from [255])

2.4.2.3 Kinematic, Kinetic and Power Studies in Lower Limb Amputees

The kinematic differences are evident in lower limb amputees. The largest difference is observed at the PL ankle in late stance due to the lack of active plantarflexor to advance the body forward as compared to the IL and able-bodied [254]. It was reported that ankle plantarflexors generate over 80% of the power during normal gait [231]. Lack of knee flexion/extension is one of the other major differences between TFA and HS (K1 and K2) during the stance phase as shown in (Figure 2.12 (B)). Since amputees cannot resist the knee flexion by generating an adequate extension moment at the knee, knee flexion is frequently restricted by the prostheses in the stance phase [259]. Therefore, TFA exhibit distinctly abnormal movements and power patterns as compared to the HS. Due to the locking mechanism of the passive prosthesis during stance phase, K1 and K2 illustrate no power generation or absorption as shown in Figure 2.12 (B). The epoch where K3 occurs is significantly lagged in TFA IL as compared to the TFA PL and HS (Figure 2.12 (A) and (B)). Significantly larger concentric hip power is generated by the hip joint of the TFA IL in H1 than the HS and TFA PL. More noticeable differences are shown at the TFA PL in H2 (negative work) as compared to the HS and TFA IL (Figure 2.12 (B)). This is due to the lack of knee flexion during stance phase in sub-phases K1 and K2 (Figure 2.12 (A)) therefore, significant hip power is required to pull the body over the predominantly straight leg [256]. The abrupt transition from H2 to H3 is observed in TFA PL in comparison with the HS and TFA IL (Figure 2.12 (B)). The power required to propel

the body forward at the beginning of the swing phase H3 is greater and less in PL and IL as compared to the HS, respectively. In previous studies, the TFA showed approximately three times more hip power on the amputated sidew compared to the HS [96, 117]. It has been reported that the metabolic energy expenditure is approximately 60% more than the HS in level ground walking due to asymmetric gait kinematics and absence of net power at the TFA ankle and knee [45, 260]. Consequently, TFA hip compensates for the power deficiency in passive devices by generating considerably higher hip power

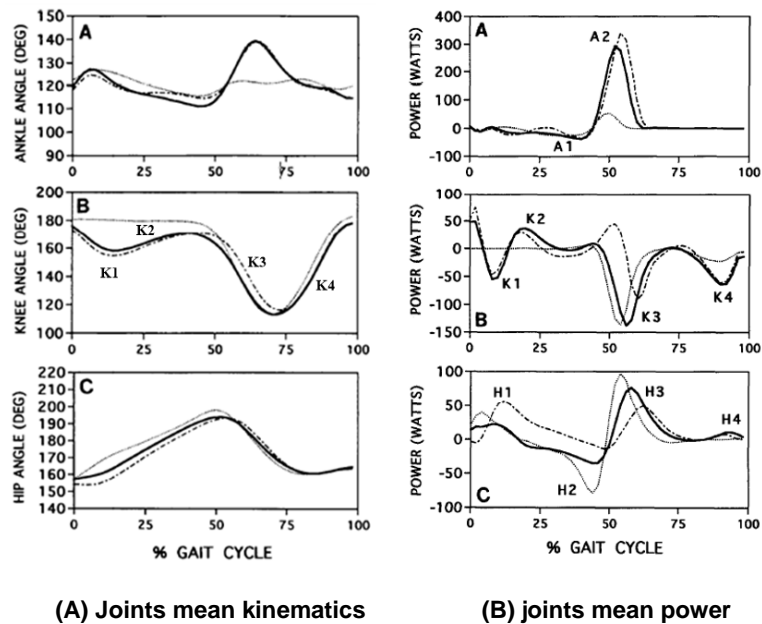


Figure 2.12: (A) joints kinematic patterns and (B) power comparison in HS and TFA. A: ankle, B: knee, and C: hip (adapted from [256]). HS (solid line), TFA IL (dotted dash) and TFA PL (dotted)

The study on the TTA IL kinematic showed less ankle plantarflexion than the able-bodied despite the healthy musculature. On the TTA PL side, the knee flexion decreased during the weighting acceptance. However, reasonable peak knee flexion was observed (60°) during the MSW and TSW [254, 261]. At the hip level, decrease in flexion during the stance phase, however, increase in flexion during the MSW and TSW were reported [254, 261]. This is the consequence of not having active dorsiflexion at the PL for foot clearance [254].

In TTA PL, the ankle and knee internal moments are significantly smaller across speeds [34, 254]. Previous literature showed the demands on the knee extensor muscles decreases considerably because of the knee moments is approximately zero, which illustrates the compensatory strategy to avoid the knee from collapsing [254, 262]. Winter reported, At the PL knee, power absorption (K1) during early stance and power generation (K2) during the terminal stance are missing in TTA PL. As a result, TTA tend to keep the thigh and shank in a more extended position to lessen the stress on the IL.

At the PL hip, decreased hip extensor moment during the weighting acceptance has been observed [34]. Power generation by the hip extensors (H1) during weighting acceptance and power generation by the hip flexor (H3) during push off occurred as a compensatory mechanism for the lack of plantarflexor muscles to propel the body forward and provide adequate foot clearance, respectively [34, 56].

Generally, the net joint moments and power in the ankle, knee, and hip of amputees' contralateral limb were increased as compared to the normal subjects to compensate for the functional loss of the one or more joints (Figure 2.8 (A) and (B)) [21, 235, 253]. It has been shown in lower limb amputees that peak dorsiflexor moment and power generation in PSW increase in the intact limb ankle (Figure 2.8 (A) and (B)). At the IL knee, the increase is observed in the power generation in stance phase and the extensor moment and power absorption in PSW. At the IL hip, extensor moment and power absorption in stance phase, and hip flexor moment and power generation in PSW are increased (Figure 2.8 (A) and (B)) [34, 235, 253].

2.4.2.4 GRF Studies in Lower Limb Amputees

Studies conducted on the GRF of unilateral amputees found higher force asymmetry (23%) as compared to the normal subjects (less than 10%) which depend on the type of prostheses being used [20, 263, 264]. Other studies found higher vertical GRF, vertical impulse and anterior/posterior on the IL than the PL for amputees [253, 265].

2.4.2.5 Gait Deficiencies in Lower Limb Amputees

One of the main purposes of the gait analysis is to identify gait deviations and the causes associated with each and thus require detailed information about the principles of locomotion, biomechanics, prosthetic fitting and alignment [105]. Gait deviations are described as a different walking pattern than in normal walking. Some factors such as individual characteristics, walking speed and age may change the normal patterns. Symmetry is the most important characteristic of normal locomotion which has been affected in individuals with amputation [105]. Poor socket fitting, prosthetic misalignment, muscle weakness, pain at the stump are the main results in gait deviation.

Common gait deficiencies and deviations in transfemoral amputees are summarized as follows [105]:

1. Lateral trunk bending: when the amputee is in stance phase, the subject tends to bend toward the amputated side as shown in Figure 2.13 (A).
2. Wide walking base (Abducted gait): step width is significantly larger than the normal range throughout the gait cycle as shown in Figure 2.13 (B). There is side to side displacement of the pelvis and trunk.

3. Circumduction: the amputee follows a wide arc movement during swing phase as shown in Figure 2.13 (C).
4. Vaulting: during swing phase, the amputee lifts the whole body by excessive plantarflexion of the IL as shown in Figure 2.13 (D).
5. Swing phase whips: heel rotates medially or laterally known as medial whip or lateral whip at and just after toe-off as shown in Figure 2.13 (E).
6. Foot rotation at HS: as the heel touches the ground; the foot rotates laterally and sometimes with vibratory motion as shown in Figure 2.13 (F).
7. Foot slap: the prosthetic foot plantarflexes quickly and just after HS, prosthetic foot strikes the ground with a slap as shown in Figure 2.13 (G).
8. Uneven heel rise: The prosthetic heel rises to a higher position than the intact heel during the initial part of swing phase as shown in Figure 2.13 (H).
9. Terminal impact: the prosthetic shank suddenly comes to a stop with visible and audible impact at the end of swing phase when the prosthetic knee has reached full extension as shown in Figure 2.13 (I).
10. Uneven step length: During consecutive periods of double limb support, the step length of prosthetic leg differs from that of IL.
11. Exaggerated lordosis: an exaggerated bending of lordosis during stance phase and the trunk may lean towards posterior side as shown in Figure 2.13 (J).

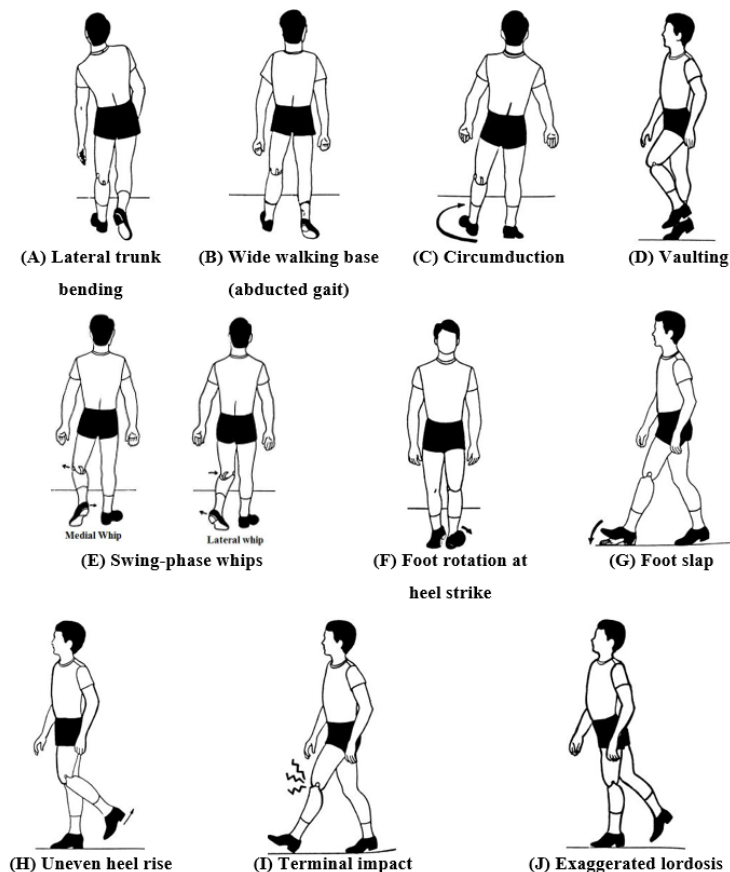


Figure 2.13 Transfemoral amputees gait deficiencies (adapted from [105]).

2.4.2.6 Consequences of Gait Deficiencies

Secondary physical conditions including osteoarthritis, osteopenia, osteoporosis and back pain could be associated with having an amputation for a long period of time. Many people had their amputation early in life and have dealt with prostheses for several years prior to the occurrence of the secondary conditions. This could be a consequence of altered gait, uneven loading and higher stress on the intact limb {Miller, 2017 #244}.

Osteoarthritis of Knee

Osteoarthritis (OA) of the knee is a common chronic joint disease which is commonly associated with pain and impaired mobility. The prevalence of OA in the US is estimated to be 12% of the population which mostly affects the elderly over the age of 60 years [266]. According to Murphy et al. [267] the lifetime risk of symptomatic knee OA is estimated to be 1 in 2 overall, more than 1 in 2 and nearly 2 in 3 for those with a history of a knee injury and for obese people, respectively. The occurrence of medial knee OA is approximately 10 times more than lateral knee OA [268]. Esposito et al. [24] reported the increase rate of Knee OA in the TFA IL is 10 times more than TTA and non-amputees. Among the TFA and TTA, the incidence rates of knee OA in veterans have been reported to be 63% and 41%, respectively as compared to the civilians which reported to be 41% and 39%, respectively [269]. Norvell et al. [270] reported both TFA and TTA higher incidence of developing knee OA as compared to the normal subjects.

2.4.2.7 Changes of EMG in Transfemoral Amputees

Generally, increased and longer muscle activity duration was observed in TFA normal walking than able-bodied individuals [37, 39, 46]. Previous studies carried out on the TFA showed the prolonged duration of the hip muscles and a similar sequence of activity in the IL as compared to the normal subjects [37]. The once bi-articulated hip muscles showed differences in phasic activity to those of able-bodied due to the morphology of the resected muscles, prosthesis types and properties and asymmetry in the walking pattern [37, 255].

Wentink et al. [36] reported longer muscle activity duration of triceps surae of the IL, as a compensatory mechanism for the loss of muscles in the PL, to generate larger push off at the TO and to advance the body forward.

Bae et al. [46] found that the hamstrings and quadriceps muscle activity and co-activity of TFA IL were larger compared to the control during steady-state of gait. the co-contraction of the knee muscles in the IL was higher than those of the healthy subjects. They also reported TA and triceps surae activities of TFA IL were significantly greater than the able-bodied.

2.4.2.8 Changes of EMG in Transtibial Amputees

In general, the magnitude of muscle activity heightened with increased speeds because of the required muscle force to propel the body forward [236]. Larger activity was observed in RF, VAS, and BFLH of the PL from ES to MS as compared to the IL as walking speed increased.

Previous research reported that the TTA PL uni-articular knee extensors, bi-articular hamstrings, and gluteus maximus activity increased in magnitude and duration as compared to the IL [26, 28, 30-34].

Power et al. [263] showed the heightened activity of the VL in the PL as compared to the IL during normal walking. Fey et al. [28] reported increased VL activity in the PL at slower walking speed to provide stability and body support in weight-bearing phase as a compensatory adjustment for the lack of ankle plantarflexor muscles.

GMED activity in the IL showed no changes as speed increased during walking. This agrees with the primary role of the GMED which is providing body support [28].

Some studies have shown the co-contraction of the quadriceps and hamstrings in early stance for TTA PL to compensate for the loss of plantar flexor which is indicative of decreased stability [32, 34, 261]. Several studies reported hypertrophy on the IL and muscle asymmetry with atrophy on the PL depending on the level of amputation [37, 253, 255, 261].

2.4.2.9 Muscle Synergy in Pathological Population

There have been studies focusing on pathological populations which show the number of muscle synergy groups was lower in people with Parkinson disease, cerebral palsy, stroke and spinal cord injuries than the normal subjects [88-91, 211, 212, 271], suggesting a lower complexity in motor control. Clark et al. [91] showed two of the muscle synergies in healthy subjects might be merged in post-stroke patients during steady-state walking. This merging of muscle synergies was observed in incomplete spinal cord injury [212], Parkinson's diseases [88], the upper extremity [271] and lower extremity of stroke patients [211]. However, two studies have found no difference in the number of modules between healthy subjects and post-stroke patients [179, 208]. The contradiction in the results of these studies could be due to the methodology analysis, number and choice of muscles included, locomotion performed, chronicity of pathology, and heterogeneity of deficits inherently present following stroke.

2.4.2.10 Muscle Synergy in Lower Limb Amputees

In previous works, muscle synergy analysis was implemented to investigate motor modules of one elderly TTA during steady-state walking [93], ramp ascending (RA) [92]

and ramp descending (RD) [94] as well as one highly active transfemoral amputee during steady-state walking [95]. The same number of muscle synergies were found between the lower limb amputees and HS, indicating analogous complexity implemented by the CNS which does not depend on the level of amputation. In addition, these studies found activation coefficient was significantly different at some regions of the GC by means of statistical parametric mapping [92-95]. However, two main limitations of these studies were the sample size, and they only account for the self-selected steady-state walking.

2.5 Lower Limb Prostheses

The use of prosthetic devices after amputation is one of the rehabilitation interventions to improve the amputees' quality of life. To be able to perform ADLs, above knee amputees require an artificial knee and below knee amputees require an artificial ankle. Several researchers categorized the prosthetic knee technology into assistance and complexity based organizations. Assistance based organization provide the assistance during stance and swing phase of walking which has been described comprehensively in [272]. The focus of complexity based organization is on the control design of prostheses. The transfemoral prosthesis comprises four main functional components: 1) foot-ankle assembly 2) knee assembly 3) socket 4) suspension (Figure 2.14). Additionally, there are two structural elements: an ankle pylon which connects foot-ankle to the knee and a thigh link connection piece which is located between the knee and the socket. In current practice, there are two types of construction endoskeletal and exoskeletal.

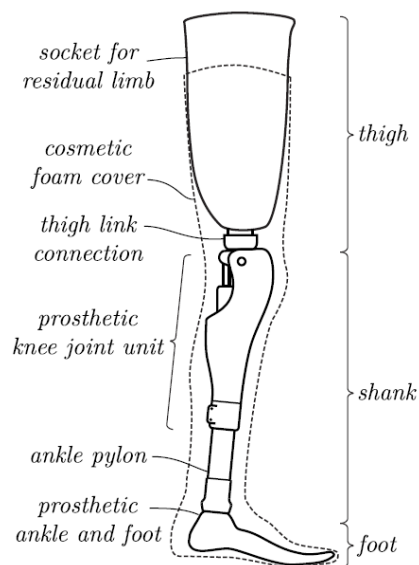


Figure 2.14: Components of the transfemoral prosthesis (adapted from [105])

2.5.1 Knee Assembly

The knee assembly consists of an extension stop, a friction device and a knee bolt which rotates around a knee shaft which each responsible for allowing the knee to bend, stopping the knee from hyperextension, and enhancing swing control, respectively. In designing a knee assembly, there are some characteristics that must be taken into consideration. These include durability, quiet functioning, acceptable cosmetic appearance during weight bearing and non-weight bearing activities and not cause excessive wear of clothing. The knee assembly is frequently made up of wood, plastic or metal. Other materials such as carbon fiber, aluminum, titanium can be used to reduce the weight. Knee units are comprised of four characteristics as follows [273]; 1) Axis-single or polycentric 2) Friction- mechanical, hydraulic or pneumatic 3) Extension aid-internal or external 4) Braking and/or locking mechanism

The modern era of advanced prostheses began by the two world wars. These prostheses were made from scrap materials. One of these prostheses was classic Long John Silver peg leg which required the patient to kneel in the prostheses.

To substitute the peg leg for more functional and natural designs, the constant friction and the friction brake design were initially introduced which had some distinct characteristics. According to [274] after World War I, the commercially available prostheses were introduced with Otto Bock house; Prostheses as the 3R22 and the 3R15. Even though these prostheses were significantly enhanced compared to the ones before the war, they had major drawbacks such as difficulty to walk at different speeds and operate in uneven terrain.

Subsequently, the new concept was developed by Hans Mauch to operate the prosthesis through fluid-control. The advent of fluid actuator prosthesis showed promise for providing users with more secure and stable gait cycle. This is due to the high resistive torque and the intrinsic property of the fluid which allows the prosthesis to extend before initial contact; producing a better harmonic cadence compared to previous designs [275]. By 1970, the development in electronics opened new horizons regarding enhancement of prostheses towards intelligent prostheses in which the first attempt was implementing power generation [276]. However, these approaches were experimental trials and this technology become only commercially available in the past few years [277]. Two major areas were under investigation since the advancement of electronics. The first one is the research done on technical assessment of prosthesis performance and the second one is the studies on control systems implemented in the intelligent prosthesis. The subsequent sections are descriptions of the three types of lower limb prostheses which can be categorized into three main categories 1) purely passive (mechanical),

energetically passive (actively controlled), and actively driven (powered) knee prostheses.

2.5.2 Mechanically Passive Prostheses

Many different types of the prosthetic knee are available which either works with simple mechanical joints or computer controlled joints. Mechanical joints have been used in the most basic passive prostheses. The two mechanically passive knees can be categorized into single-axis (Otto Bock 3R22, 3R49, 3R15 shown in Appendix A, Figure A.2 (A), (B) and (C), respectively) and multi-axis (3R66 shown in Appendix A, Figure A.2 (D)). The one degrees of freedom prostheses were reliable, low cost, and lightweight as compared to the other prosthetic knees. However, due to the lack of stance phase control, these types of prostheses require the user to exert more hip extension torque from the PL and the IL to avoid buckling [275]. To provide full extension and limit the swinging speed, friction pad (dry friction or viscous damping) is added to these prosthetic devices.

The polycentric knee has four or five bar linkage system in sagittal plane which provides multi-axial movement. They showed superior stability, compared to the single-axis, due to the ability to change the instantaneous center of rotation based on the knee flexion/extension angle [278, 279].

The Ottobock 3R15 (Appendix A, Figure A.2 (C)) is an example of weight activated knee with the constant friction property. While it would provide better stability during the stance phase, it is inefficient during the swing phase [280]. The Otto Bock 3R66 (Appendix A, Figure A.2 (D)) is a multiple axis knee prosthesis which provides stability during stance phase by kinetically locking mechanism.

Both single-axis and polycentric knees use the locking system and passive hydraulic or pneumatic cylinders to keep the mechanically passive devices stable and to prevent from buckling during stance. Mechanically passive knees stability is either can be manually or weight-activated mechanism [281]. Manual locking knees are locked and unlocked during the stance phase and swing phase, respectively. They are frequently used in the patients with muscle weakness and instability issue to prevent buckling in the knee extension during stance and to provide stability. In weight-activated stance control knee, during the stance phase, the amputee's body weight is transferred to the prosthesis, which due to the high friction the knee will not bend [281]. In swing phase, constant friction is applied to the knee's axis. Constant friction would lead to inefficient gait in swing phase when the user changes the walking speed. Therefore, the use of hydraulic and pneumatic mechanism helped to provide variable resistance at different walking speeds. It has been shown that amputees walk more comfortably at different speeds [281]. Example of single-axis (Appendix A, Figure A.3 (A)) and multi-axis

prosthetic (Appendix A, Figure A.3 (B)) devices which operate with fluid and provide resistance to the knee. As the speed increases by the user, the resistance about the axis of the knee increases. The term fluid is used because liquids vapor and gases are the main elements that comprise the fluid-control knees. Hydraulic fluid prosthetic knees are not compressible. To control the flow of fluid through ports, oil and air both are forced through a tube which adjustment screw permit alteration in the orifice size. This allows a good performance of knee resistance during swing phase.

On the other hand, pneumatic knees compress air during knee flexion and use the compressed air within the pneumatic cylinder for extension support. The air provides the pneumatic knees a springier feel to the users [273].

2.5.3 Microprocessor Knee

The intelligent prostheses or known as microprocessor controlled has a microprocessor which controls the response of actuators. Microprocessor knees consist of sensors which detect the conditions around the joint and make internal adjustment accordingly. The adjustment is made when sensors convey the information (e.g., joint angle and forces) to the microprocessor. Opening and closing of valves vary the resistance of the knee by increasing and decreasing the fluid/magnetorheolic flow through the knee's internal port. The superiority of the microprocessor compared to mechanically passive knees is the fast response of microprocessor to the tasks performed by the users regardless of tasks complexity [282]. These prostheses are programmable (Appendix A, Figure A.4). Therefore, the stability and safety can vary by altering the program. One of the most important features of these prostheses is the ability to recover stumble.

2.5.4 Motorised Knee/Power Knee

Power knee is the first commercially available active prosthesis designed for transfemoral amputees in 2007 (Appendix A, Figure A.5 (A)) ([275]. This prosthesis consists of a motorized knee which provides extension and flexion for the users; this is an added technology on microprocessor knees. Some complex tasks (e.g., stair ascent/descent or walking backward) that cause energy to dissipate in joint become easier to perform by patients as the motorized knee generates net power which mimics the function of lost muscle [275]. The working mechanism of these devices is as the sensors are placed in the IL to measure motion, load, and position which then data obtained is transmitted to the knee via Bluetooth technology. In order to determine the power or force required from the knee, the microprocessor analyses the transmitted information to produce adequate knee flexion or extension [273]. This prosthesis is large and heavy weighted due to the motors required to replace the loss of biological musculature functions.

Ossur developed the second generation of Power Knee which is the first motor powered prosthesis for the TFA in 2010 (Appendix A, Figure A.5 (B)). This prosthetic device not only provides active motion and stance stability but also has the ability to perform the locomotion tasks without thinking their next movement. However, the drawbacks of Power Knee are the expensive cost (\$120,000), the heavyweight (3 times the mass of passive prosthesis), the short battery life (4 hours), being loud and not being able to be used by bilateral amputees as it uses echo control system [283].

In 2009, a new powered prosthesis was designed by Martinez-Villalpando and Hugh Herr [284] which uses a pair of series elastic actuators, proposed by Robinson et al. [285], positioned in an agonist and antagonist arrangement.

2.5.5 Semi-Active Prosthetic Devices

A novel semi-active prosthetic device (hybrid) has been developed for transfemoral amputee in 2009 (Appendix A, Figure A.6 (A)). The power source has been added to the hydraulic knee joint such that the device benefits from the state of the art microprocessor control as well as well-established mechanically passive damped system [286]. The passive mechanism work during the stance phase (IC) providing an adequate impedance to avoid buckling. During the swing phase, the impedance was reduced to provide knee flexion for adequate heel rise. The advantage of the semi-active prosthetic approach is the improved battery life thus higher number of steps can be performed than the averaged TFA take daily [287]. Another semi-active prosthetic device was designed at the University of Leeds (Appendix A, Figure A.6 (B)). This device is comprised of various sensors which provide kinematic information, using a potentiometer and inertial measurement unit (IMU), and kinetic information, using FlexiForce sensors, strain gauges, and load cells, to modulate the prosthetic device in different terrain and environment [8].

Appendix A, Table A.10 illustrates the most common commercially available prostheses.

2.5.6 Transtibial Prostheses

Foot-ankle assembly is the terminal section of all the prosthesis which replaces the anatomical foot and ankle and fulfills some of the basic requirements. The assembly should: 1) provide a base for weight bearing 2) absorb shock at heel contact and reach foot-flat position quickly 3) provide for metatarsophalangeal hyperextension late in stance phase 4) resemble the general contour of the missing foot. Additional functions such as mediolateral motion or energy storage and return are offered by other components. There are three categories of foot prosthesis including CF, ESR and bionic feet. SACH is the most commonly CF which provides “pseudo-plantar flexion” and

stability during the ES and MS, respectively [7]. This type of foot is directly attached to the shank without any articulating movements. This prosthesis is the most prescribed foot in low-income countries and is famous for their streamlined appearance at the ankle, their relative durability, lightweight, inexpensiveness, robustness and quite as compared to the articulated Foot-ankle. One of the other frequently used prosthesis is the Single-Axis foot with a sagittal joint. Similar to the SACH (Appendix A, Figure A.7 (A)), Single-Axis does not provide lateral movement during the MS. However, it is heavier, and it requires more maintenance as the bumper mechanism is prone to dirt. Since the Single-Axis feet comprised of springs which have fixed stiffness properties, they can only flex back to the neutral position from the instant TO. This is different from the healthy foot which establishes plantarflexion relative to the standing upright. One of the most advanced foot that has been commercialized is 'Proprio Foot' by Ossur (Appendix A, Figure A.7 (C)). It is a motor-powered ankle prosthesis which has several features: increases ground clearance, provide a high degree of terrains compliance, improves the stability for sloped surfaces and stairs, decreases the risk of trips and fall, improves safety and gait quality [260, 261, 288-290]. Although improved performance has been observed using the ESR prostheses (Appendix A, Figure A.7 (B)), none of them is capable of reducing gait asymmetries and energy cost of walking [7].

2.6 Control Strategies in Lower Limb Prostheses

Control approaches that have been proposed in the active TFA prostheses are categorized into the 'echo control' and 'pattern recognition' [45]. Echo control is a combination of time-based and normalized-trajectory control from different sensor modalities recorded from the IL and replayed on the PL with some time delay [291]. Pattern recognition (PR) is the most commonly used control strategy for powered prostheses. Intent and activity recognition based on pattern recognition approach to control powered prostheses has been studied using different sensor modalities [16, 292-295]. One of the sensor modalities which is a major source of biological signals in neural control is surface EMG. This signal can be detected from the muscles of lower extremities using EMG electrodes to control lower limb prostheses. EMG electrodes have been used to record muscle activities signals from amputees wearing passive prostheses [12] and powered prostheses [295]. Early application of EMG for control was mostly based on the amplitude-based threshold (onset and offset control strategy) to lock/unlock the prosthetic knee joint during some activities [11, 12]. EMG signals also have been used for direct proportional control of different joints of lower limb prosthetics including knee [13] and ankle joints [14]. Other studies investigated EMG pattern recognition to identify the user intent in different activities [15-19]. The purpose of using the EMG pattern

recognition is to control the prosthetic device in different terrains and activities smoothly, intuitively and naturally. Appendix A, Table A.11 shows more studies that have used EMG from lower limb muscles to control prostheses.

2.7 Gap of Knowledge

Neuromuscular behavior can be studied at two levels namely HD EMG/muscle activation pattern and low dimensional muscle synergy/modular motor control. Based on the previous studies discussed in this chapter, muscle coordination in terms of HD EMG and low dimensional muscle synergy have been investigated in healthy subjects during a range of ADLs using traditional statistical analysis. However, there is little information on lower limb amputees. Furthermore, not much work has been done on muscle coordination in high and low dimensions in response to increasing transient-state (the stride after gait initiation) walking speeds for both healthy subjects and transfemoral amputees. Therefore, the motivation of this research is to fill this gap of knowledge by focusing on understanding neuromuscular modularity of HS and lower limb amputees during transient-state walking at different speeds from biomechanics (considers inter-neuromuscular variable covariance) and robotic control (considers individual neuromuscular variable) perspectives. In addition, the developed muscle synergy algorithm is applied to elucidate the muscle recruitment strategies in transtibial amputee to investigate modular motor control at a different state of walking task (i.e., steady-state), accounting for intact leg and prosthetic leg and a different number of muscles.

2.8 Summary

A general overview of lower limb biomechanics including muscles and movements as well as the biomechanics terminologies in association with the gait, kinematics and kinetics were discussed. In addition, information about the different means of gait measurement devices was studied. In the second part of this chapter, the use of surface EMG in two aspects namely high dimensional EMG and muscle synergies were studied. Furthermore, the drawbacks intrinsic to surface EMG and different methodological concerns using surface EMG in muscle synergies were investigated. Comprehensive research has been conducted on some of the biomechanics variables including EMG profile and muscle synergies in healthy subjects and lower limb amputees during walking. The biomechanics aspects of amputation (e.g., gait deficiencies) and consequences of gait deficiencies (e.g., osteoarthritis) were studied. Various lower limb prostheses were studied including knee and ankle joints, focusing on the types and control strategies implemented for movement of lower limb amputees.

Chapter 3

HIGH DIMENSIONAL MUSCLE ACTIVATION PATTERNS IN TRANSFEMORAL AMPUTEES DURING TRANSIENT-STATE WALKING

3.1 Introduction

This chapter reports on the EMG recorded from muscles of healthy subjects' (HS) dominant leg and transfemoral amputees' (TFA) intact leg (IL) during transient-state walking at three different speeds (slow, normal and fast). The muscle activation patterns are obtained by calculating the linear envelope of the EMG signals for each group. The muscle activation patterns are compared within- and between-subject by means of statistical parametric mapping (SPM). This study is regarded as exploratory; thereby two approaches are taken into account, namely biomechanics, and robotic control to investigate *a priori* hypotheses. The biomechanics related hypotheses consider the inter-muscle covariance which effectively accounts for high dimensional sensorimotor modules (multi-muscle synergy) concept whereas the robotic control related hypotheses take individual muscle activations into account. A total of six hypotheses is tested to compare the effect of speed on muscle activities of HS and TFA as well as to assess the differences between groups at each speed. Therefore, the within-subject analysis is performed for each group separately across speeds, and the between-subject analysis accounted for individual speed as a different task under the walking control. Previous literature on HS and TFA predominantly focused on the individual muscle activity during steady-state walking and taking into account parts of the gait cycle (phasic activity) rather than the whole time-series for statistical analysis [36, 37, 255]. To the best of the author's knowledge, little to no details are provided regarding the differences in muscle activation patterns of HS and TFA during transient-state walking across speeds, accounting for inter-muscle covariance (biomechanics perspective), individual muscle activities (robotic control perspective) and the whole time-series.

3.2 Experimental Protocol

3.2.1 Methodology

In this study, thirteen HS (mean (SD): age 41 (14) years, weight 82.9 (11.8) kg, height 174.2 (3.1) cm) and eleven unilateral above knee male amputees (mean (SD): age 55 (8) years, weight 78 (15.3) kg, height 170.9 (7.9) cm) were involved (anthropometric characteristics of individual HS and TFA, as well as details of prosthesis used by each

one of the TFA, are presented in Appendix B, Table B.1, Table B.2 and Table B.3, respectively). The TFA subjects were recruited from the “Disabled Iranian Veterans” prosthetic clinic, a sports complex related to the “Disabled Iranian Veterans” community and the “Iranian Handicapped Society” in Tehran, Iran. All subjects were free from any orthopedic or neurological pathology. The amputee subjects were above knee amputees, and they were able to walk comfortably with their prosthesis at least for a year without the use of an additional ambulation aid. Bilateral amputees regardless of the level of amputation were excluded from the study. All TFA subjects were fitted with mechanically passive devices with the SACH foot. All subjects wore their own normal daily activity shoes. The experiment conducted in the Motion Laboratory at “Djavad Mowafaghian Research Centre of Intelligent Neuro-Rehabilitation Technologies”; the Sharif University of Technology in Tehran-Iran.

Myon wireless surface EMG (Myon AG, Schwarzenberg, Switzerland) at a sampling rate of 1200 Hz and disposable, self-adhesive Ag/AgCl dual snap electrodes with inter-electrode distance of 20 mm (Noraxon System, Inc., Scottsdale, AZ, USA) were attached to the muscles to record electrical activity during self-initiated gait at three self-selected speeds (slow, normal and fast) (Table 3.1). This system consists of a receiver which has 12 electrodes and channels connected to a computer with a visual feedback program (Vicon Nexus software). The electrodes were attached to twelve lower limb muscles of HS dominant leg and TFA IL including rectus femoris (RF), and vasti (i.e. vastus medialis (VM) and vastus lateralis (VL)), biceps femoris long head (BFLH), semitendinosus (SEM), gluteus medius (GMED), tensor fascia latae (TFL), gracilis (GR), tibialis anterior (TA) and triceps surae (i.e. gastrocnemius medialis (GM), gastrocnemius lateralis (GL), and soleus (SOL)). However, GMED and GR were eliminated because of lost (the prosthesis belt covering the gluteus muscles of the IL in six of TFA subjects and not being able to record from the deep adductor muscle). Therefore, ten muscles were chosen for data analysis in this chapter. Prior to the electrodes attachment, the skin was shaved and cleaned with an alcohol pad to reduce impedance. Surface EMG for Non-Invasive Assessment of Muscles (SENIAM) was followed to find the muscle bellies and electrodes were attached longitudinally with respect to the underlying muscle fiber direction [296].

Table 3.1: Participants’ walking speed; mean \pm standard deviation (m/s)

	Slow	Normal	Fast
HS	0.78 \pm 0.08	1.02 \pm 0.07	1.45 \pm 0.1
TFA	0.61 \pm 0.09	0.76 \pm 0.16	0.97 \pm 0.14

The subjects walked across a 7-m walkway in the laboratory with two 40cm \times 60cm and 80cm \times 60cm Kistler force platforms embedded in the floor and six

infrared cameras which were fixed on the wall in the height of 2m around a 2m×5m walking path to cover a measurement field of view approximately 1.5m×4m×2m around the force platform area. Calibration was done, so the spatial accuracy of the system was lower than 1 mm (root mean square). Calibration of the system was done for each test session separately according to Vicon protocol and guidelines. The GRF from 2 Kistler force platforms and position of markers were recorded synchronically in sampling frequency of 1200 Hz and 120 Hz respectively during each test.

The marker placement and tests protocols were same for all participants. After calibration of the movement space according to the calibration protocol of related motion analysis system; 14 mm spherical passive reflective markers were attached to the skin by using double-sided adhesive tape to define body segments. The anatomical landmarks were identified for marker placement according to Qualysis Track Manager's user manual and body modeling requirements in Visual 3D software on basis of the markers to be visible as much of the test time as possible. The anatomical landmarks were: right and left 1st and 5th metatarsal heads and bases, right and left medial and lateral calcaneus, right and left medial and lateral malleolus, right and left medial and lateral epicondyles of femurs, right and left greater trochanters, right and left iliac crests, right and left anterior superior iliac spine (ASIS), right and left posterior superior iliac spine (PSIS), right and left acromion processes, right and left coracoid processes, right and left medial and lateral epicondyles of humerus, medial and lateral of wrists for right and left upper limbs, 7th cervical spine and sternum. In addition, 4 markers in the quadrilateral arrangement were attached to shanks, femurs, arms and 3 markers with fixed positions were attached to forearms in left and right sides as tracking targets. The markers for the prosthetic side were placed in accordance with the intact side and rotational axis of the prosthetic knee. After marker placement and at the starting of each test session, the participants stood in anatomical posture in the middle of calibrated space to record a static data set.

A Minimum of three successful trials was recorded from each subject with an increased self-selected walking speed which was determined as a consequent contact of HS dominant leg and TFA IL with one of the force platforms. In addition, the trajectories from reflective markers placed on the instrumented foot (calcaneus and 1st metatarsal) were used to identify the GC. It is worth noting, the next gait cycle after gait initiation of leading or trailing limbs was considered such that the gait would still be in transient-state (Figure 2.4 C and/or D) [52, 54, 60, 109]. This was done due the nature of study however, it noteworthy that pragmatic difficulties such as space limitation did not allow recording of steady-state walking for all subjects (chapter 3 and chapter 4). Vicon software was used to display EMG signals from each subject when performing gait. The data was then extracted and exported to Excel Microsoft for further modification. MATLAB R2017

software (The Mathworks, Natick, Massachusetts) was used for data analyses. Figure 3.1 shows the electrodes and reflective markers attachment configuration on one of the TFA. Appendix B, Figure B.1 shows markers and electrode attachment on one of the HS.

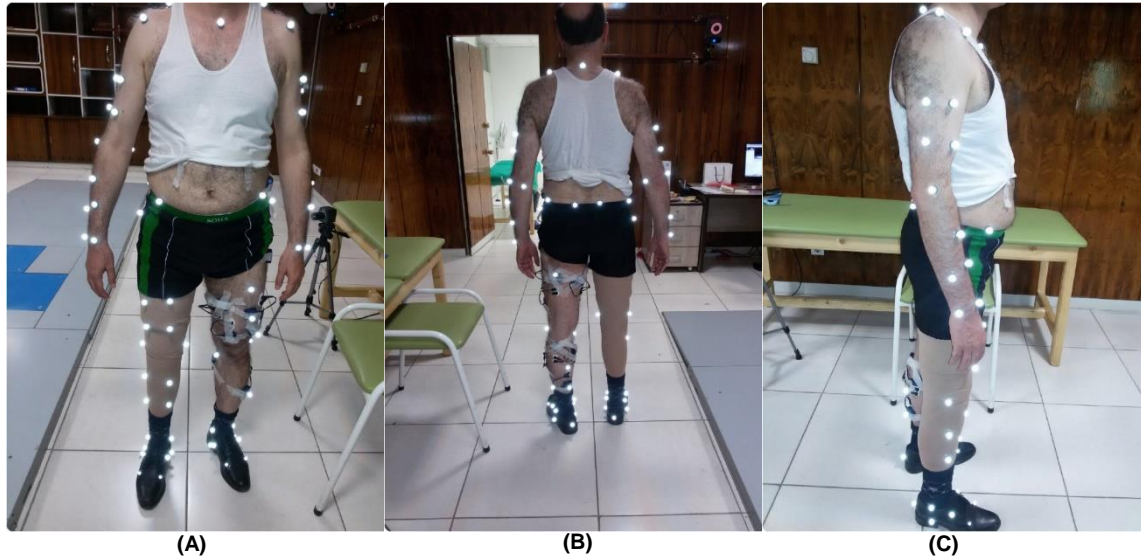


Figure 3.1: EMG attachments on TFA (A) front IL, (B) back IL, and (C) side PL.

The study carried out on thirteen HS, and eleven TFA received approval from the University of Leeds Ethical Review board and the ethics committee of “Djavad Mowafaghian Research Centre of Intelligent Neuro-Rehabilitation Technologies”; the Sharif University of Technology in Tehran-Iran. The information sheet was provided, and consent was obtained from the participants. In addition, consent for participation and the agreement to photographic and video records were signed by participants before the experiment.

3.2.2 Surface EMG Signal Processing

This section outlines the methodology used to process the EMG signals prior to the EMG comparison within- and between-subject. The author adopted the signal processing according to the SENIAM recommendation [296]. To illustrate the procedures, the data acquired from one of the HS was used as an example (Appendix B, Figure B.2). Ten muscles were recorded and processed. The analytical work was implemented in MATLAB R2013 (Mathworks, Inc, Natick, MA). In order to scale down the data, the mean of the amplitude of each muscle was subtracted from the corresponding data column. Furthermore, the raw EMG data was filtered using bandpass filter. The data was rectified and low pass filtered. Amplitude normalization was performed with respect to the highest peak obtained from the fast walking condition. By. The data were normalized to 101 points to represent a GC from 0% to 100%.

3.2.2.1 Raw Surface EMG

EMG signals can be detected by placing one or more differential electrodes on the skin of the subject. Appendix B, Figure B.2 shows the raw EMG taken from one subject's muscles. In this case, the x-axis was time normalized to 101 points using the interpolation technique. The Y-axis shows amplitude in Volts (V). The signal passes zero from both negative and positive sides. The muscle contraction causes the amplitude of the EMG signal increases whereas, during muscle relaxation, the amplitude of EMG signals decreases. The signal obtained from each muscle was separated, and similar filtering technique was applied to all the acquired signals of all subjects.

3.2.2.2 Filtration Technique

Following the EMG signal detection, filtration was applied to the EMG signals of both HS and TFA. Due to baseline drifts associated with motion (e.g., wires being pulled) and equipment noise, a high pass filter (HPF) was used. A low pass filter (LPF) was implemented to remove high frequency components due to unsteadiness of the interface between skin and electrode. According to several studies, the range of sampling rate used in EMG is 1000-2000 Hz and the commonly used cut off frequency for low, and high pass filter is approximately 450-500 Hz and 5-20 Hz, respectively [296-298]. In this study, A fourth order Butterworth with the HPF of 20 Hz, and an LPF of 500 Hz were applied (Appendix B, Figure B.2). In order to prevent phase shift after filtration, a Butterworth filter was used. This type of filtration is "infinite impulse response" filters which are applied in both the forward and backward direction to avoid phase shift [299].

3.2.2.3 Linear Envelope

The linear envelope was obtained by performing the rectification and LPF of the EMG signal. The full wave rectification was done by taking an absolute value of the signal. The rectified signal was then filtered using the 2nd order Butterworth with the cut off frequency of 6Hz to get the shape of "envelope" (Appendix B, Figure B.2). An ensemble average of each EMG was obtained from all the GCs of each subject.

3.2.3 Statistical Parametric Mapping (High Dimensional EMG)

All linear envelopes were statistically evaluated over the GC since a *priori* hypothesis pertains to the whole time-series rather than specific time points. Therefore, the scalar and qualitative analyses were not performed in this chapter.

Muscle synergies consider inter-muscle covariance, however; the hypothesis may also pertain to a specific muscle and/or application. Here, statistical analyses were selected based on a *priori* null hypotheses made before the experiment was conducted:

- 1) Non-directed null hypothesis (**biomechanics perspective**): There is no difference between muscles corresponded to each biomechanical subtask

(associated with muscle synergies) as well as muscles contribute to the ankle and knee co-contraction for both HS dominant leg and TFA IL during gait across different speeds.

- 2) Non-directed null hypothesis (**robotic control perspective**): There is no difference between individual EMG signals of HS dominant leg and TFA IL during gait across different speeds

The biomechanics hypothesis considers the inter-muscle activation covariance whereas the robotic control involves individual muscle activations comparison. The rationale behind the first hypothesis is the concept of inter-muscle co-activation [300], and multi-muscle synergy [80] implying groups of muscles contribute primarily to high dimensional sensorimotor Modules based on their temporal covariance. In addition, the high similarity was observed in the temporal EMG profiles of functionally related muscles [171, 172, 238]. Therefore, muscles were selected based on their contribution to biomechanical subtasks, which also associated with the low dimensional muscle synergies, according to the study conducted by [77]. High dimensional sensorimotor Module 1 (HD M1) consisted of knee and hip extensors muscles which contributed to body support in early stance while acting to decelerate forward motion. High dimensional sensorimotor Module 2 (HD M2) comprised plantarflexor muscles which contributed to loading and propulsion in late stance. High dimensional sensorimotor Module 3 (HD M3) comprised dorsiflexors and hip extensors which contributed to deceleration of the leg in early and late swing as well as trunk stabilization throughout swing phase. High dimensional sensorimotor Module 4 (HD M4) consisted primarily of knee flexors which contributed to deceleration of leg in late swing. In this chapter, the muscles contributing to the ankle and knee co-contraction have been considered because it is believed that the CNS implements co-contraction as a task-independent strategy to improve the stability and increase the stiffness of the joints [301-304]. Therefore, all the ankle muscles (which consisted of plantarflexors and dorsiflexor) in one group and all the knee muscles (which consisted of all knee extensors and flexors) in another group were studied to account for co-contraction of the agonist and antagonist muscles in ankle and knee, respectively.

It is worth mentioning, the null hypotheses with regards to the high dimensional Modules were formulated prior to the muscle synergy analyses. Therefore the selection of muscles was based on the literature [77] rather than the exact contribution of the muscle synergy vectors of HS and TFA in the present study (chapter 4). Table 3.2 divides the muscles into the corresponding category based on the task-specific biomechanical function and temporal relevance (HD M1-M4), and co-contraction (ankle and knee).

Table 3.2: Muscles corresponded to each HD Module which is associated with the biomechanical subtasks are considered for biomechanics hypotheses.

	HD Module 1	HD Module 2	HD Module 3	HD Module 4	Ankle Co-contraction	Knee Co-contraction
Muscles	RF, VM, VL	GM, GL, SOL	RF, TA	BFLH, SEM	TA, GM, GL, SOL,	RF, VM, VL, BFLH, SEM

With regards to the robotic control hypothesis, individual muscle activities become important in within- and between-subject comparison. This has an important application in controlling robotic devices similar to the clinical state of the art myoelectric prostheses in upper and lower limb prostheses [13, 18, 44, 113, 297, 305-309]. In this chapter, six different null hypotheses were proposed based on the biomechanics and robotic control perspectives before observing the data.

3.2.3.1 Within-Subject Hypotheses

- 1) Biomechanics null hypothesis 1: There is no effect of walking speeds on HS temporal EMG profiles of functionally related muscles contributing to biomechanical subtasks of gait as well as all muscles that contribute to the co-contraction of ankle and knee joints during gait. The following hypotheses were tested:
 - a. There is no difference in HD M1 activity of the HS across speeds.
 - b. There is no difference in HD M2 activity of the HS across speeds.
 - c. There is no difference in HD M3 activity of the HS across speeds.
 - d. There is no difference in HD M4 activity of the HS across speeds.
 - e. There is no difference in the activation of muscles contribute to the HS ankle co-contraction across speeds.
 - f. There is no difference between the activation of muscles contribute to the HS knee co-contraction across speeds.
- 2) Robotic control null hypothesis 2: There is no effect of walking speeds on HS individual muscle activities during gait.
- 3) Biomechanics null hypothesis 3: There is no effect of walking speeds on TFA temporal EMG profiles of functionally related muscles contributing to biomechanical subtasks of gait as well as all muscles that contribute to co-contraction of ankle and knee joints during gait. The following hypotheses were tested:
 - a. There is no difference in HD M1 activity of the TFA across speeds.
 - b. There is no difference in HD M2 activity of the TFA across speeds.
 - c. There is no difference in HD M3 activity of the TFA across speeds.
 - d. There is no difference in HD M4 activity of the TFA across speeds.

- e. There is no difference in the activation of muscles contribute to the TFA ankle co-contraction across speeds.
 - f. There is no difference in the activation of muscles contribute to the TFA knee co-contraction across speeds.
- 4) Robotic control null hypothesis 4: There is no effect of walking speeds on TFA individual muscle activities during gait.

3.2.3.2 Between-Subject Hypotheses

- 5) Biomechanics null hypothesis 5: There is no difference in temporal EMG profiles of functionally related muscles contributing to biomechanical-subtasks of gait as well as all muscles that contribute to co-contraction of ankle and knee joints between HS and TFA during transient-state walking at different speeds. The following hypotheses were tested for each speed separately
- a. There is no difference in HD M1 activity between the HS and TFA at each speed.
 - b. There is no difference in HD M2 activity between the HS and TFA at each speed.
 - c. There is no difference in HD M3 activity between the HS and TFA at each speed.
 - d. There is no difference in HD M4 activity between the HS and TFA at each speed.
 - e. There is no difference in activation of muscles contribute to the ankle co-contraction between HS and TFA at each speed.
 - f. There is no difference in activation of muscles contribute to the knee co-contraction between HS and TFA at each speed.
- 6) Robotic control null hypothesis 6: There is no difference in individual muscle activities between HS and TFA during walking at each speed (two-sample t-test).

To account for inter-muscle covariance (biomechanics hypotheses), SPM paired Hotelling's T^2 (hypothesis 1 (a-f) and 3 (a-f)) and Hotelling's T^2 (hypothesis 5 (a-f)) statistics were used within- and between-subject, respectively. Furthermore, a pairwise comparison was made using a Bonferroni correction to correct for the alpha, due to the limited multivariate ANOVA (MANOVA) functionality in the SPM, within each population between speeds to test the biomechanics null hypotheses, i.e., HS (Normal vs Slow), HS (Fast vs Normal) and HS (Fast vs Slow). A similar approach was followed for the TFA. The muscles were analyzed in HD Modules contribute to biomechanical subtask as well as contribute to the ankle and knee co-contraction. Therefore,

For HD M1, 3-component vector-field $I = 3$ (number of muscle), $J = 24$ (total number of subjects HS and TFA), $Q = 100$ (time normalized) (i.e. HS HD M1 = [13x100x3] and TFA HD M1 = [11x100x3] at each speed).

For HD M2, HS HD M2 = [13x100x3] and TFA HD M2 = [11x100x3] at each speed.

For HD M3, HS HD M3 = [13x100x2] and TFA HD M3 = [11x100x2] at each speed.

For HD M4, HS HD M4 = [13x100x4] and TFA HD M4 = [11x100x4] at each speed.

For ankle muscles, HS ankle = [13x100x4] and TFA ankle = [11x100x4] at each speed.

For knee muscles, HS knee = [13x100x5] and TFA knee = [11x100x5] at each speed.

Hotelling's T^2 is conceptually similar to the scalar two-sample t-test, but it is equivalent to vector fields of scalar values [225]. The comparison was made between two populations with the same speed category (hypothesis 5), i.e., HS slow Vs. TFA slow; HS normal Vs. TFA normal and HS fast Vs. TFA fast rather than matching group's similar speed (i.e., HS slow vs TFA normal or HS normal vs TFA fast). The EMG signals were analyzed as an I , J and Q stated in paired Hotelling's T^2 . For the robotic control hypotheses, SPM RM ANOVA (hypothesis 2 and 4) and two-sample t-test (hypothesis 6) was implemented within- and between-subject, respectively. For more information about the SPM tests refer to chapter 2, section 2.3.4 (page 30). All SPM statistics was implemented in MATLAB R2017 (Mathworks, Inc, Natick, MA).

3.2.4 Justification for Separating Group and Speed Factors for Statistical Analysis

This study is regarded as exploratory, and a *priori* hypotheses are formulated in such a way that no interactions from the other group were considered in within-subject comparison as well as no interaction from other speeds was considered in between-subject comparison. Therefore, the effect of speeds (intra or within-subject) on neuromuscular modulation (i.e., HD EMG) was considered for each population (i.e., biomechanics (paired-Hotelling's T^2) and robotic control (RM ANOVA)) and the effect of groups (inter- or between-subject) on neuromuscular modulation (i.e., HD EMG) was considered at each speed category separately (i.e., HS slow speed vs TFA slow speed). Therefore, each speed was considered as a different task under walking control.

3.3 Results

Figure 3.2 and Figure 3.3 show HS and TFA EMG ensemble averages of individual muscle activities during transient-state walking at slow, normal, and fast speeds (the process of obtaining linear envelope is given in Appendix B, Figure B.2).

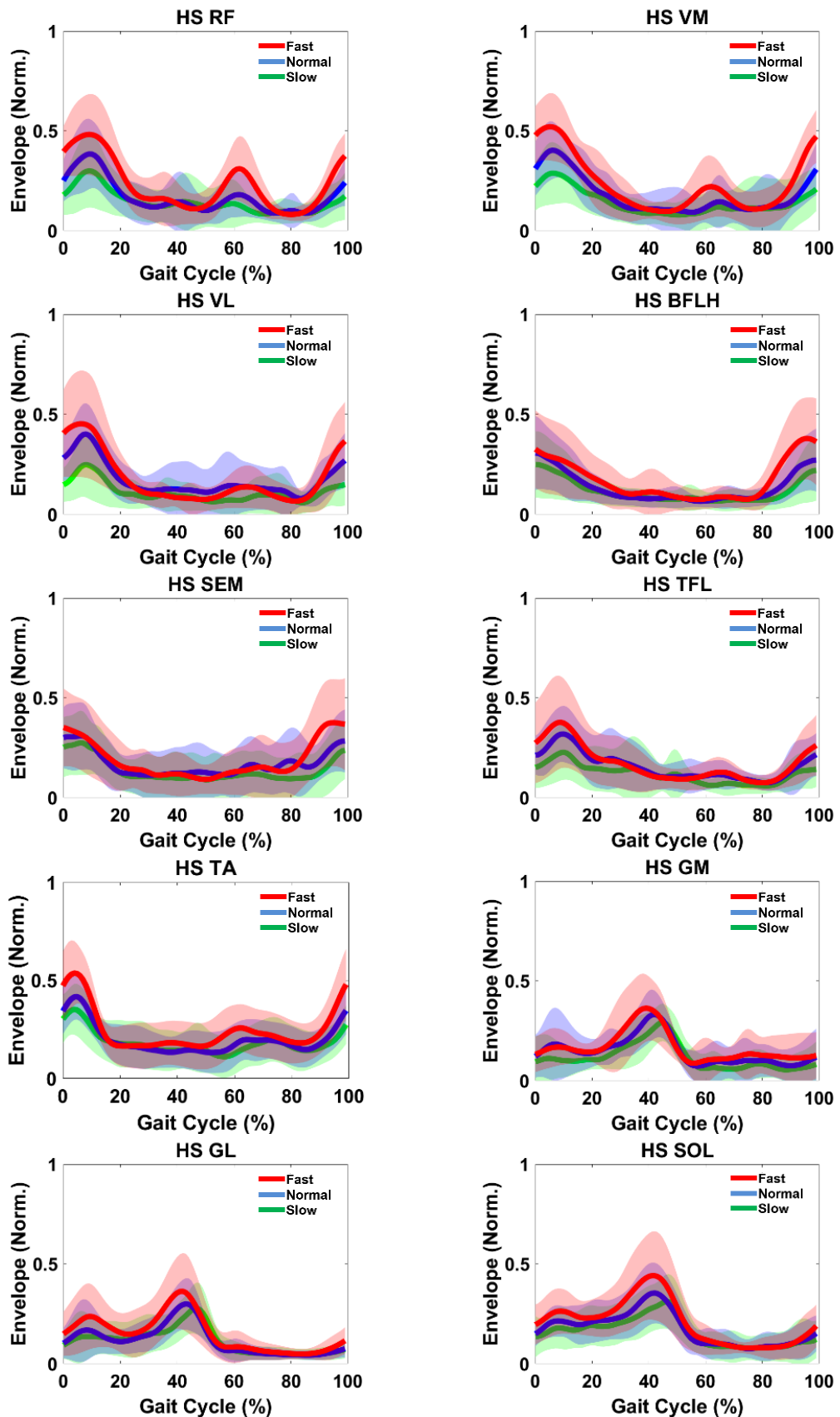


Figure 3.2: HS EMG ensemble averages of individual muscle over all trials at slow, normal, and fast speeds. The thick line and shaded area indicate mean EMG and \pm one standard deviation, respectively.

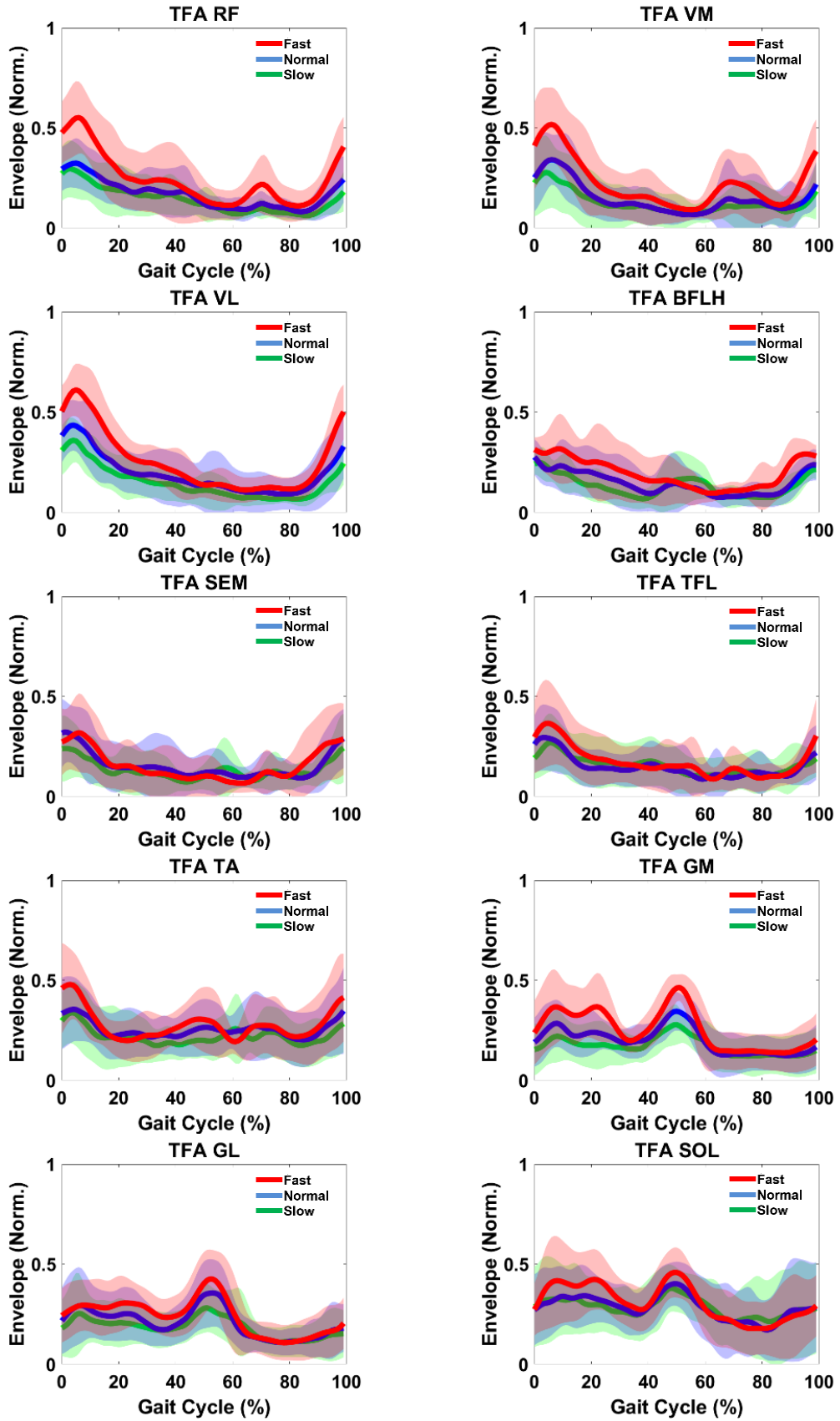


Figure 3.3: TFA EMG ensemble averages of individual muscle over all trials at slow, normal, and fast speeds. The thick line and shaded area indicate mean EMG and \pm one standard deviation, respectively.

3.3.1 Muscle Activation Patterns and Magnitudes Description

3.3.1.1 Slow Transient-State Walking

Figure 3.4 shows EMG ensemble averages of HS and TFA (averaged over all trials) for each muscle during the transient-state walking at slow speed. The descriptive analysis of each muscle activity patterns was described for HS and TFA.

RF

One major burst was observed in both HS and TFA RF activity at slow speed which contributed to control knee flexion as well as to extend the knee during the MS. In HS, the major activity occurred during the weighting acceptance peaking at 10% of GC. In TFA, RF activity started from TSW and continued to the weighting acceptance however the peak occurred at 4% of GC. In addition, on some HS, RF second minor peak occurred approximately prior to the TO continuing to the ISW peaking approximately at 60%. This served to control the swinging leg and foot by knee extension and flexing the hip to forward the swinging leg

Vasti

One major burst was observed in both HS and TFA vasti activity at slow speed which contributed to control the knee flexion as well as to assist the knee in extension during the MS. In HS, VM major activity began during the TSW and continued into weighting acceptance peaking at 7% of GC and VL activity occurred only during the weighting acceptance peaking at 9% of GC. In TFA, vasti activity started from TSW and continued into the weighting acceptance peaking at 5% of GC. In addition, on some HS and TFA, VM minor peak occurred approximately around the TO continuing to the ISW peaking at 66% and 81%, respectively, which contributed to deceleration of backward swinging leg and foot by assisting RF.

Hamstrings

One major burst was observed in both HS and TFA hamstring activities at slow speed which contributed to deceleration of the leg in the transition from swing to stance phase as a hip extensor assisting gluteus maximus. HS hamstrings major activity began during the TSW and continued into weighting acceptance, peaking at 5% (BFLH) and 7% (SEM) of GC, where they act as hip extensors to control the forward rotation of the thigh. In TFA, hamstrings major activity began during the TSW and continued into weighting acceptance peaking at 3% (BFLH) and 2% (SEM) of GC. Another major activity occurred in TFA BFLH and SEM during the TS peaking at 56% and 59% of GC, respectively.

TFL

The major burst in both HS and TFA TFL contributed to controlling the pelvis drop during weighting acceptance. HS TFL major activity began in ES and continued into MS peaking at 11% of GC. In addition, a minor peak occurred in HS during the MS peaking at 35% of GC. In TFA, TFL major activity started during the TSW and continued into weighting acceptance peaking at 7% of GC. The second minor peak occurred at 42% of GC.

TA

The major activity in both HS and TFA TA began in TSW and continued into weighting acceptance peaking at 5% of GC which contributed to dorsiflexion of the foot. Additional peaks occurred in HS at 74% and TFA at 62% and 74% of GC.

Triceps Surae

The major burst in HS and TFA triceps surae contributed to plantarflexion of the foot during push off. HS GM, GL and SOL major activities began in MS and continued into TS peaking at 46%, 48% and 47% of GC. In TFA, GM, GL and SOL major activity started during the foot-flat phase, peaking at 9%, 7% and 15% of GC, to reduce the tibia rotation. In addition, the most important mechanical power burst occurred at TS, peaking at 51% (GM), 52% (GL) and 49% (SOL) to plantarflex the foot.

3.3.1.2 Normal Transient-State Walking

Figure 3.5 shows the EMG ensemble averages of HS and TFA (averaged over all trials) for each muscle during the transient-state walking at normal speed. The descriptive analysis of each muscle activity patterns was described for HS and TFA.

RF

One major burst was observed in both HS and TFA RF activity at normal speed which contributed to control the knee flexion as well as to extend the knee during the MS. In HS, the major activity occurred during the weighting acceptance peaking at 10% of GC. In TFA, RF activity started from TSW and continued to the weighting acceptance however the peak occurred at 6% of GC. In addition, on some HS, RF second minor peak occurred approximately prior to the TO continuing to the ISW peaking approximately at 63%. This served to control the swinging leg and foot by knee extension and flexing the hip to forward the swinging leg.

Vasti

One major burst was observed in both HS and TFA vasti activity at normal speed which contributed to control the knee flexion as well as to assist the knee in extension during the MS. In HS, In HS, VM and VL major activities began during the TSW and continued

into weighting acceptance peaking at 7% and 9% of GC, respectively. In TFA, VM and VL activities started from TSW and continued into the weighting acceptance peaking at 7% and 5% of GC, respectively. In addition, on some HS and TFA, VM minor peak occurred approximately around the TO continuing to the ISW peaking at 66% and 70%, respectively, which contributed to deceleration of backward swinging leg and foot by assisting RF.

Hamstrings

One major burst was observed in both HS and TFA hamstring activities at normal speed which contributed to deceleration of the leg in the transition from swing to stance phase as a hip extensor assisting gluteus maximus. HS hamstrings major activity began during the TSW and continued into weighting acceptance, peaking at 0% (BFLH) and 7% (SEM) of GC, where they act as hip extensors to control the forward rotation of the thigh. In TFA, hamstrings major activity began during the TSW and continued into MS peaking at 99% (BFLH) and 2% (SEM) of GC. Another major activity occurred in TFA BFLH during the TS peaking at 50% of GC, respectively.

TFL

The major burst in both HS and TFA TFL contributed to controlling the pelvis drop during weighting acceptance. HS TFL major activity began during the TSW and continued into MS peaking at 11% of GC. In addition, a minor peak occurred in HS during the MS peaking at 28% of GC. In TFA, TFL major activity started during the TSW and continued into weighting acceptance peaking at 4% of GC. The second minor peak occurred at 42% of GC.

TA

The major activity in both HS and TFA TA began in TSW and continued into weighting acceptance peaking at 6% of GC which contributed to dorsiflexion of the foot. Additional peaks occurred in HS at 65% and TFA at 52% and 69%.

Triceps Surae

The major burst in HS and TFA triceps surae contributed to plantarflexion of the foot during push off. HS GM, GL and SOL major activities began in MS and continued into TS peaking at 43%, 44% and 43% of GC. In TFA, GM, GL and SOL major activity started during the foot-flat phase, peaking at 9%, 8% and 19% of GC, to reduce the tibia rotation. In addition, the most important mechanical power burst occurred at TS, peaking at 51% (GM), 54% (GL) and 50% (SOL) to plantarflex the foot.

3.3.1.3 Fast Transient-State Walking

Figure 3.6 shows the EMG ensemble averages of HS and TFA (averaged over all trials) for each muscle during the transient-state walking at slow speed. The descriptive analysis of each muscle activity patterns was explained for HS and TFA.

RF

One major burst was observed in both HS and TFA RF activity at fast speed which contributed to control the knee flexion as well as to extend the knee during the MS. In HS, the major activity occurred during the weighting acceptance peaking at 10% of GC. In TFA, RF activity started from TSW and continued to the weighting acceptance however the peak occurred at 7% of GC. In addition, on some HS, RF minor second and third peaks occurred approximately prior TO continuing to the ISW peaking approximately at 35% and 63%. Similarly, two minor bursts were observed in TFA RF peaking at 35% and 71%. The peak around the TO acted to decelerate the backward swinging leg and foot by extending the knee as well as flexing the hip to pull the swinging leg forward.

Vasti

One major burst was observed in both HS and TFA vasti activity at fast speed which contributed to control the knee flexion as well as to assist the knee in extension during the MS. In HS, VM and VL major activities began during the TSW and continued into weighting acceptance peaking at 6% and 7% of GC, respectively. In TFA, VM and VL activities started from TSW and continued into the weighting acceptance peaking at 7% and 6% of GC, respectively. In addition, on some HS and TFA, VM minor peak occurred approximately around the TO continuing to the ISW peaking at 63% and 70%, respectively, which contributed to deceleration of backward swinging leg and foot by assisting RF.

Hamstrings

One major burst was observed in both HS and TFA hamstring activities at fast speed which contributed to deceleration of the leg in the transition from swing to stance phase as hip extensor assisting gluteus maximus. HS hamstrings major activity began during the TSW and continued into weighting acceptance, peaking at 97% (BFLH) and 96% (SEM) of GC, where they act as hip extensors to control the forward rotation of the thigh. In TFA, hamstrings major activity began during the TSW and continued into MS peaking at 10% (BFLH) and 7% (SEM) of GC.

TFL

The major burst in both HS and TFA TFL contributed to controlling the pelvis drop during weighting acceptance. HS TFL major activity began during the TSW and continued into MS peaking at 10% of GC. In addition, a minor peak occurred in HS around TO peaking at 66% of GC. In TFA, TFL major activity started during the TSW and continued into weighting acceptance peaking at 6% of GC. The second minor peak occurred at 55% of GC.

TA

The major burst in both HS and TFA TA began in TSW and continued into weighting acceptance peaking at 5% of GC which contributed to dorsiflexion of the foot. In addition, the minor bursts occurred in HS peaking at 63% and in TFA peaking at 49% and 71% which contributed to the dorsiflexion of the foot in swing phase for foot clearance.

Triceps Surae

The major burst in HS and TFA triceps surae contributed to plantarflexion of the foot during push off. HS GM, GL and SOL major activities began in MS and continued into TS peaking at 40%, 43% and 43% of GC. In addition, in GL and SOL, the earlier peak occurred during the foot-flat peaking at 10% of GC. In TFA, GM, GL and SOL major activity started during the foot-flat phase, peaking at 23%, 23% and 22% of GC, to reduce the tibia rotation. In addition, the most important mechanical power burst occurred at TS, peaking at 52% (GM), 53% (GL) and 50% (SOL) to plantarflex the foot.

Table 3.3 shows the major and minor peaks occurred in HS and TFA during transient-state walking at different speeds. In addition, literature review results were also included.

Table 3.3: HS and TFA major and minor bursts (peaks) muscle activities during transient-state walking at each speed. The approximate peak values available from the muscles in the literature review are included for HS [9, 96] and TFA [36, 47]. NF indicates not found.

Major and Minor Peaks								
	Slow (%)		Normal (%)		Fast (%)		Literature Review	
	HS	TFA	HS	TFA	HS	TFA	HS	TFA
RF	10,43,60	4,39	10,63,41	6,31	10,35,63	7,35,71	10,66	NF
VM	7,66	5,81	7,66	7,70	6,63	7,70	15,60	NF
VL	9,24	5,24	9,60	5,32	7,65	6,56	10,70	22
BFLH	0,55	3,56	0,50	99,10	97,42	10,96	4,70	14
SEM	7,66	2,59	7,3	2,32	96,70	7,23	95,65	NF
TFL	11,35	7,42	11,28	4,42	10,66	6,55	15,40	NF
TA	5,74	5,62,74	6,65	5,69,52	5,63	4,49,71	5,75	8,68
GM	46,6	51,9	43,8	51,9	40,9	52,23	45,10	60,24
GL	48,9	52,7	44,9	54,8	43,10	53,23	45,10	52
SOL	47,21	49,15	43,9	50,19	43,10	50,22	50,20	53,20

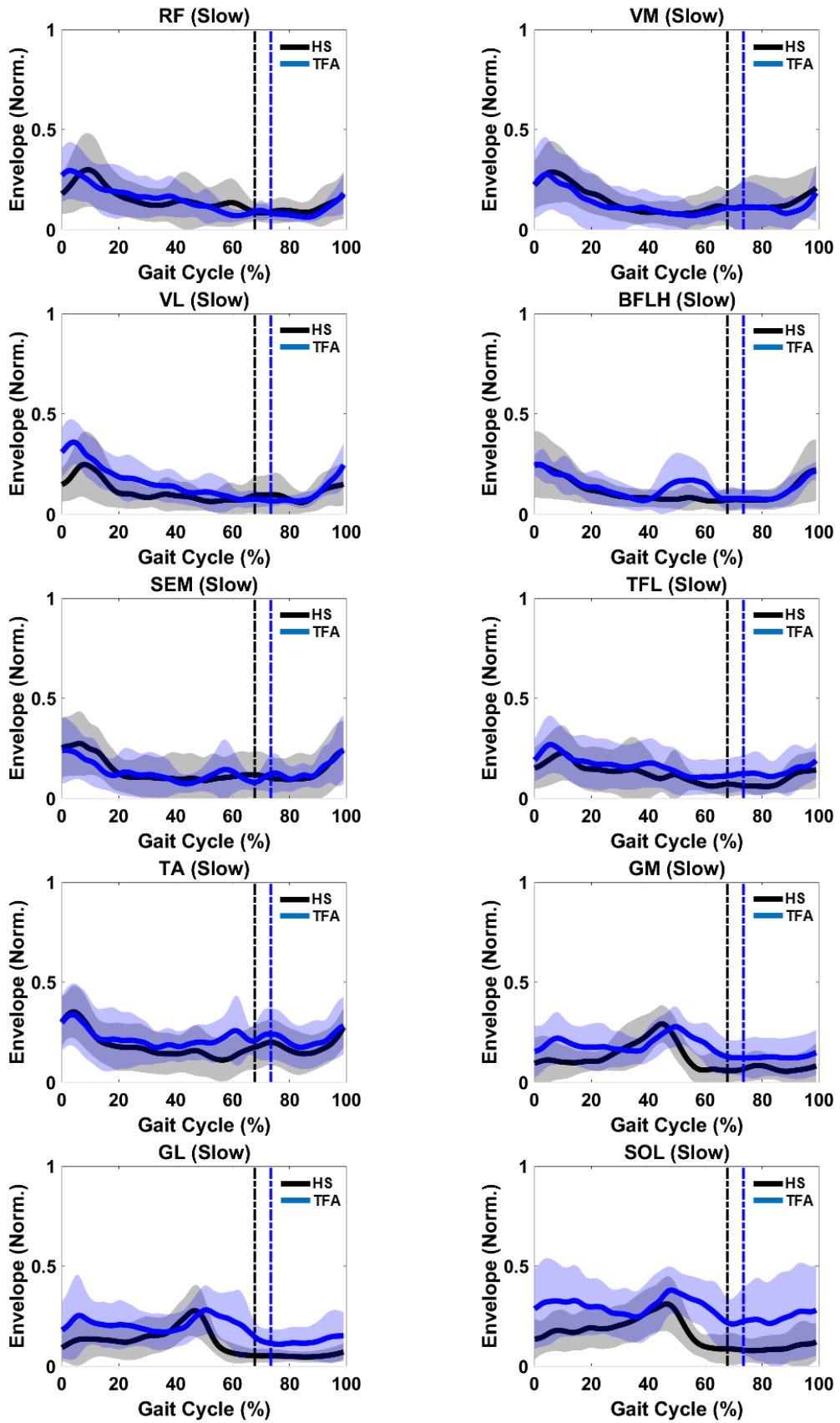


Figure 3.4: EMG ensemble averages of HS and TFA (averaged over all trials) for each muscle at slow speed. The thick line and shaded area indicate mean EMG and \pm one standard deviation. The vertical dashed line indicates TO.

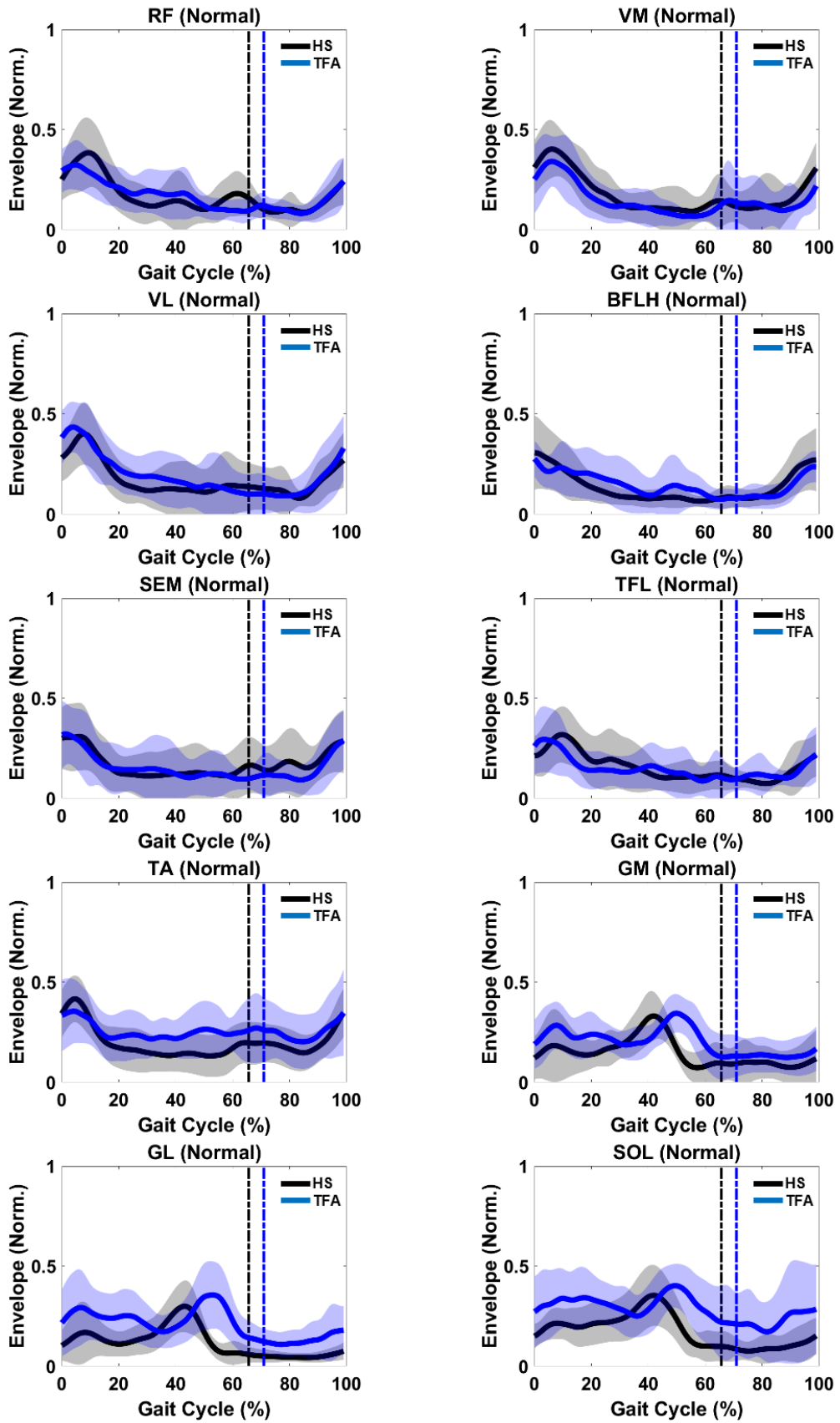


Figure 3.5: EMG ensemble averages of HS and TFA (averaged over all trials) for each muscle at normal speed. The thick line and shaded area indicate mean EMG and \pm one standard deviation. The vertical dashed line indicates TO.

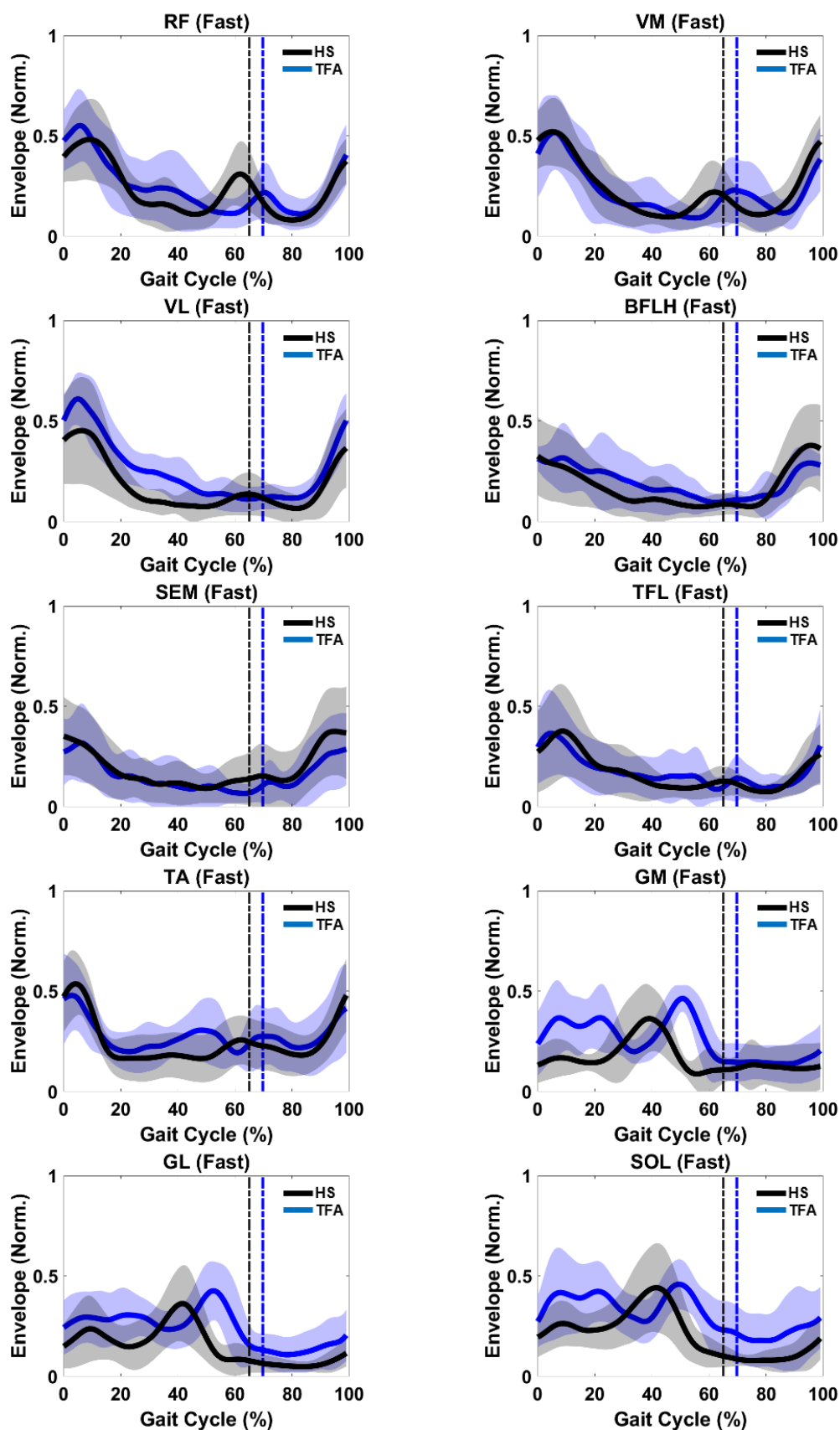


Figure 3.6: EMG ensemble averages of HS and TFA (averaged over all trials) for each muscle at fast speed. The thick line and shaded area indicate mean EMG and \pm one standard deviation. The vertical dashed line indicates TO.

3.3.2 Statistical Parametric Mapping

3.3.2.1 Within-Subject (Biomechanics Perspective)

Due to the limitations of SPM, repeated-measures MANOVA could not be performed. In addition, the design of this study is regarded as exploratory which searches for the effect of speeds on EMG profiles of functionally related muscles contributing to biomechanical subtasks of gait as well as all muscles that contribute to the co-contraction of ankle and knee joints during walking in each group separately. Therefore, paired Hotelling's T^2 for hypothesis 1 (a-f) and 3 (a-f) was deployed using a Bonferroni correction across speeds. Post hoc SPM vector field analysis was performed pairwise between speeds. The threshold was corrected for the Bonferroni threshold of 0.02.

Speed Dependence of the HS HD Module 1

As shown in Figure 3.7, HS HD M1 were significantly greater at 4-13% ($p=0.002$) and 0-1% ($p=0.016$) in normal-slow and fast-normal speed comparison, respectively. In addition, two suprathreshold clusters were found in HS HD M1 between fast-slow at 0-22% ($p=0.001$) and 92-100% ($p=0.001$) GC. Therefore, null hypothesis 1a was rejected as significant differences were observed in activations of muscles consisted in HD M1 of HS between speeds.

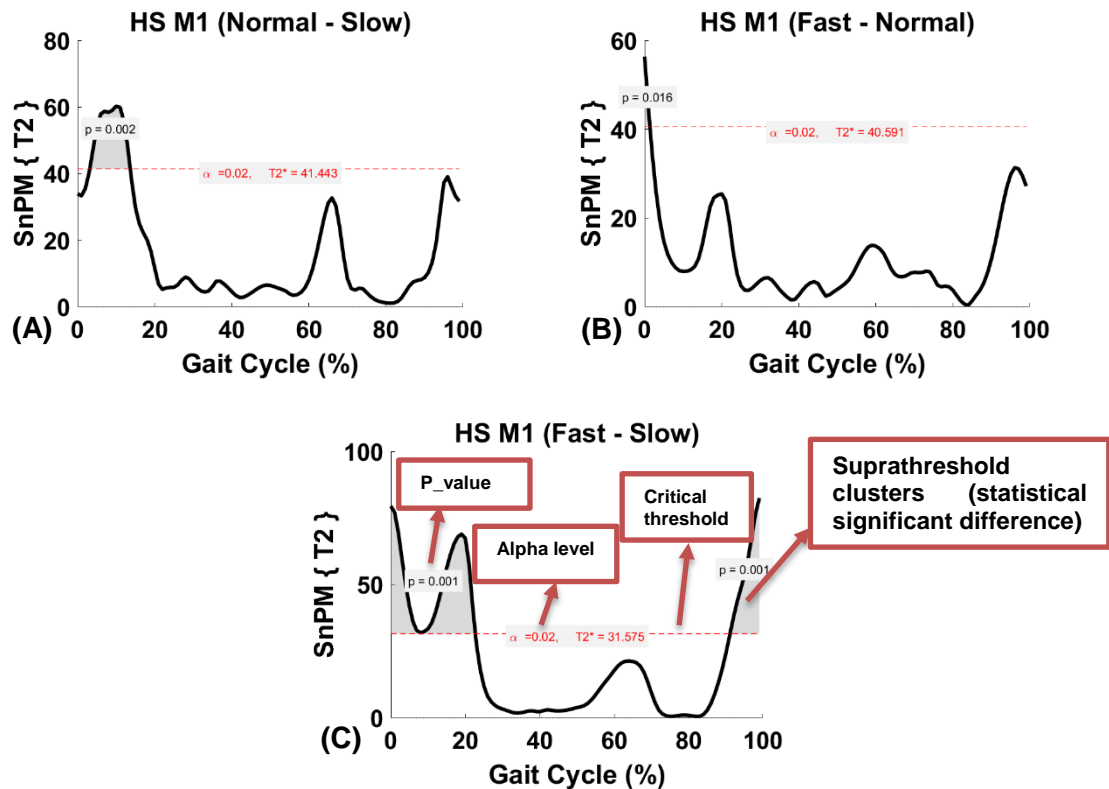


Figure 3.7: HS M1 non-parametric post hoc SPM vector field results (paired Hotelling's T² test) depicting significant differences between speeds. The red dashed lines indicate critical thresholds of $T_2^* = 41.443$, 40.591 and 31.575 for (A), (B), and (C), respectively. Suprathreshold clusters are shown in grey where $p < 0.02$.

As an example, Figure 3.7 (C) has been annotated to facilitate understanding of the SPM figures. T²-values above the threshold (T² critical threshold) suggest significant difference between the two speeds. For regions of the SnPM {T²} which fail to cross the threshold, the interpretation is the same as in all classical hypothesis tests: insufficient evidence to reject the null hypothesis. More simply, in areas which do not cross the threshold the mean difference is not large relative to the variance. It is noteworthy that if results fail to reach significance, but come close to breaching the critical threshold, it is possible that other post hoc analyses would find them statistically significant. It is, therefore, best to interpret non-significant results cautiously when using Bonferroni corrections.

Speed Dependence of the HS HD Module 2

As shown in Figure 3.8, no significant differences were found in HS HD M2 between normal-slow. In fast-normal and fast-slow speed comparison, HS HD M2 was significantly greater at 76% ($p=0.045$) and 36-40% ($p=0.006$) GC, respectively. Therefore, null hypothesis 1b was rejected as significant differences were observed in activations of muscles consisted in HD M2 of HS between speeds.

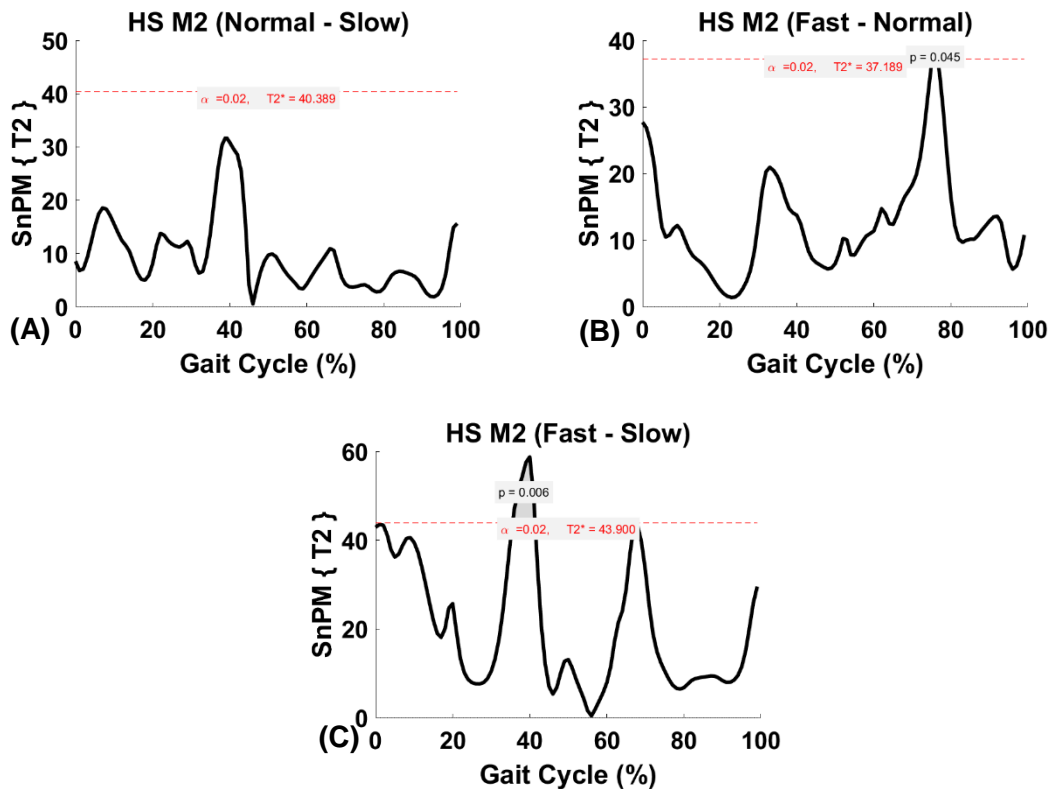


Figure 3.8: HS M2 non-parametric post hoc SPM vector field results (paired Hotelling's T2 test) depicting significant differences between speeds. The red dashed lines indicate critical thresholds of $T2^* = 40.389$, 37.189 and 43.900 for (A), (B), and (C), respectively. Suprathreshold clusters are shown in grey where $p < 0.02$.

Speed Dependence of the HS HD Module 3

As shown in Figure 3.9, HS HD M3 were significantly greater between normal-slow at 97-100% ($p=0.013$), between fast-normal at 0-1% ($p=0.005$), 15-21% ($p=0.001$) and 97-100% ($p=0.021$), and between fast-slow at 0-8% ($p=0.001$), 16-21% ($p=0.001$), 57-65% ($p=0.007$) and 93-100% ($p=0.001$) GC. Therefore, null hypothesis 1c was rejected as significant differences were observed in activations of muscles consisted in HD M3 of HS between speeds.

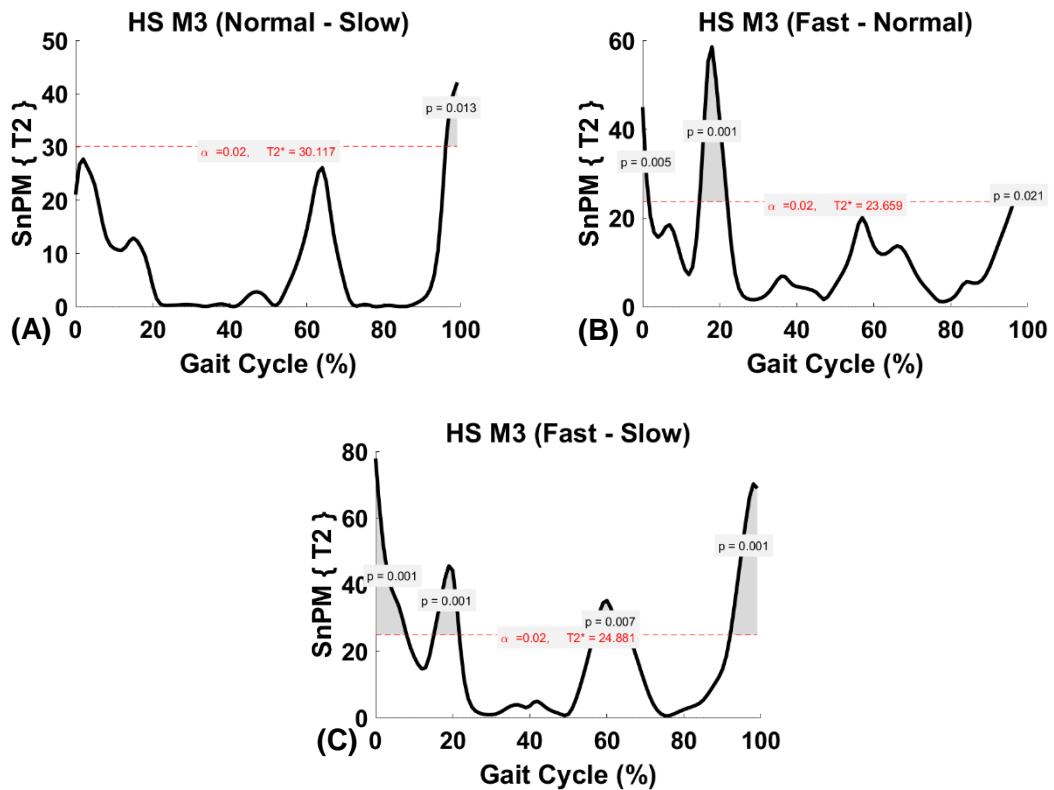


Figure 3.9: HS M3 non-parametric post hoc SPM vector field results (paired Hotelling's T2 test) depicting significant differences between speeds. The red dashed lines indicate critical thresholds of $T2^* = 30.117$, 23.659 and 24.881 for (A), (B), and (C), respectively. Suprathreshold clusters are shown in grey where $p < 0.02$.

Speed Dependence of the HS HD Module 4

As shown in Figure 3.10, no significant differences were found in HS HD M4 between fast-normal. HS HD M4 was significantly greater between normal-slow at 90% ($p=0.045$) and between fast-slow at 85-95% ($p=0.01$) GC. Therefore, null hypothesis 1d was rejected as a significant difference was observed in activations of muscles consisted in HD M4 of HS between speeds.

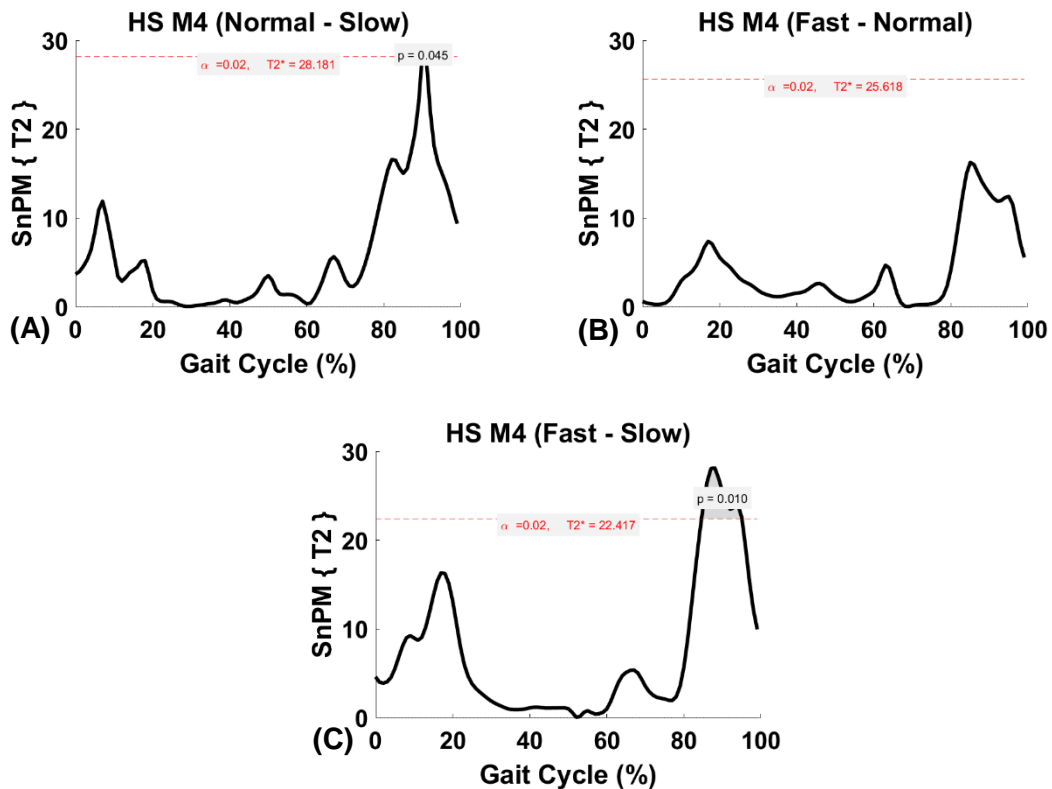


Figure 3.10: HS M4 non-parametric post hoc SPM vector field results (paired Hotelling's T2 test) depicting significant differences between speeds. The red dashed lines indicate critical thresholds of $T2^* = 28.181$, 25.618 and 22.417 for (A), (B), and (C), respectively. Suprathreshold clusters are shown in grey where $p < 0.02$.

Speed Dependence of the HS Ankle Co-Contraction

As shown in Figure 3.11 no significant differences were found in HS ankle muscles between normal-slow and fast-normal. In fast-slow speed comparison, HS ankle was significantly greater at 47-40% ($p=0.023$) GC. Therefore, null hypothesis 1e was rejected as a significant difference was observed in activations of muscles consisted in the ankle co-contraction of HS between speeds.

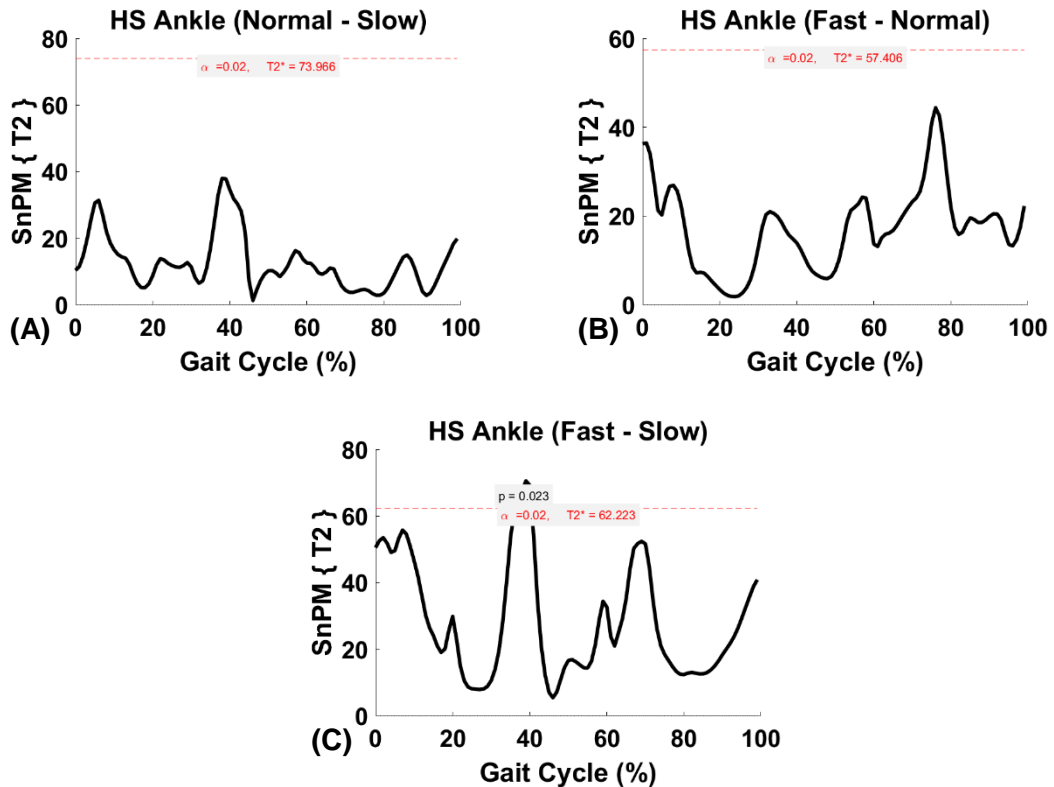


Figure 3.11: HS ankle co-contraction non-parametric post hoc SPM vector field results (paired Hotelling's T2 test) depicting significant differences between speeds. The red dashed lines indicate critical thresholds of $T2^* = 73.966$, 57.406 and 62.223 for (A), (B), and (C), respectively. Suprathreshold clusters are shown in grey where $p < 0.02$.

Speed Dependence of the HS Knee Co-Contraction

As shown in Figure 3.12, no significant differences were found in HS knee muscles between fast-normal. HS knee muscles was significantly greater between normal-slow at 98-100% ($p=0.032$) and between fast-slow at 0% ($p=0.049$) and 99% ($p=0.049$) GC. Therefore, null hypothesis 1f was rejected as a significant difference was observed in activations of muscles consisted in the knee co-contraction of HS between speeds.

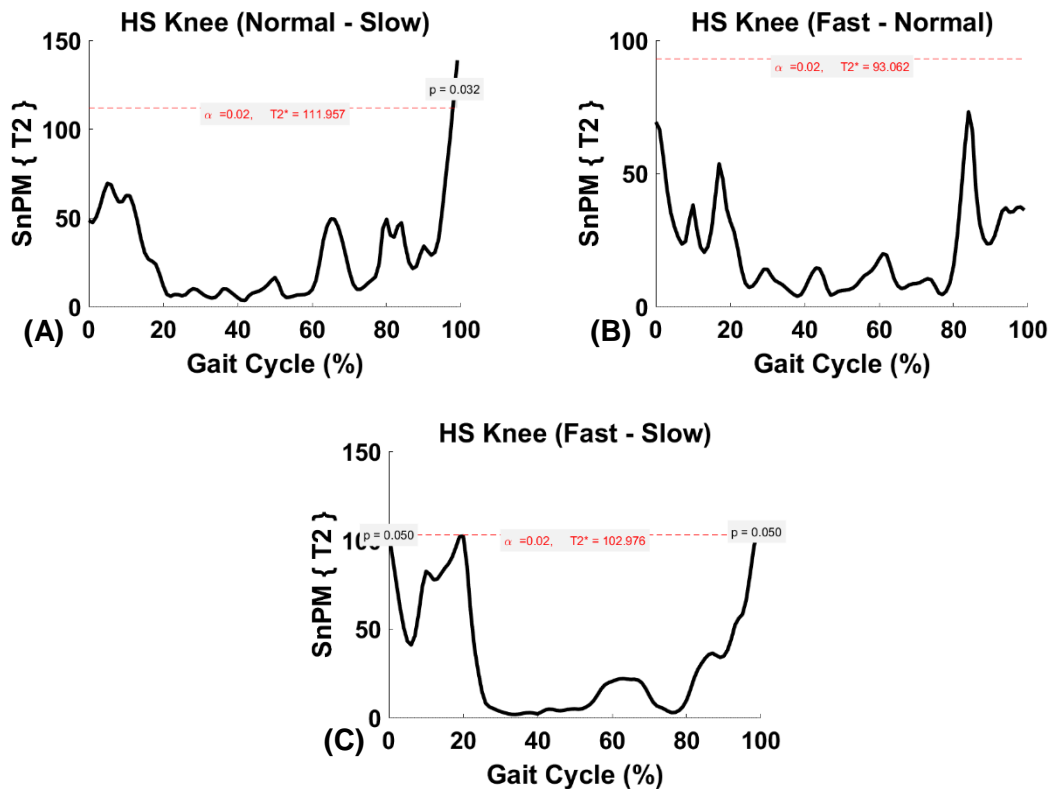


Figure 3.12: HS knee co-contraction non-parametric post hoc SPM vector field results (paired Hotelling's T2 test) depicting significant differences between speeds. The red dashed lines indicate critical thresholds of $T2^* = 111.957$, 93.062 and 102.976 for (A), (B), and (C), respectively. Suprathreshold clusters are shown in grey where $p < 0.02$.

Speed Dependence of the TFA HD Module 1

As shown in Figure 3.13, no significant differences were found in TFA HD M1 between normal-slow and fast-normal. In fast-slow speed comparison, TFA HD M1 was significantly greater at 0-1% ($p=0.028$), 6-11% ($p=0.015$) and 92-100% ($p=0.001$) GC. Therefore, null hypothesis 3a was rejected as significant differences were observed in activations of muscles consisted in HD M1 of TFA between speeds.

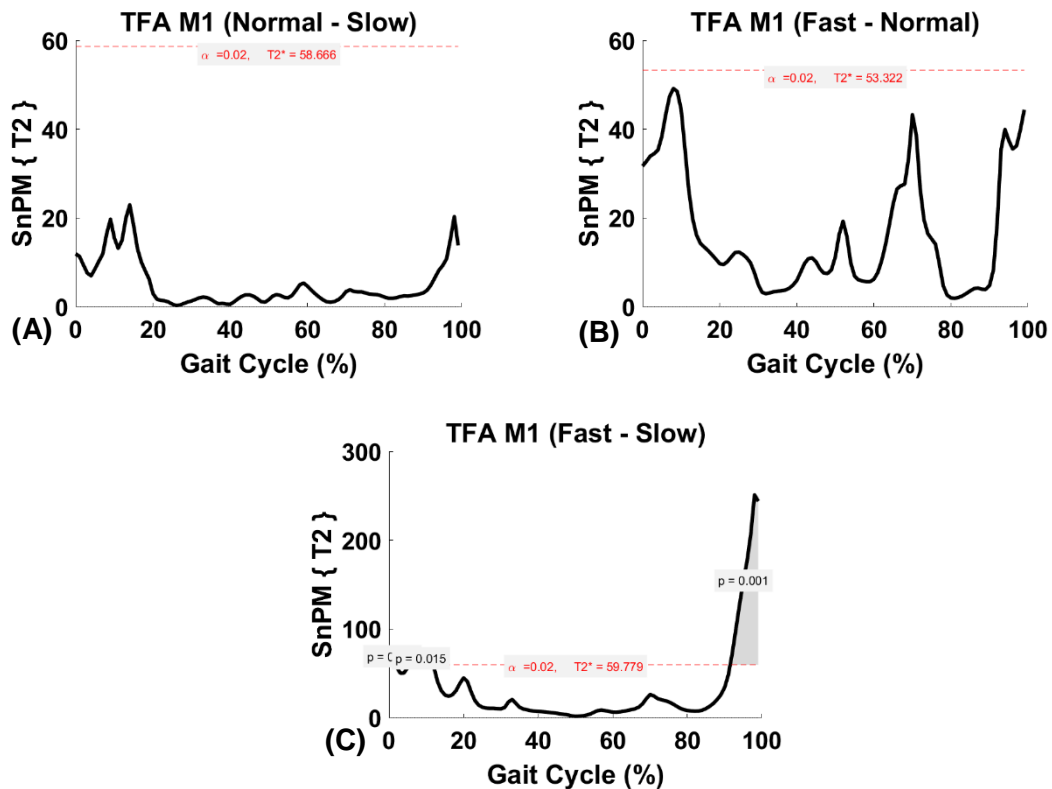


Figure 3.13: TFA M1 non-parametric post hoc SPM vector field results (paired Hotelling's T2 test) depicting significant differences between speeds. The red dashed lines indicate critical thresholds of $T2^* = 58.666$, 53.322 and 59.779 for (A), (B), and (C), respectively. Suprathreshold clusters are shown in grey where $p < 0.02$.

Speed Dependence of the TFA HD Module 2

As shown in Figure 3.14, no significant differences were found in TFA HD M2 between normal-slow and fast-normal. In fast-slow speed comparison, TFA HD M2 was significantly greater at 6-7% ($p=0.007$) and 51-54% ($p=0.003$) GC. Therefore, null hypothesis 3b was rejected as significant differences were observed in activations of muscles consisted in HD M2 of TFA between speeds.

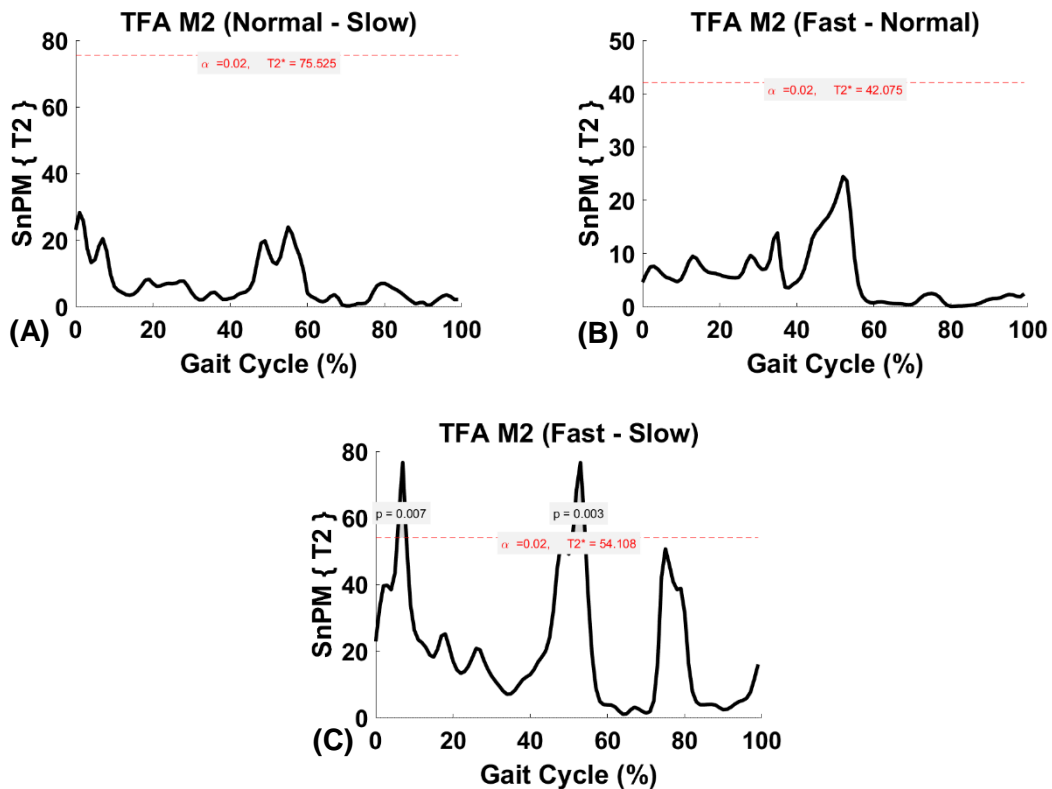


Figure 3.14: TFA M2 non-parametric post hoc SPM vector field results (paired Hotelling's T2 test) depicting significant differences between speeds. The red dashed lines indicate critical thresholds of $T_2^* = 75.525$, 42.075 and 54.108 for (A), (B), and (C), respectively. Suprathreshold clusters are shown in grey where $p < 0.02$.

Speed Dependence of the TFA HD Module 3

As shown in Figure 3.15, no significant differences were found in TFA HD M3 between normal-slow. TFA HD M3 was significantly greater between fast-normal at 0-11% ($p=0.001$) and between fast-slow at 0-12% ($p=0.001$) and 92-100% ($p=0.001$) GC. Therefore, null hypothesis 3c was rejected as significant differences were observed in activations of muscles consisted in HD M3 of TFA between speeds.

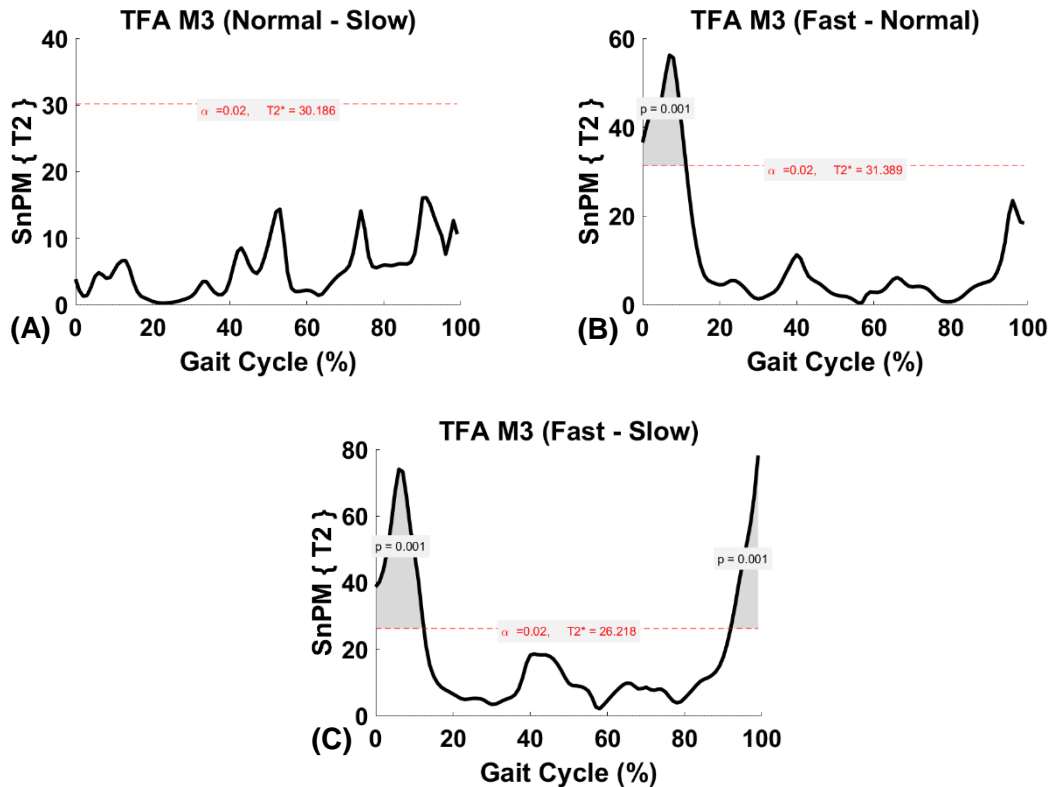


Figure 3.15: TFA M3 non-parametric post hoc SPM vector field results (paired Hotelling's T2 test) depicting significant differences between speeds. The red dashed lines indicate critical thresholds of $T2^* = 30.186$, 31.389 and 26.218 for (A), (B), and (C), respectively. Suprathreshold clusters are shown in grey where $p < 0.02$.

Speed Dependence of the TFA HD Module 4

As shown in Figure 3.16, no significant differences were found in TFA HD M4 between normal-slow and fast-slow. TFA HD M4 was significantly greater between fast-normal at 89-91% ($p=0.004$) GC. Therefore, null hypothesis 3d was rejected as a significant difference was observed in activations of muscles consisted of HD M4 of TFA between speeds.

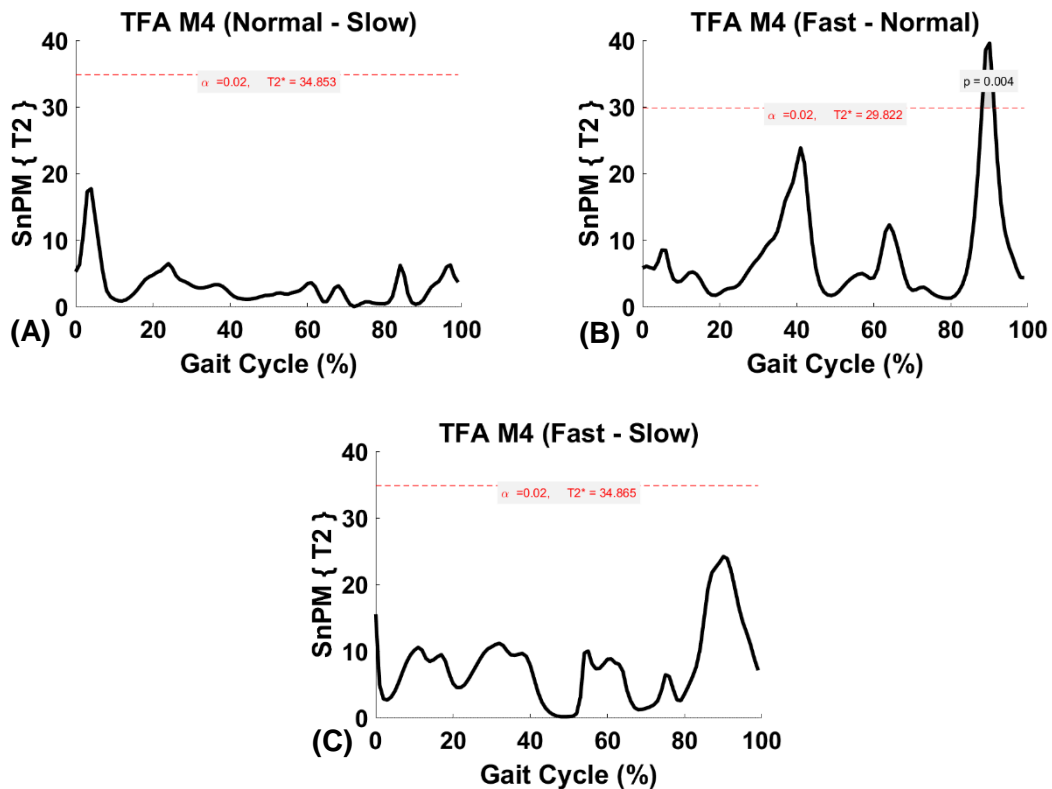


Figure 3.16: TFA M4 non-parametric post hoc SPM vector field results (paired Hotelling's T2 test) depicting significant differences between speeds. The red dashed lines indicate critical thresholds of $T2^* = 34.853$, 29.822 and 34.865 for (A), (B), and (C), respectively. Suprathreshold clusters are shown in grey where $p < 0.02$.

Speed Dependence of the TFA Ankle Co-Contraction

As shown in Figure 3.17, no significant differences were found in TFA ankle muscle between fast-normal. TFA ankle muscles were significantly greater between normal-slow at 53-54% ($p=0.013$) and fast-slow at 74% ($p=0.037$) GC. Therefore, null hypothesis 3e was rejected as significant differences were observed in activations of muscles consisted in the ankle co-contraction of HS between speeds.

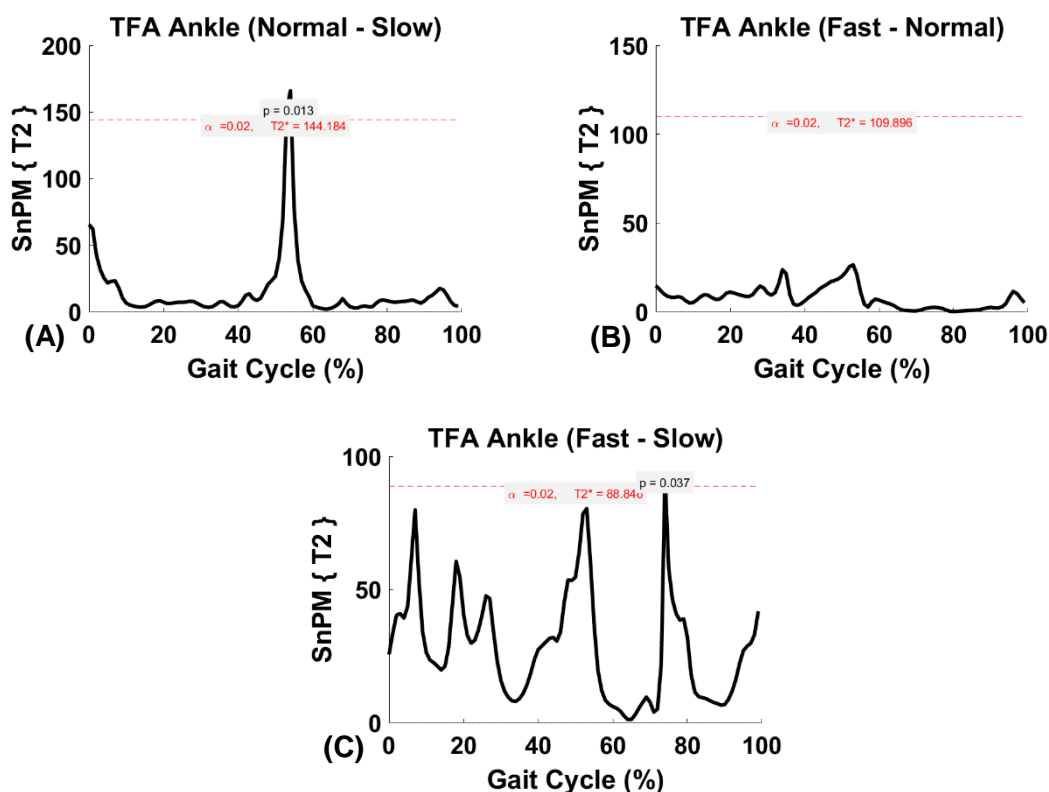


Figure 3.17: TFA ankle co-contraction non-parametric post hoc SPM vector field results (paired Hotelling's T2 test) depicting significant differences between speeds. The red dashed lines indicate critical thresholds of $T2^* = 144.184$, 109.896 and 88.846 for (A), (B), and (C), respectively. Suprathreshold clusters are shown in grey where $p < 0.02$.

Speed Dependence of the TFA Knee Co-Contraction

As shown in Figure 3.18, no significant differences were found in TFA knee muscles between normal-slow. TFA knee muscles were significantly greater between fast-normal at 1% ($p=0.049$) and between fast-slow at 97-100% ($p=0.001$) GC. Therefore, null hypothesis 3f was rejected as a significant difference was observed in activations of muscles consisted in the knee co-contraction of TFA between speeds.

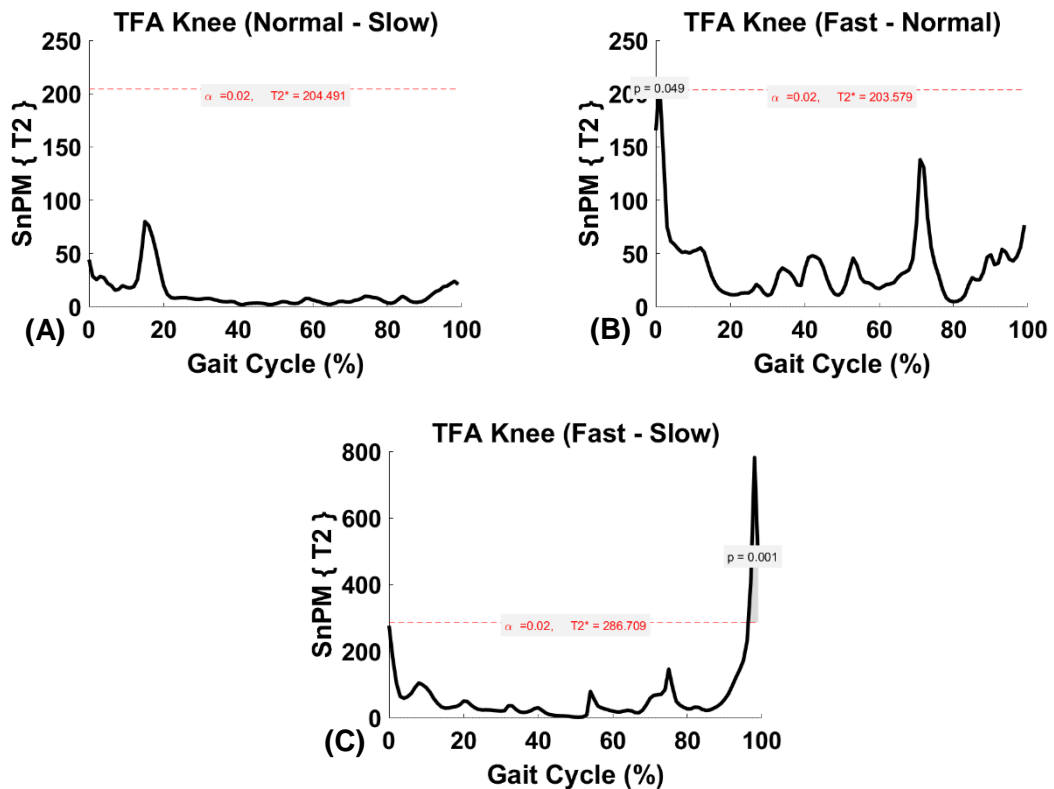


Figure 3.18: TFA knee co-contraction non-parametric post hoc SPM vector field results (paired Hotelling's T_2 test) depicting significant differences between speeds. The red dashed lines indicate critical thresholds of $T_2^* = 204.491$, 203.579 and 286.709 for (A), (B), and (C), respectively. Suprathreshold clusters are shown in grey where $p < 0.02$.

3.3.2.2 Within-Subject (Robotic Control Perspective)

A *priori* hypothesis in this section was to investigate the effect of speeds on individual muscle activities during transient-state walking in each group separately. Therefore, one-way RM ANOVA (represented as a black trajectory in Figure 3.19) was implemented to investigate the within-subject F statistics for hypothesis 2 and 4.

It is worth mentioning that one-way ANOVA was performed between-subject for demonstration (represented as a red trajectory in Figure 3.19) however, this is not an appropriate test since the same subjects performed transient-state walking at different speeds. Moreover, the between-subject analysis yields a small F value because between-subject variability is large relative to between-condition variability. The within-subject analysis yields a large F value because paired effects are large relative to paired variability.

Post hoc analysis was done to investigate further the differences between speeds. Multiple post hoc paired t-tests increases the chances of making a type I error (false positive). Therefore, alpha was corrected according to the number of comparisons made to decrease the likelihood of a type I error, to increase the critical threshold, and to ensure the false positive error rate is appropriate for the number of comparisons made. In this case, Bonferroni threshold of $p = 0.017$ was adopted for the three walking speeds to retain a family-wise error of $\alpha = 0.05$ which was then used for inference calculation.

It is noted that the post hoc analyses are meant to qualify the original hypotheses provided - they do not disagree with the main analyses. Where differences exist, one must not make the conclusion that disagrees with the main results. Therefore, the main analysis answered the null hypothesis completely in the case of those muscles whose main and post hoc disagreed.

Speed Dependence of the HS Muscles

HS RF

As shown in Figure 3.19, statistically significant differences occurred in HS RF across different speeds. Three suprathreshold clusters were found at 0-23% ($p=0.001$), 63-67% ($p=0.022$) and 92-100% ($p=0.008$) GC intra-subjectively. Post hoc paired t-test revealed RF was significantly greater between fast-normal at approximately 0-1% ($p=0.041$), 19-21% ($p=0.020$) and 97-100% ($p=0.020$) GC as well as between fast-slow 0-3% ($p=0.023$), 15-21% ($p=0.001$) and 94-100% ($p=0.005$) (Figure 3.20).

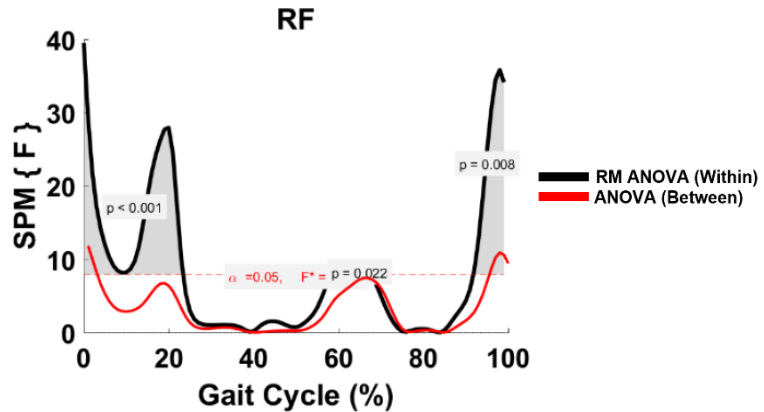


Figure 3.19: HS RF parametric RM ANOVA within- and between-subjects, depicting significant differences between speeds. The horizontal red dotted line indicates the critical threshold of 7.908. Suprathreshold clusters are shown in grey where $p < 0.05$.

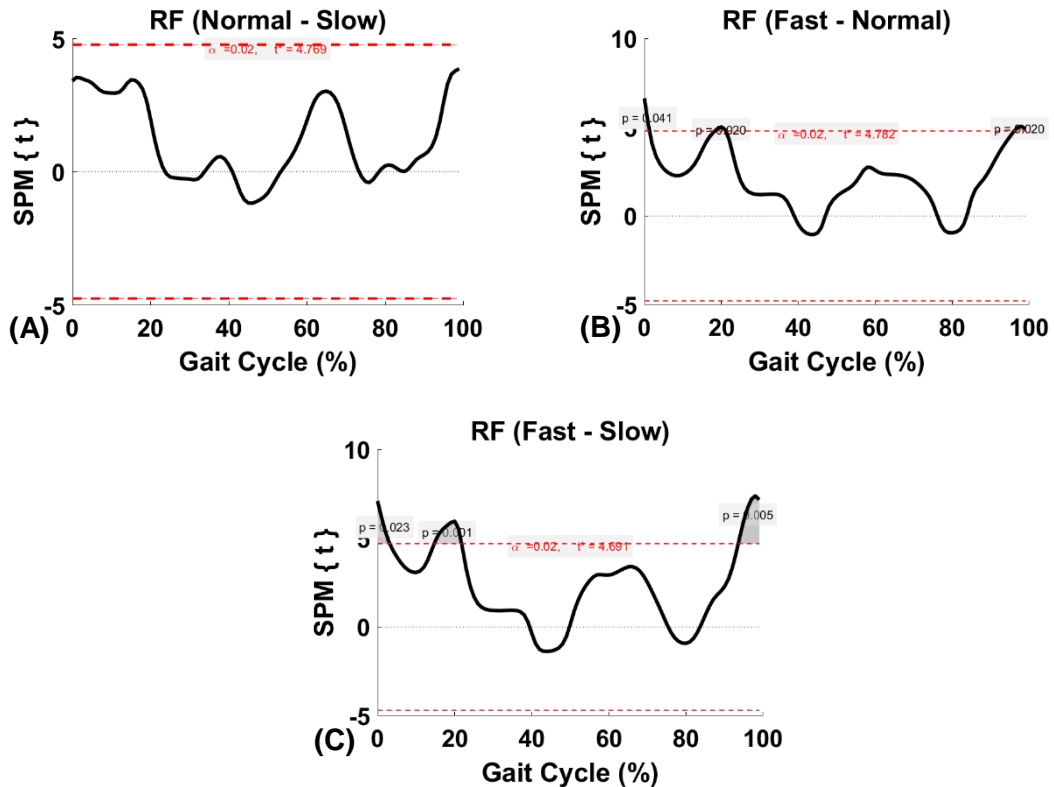


Figure 3.20: HS RF within-subject post hoc paired t statistic between speeds. The red dashed lines indicate critical thresholds of $t^* = 4.77$, 4.78 and 4.69 for (A), (B), and (C), respectively. Suprathreshold clusters are shown in grey where $p < 0.02$.

HS VM

As shown in Figure 3.21, SPM analysis revealed two suprathreshold clusters between three speeds in VM intra-subjectively at approximately 0-19% ($p=0.00$) and 92-100% ($p=0.015$) GC. Post hoc paired t-test was conducted between speeds where significant differences occurred between normal-slow at 5-8% ($p=0.014$), fast-normal at 95-98% ($p=0.020$) and fast-slow at 0-2% ($p=0.037$) and 96-100% ($p=0.034$) GC (Figure 3.22).

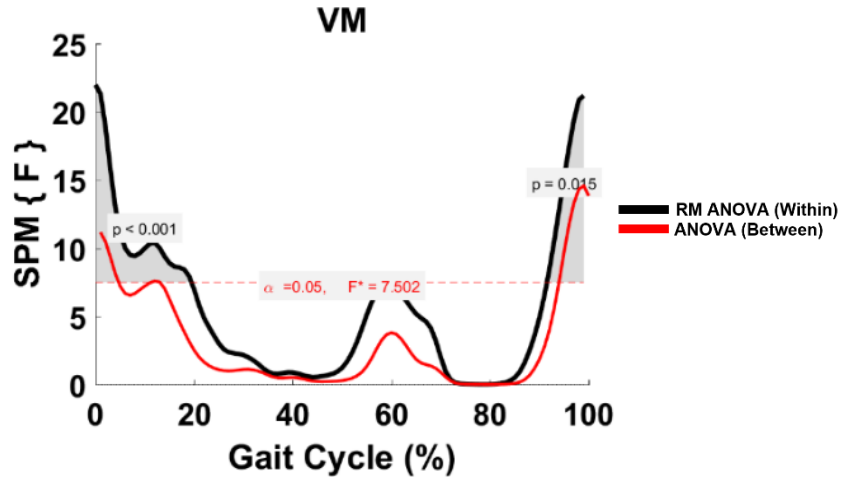


Figure 3.21: HS VM parametric RM ANOVA within- and between-subjects, depicting significant differences between speeds. The horizontal red dotted line indicates the critical threshold of 7.502. Suprathreshold clusters are shown in grey where $p < 0.05$.

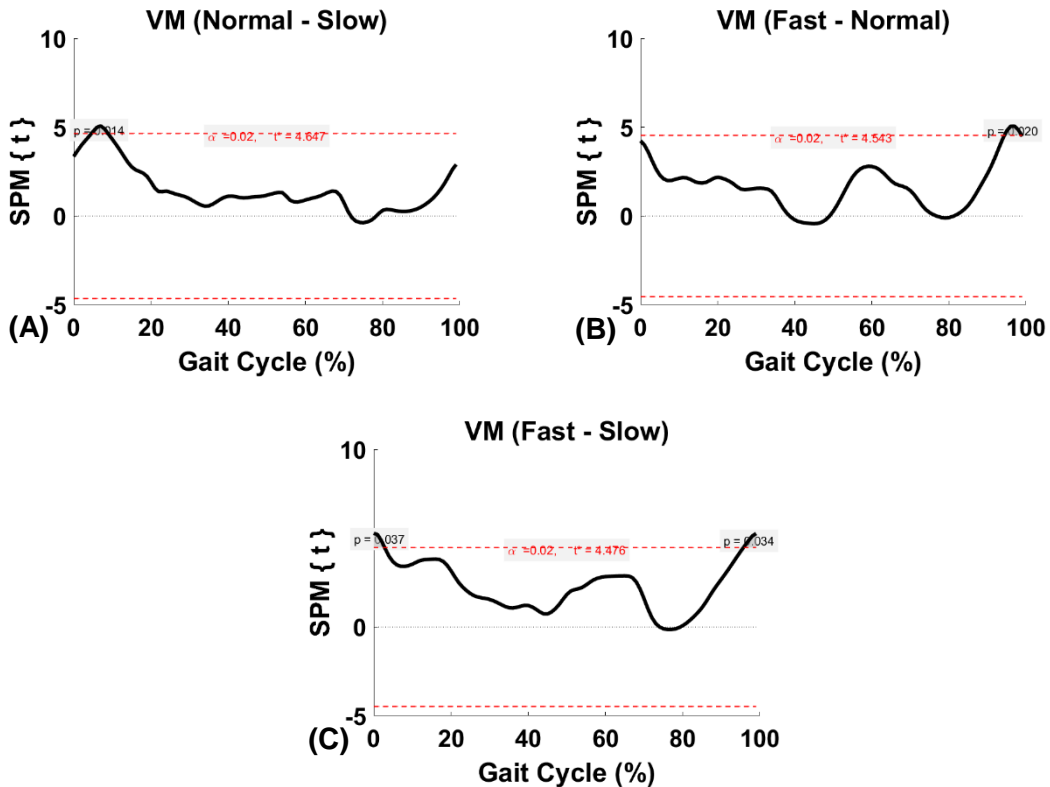


Figure 3.22: HS VM within-subject post hoc paired t statistic between speeds. The red dashed lines indicate critical thresholds of $t^* = 4.65$, 4.54 and 4.48 for (A), (B), and (C), respectively. Suprathreshold clusters are shown in grey where $p < 0.02$.

HS VL

As shown in Figure 3.23, SPM analysis revealed two suprathreshold clusters between three speeds in VL intra-subjectively at approximately 0-20% ($p=0.00$) and 97-100% ($p=0.040$) GC. In post hoc paired t-test, significant differences were observed between normal-slow at 0-14% ($p=0.00$) and fast-slow at 11-23% ($p=0.00$) GC (Figure 3.24).

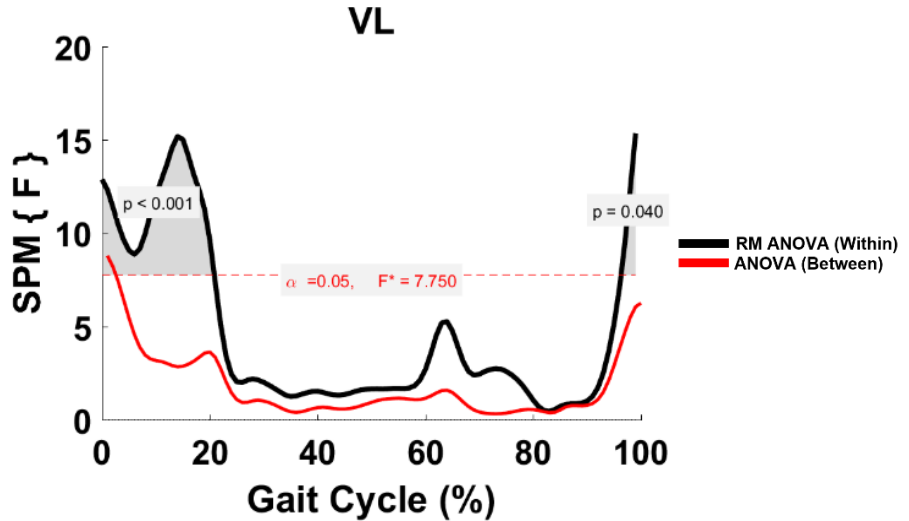


Figure 3.23: HS VL parametric RM ANOVA within- and between-subjects, depicting significant differences between speeds. The horizontal red dotted line indicates the critical threshold of 7.750. Suprathreshold clusters are shown in grey where $p < 0.05$.

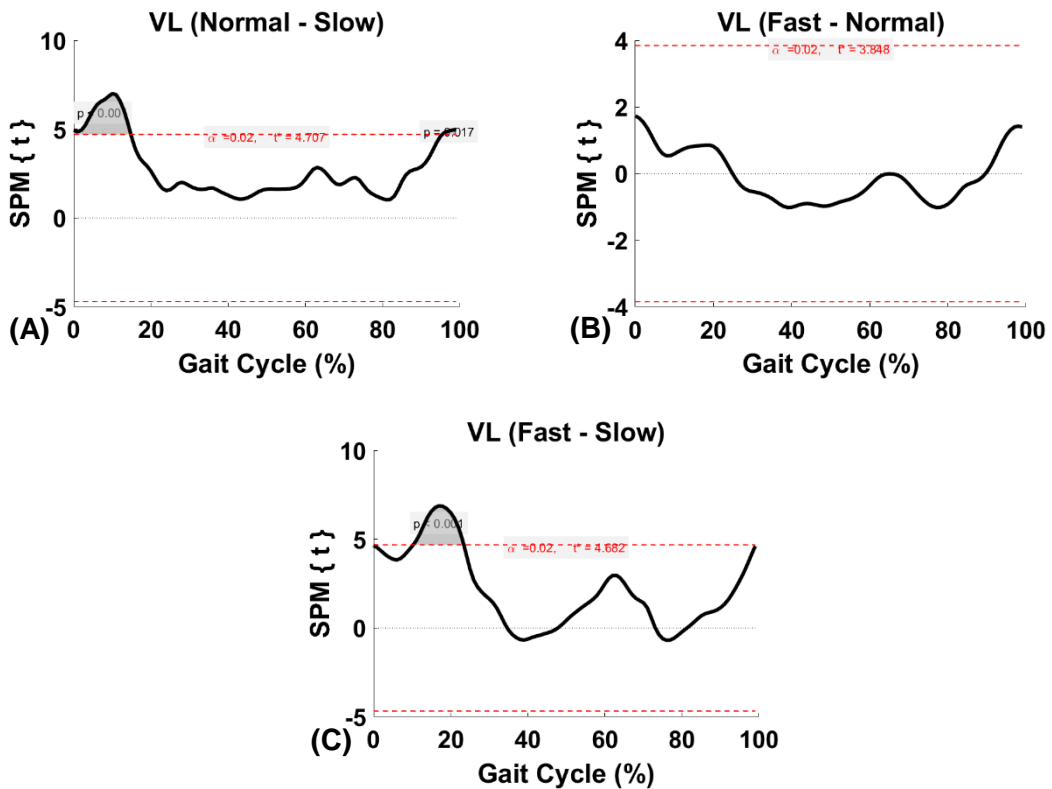


Figure 3.24: HS VL within-subject post hoc paired t statistic between speeds. The red dashed lines indicate critical thresholds of $t^* = 4.71$, 4.55 and 4.68 for (A), (B), and (C), respectively. Suprathreshold clusters are shown in grey where $p < 0.02$.

HS BFLH

As shown in Figure 3.25, SPM analysis revealed two suprathreshold clusters between three speeds in BFLH intra-subjectively at approximately 16-19% ($p=0.032$) and 82-100% ($p=0.00$) GC. In post hoc paired t-tests, significant differences occurred between normal-slow at 90-91% ($p=0.025$) and fast-slow at 85-94% ($p=0.00$) GC (Figure 3.26).

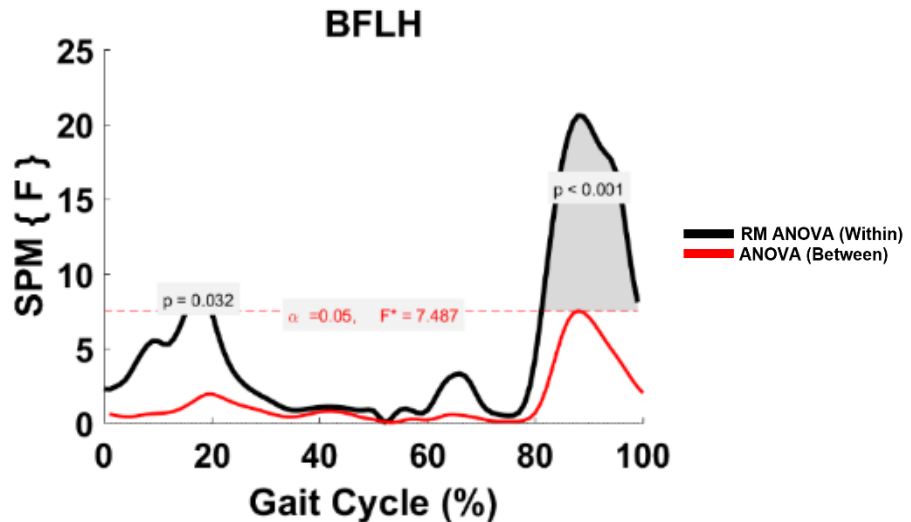


Figure 3.25: HS BFLH parametric RM ANOVA within- and between-subjects, depicting significant differences between speeds. The horizontal red dotted line indicates the critical threshold of 7.487. Suprathreshold clusters are shown in grey where $p < 0.05$.

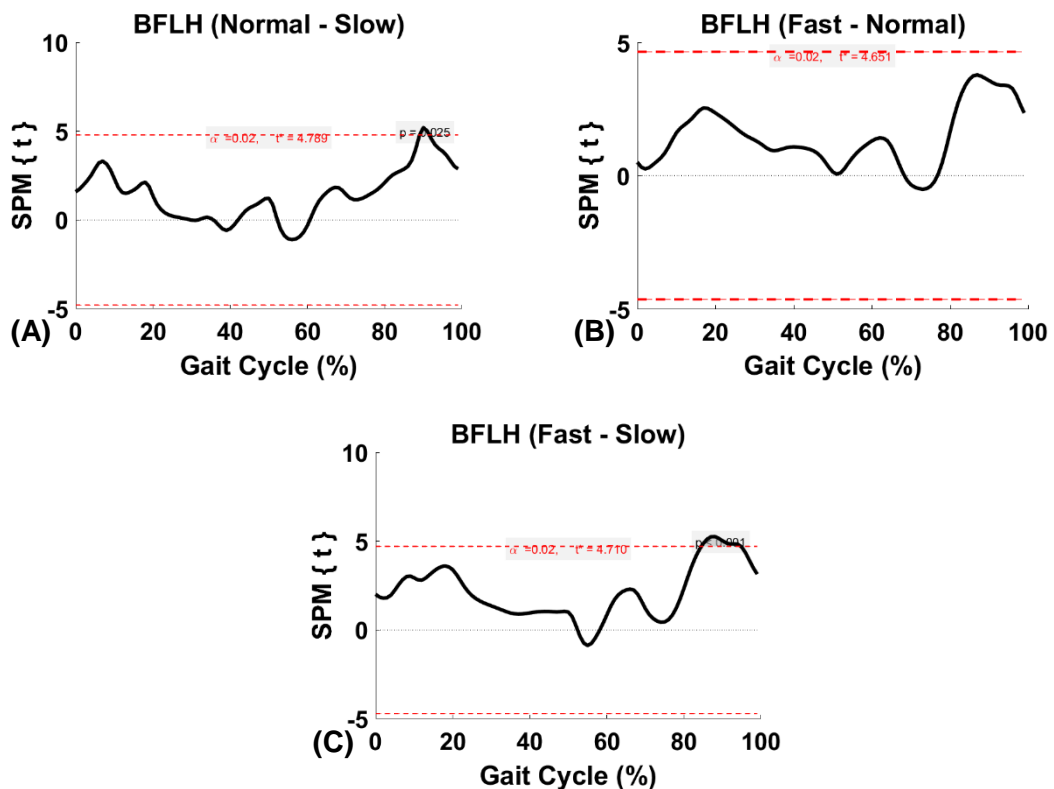


Figure 3.26: HS BFLH within-subject post hoc paired t statistic between speeds. The red dashed lines indicate critical thresholds of $t^* = 4.79$, 4.65 and 4.71 for (A), (B), and (C), respectively. Suprathreshold clusters are shown in grey where $p < 0.02$.

HS SEM

As shown in Figure 3.27, SPM analysis revealed one suprathreshold cluster between three speeds in SEM intra-subjectively at approximately 87-93% ($p=0.021$) GC. Post hoc test showed no significant difference between speeds (Figure 3.28).

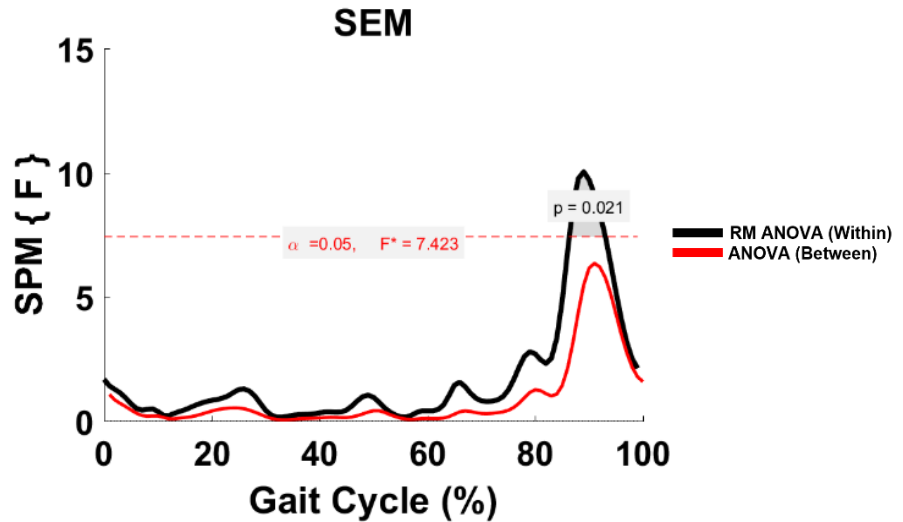


Figure 3.27: HS SEM parametric RM ANOVA within- and between-subjects, depicting significant differences between speeds. The horizontal red dotted line indicates the critical threshold of 7.423. Suprathreshold clusters are shown in grey where $p < 0.05$.

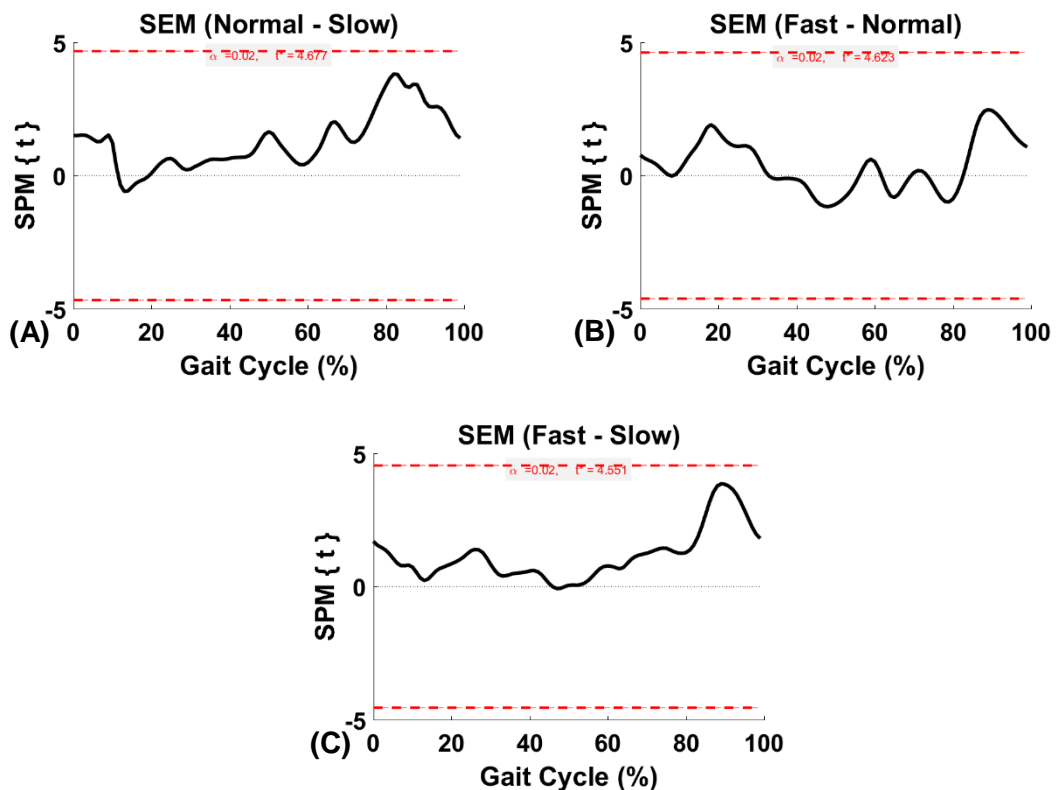


Figure 3.28: HS SEM within-subject post hoc paired t statistic between speeds. The red dashed lines indicate critical thresholds of $t^* = 4.68$, 4.62 and 4.55 for (A), (B), and (C), respectively. Suprathreshold clusters are shown in grey where $p < 0.02$.

HS TFL

As shown in Figure 3.29, SPM analysis revealed three suprathreshold clusters between three speeds in TFL intra-subjectively at approximately 4-17% ($p=0.00$), 66-69% ($p=0.026$) and 95-100% ($p=0.025$) GC. In Post hoc paired t-test, a significant difference was observed between normal-slow at 4-9% ($p=0.00$) GC (Figure 3.30).

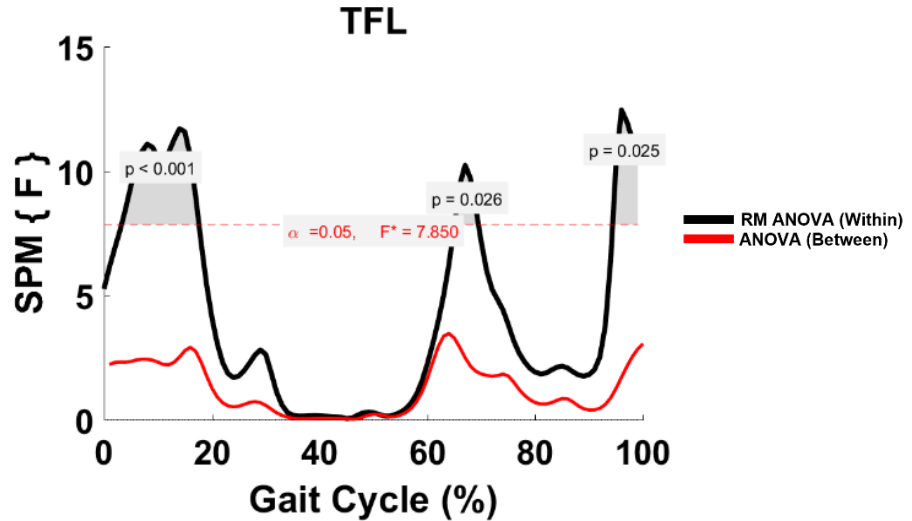


Figure 3.29: HS TFL parametric RM ANOVA within- and between-subjects, depicting significant differences between speeds. The horizontal red dotted line indicates the critical threshold of 7.850. Suprathreshold clusters are shown in grey where $p < 0.05$.

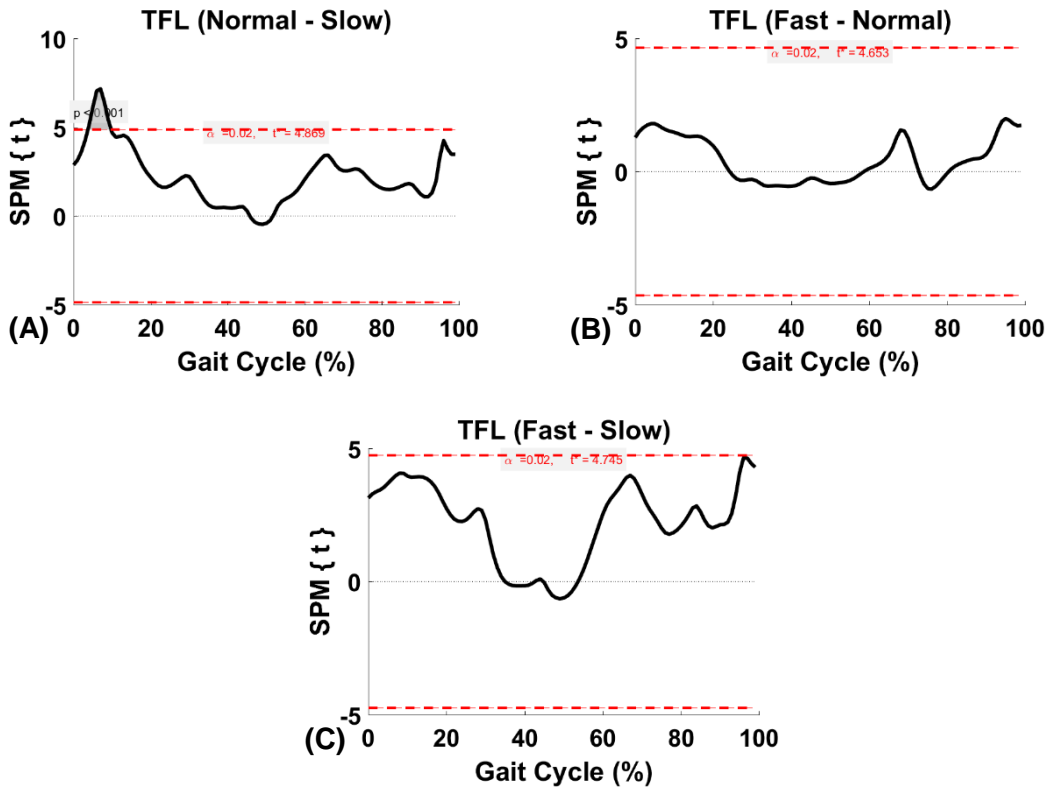


Figure 3.30: HS TFL within-subject post hoc paired t statistic between speeds. The red dashed lines indicate critical thresholds of $t^* = 4.87, 4.65$ and 4.75 for (A), (B), and (C), respectively. Suprathreshold clusters are shown in grey where $p < 0.02$.

HS TA

As shown in Figure 3.31, SPM analysis revealed three suprathreshold clusters between three speeds in TA intra-subjectively at approximately 0-10% ($p=0.008$), 55-67% ($p=0.003$) and 92-100% ($p=0.019$) GC. In Post hoc paired t-test, significant differences were observed between fast-slow at 5-7% ($p=0.039$), 59-61% ($p=0.029$) and 97-100% ($p=0.037$) GC (Figure 3.32).

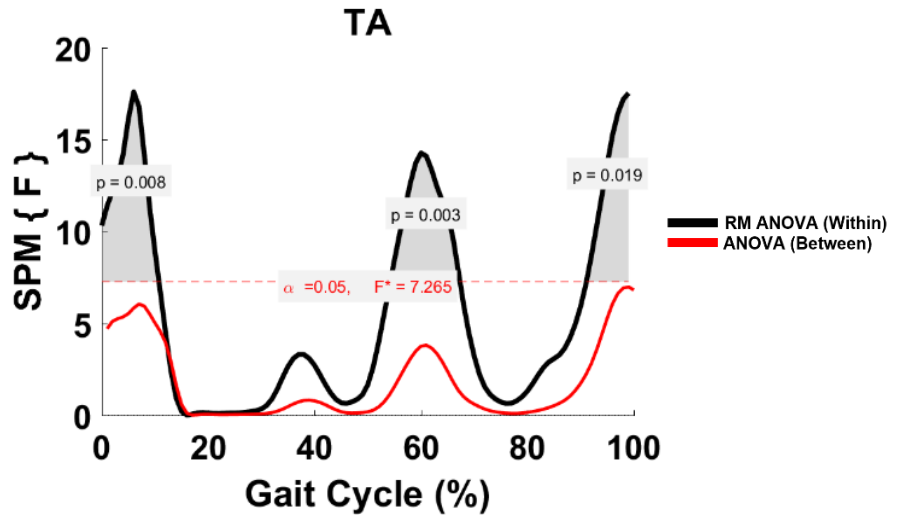


Figure 3.31: HS TA parametric RM ANOVA within- and between-subjects, depicting significant differences between speeds. The horizontal red dotted line indicates the critical threshold of 7.265. Suprathreshold clusters are shown in grey where $p < 0.05$.

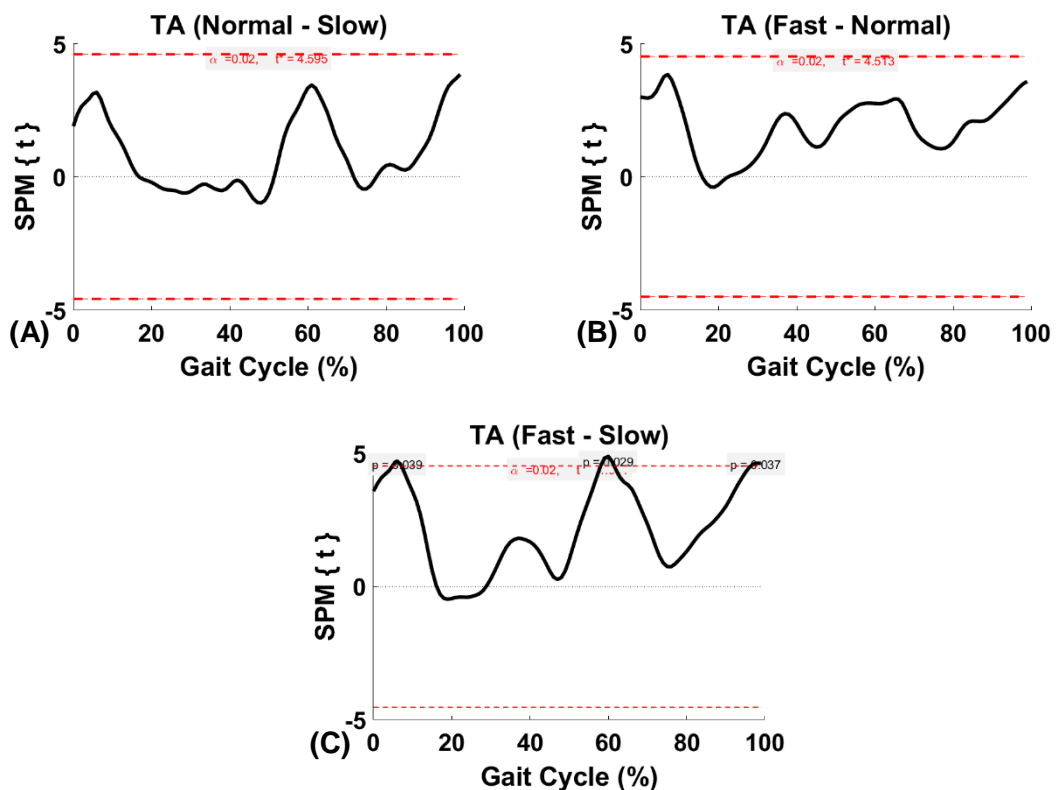


Figure 3.32: HS TA within-subject post hoc paired t statistic between speeds. The red dashed lines indicate critical thresholds of $t^* = 4.60$, 4.51 and 4.69 for (A), (B), and (C), respectively. Suprathreshold clusters are shown in grey where $p < 0.02$.

HS GM

As shown in Figure 3.33, SPM analysis revealed one suprathreshold cluster between three speeds in GM intra-subjectively at approximately 34-39% ($p=0.001$) GC. No significant difference was observed in the post hoc paired t-test (Figure 3.34).

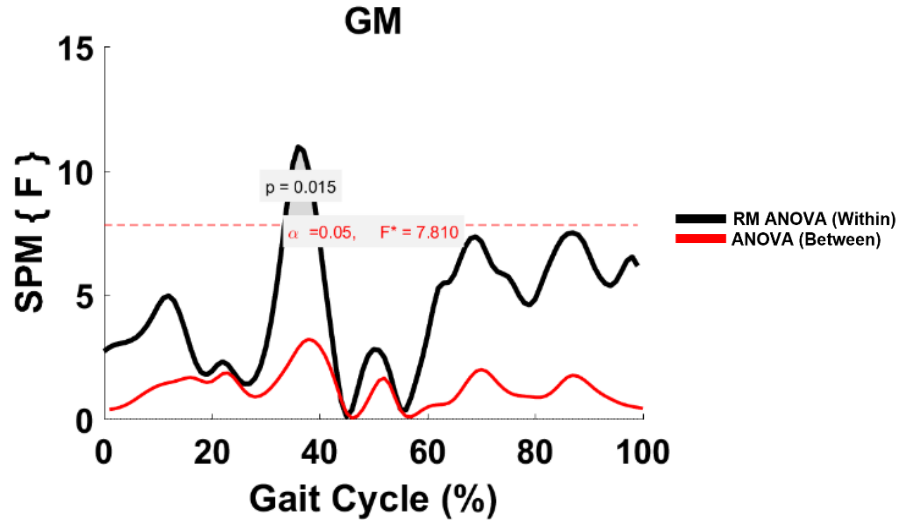


Figure 3.33: HS GM parametric RM ANOVA within- and between-subjects, depicting significant differences between speeds. The horizontal red dotted line indicates the critical threshold of 7.810. Suprathreshold clusters are shown in grey where $p < 0.05$.

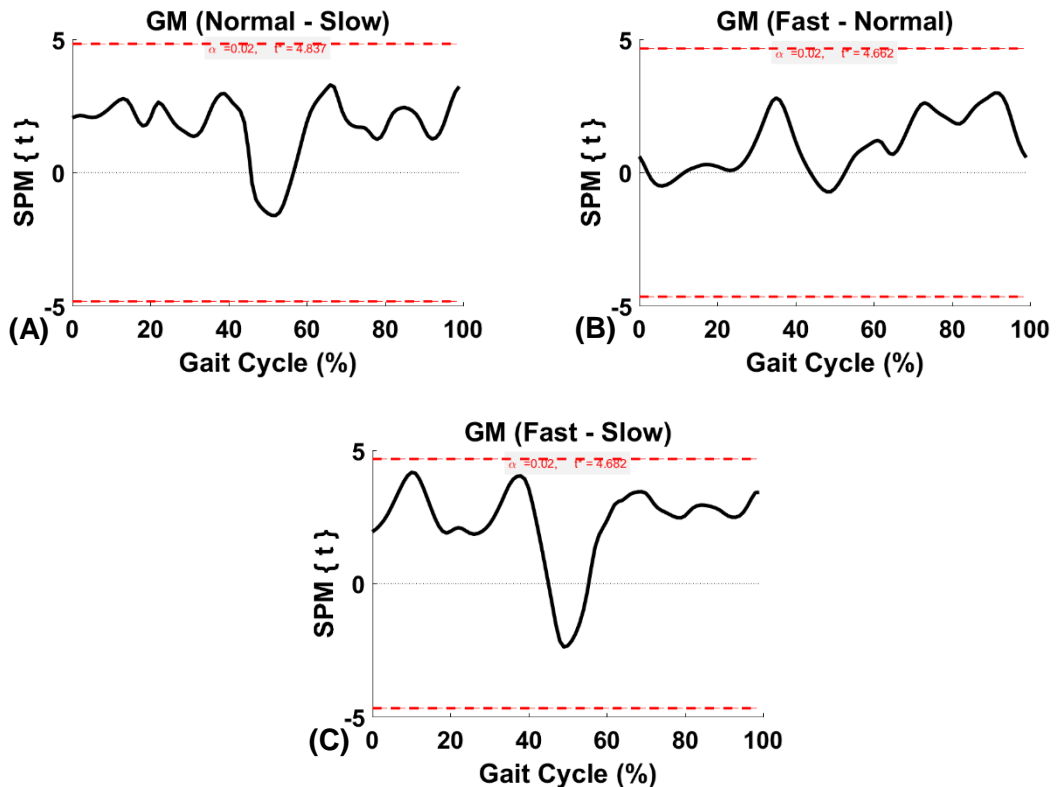


Figure 3.34: HS GM within-subject post hoc paired t statistic between speeds. The red dashed lines indicate critical thresholds of $t^* = 4.84$, 4.66 and 4.68 for (A), (B), and (C), respectively. Suprathreshold clusters are shown in grey where $p < 0.02$.

HS GL

As shown in Figure 3.35, SPM analysis revealed three suprathreshold clusters between three speeds in GL intra-subjectively at approximately 0-8% ($p=0.008$), 33-42% ($p=0.005$) and 99-100% ($p=0.049$) GC. In Post hoc paired t-test, a significant difference was observed between fast-slow at 35-40% ($p=0.007$) GC (Figure 3.36).

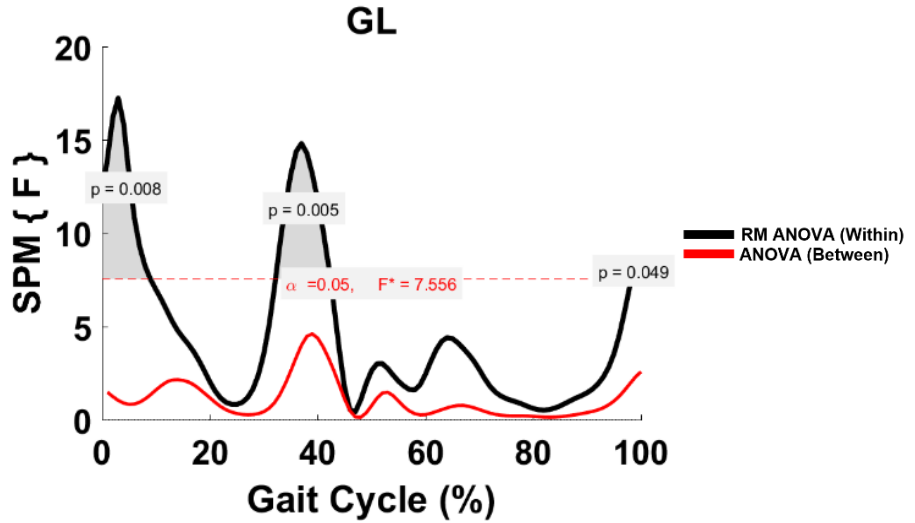


Figure 3.35: HS GL parametric RM ANOVA within- and between-subjects, depicting significant differences between speeds. The horizontal red dotted line indicates the critical threshold of 7.556. Suprathreshold clusters are shown in grey where $p < 0.05$.

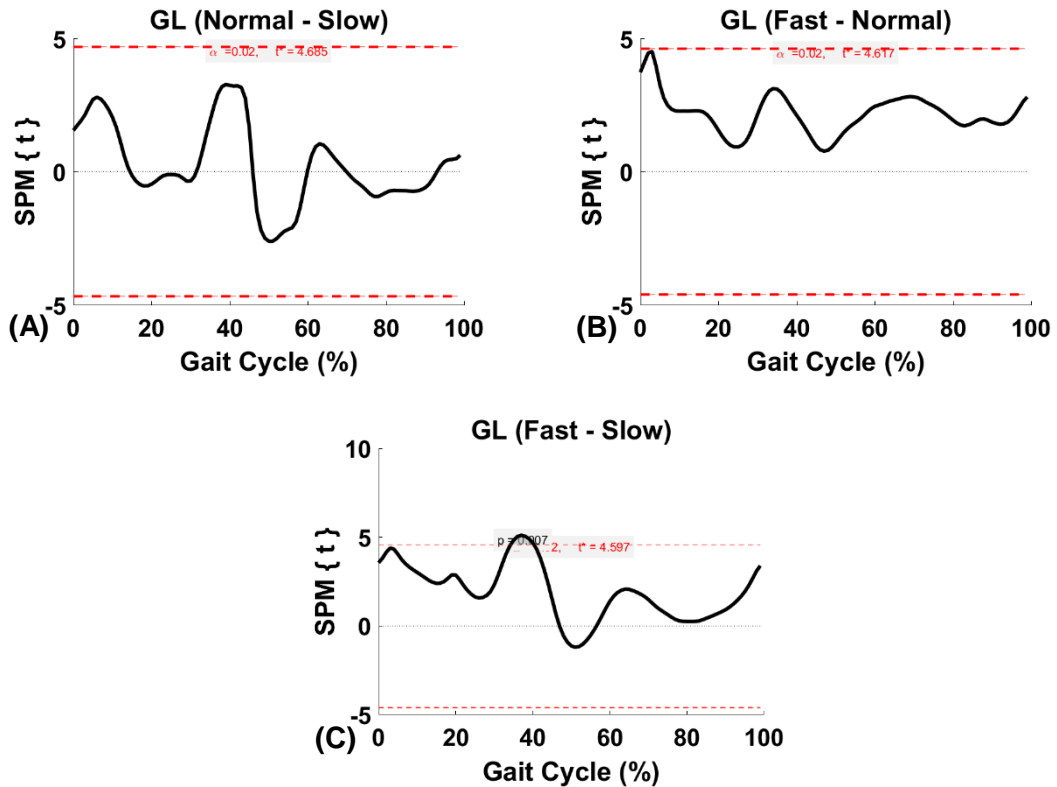


Figure 3.36: HS GL within-subject post hoc paired t statistic between speeds. The red dashed lines indicate critical thresholds of $t^* = 4.69$, 4.62 and 4.60 for (A), (B), and (C), respectively. Suprathreshold clusters are shown in grey where $p < 0.02$.

HS SOL

As shown in Figure 3.37, SPM analysis revealed three suprathreshold clusters between three speeds in SOL intra-subjectively at approximately 7-13% ($p=0.014$), 30-44% ($p=0.00$) and 98-100% ($p=0.046$) GC. In Post hoc paired t-test, a significant difference was observed between fast-slow at 34-36% ($p=0.025$) GC (Figure 3.38).

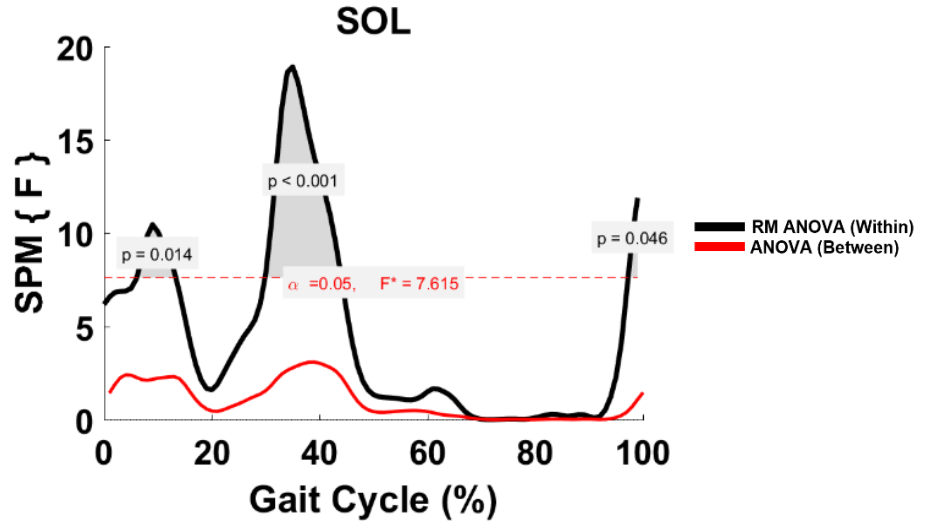


Figure 3.37: HS SOL parametric RM ANOVA within- and between-subjects, depicting significant differences between speeds. The horizontal red dotted line indicates the critical threshold of 7.615. Suprathreshold clusters are shown in grey where $p<0.05$.

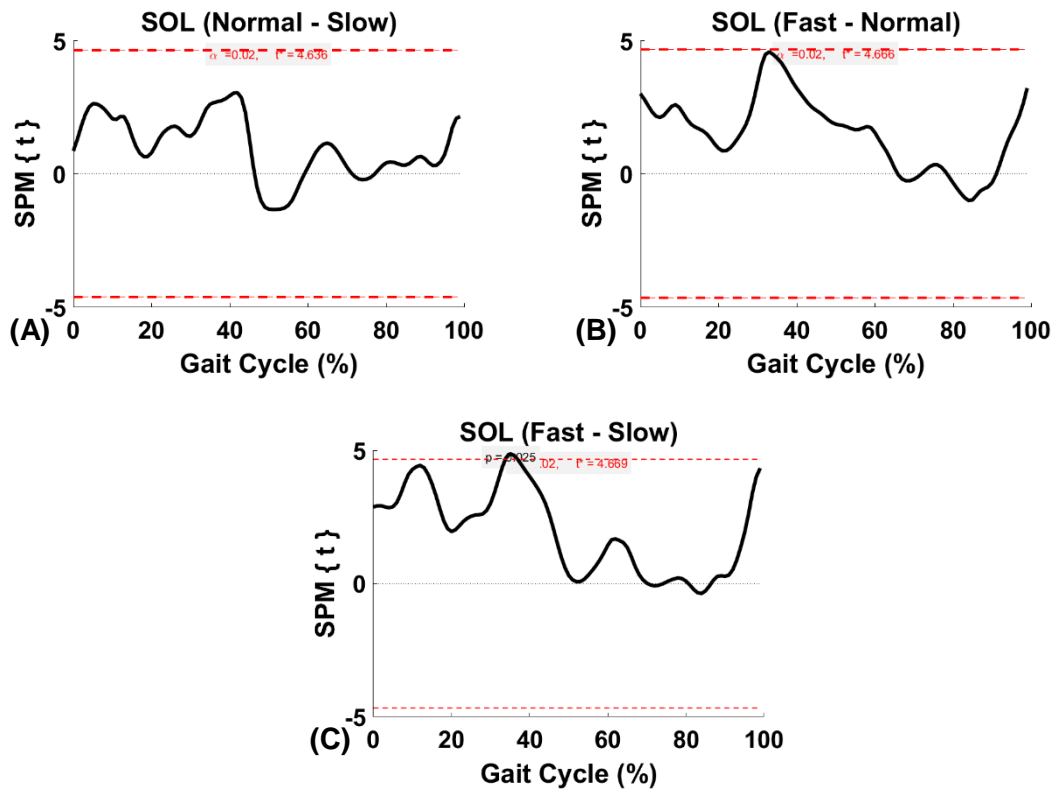


Figure 3.38: HS SOL within-subject post hoc paired t statistic between speeds. The red dashed lines indicate critical thresholds of $t^* = 4.64$, 4.67 and 4.67 for (A), (B), and (C), respectively. Suprathreshold clusters are shown in grey where $p<0.02$.

Speed Dependence of the TFA Muscles

TFA RF

As shown in Figure 3.39, statistically significant differences occurred in TFA RF across speeds. Two suprathreshold clusters were found at 0-15% ($p=0.000$) and 92-100% ($p=0.007$) GC intra-subjectively. Post hoc paired t-test revealed RF was significantly greater between fast-normal at approximately 5-10% ($p=0.003$) GC and between fast-slow at 3-12% ($p=0.000$) and 92-100% ($p=0.001$) (Figure 3.40).

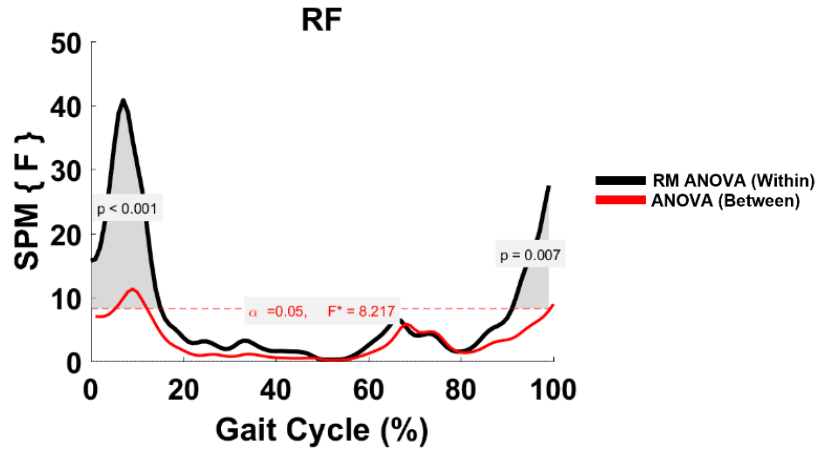


Figure 3.39: TFA RF parametric RM ANOVA within- and between-subjects, depicting significant differences between speeds. The horizontal red dotted line indicates the critical threshold of 8.217. Suprathreshold clusters are shown in grey where $p < 0.05$.

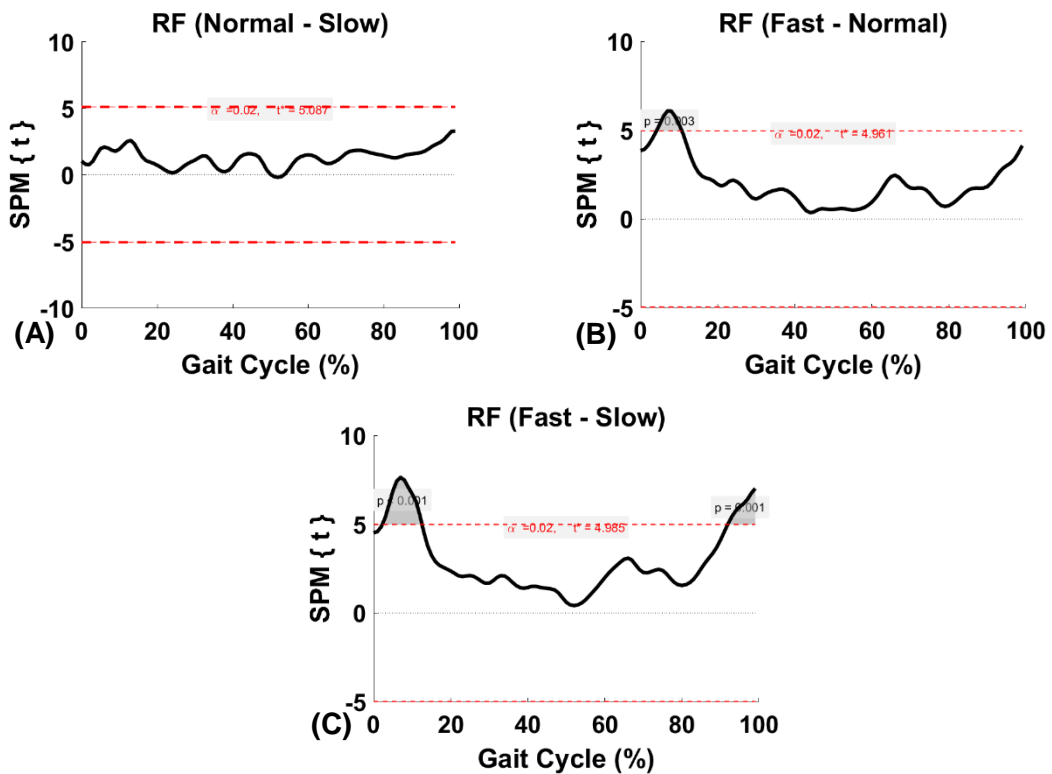


Figure 3.40: TFA RF within-subject post hoc paired t statistic between speeds. The red dashed lines indicate critical thresholds of $t^* = 5.09$, 4.96 and 4.99 for (A), (B), and (C), respectively. Suprathreshold clusters are shown in grey where $p < 0.02$.

TFA VM

As shown in Figure 3.41, SPM analysis revealed three suprathreshold clusters between three speeds in VM intra-subjectively at approximately 0-17% ($p=0.00$), 69-74% ($p=0.010$) and 92-100% ($p=0.004$) GC. Post hoc paired t-test was conducted between speeds where significant differences occurred between fast-normal at 93-95% ($p=0.022$) and fast-slow at 0-1% ($p=0.040$) and 93-100% ($p=0.000$) GC (Figure 3.42).

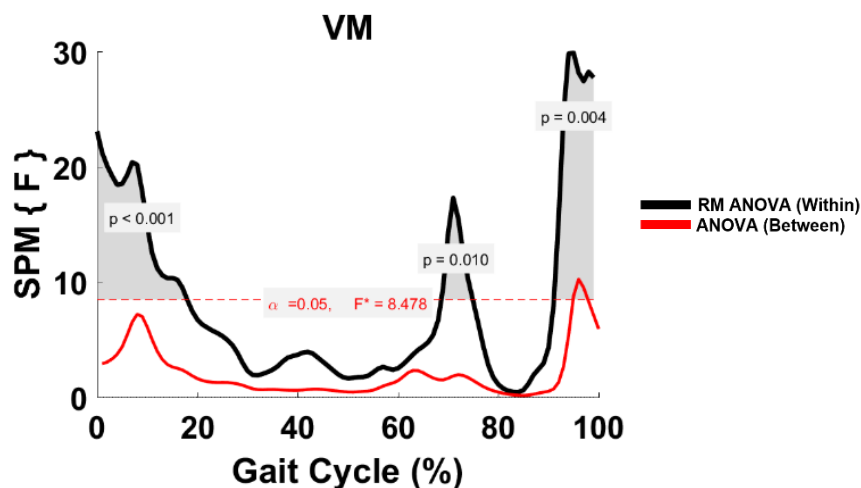


Figure 3.41: TFA VM parametric RM ANOVA within- and between-subjects, depicting significant differences between speeds. The horizontal red dotted line indicates the critical threshold of 8.478. Suprathreshold clusters are shown in grey where $p < 0.05$.

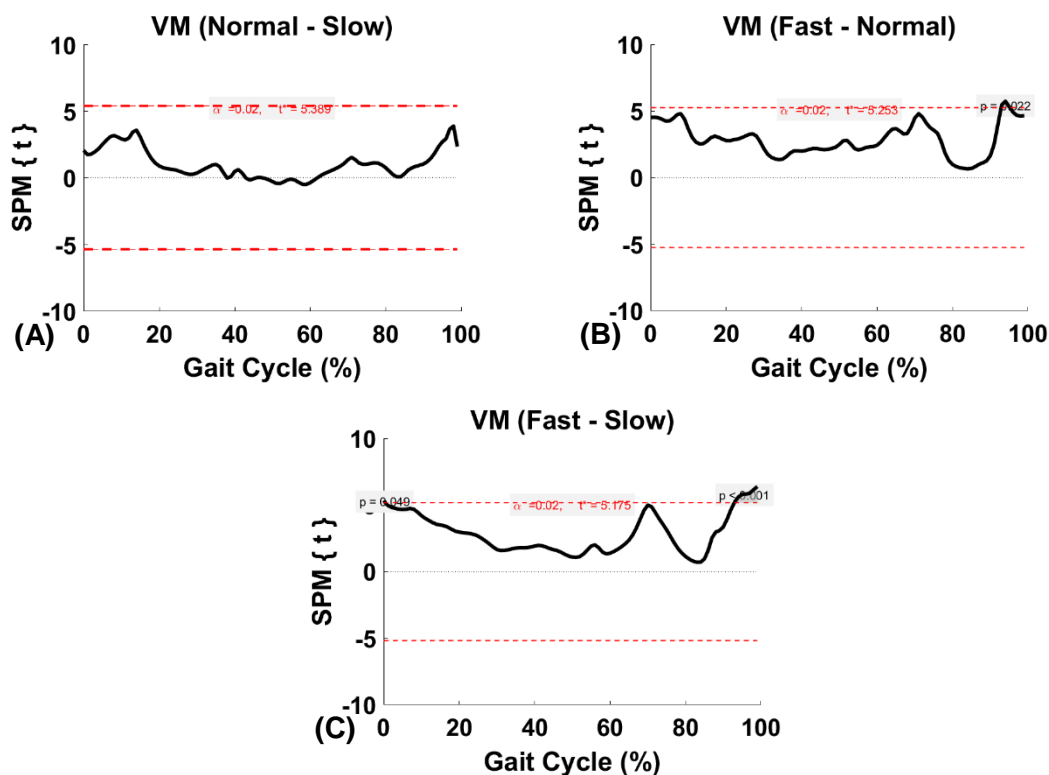


Figure 3.42: TFA VM within-subject post hoc paired t statistic between speeds. The red dashed lines indicate critical thresholds of $t^* = 5.39$, 4.25 and 5.18 for (A), (B), and (C), respectively. Suprathreshold clusters are shown in grey where $p < 0.02$.

TFA VL

As shown in Figure 3.43, SPM analysis revealed two suprathreshold clusters between three speeds in VL intra-subjectively at approximately 0-20% ($p=0.00$) and 93-100% ($p=0.019$) GC. In post hoc paired t-test, significant differences were observed between fast-slow at 0-13% ($p=0.000$), 19-21% ($p=0.032$), and 92-100% ($p=0.000$) GC (Figure 3.44).

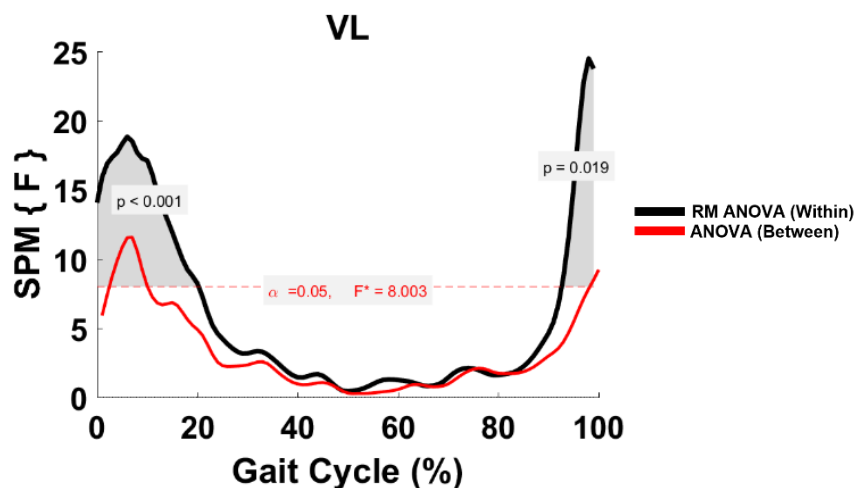


Figure 3.43: TFA VL parametric RM ANOVA within- and between-subjects, depicting significant differences between speeds. The horizontal red dotted line indicates the critical threshold of 8.003. Suprathreshold clusters are shown in grey where $p < 0.05$.

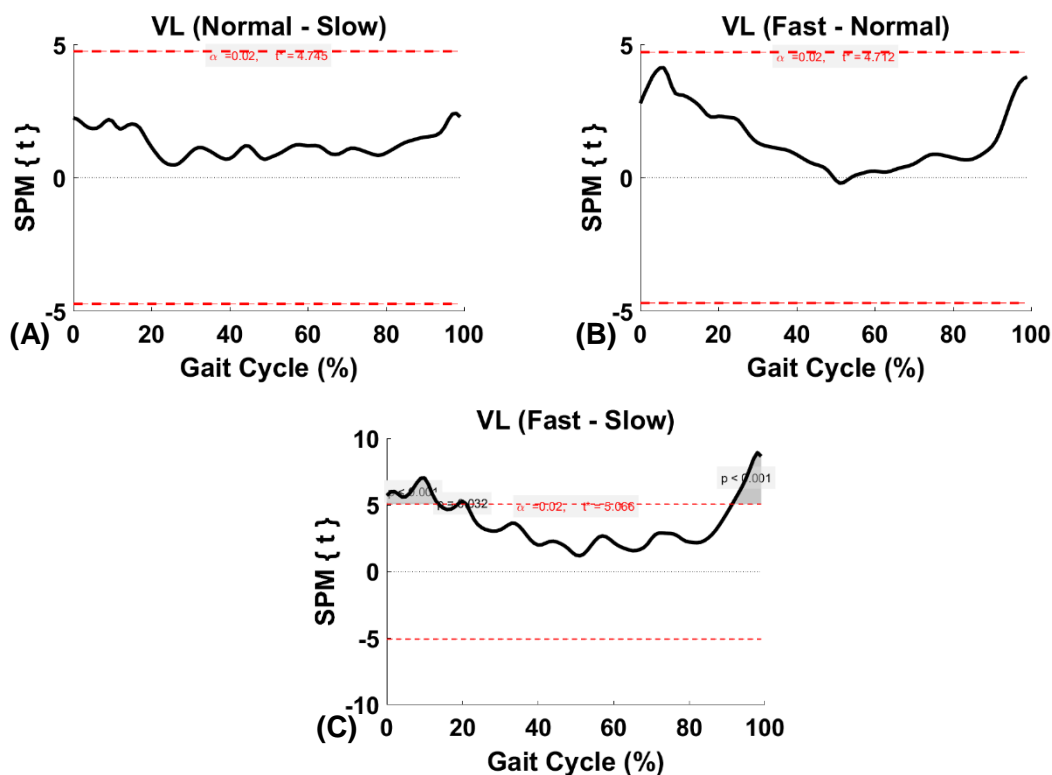


Figure 3.44: TFA VL within-subject post hoc paired t statistic between speeds. The red dashed lines indicate critical thresholds of $t^* = 4.75$, 4.71 and 5.07 for (A), (B), and (C), respectively. Suprathreshold clusters are shown in grey where $p < 0.02$.

TFA BFLH

As shown in Figure 3.45, SPM analysis revealed two suprathreshold clusters between three speeds in BFLH intra-subjectively at approximately 87-95% ($p=0.001$) GC. In post hoc paired t-test, significant differences occurred between fast-normal at 89-91% ($p=0.020$) GC (Figure 3.46).

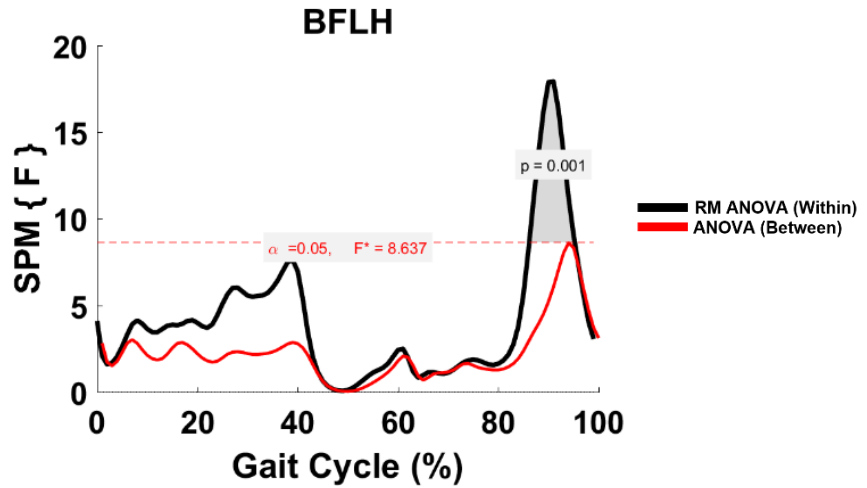


Figure 3.45: TFA BFLH parametric RM ANOVA within- and between-subjects, depicting significant differences between speeds. The horizontal red dotted line indicates the critical threshold of 8.637. Suprathreshold clusters are shown in grey where $p < 0.05$.

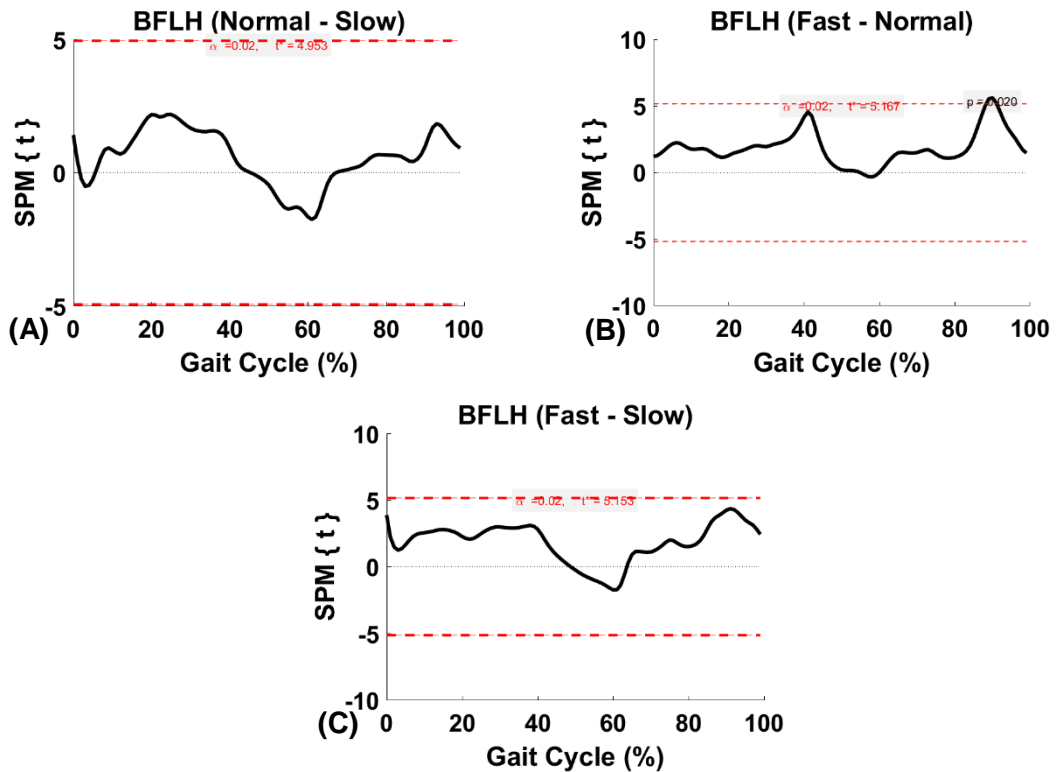


Figure 3.46: TFA BFLH within-subject post hoc paired t statistic between speeds. The red dashed lines indicate critical thresholds of $t^* = 4.953$, 5.167 and 5.153 for (A), (B), and (C), respectively. Suprathreshold clusters are shown in grey where $p < 0.02$.

TFA TA

As shown in Figure 3.47, SPM analysis revealed three suprathreshold clusters between three speeds in TA intra-subjectively at approximately 0-3% ($p=0.033$), 42-43% ($p=0.044$) and 94-98% ($p=0.019$) GC. No differences were found in post hoc analyses within-subject even though the main SPM analysis showed significant differences (Figure 3.48). The null hypothesis was answered completely by the main RM ANOVA.

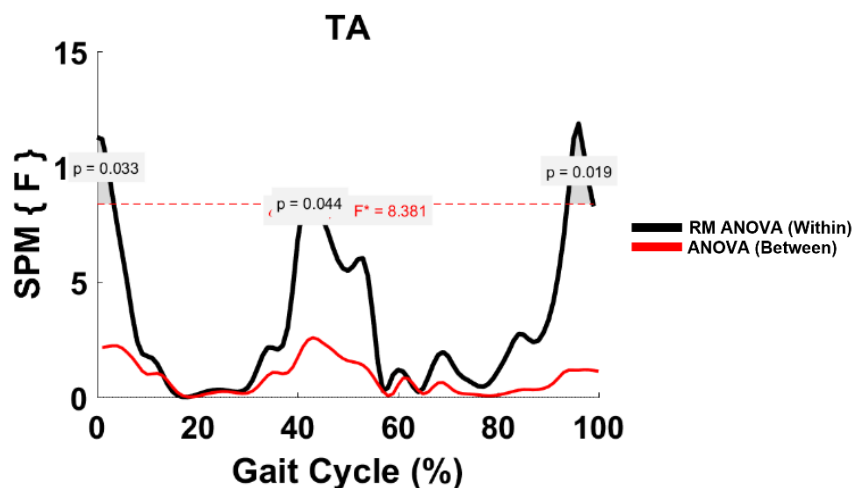


Figure 3.47: TFA TA parametric RM ANOVA within- and between-subjects, depicting significant differences between speeds. The horizontal red dotted line indicates the critical threshold of 8.381. Suprathreshold clusters are shown in grey where $p < 0.05$.

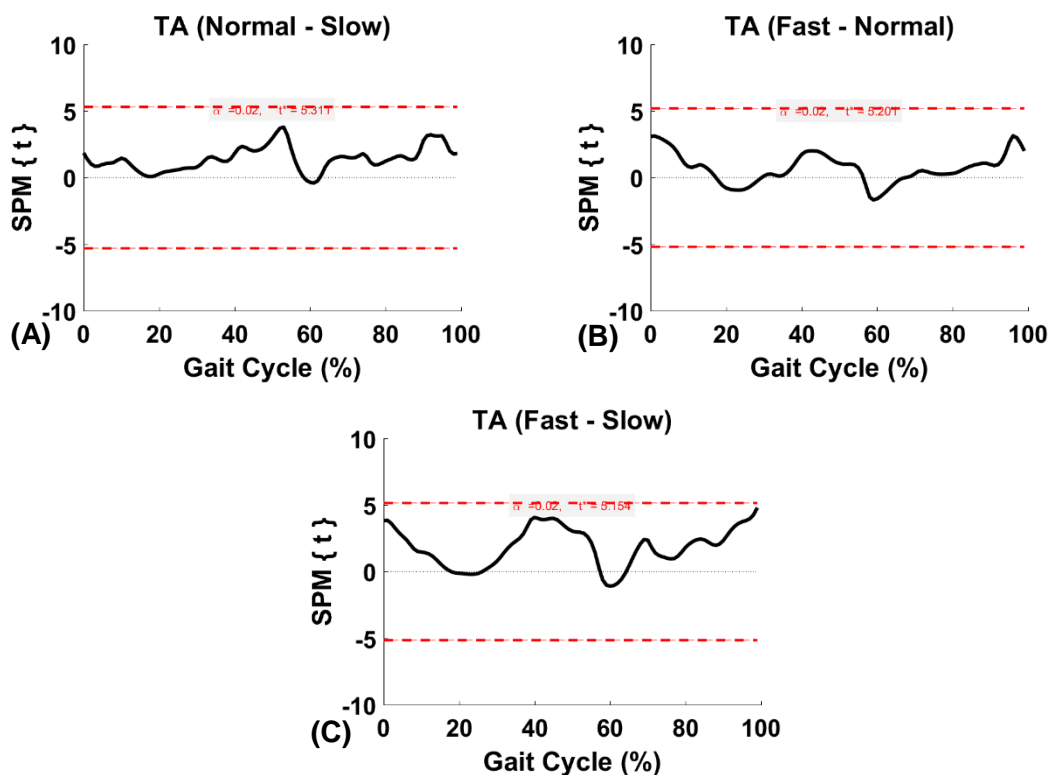


Figure 3.48: TFA TA within-subject post hoc paired t statistic between speeds. The red dashed lines indicate critical thresholds of $t^* = 5.31$, 5.20 and 5.15 for (A), (B), and (C), respectively. Suprathreshold clusters are shown in grey where $p < 0.02$.

TFA GM

As shown in Figure 3.49, SPM analysis revealed three suprathreshold clusters between three speeds in GM intra-subjectively at approximately 3% ($p=0.018$), 11-19% ($p=0.004$) and 46-56% ($p=0.00$) GC. In Post hoc paired t-test, a significant difference was observed between fast-slow at 47-55% ($p=0.00$) GC (Figure 3.50).

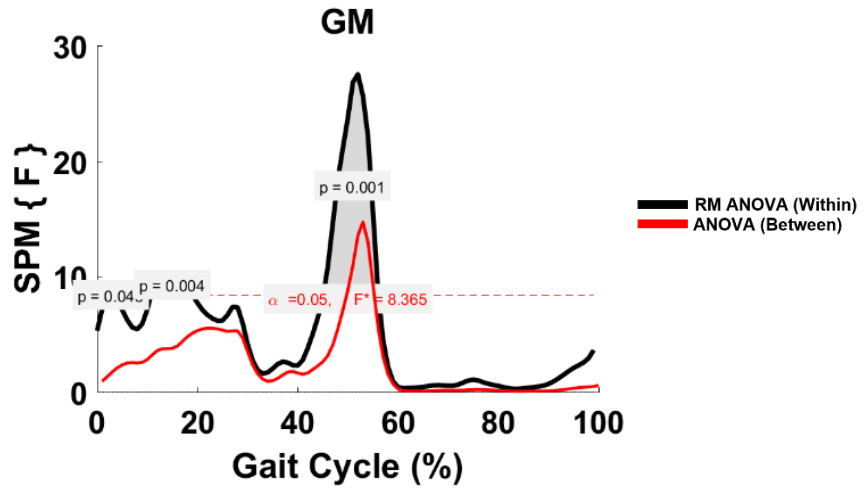


Figure 3.49: TFA GM parametric RM ANOVA within- and between-subjects, depicting significant differences between speeds. The horizontal red dotted line indicates the critical threshold of 7.365. Suprathreshold clusters are shown in grey where $p < 0.05$.

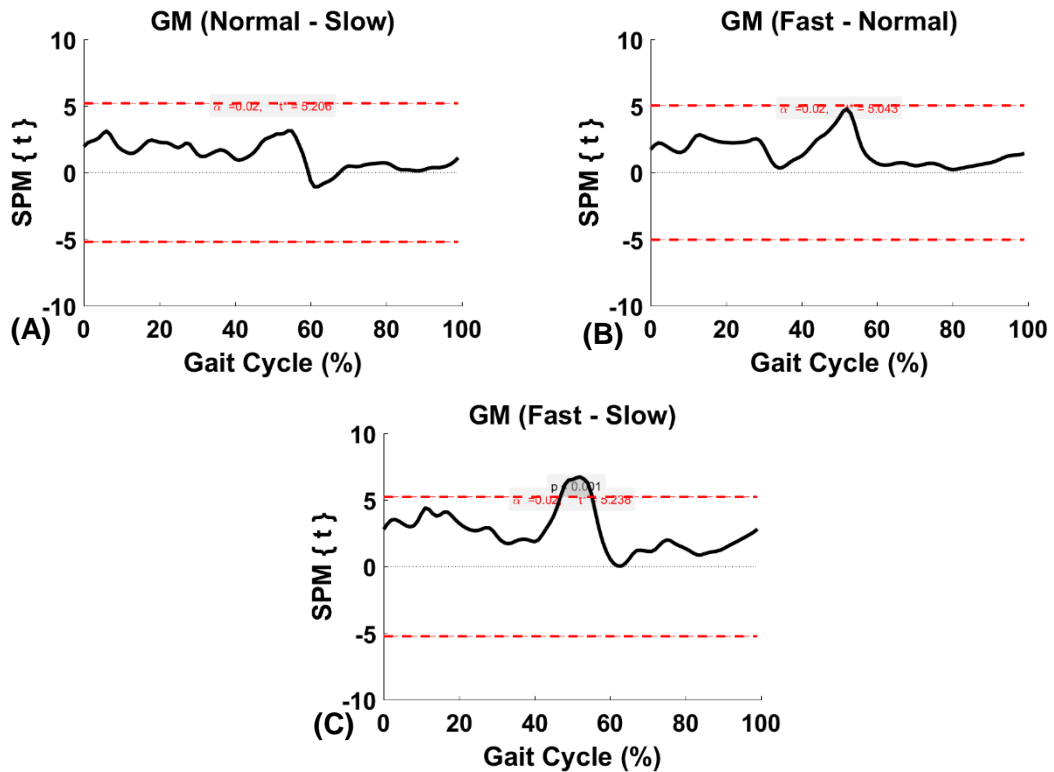


Figure 3.50: TFA GM within-subject post hoc paired t statistic between speeds. The red dashed lines indicate critical thresholds of $t^* = 5.21$, 5.04 and 4.24 for (A), (B), and (C), respectively. Suprathreshold clusters are shown in grey where $p < 0.02$.

TFA GL

As shown in Figure 3.51, SPM analysis revealed three suprathreshold clusters between three speeds in GL intra-subjectively at approximately 26-30% ($p=0.034$) and 47-55% ($p=0.008$) GC. In post hoc paired t-test, a significant difference was observed between fast-slow at 51-54% ($p=0.006$) GC (Figure 3.52).

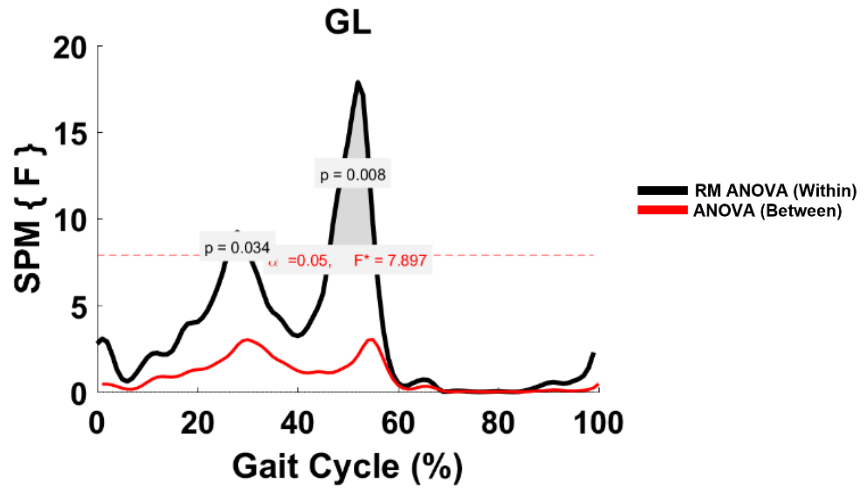


Figure 3.51: TFA GL parametric RM ANOVA within- and between-subjects, depicting significant differences between speeds. The horizontal red dotted line indicates the critical threshold of 7.897. Suprathreshold clusters are shown in grey where $p < 0.05$.

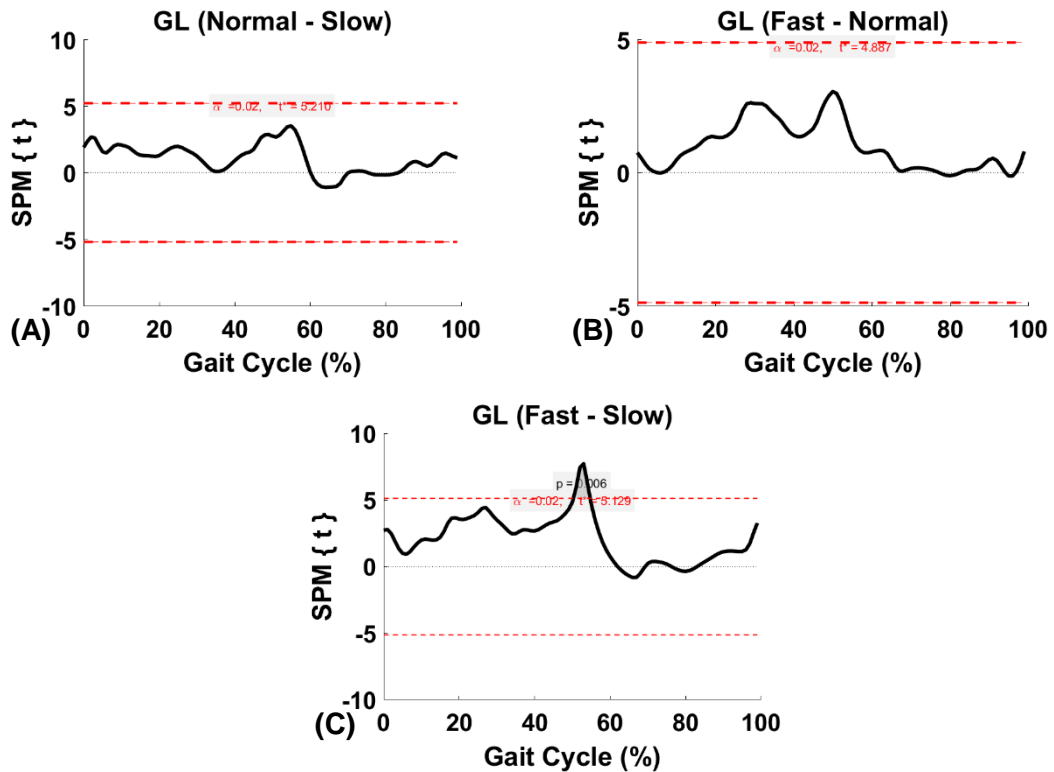


Figure 3.52: TFA GL within-subject post hoc paired t statistic between speeds. The red dashed lines indicate critical thresholds of $t^* = 5.21$, 4.89 and 5.13 for (A), (B), and (C), respectively. Suprathreshold clusters are shown in grey where $p < 0.02$.

TFA SEM, TFL, and SOL

No significant differences were found in SEM (Figure 3.53), TFL (Figure 3.54) and SOL (Figure 3.55) across speeds intra-subjectively.

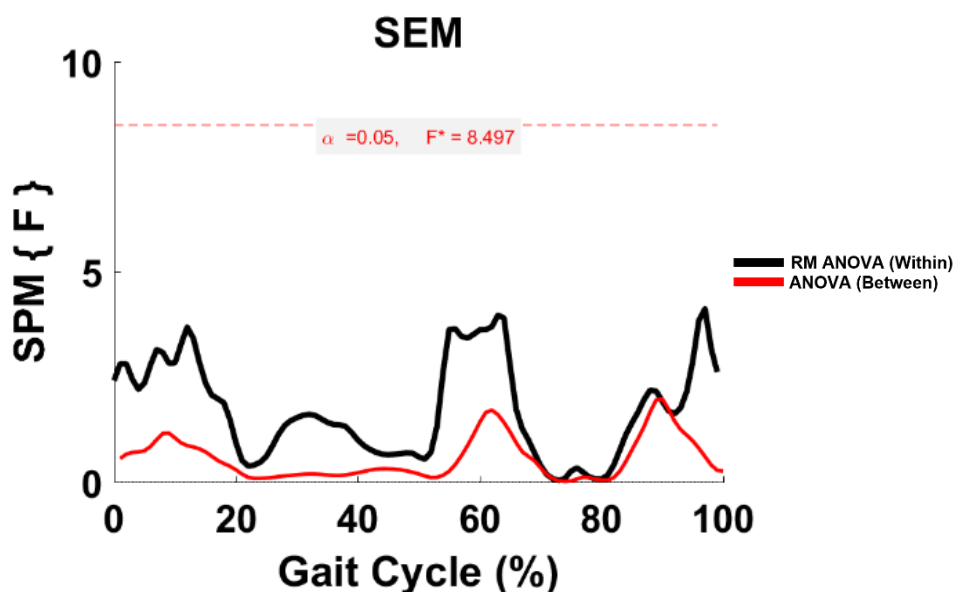


Figure 3.53: TFA SEM parametric RM ANOVA within- and between-subjects, depicting significant differences between speeds. The horizontal red dotted line indicates the critical threshold of 8.497. Suprathreshold clusters are shown in grey where $p < 0.05$.

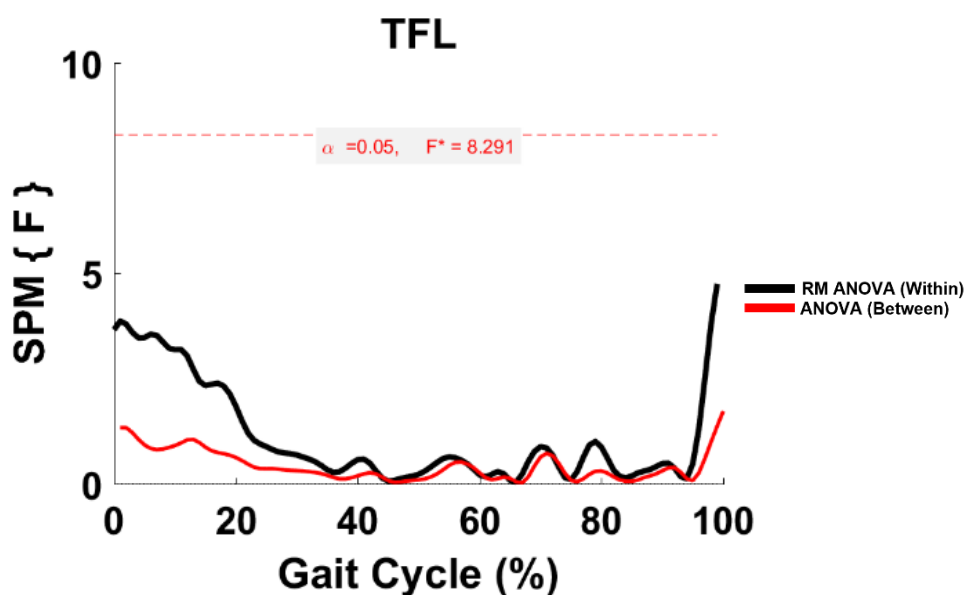


Figure 3.54: TFA TFL parametric RM ANOVA within- and between-subjects, depicting significant differences between speeds. The horizontal red dotted line indicates the critical threshold of 8.291. Suprathreshold clusters are shown in grey where $p < 0.05$.

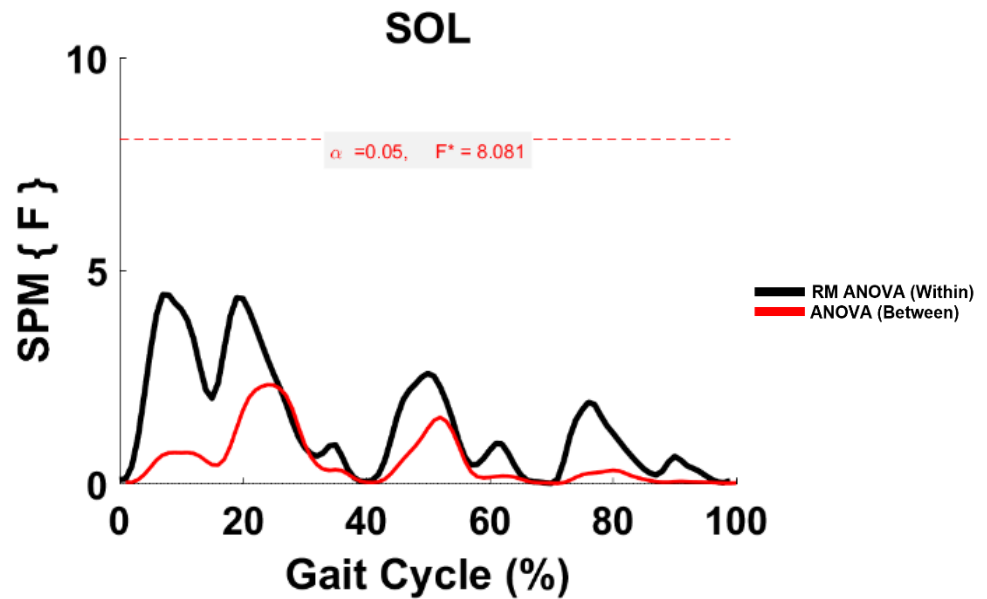


Figure 3.55: TFA SOL parametric RM ANOVA within- and between-subjects, depicting significant differences between speeds. The horizontal red dotted line indicates the critical threshold of 8.081. Suprathreshold clusters are shown in grey where $p < 0.05$.

3.3.2.3 Between-Subject (Biomechanics Perspective)

A *priori* hypothesis accounted for individual speed as a different task under the walking control between-subject. Therefore, the effect of groups on HD EMG profiles of functionally related muscles contributed to biomechanical subtasks of gait as well as all muscles that contribute to co-contraction of ankle and knee joints during walking was compared at each speed category. Consequently, Hotelling's T^2 was implemented for hypothesis 5 (a-f).

HS vs. TFA HD Module 1 (Slow)

As shown in Figure 3.56, no significant differences were observed between HD M1 of HS and TFA at slow speed.

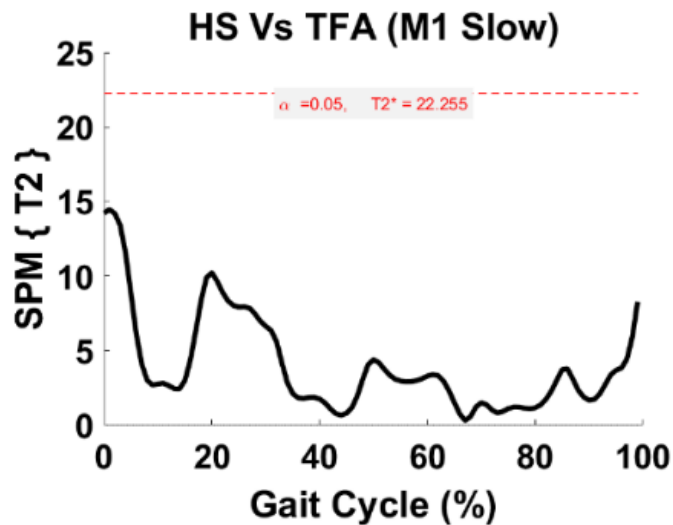


Figure 3.56: HD M1 SPM vector field result (Hotelling's T^2) depicting HS vs. TFA differences at slow speed. The red dashed line indicates critical threshold of $T2^*=22.255$. Suprathreshold clusters are shown in grey where $p<0.05$.

HS vs. TFA HD Module 2 (Slow)

As shown in Figure 3.57, SPM vector field found one suprathreshold cluster indicating a significant difference between HD M2 of HS and TFA at 53-61% during slow gait. Identically, smooth random 1D data would produce clusters of this breadth with a probability of $p=0.006$. Therefore, the null hypothesis was rejected as significant differences were observed between HS and TFA HD M2 in slow gait.

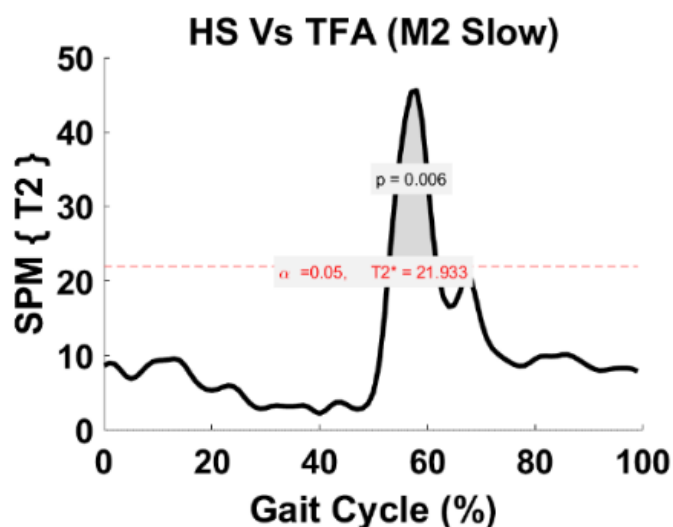


Figure 3.57: HD M2 SPM vector field result (Hotelling's T^2) depicting HS vs. TFA differences at slow speed. The red dashed line indicates critical threshold of $T2^*=21.933$. Suprathreshold clusters are shown in grey where $p<0.05$.

HS vs. TFA HD Module 3 (Slow)

As shown in Figure 3.58, no significant differences were observed between HD M3 of HS and TFA at slow speed.

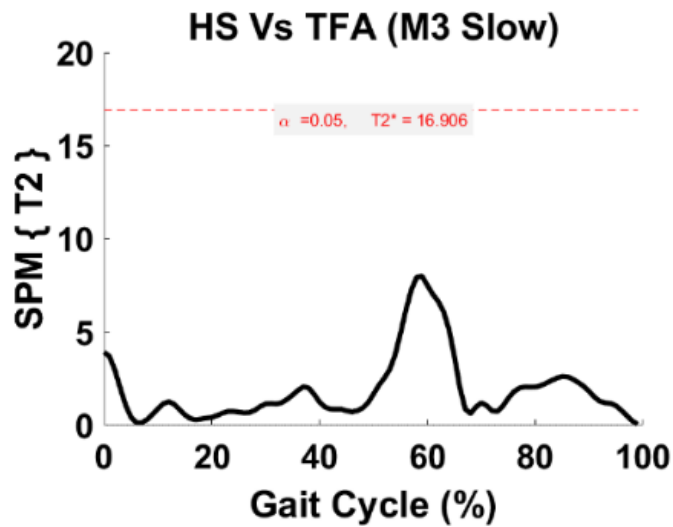


Figure 3.58: HD M3 SPM vector field result (Hotelling's T^2) depicting HS vs. TFA differences at slow speed. The red dashed line indicates critical threshold of $T2^*=16.906$. Suprathreshold clusters are shown in grey where $p<0.05$.

HS vs. TFA HD Module 4 (Slow)

As shown in Figure 3.59, no significant differences were observed between HD M4 of HS and TFA at slow speed.

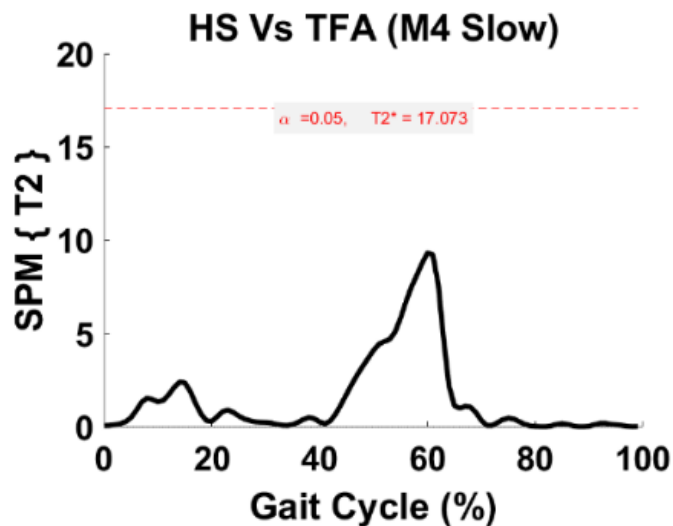


Figure 3.59: HD M4 SPM vector field result (Hotelling's T^2) depicting HS vs. TFA differences at slow speed. The red dashed line indicates critical threshold of $T2^*=17.073$. Suprathreshold clusters are shown in grey where $p<0.05$.

HS vs. TFA HD Ankle Co-Contraction (Slow)

As shown in Figure 3.60, SPM vector field found one suprathreshold cluster indicating a significant difference between ankle muscles of HS and TFA at 54-61% during slow gait. Identically, smooth random 1D data would produce clusters of this breadth with a probability of $p=0.009$. Therefore, the null hypothesis was rejected as significant differences were observed between HS and TFA HD M2 in slow gait.

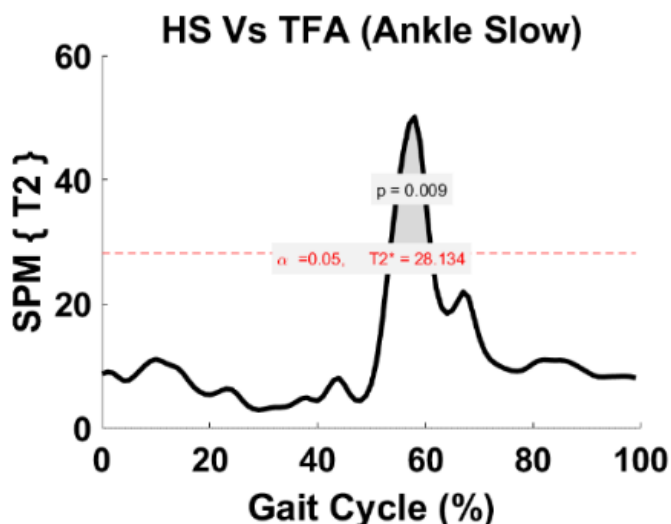


Figure 3.60: Ankle SPM vector field result (Hotelling's T^2) depicting HS vs. TFA differences at slow speed. The red dashed line indicates critical threshold of $T2^*=28.134$. Suprathreshold clusters are shown in grey where $p<0.05$.

HS vs. TFA HD Knee Co-Contraction (Slow)

As shown in Figure 3.61, no significant differences were observed between knee muscles of HS and TFA at slow speed.

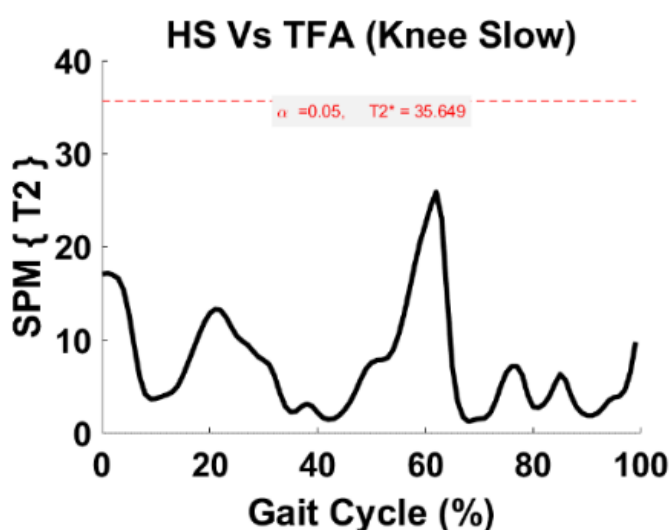


Figure 3.61: Knee SPM vector field result (Hotelling's T^2) depicting HS vs. TFA differences at slow speed. The red dashed line indicates critical threshold of $T2^*=35.649$. Suprathreshold clusters are shown in grey where $p<0.05$.

HS vs. TFA HD Module 1 (Normal)

As shown in Figure 3.62, no significant differences were observed between HD M1 of HS and TFA at normal speed.

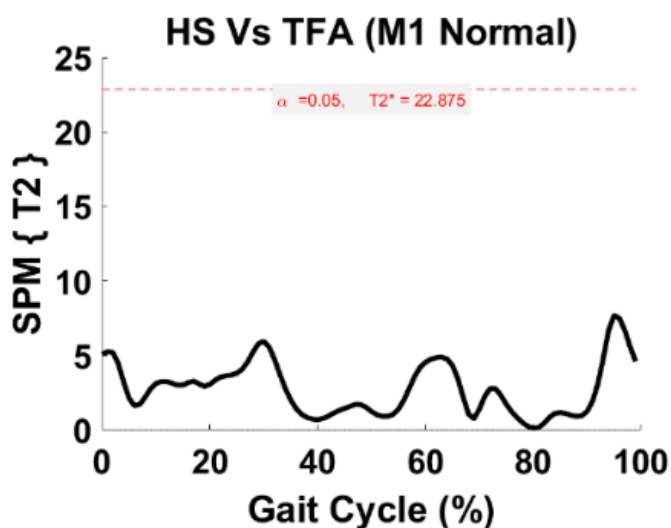


Figure 3.62: HD M1 SPM vector field result (Hotelling's T^2) depicting HS vs. TFA differences at normal speed. The red dashed line indicates critical threshold of $T2^*=22.875$. Suprathreshold clusters are shown in grey where $p<0.05$.

HS vs. TFA HD Module 2 (Normal)

As shown in Figure 3.63, SPM vector field found one suprathreshold cluster indicating a significant difference between HD M2 of HS and TFA at 49-60% during normal gait. Identically, smooth random 1D data would produce clusters of this breadth with a probability of $p=0.001$. Therefore, the null hypothesis was rejected as significant differences were observed between HS and TFA HD M2 in normal gait.

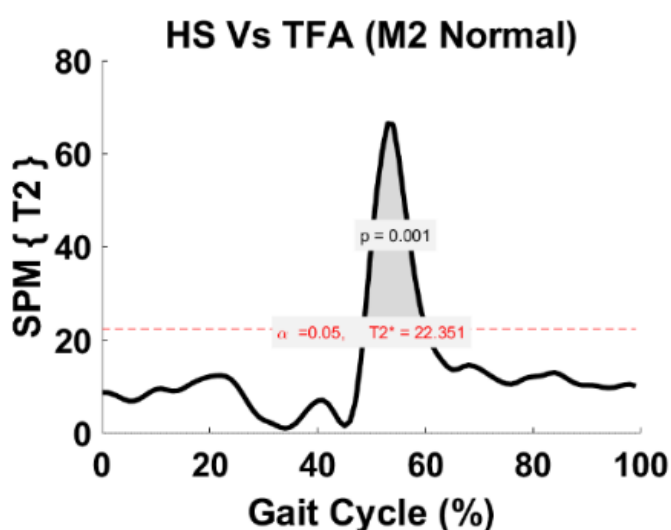


Figure 3.63: HD M2 SPM vector field result (Hotelling's T^2) depicting HS vs. TFA differences at normal speed. The red dashed line indicates critical threshold of $T2^*=22.351$. Suprathreshold clusters are shown in grey where $p<0.05$.

HS vs. TFA HD Module 3 (Normal)

As shown in Figure 3.64, no significant differences were observed between HD M3 of HS and TFA at normal speed.

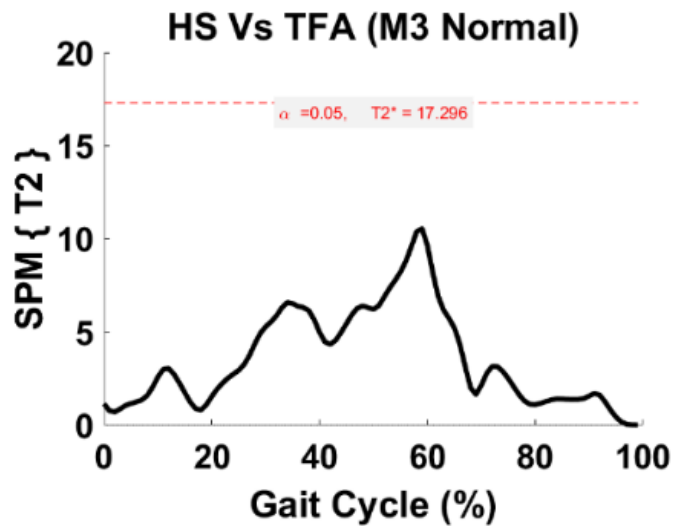


Figure 3.64: HD M3 SPM vector field result (Hotelling's T^2) depicting HS vs. TFA differences at normal speed. The red dashed line indicates critical threshold of $T2^*=17.296$. Suprathreshold clusters are shown in grey where $p<0.05$.

HS vs. TFA HD Module 4 (Normal)

As shown in Figure 3.65, no significant differences were observed between HD M4 of HS and TFA at normal speed.

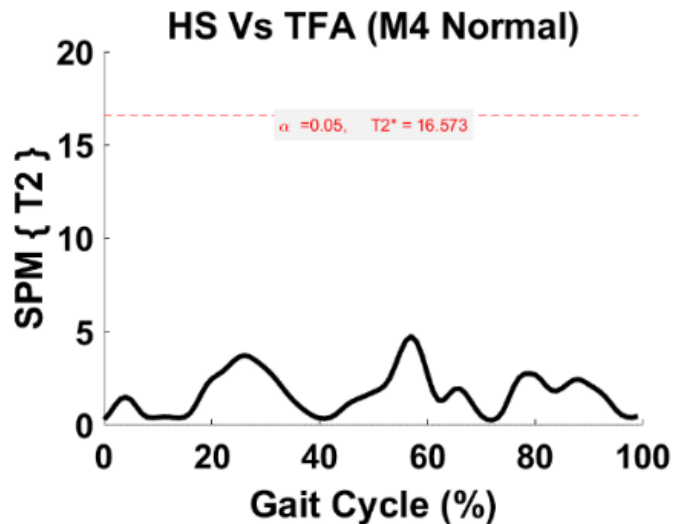


Figure 3.65: HD M4 SPM vector field result (Hotelling's T^2) depicting HS vs. TFA differences at normal speed. The red dashed line indicates critical threshold of $T2^*=16.573$. Suprathreshold clusters are shown in grey where $p<0.05$.

HS vs. TFA HD Ankle Co-Contraction (Normal)

As shown in Figure 3.66, SPM vector field found one suprathreshold cluster indicating a significant difference between ankle muscles of HS and TFA at 50-58% during normal gait. Identically, smooth random 1D data would produce clusters of this breadth with a probability of $p=0.002$. Therefore, the null hypothesis was rejected as significant differences were observed between HS and TFA ankle muscles in normal gait.

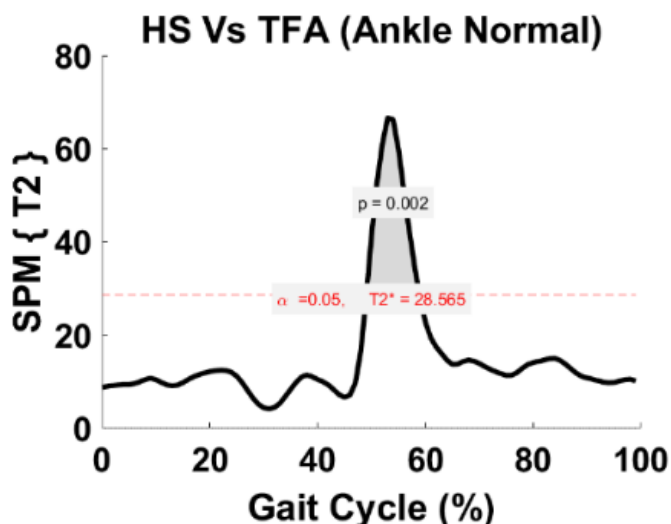


Figure 3.66: Ankle SPM vector field result (Hotelling's T^2) depicting HS vs. TFA differences at normal speed. The red dashed line indicates critical threshold of $T2^*=28.565$. Suprathreshold clusters are shown in grey where $p<0.05$.

HS vs. TFA HD Knee Co-Contraction (Normal)

As shown in Figure 3.67, no significant differences were observed between knee muscles of HS and TFA at normal speed.

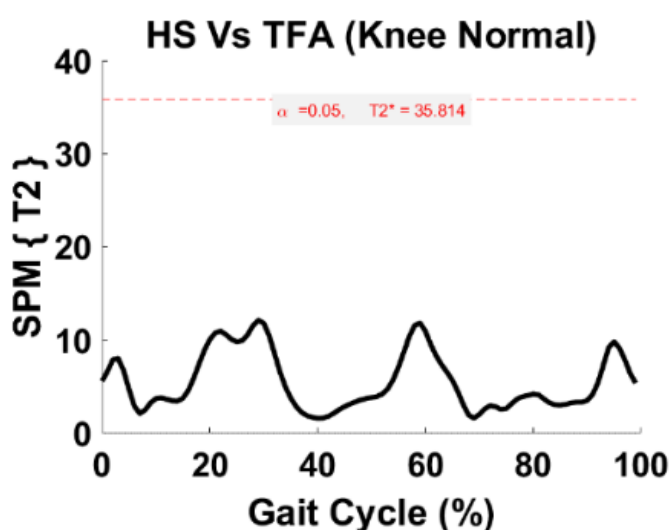


Figure 3.67: Knee SPM vector field result (Hotelling's T^2) depicting HS vs. TFA differences at normal speed. The red dashed line indicates critical threshold of $T2^*=35.814$. Suprathreshold clusters are shown in grey where $p<0.05$.

HS vs. TFA HD Module 1 (Fast)

As shown in Figure 3.68, no significant differences were observed between HD M1 of HS and TFA at fast speed.

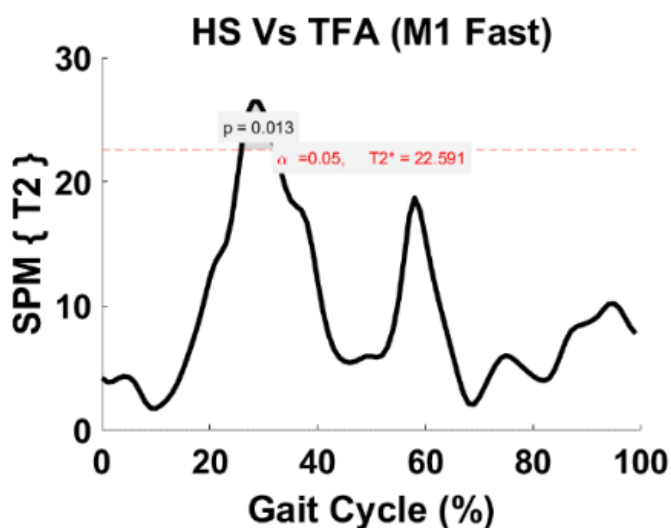


Figure 3.68: HD M1 SPM vector field result (Hotelling's T^2) depicting HS vs. TFA differences at fast speed. The red dashed line indicates critical threshold of $T2^*=22.591$. Suprathreshold clusters are shown in grey where $p<0.05$.

HS vs. TFA HD Module 2 (Fast)

As shown in Figure 3.69, SPM vector field found one suprathreshold cluster indicating a significant difference between HD M2 of HS and TFA at 17-21% and 48-59% during fast gait. Identically, smooth random 1D data would produce clusters of this breadth with a probability of $p=0.023$ and $p=0.001$. Therefore, the null hypothesis was rejected as significant differences were observed between HS and TFA HD M2 in fast gait.

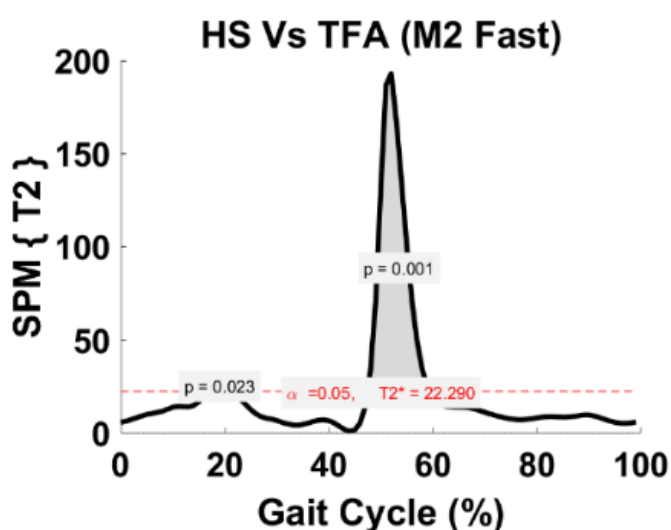


Figure 3.69: HD M2 SPM vector field result (Hotelling's T^2) depicting HS vs. TFA differences at fast speed. The red dashed line indicates critical threshold of $T2^*=22.290$. Suprathreshold clusters are shown in grey where $p<0.05$.

HS vs. TFA HD Module 3 (Fast)

As shown in Figure 3.70, no significant differences were observed between HD M3 of HS and TFA at fast speed.

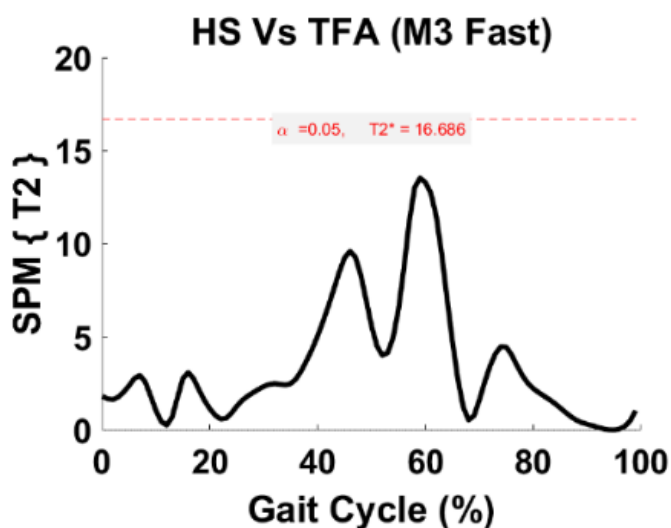


Figure 3.70: HD M3 SPM vector field result (Hotelling's T^2) depicting HS vs. TFA differences at fast speed. The red dashed line indicates critical threshold of $T2^*=16.686$. Suprathreshold clusters are shown in grey where $p < 0.05$.

HS vs. TFA HD Module 4 (Fast)

As shown in Figure 3.71, no significant differences were observed between HD M4 of HS and TFA at fast speed.

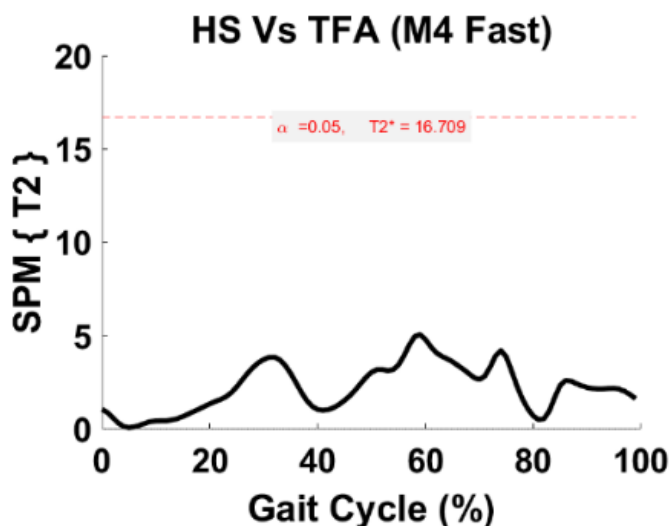


Figure 3.71: HD M4 SPM vector field result (Hotelling's T^2) depicting HS vs. TFA differences at fast speed. The red dashed line indicates critical threshold of $T2^*=16.709$. Suprathreshold clusters are shown in grey where $p < 0.05$.

HS vs. TFA HD Ankle Co-Contraction (Fast)

As shown in Figure 3.72, SPM vector field found one suprathreshold cluster indicating a significant difference between ankle muscles of HS and TFA at 18-19% and 48-58% during fast gait. Identically, smooth random 1D data would produce clusters of this breadth with a probability of $p=0.048$ and $p=0.001$. Therefore, the null hypothesis was rejected as significant differences were observed between HS and TFA ankle muscles in fast gait.

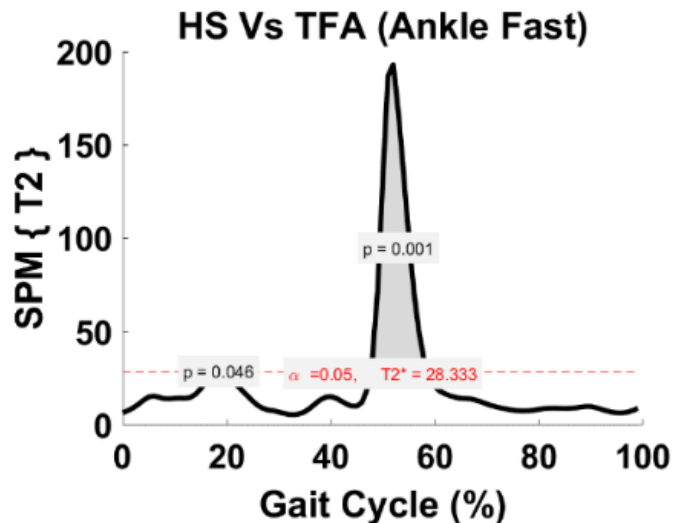


Figure 3.72: Ankle SPM vector field result (Hotelling's T^2) depicting HS vs. TFA differences at fast speed. The red dashed line indicates critical threshold of $T2^*=28.333$. Suprathreshold clusters are shown in grey where $p<0.05$.

HS vs. TFA HD Knee Co-Contraction (Fast)

As shown in Figure 3.73, no significant differences were observed between ankle muscles of HS and TFA at fast speed.

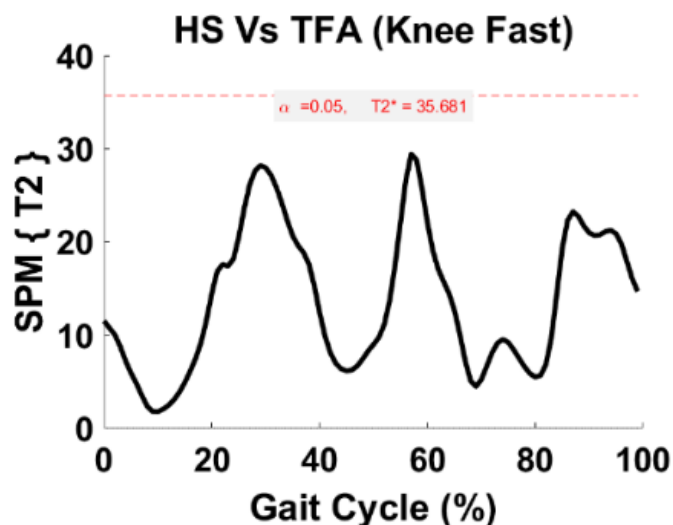


Figure 3.73: Knee SPM vector field result (Hotelling's T^2) depicting HS vs. TFA differences at fast speed. The red dashed line indicates critical threshold of $T2^*=35.681$. Suprathreshold clusters are shown in grey where $p<0.05$.

3.3.2.4 Between-Subject (Robotic Control Perspective)

A *priori* hypothesis accounted for individual speed as a different task under the walking control between-subject. Therefore, the effect of groups on individual muscle activities during walking at each speed. Consequently, SPM two-sample t-test ($\alpha=0.05$) was implemented for hypothesis 6.

As shown in Figure 3.74, RF, VM, SEM and GMED showed no significant differences between HS and TFA at slow speed. TFA VL was significantly greater than HS VL at 0-6% ($p=0.014$), 18-22% ($p=0.027$) and 26-32% ($p=0.011$) GC. One suprathreshold cluster was found in BFLH at 48-62% ($p=0.00$), TFL at 73-75% ($p=0.033$) and TA at 53-63% ($p=0.001$) in which TFA was significantly greater than HS at slow speed. TFA was significantly greater than HS in GM at 6-25% ($p=0.00$), 51-73% ($p=0.00$) and 84-91% ($P=0.006$) gait, in GL at 13-26% ($p=0.00$) and 52-100% ($p=0.00$) gait as well as in SOL at 0-26% ($p=0.00$) and 50-100% ($p=0.00$) gait at slow speed.

As shown in Figure 3.75, VL, SEM and TFL showed no significant differences between HS and TFA at normal speed. HS was significantly greater than TFA in RF at 11% ($p=0.046$) and 60-66% ($p=0.012$), in VM at 93-97% ($p=0.024$), in GM at 39-42% ($p=0.033$) and in GL at 39-42% ($p=0.027$) gait. One suprathreshold cluster was found in BFLH at 55-58% ($p=0.033$) and TA at 34-58% ($p=0.00$) in which TFA was significantly greater than HS at normal speed. TFA was significantly greater than HS in GM at 15-23% ($p=0.004$) and 48-61% ($p=0.00$) gait, in GL at 0-2% ($p=0.00$), 13-27% ($p=0.00$) and 49-100% ($p=0.00$) gait as well as in SOL at 0-28% ($p=0.00$) and 84-100% ($p=0.00$) gait at normal speed.

As shown in Figure 3.76, SEM and TFL showed no significant differences between HS and TFA at fast speed. HS was significantly greater than TFA in RF at 56-65% ($p=0.004$), in VM at 91-95% ($p=0.03$), and in GM at 36-38% ($p=0.037$) gait. TFA was significantly greater than HS in RF at 41-55% ($p=0.03$) and 73-75% ($p=0.043$), in VM at 71-75% ($p=0.028$), in VL at 0-8% ($p=0.009$), 17-46% ($p=0.00$), 80-88% ($p=0.00$) and 95-100% ($p=0.031$) and in BFLH at 25-37% ($p=0.001$), 47-56% ($p=0.004$) and 74-75% ($p=0.045$) gait in fast speed. One suprathreshold cluster was found in TA at 39-54% ($p=0.001$) in which TFA was significantly greater than HS at fast speed. TFA was significantly greater than HS in GM at 0-27% ($p=0.00$) and 46-61% ($p=0.00$) gait, in GL at 16-30% ($p=0.00$) and 48-100% ($p=0.00$) gait as well as in SOL at 0-28% ($p=0.00$) and 48-100% ($p=0.00$) gait at fast speed.

HS vs. TFA (Slow)

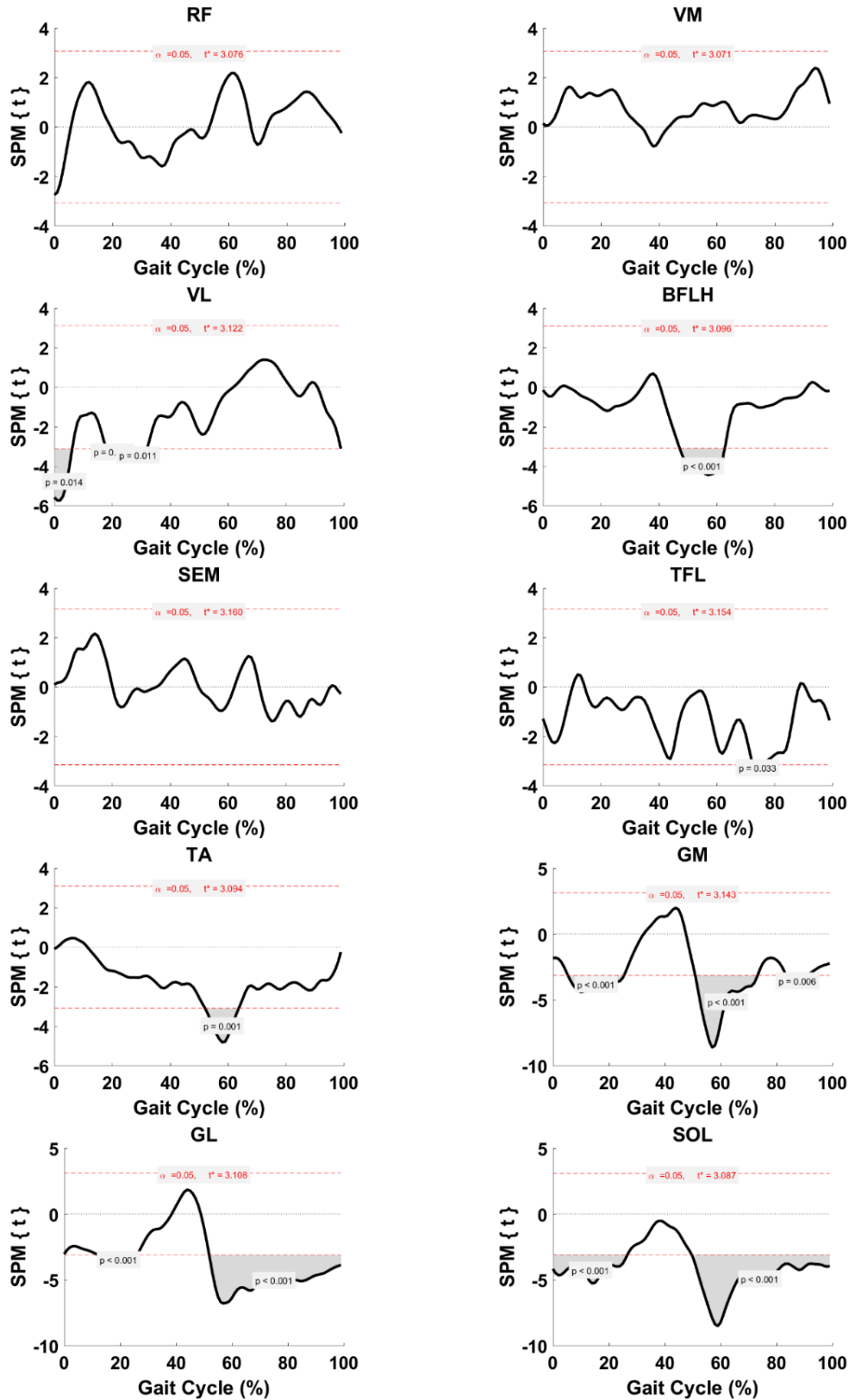


Figure 3.74: A statistical inference curve indicating a significant relationship between HS and TFA muscles at slow speed. Red dashed line indicates critical threshold ($t^*_{RF}=3.076$, $t^*_{VM}=3.071$, $t^*_{VL}=3.122$, $t^*_{BFLH}=3.096$, $t^*_{SEM}=3.160$, $t^*_{TFL}=3.154$, $t^*_{TA}=3.094$, $t^*_{GM}=3.143$, $t^*_{GL}=3.108$, $t^*_{SOL}=3.087$). Suprathreshold clusters are shown in grey where $p < 0.05$.

HS vs. TFA (Normal)

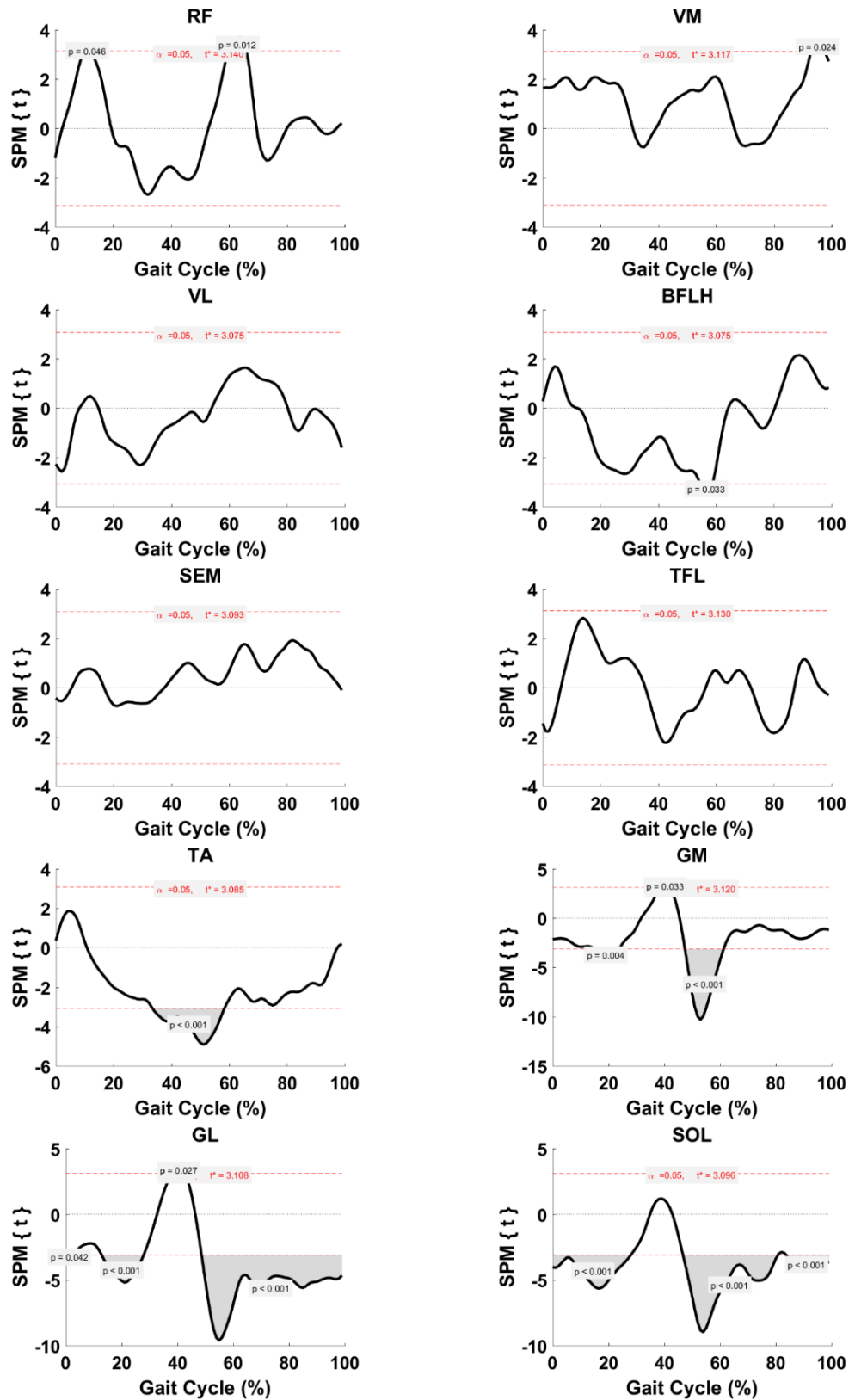


Figure 3.75: A statistical inference curve indicating a significant relationship between HS and TFA muscles at normal speed. Red dashed line indicates critical threshold ($t^*_{RF}=3.140$, $t^*_{VM}=3.117$, $t^*_{VL}=3.075$, $t^*_{BFLH}=3.075$, $t^*_{SEM}=3.093$, $t^*_{TFL}=3.130$, $t^*_{TA}=3.085$, $t^*_{GM}=3.120$, $t^*_{GL}=3.108$, $t^*_{SOL}=3.096$). Suprathreshold clusters are shown in grey where $p < 0.05$.

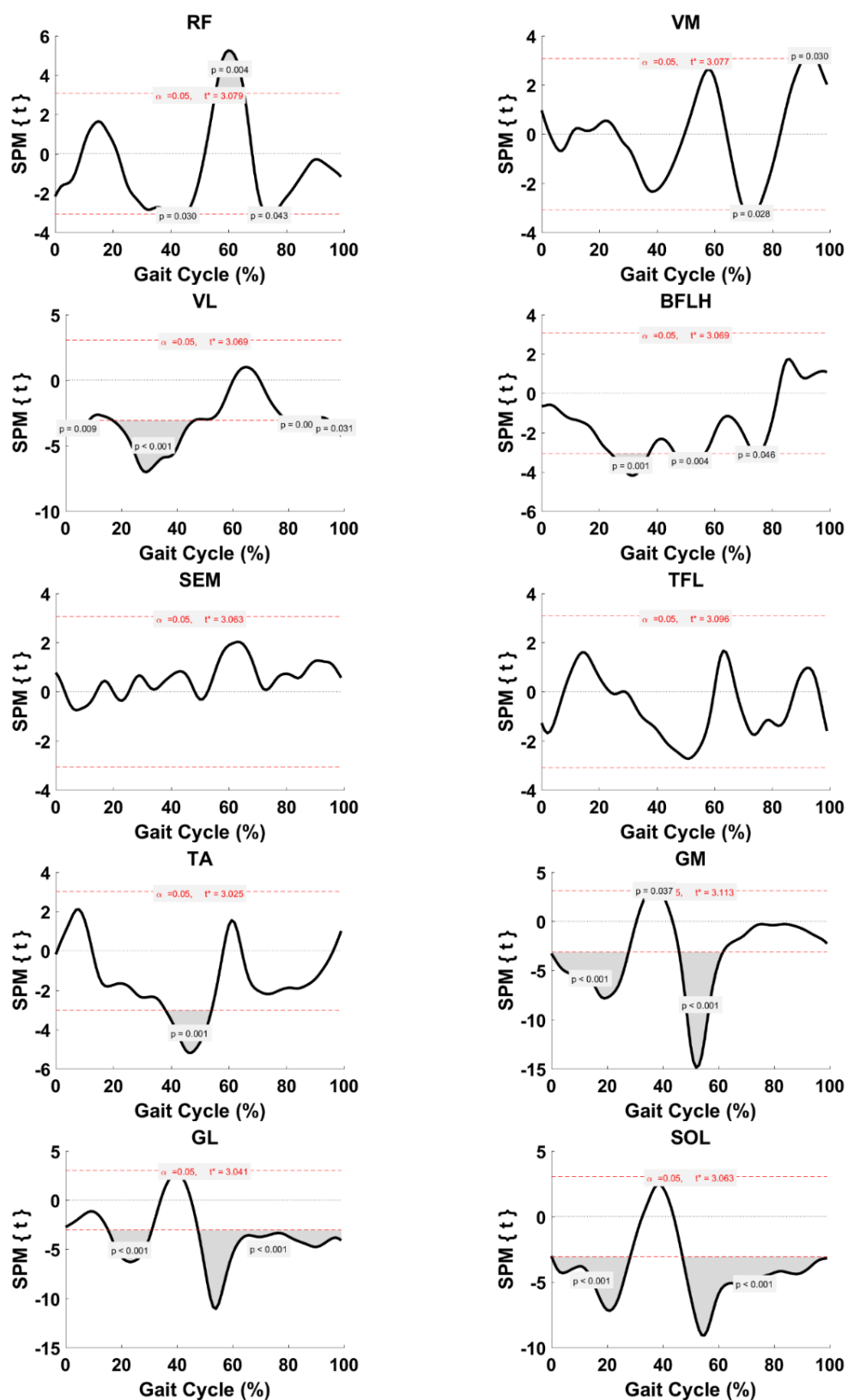
HS vs. TFA (Fast)

Figure 3.76: A statistical inference curve indicating a significant relationship between HS and TFA muscles at fast speed. Red dashed line indicates critical threshold ($t^*_{RF}=3.079$, $t^*_{VM}=3.077$, $t^*_{VL}=3.069$, $t^*_{BFLH}=3.069$, $t^*_{SEM}=3.063$, $t^*_{TFL}=3.096$, $t^*_{TA}=3.025$, $t^*_{GM}=3.113$, $t^*_{GL}=3.041$, $t^*_{SOL}=3.063$). Suprathreshold clusters are shown in grey where $p < 0.05$.

3.4 Discussion

3.4.1 Statistical Analyses (HD Muscle Activation Patterns)

In this chapter, two different approaches were investigated to assess the differences between HS and TFA within- and between-subject. The first approach, i.e., biomechanics approach was based on the concept of inter-muscle co-variance and muscle synergies hence the muscles were divided up into Modules corresponded to biomechanical subspecific tasks. The second approach, i.e., robotic control was inspired by the concept of the clinical state of the art myoelectric control in which individual muscles activation becomes crucial. Therefore, each muscle was compared individually.

To the best of the author's knowledge, no study was found to investigate the differences in muscle activities between HS and TFA IL in response to increasing transient-state walking speeds considering the HD sensorimotor Modules (biomechanics perspective), individual muscle activities (robotic control perspective) and whole EMG time-series (SPM). However, the previous literature examined the differences in individual muscle activities of HS and TFA IL on discrete points in GC using traditional statistical analysis [36, 37, 46, 47]. The between-subject analysis was the comparison based on the speed category (i.e., HS slow vs. TFA slow or HS normal vs. TFA normal) rather than matching group's similar speed (i.e., HS slow vs TFA normal or HS normal vs TFA fast). Therefore, results could be biased as the interaction between different speeds have not been considered. In addition, both groups walking at the same speed may have similar mechanics. However, similar speed does not mean it is their comfortable speed (especially in TFA) thereby, the speeds were compared categorically between-subject.

3.4.1.1 Within-Subject (Biomechanics Perspective)

The goal of this section was to investigate the effect of speeds on the groups of muscles which has similar activation pattern and/or contributed to the same biomechanical subtask (i.e., HD sensorimotor Modules). In addition, the muscles contributed to the co-contraction of the ankle and knee were compared with respect to the change of speeds.

Generally, in this study, the basic structure, i.e., the pattern of muscle activations was relatively consistent across speeds for both HS and TFA. However, the major burst in muscles heightened with increased speed (Figure 3.2 and Figure 3.3, respectively) which agree with the earlier investigations [28, 52, 96, 239]. In addition, as suggested by [240], tight coupling occurred between the EMG bursts and events in the GC. In other words, the timing where the major peaks occurred for all muscles across speeds were approximately in a close range for both HS and TFA (Table 3.3).

The change in the motor output of the extensor and flexor groups across speeds could be the result of pre-programmed neural control [240, 290, 310]. Notwithstanding, this does not exclude the possible influence the reflex activity has on the overall muscle activation [239, 289, 311]. Moreover, previously it has been shown that descending activity influenced the transition from the quiet state to movement by a specific tuning of spinal cord circuitry [312, 313].

Speed Dependence of the HS HD Modules

HS HD M1 muscles were activated at the weighting acceptance to support the body, control the knee flexion and extend the knee during the MS. The hypothesis (biomechanics null hypothesis 1a) that there would be no difference in M1 muscle activity with increased transient-state walking speed was not supported as significant differences were observed in ES, MS, and TSW where the main bursts occurred. These differences were more prominent in HD M1 between fast-slow (Figure 3.7).

HS HD M2 muscles were activated in TS which contributed to body support and plantarflexion during propulsion. The hypothesis (biomechanics null hypothesis 1b) that there would be no difference in HD M2 muscle activity with increased transient-state walking speed was not supported as significant differences were observed in MSW (fast-normal) and TS (fast-slow) (Figure 3.8).

HS HD M3 muscles were activated in TSW to ES. TA contributed to dorsiflexion of the foot in TSW and acted to decelerate the foot during the foot flat phase after IC. Moreover, TA second burst occurred in PSW where TA activated for foot clearance. In addition, RF in HD M3 contributed to decelerate the leg in ES and TSW. The hypothesis (biomechanics null hypothesis 1c) that there would be no difference in HD M3 muscle activity with increased transient-state walking speed was not supported as significant differences were observed in ES, MS, PSW-ISW, and TSW. These differences were more prominent in HD M3 between fast-slow (Figure 3.9).

HS HD M4 muscles were activated in TSW and ES which contributed to decelerate the leg while increasing the leg energy during weight acceptance. The hypothesis (biomechanics null hypothesis 1d) that there would be no difference in HD M4 muscle activity with increased transient-state walking speed was not supported as a significant difference was observed in HD M4 during TS between normal-slow and fast-slow (Figure 3.10).

HS co-contraction of ankle and knee muscles were considered in this study. The hypotheses (biomechanics null hypothesis 1e and 1f) that there would be no difference in activation of muscles contributed to the HS ankle and knee co-contractions with increased transient-state walking speed were not supported as significant differences

were observed during TS (ankle co-contraction) and ES and TSW (knee co-contraction) (Figure 3.11 and Figure 3.12).

The observed significant differences in HS HD sensorimotor Modules between speeds are indicative of neuromuscular adaptation to the kinematic and kinetic demands of increased transient-state walking speed. Similarly, the muscles contributed to the co-contraction showed adaptation mechanism required to stabilize HS ankle and knee joints with increased speeds which should not be considered as a pathological issue.

Speed Dependence of the TFA HD Modules

TFA HD M1 muscles were activated at the weighting acceptance to support the body, control the knee flexion and extend the knee during the MS. The hypothesis (biomechanics null hypothesis 3a) that there would be no difference in HD M1 muscle activity with increased transient-state walking speed was not supported as a significant difference was observed in ES, MS, and TSW between fast-slow (Figure 3.13).

TFA HD M2 showed two main bursts; one occurred during the foot-flat which contributed to body support and deceleration of the tibial rotation, and the other one occurred during propulsive phase to generate enough force to plantarflex. The hypothesis (biomechanics null hypothesis 3b) that there would be no difference in HD M2 muscle activity with increased transient-state walking speed was not supported as significant differences were observed during foot flat and TS between fast-slow (Figure 3.14).

TFA HD M3 muscles were activated in TSW to ES. TA contributed to dorsiflexion of the foot in TSW and acted to decelerate the foot during the foot flat phase after IC. Moreover, TA second burst occurred in PSW where TA activated for foot clearance. In addition, RF in HD M3 contributed to decelerate the leg in ES and TSW. The hypothesis (biomechanics null hypothesis 3c) that there would be no difference in HD M3 muscle activity with increased transient-state walking speed was not supported as significant differences were observed in ES and TSW. These differences were more prominent in HD M3 between fast-slow (Figure 3.15).

TFA HD M4 muscles were activated in TSW and ES which contributed to decelerate the leg while increasing the leg energy during weight acceptance. The hypothesis (biomechanics null hypothesis 3d) that there would be no difference in HD M4 muscle activity with increased transient-state walking speed was not supported as a significant difference was observed in TSW between fast-normal (Figure 3.16).

TFA co-contraction of ankle and knee muscles were considered in this study. The hypotheses (biomechanics null hypothesis 3e and 3f) that there would be no difference

in activation of muscles contributed to the TFA ankle and knee co-contractions with increased transient-state walking speed were not supported as a significant difference was observed in ankle muscles during the TS (between normal-slow) and ISW (between fast-normal) as well as in knee muscles during the ES (between fast-normal) and TSW (between fast-slow) (Figure 3.17 and Figure 3.18).

The observed significant differences in TFA HD sensorimotor Modules between speeds are indicative of neuromuscular adaptation to the kinematic and kinetic demands of increased transient-state walking speed. The TFA co-contraction may be indicative of compensatory mechanism required to stabilize TFA IL joints as transient-state walking speed increased. However, the regions which found to be statistically significant were similar to those of HS; thereby this may be just the adaptation adjustment to change of speeds rather than a compensatory mechanism.

3.4.1.2 Within-Subject (Robotic Control Perspective)

The goal of this section was to investigate the changes in HS and TFA individual muscle activity as speed increased during transient-state walking. Generally, the magnitude of muscle activity heightened with increased speeds because of the required muscle force to propel the body forward [236]. It has been shown in the literature that, in slow walking, larger muscular efforts required to provide the balance of frontal plane [236, 314]. Neptune et al. [315] reported the functional role of individual muscles does not change with an increase in speeds. However, none of the previous studies considered the whole time-series and statistical parametric mapping as means of comparison.

Speed Dependence of the HS Muscles

The robotic control null hypothesis 2 regarding the effect of speeds on HS muscle activity was not supported in all the muscles. The results showed increased activity in the HS quadriceps as speed increased in the transient-state walking (Figure 3.2).

The main analysis (RM ANOVA) showed significant differences of HS RF, VM, and VL in ES, MS, and TSW across speeds. In, addition, another suprathreshold cluster was observed in RF during the ISW across speeds. This is also evident in the previous study by [236]. The post hoc analysis between fast-normal and fast-slow illustrated RF fast was significantly greater than normal and slow, respectively (Figure 3.20) which is consistent with the literature on HS showing RF activity increased to a greater extent at higher speeds [28, 236, 238, 240].

HS VM post hoc test showed normal was significantly greater than slow and fast was significantly greater than normal and slow (Figure 3.22). HS VL post hoc analysis

showed normal and fast was significantly greater than slow in normal-slow and fast-slow comparison, respectively (Figure 3.24).

HS BFLH analysis showed significant differences in MS and TSW. Post hoc analysis showed normal and fast was significantly greater than slow between normal-slow and fast-slow comparison, respectively (Figure 3.26) which agreed with previous studies [28, 236, 238, 240].

HS TFL main analysis showed significant differences in ES-MS, ISW, and TSW. The post hoc test showed normal was significantly greater than slow (Figure 3.30).

HS TA main analysis showed significant differences in ES to MS, PSW to ISW and TSW. TA fast showed to be significantly greater than slow in the post hoc test (Figure 3.32). The significant differences in TSW and ES of TA were supported by [236] as they concluded the activities during the weight bearing phase is velocity-dependent. However, they pointed out that TA activity during ISW was insensitive to change of speeds which are not in agreement with the results obtained in this study. The possible explanation is that the gait was performed in steady-state and the range of walking speeds was different from the present study.

The main significant difference in triceps surface muscles was observed in TS (Figure 3.33, Figure 3.35 and Figure 3.37). In addition, during ES and TSW, GL and SOL were significantly different across speeds. The post hoc results illustrated GL and SOL at fast was significantly greater than slow. This is in agreement with [236] showing that triceps surae affected strongly by increased speeds during the TS (50-80% of the stance phase). An extra burst occurred during the foot flat in triceps surae at fast speed (Figure 3.2). In addition, [236] and [231] found no change in triceps surae activity during weighting acceptance across speeds which contradicted the present study as significant differences were found during this time. The discrepancy between the results may be due to the change in neuromuscular strategy between the transient-state and steady-state walking and the difference in the range of walking speeds.

Even though HS SEM in MSW (Figure 3.27) and GM in MS (Figure 3.33) showed a significant difference across speeds, no significant difference was observed in their post hoc analysis. It is worth mentioning, the null hypothesis was answered completely by the main RM ANOVA, and the discrepancy between main and post hoc is due to the Bonferroni post hoc procedures which are approximate. Different post hoc procedures are needed to yield a precise probabilistic agreement between the main analysis and post hoc result.

The post hoc results showed no significant differences in HS RF normal-slow, VL fast-normal, BFLH fast-normal, TFL fast-normal, TA normal-slow and fast-normal, GL

normal-slow and SOL normal-slow, suggesting the muscle activation was less affected by the change of speeds.

It is noteworthy that if results fail to reach significance, but come close to breaching the critical threshold (TFL fast-slow, GL fast-normal, SOL fast-normal), it is possible that other post hoc analyses would find them statistically significant. It is, therefore, best to interpret non-significant results cautiously when using Bonferroni corrections.

In general, the previous studies on the HS reported higher activity and heightened magnitude with increasing steady-state walking speed irrespective of the EMG processing method for quantification (absolute mean value, peak magnitude, integrated of full wave rectification, gain functions) [28, 236, 238, 239, 316]. Although the present study was associated with the transient-state walking, increased activity was perceived in some of the muscles more than the others throughout GC. The hamstring muscles showed less increase in magnitude during the stance phase, however, heightened magnitude in MSW to TSW across speeds.

Speed Dependence of the TFA Muscles

The null hypothesis 4 (robotic control) that there would be no effect of speeds on TFA muscle activity was not supported in all the muscles except SEM, TFL, and SOL with increased speed. One possible explanation is that other functionally related muscles are compensating for those which no significant differences were observed. Therefore, BFLH which has a similar functional role to SEM showed to be statistically significant across speeds. Likewise, the activity of SOL was insensitive to change of speed which seems to be compensated by higher activation in GM and GL. However, this is in contrast with the results found in the HS muscle activities of the literature [236]. The information from SEM and SOL could be used in prosthetic application to control the onset of stance and swing at a different range of speeds, respectively. In addition, the temporal features of these muscles may facilitate the middle level control complexity (phase/event detection) to modulate prosthetic devices without any concerns about the effects of walking speeds.

TFA quadricep muscles were significantly different in ES to MS and TSW across speeds. In addition, VM was statistically significant in PSW to ISW as speed increased. The post hoc analysis of TFA between fast-normal and fast-slow illustrated RF and VM at fast was significantly greater than normal and slow, respectively (Figure 3.40 and Figure 3.42). VL was significantly greater at fast compared to slow only (Figure 3.44).

TFA BFLH showed significant differences in MSW to TSW. Post hoc analysis showed fast was significantly greater than normal (Figure 3.46).

The main analysis showed significant differences in TFA GM in ES, foot flat and MS to TS between speeds (Figure 3.49). Similarly, TFA GL was statistically significant during foot flat and MS to TS (Figure 3.51). Post hoc analysis showed GM (Figure 3.50), and GL (Figure 3.52) were significantly greater at fast compared to slow.

TFA SEM (Figure 3.53), TFL (Figure 3.54) and SOL (Figure 3.55) showed no significant differences across speeds.

TA was significantly different in ES, MS, and TSW (Figure 3.47). No significant difference was observed in TA post hoc analysis, but the null hypothesis was answered completely by the main RM ANOVA (Figure 3.48).

Significant differences were not observed in post hoc analyses of RF normal-slow, VM normal-slow, VL normal-slow and fast-normal, BFLH normal-slow, GM normal-slow, as well as GL normal-slow and fast-normal. This suggests less dependency of these muscles activities to the change of speeds.

Generally, the results showed increased activity in the TFA quadriceps, dorsiflexor, GM, and GL more than the other muscles with increased transient-state walking. Two bursts occurred in triceps surae in which the first was long, and both peaks were heightened with increased walking speed. This can be due to the fact that the IL compensates for the lack of push off on the PL in order to contribute to the propulsion in TS [36].

3.4.1.3 Between-Subject (Biomechanics Perspective)

Since the biomechanics hypothesis does not pertain to a specific muscle and time point, inter-muscle covariance and whole time-series have been considered for statistical testing. No significant difference was observed between groups for HD M1, HD M3, HD M4 and knee co-contraction muscles at slow, normal and fast speed. However, SPM analysis rejected the biomechanics null hypothesis between groups for HD M2 and ankle co-contraction at slow, normal and fast speed (biomechanics hypothesis 5b and 5e across speeds).

The hypothesis (biomechanics null hypothesis 5b) that there would be no difference between groups for HD M2 at all speeds was not supported as significant differences were observed approximately where the major burst of TFA triceps surae occurred. In addition, HD M2 showed another significant difference at fast speed in MS where TFA plantarflexor were highly activated. The difference attributed to the TFA longer stance phase, heightened activity, prolonged duration and the need for larger push off of the HD M2 muscles to compensate for the lack of plantarflexor in the PL which agreed with the results in [46]. This was also supported by the kinetic studies of TFA in which greater work at hip and plantarflexors of IL were observed [36, 39, 235, 256].

The hypothesis (biomechanics null hypothesis 5E) that there would be no difference between groups for the muscles contributed to the ankle co-contractions of HS at each speed was not supported as a significant difference was observed approximately before the transition from stance to swing phase. This may suggest compensatory mechanism required to stabilize TFA IL ankle joint during double support before PL enter the single limb support phase which could be indicative of reduced stability during this time. In addition, another significant difference occurred at fast speed in MS where TFA plantarflexors were highly activated. This may suggest increased ankle stiffness to control the balance concerns during single limb support [304]. These results are in agreement with the findings of [46] which reported increased activity and co-activity of IL dorsiflexor and plantarflexor muscles during gait as compared to the HS.

3.4.1.4 Between-Subject (Robotic Control Perspective)

The null hypothesis 6 (robotic control) that there would be no difference in individual muscle activity between HS and TFA during walking at different speeds was supported for RF, VM and SEM during slow, for VL, SEM, TFL during normal and for SEM and TFL during fast. Commonly, SEM activity was similar between groups at all speeds which suggests a similar neuromotor mechanism underlying the motor control regulation of both groups.

HS vs. TFA (Slow)

No significant difference was observed in RF and VM activity between HS and TFA. In contrast, significant differences occurred in VL during the LR and MS due to the TFA VL activity was heightened to a greater extent as compared to the HS.

No significant difference was observed in SEM whereas BFLH significant difference occurred during the TS to PSW where the second major contraction presented in TFA. This could be the compensatory reaction of the knee flexor during push off to bring the intact limb forward due to the instability of PL during the weighting acceptance.

A significant difference was observed between groups during the ISW due to the larger activity variation of the TFL in that region. One possible explanation is that TFL contributed as a minor hip flexor as well as co-contracting with the hip adductors to stabilize the hip joint in ISW.

A significant difference was observed between groups during the TS to PSW where the second peak occurred in TFA TA. One possible explanation is that TA contributed more to dorsiflexion of the foot for foot clearance around the transition between stance to swing phase as compared to the HS.

GM showed three suprathreshold clusters during the foot-flat, TS to ISW and MSW. GL illustrated two suprathreshold clusters in foot-flat and TS to the whole swing phase. SOL showed two suprathreshold clusters during the weighting acceptance and TS to the whole swing phase. The significant differences were due to the foot-flat activation and heightened activity of triceps surae in TFA as compared to the HS. Even though the activity of triceps surae decreased significantly after TO, there is minimal low activity in both groups during swing phase, however, larger in TFA. This could be caused by the fact that triceps surae co-contracted against the quadriceps muscle in order to provide enough knee flexion during swing phase. Refer to Figure 3.74 for the comparison between HS and TFA during slow transient-state walking.

HS vs. TFA (Normal)

RF activity showed two suprathreshold clusters during the LR and PSW where the first and second peaks in HS heightened as compared to TFA.

No significant difference was observed in VL activity between HS and TFA. However, a significant difference occurred in TSW due to the HS VM activity was heightened to a greater extent than the TFA.

No significant difference was observed in SEM whereas in BFLH a significant difference occurred during the TS where the second major contraction presented in TFA. This could be the compensatory reaction of the knee flexor during push off to bring the intact limb forward due to the instability of PL during the weighting acceptance. No significant difference in TFL was observed between HS and TFA at normal speed.

A significant difference was observed between groups during the TS to PSW where the second peak is occurring in TFA TA. One possible explanation is that TA contributed to dorsiflexion of the foot for foot clearance in transition between stance to swing phase.

GM showed three suprathreshold clusters during the foot-flat, TS and TS to PSW. GL illustrated four suprathreshold clusters in weighting acceptance, foot-flat and TS and TS to the whole swing phase. SOL showed three suprathreshold clusters during the weighting acceptance, TS, and TS to the whole swing phase. The significant differences occurred during the ES and MS were due to the foot-flat activation and heightened activity of triceps surae in TFA as compared to the HS. The significant difference in TS was due to the HS peak presented earlier than the TFA. The significant difference in TS to swing phase was due to the heightened activity of TFA triceps surae caused by co-contraction against quadriceps muscle in order to provide enough knee flexion during swing phase. Refer to Figure 3.75 for the comparison between HS and TFA during normal transient-state walking.

HS vs. TFA (Fast)

RF activity showed three suprathreshold clusters during the TS, PSW, and ISW. The TS and ISW significant differences were due to the TFA RF higher activation and shifted second and third minor bursts as compared to the HS, respectively. The PSW significant difference was due to the heightened activity of HS RF third peak.

Two suprathreshold clusters were observed in VM activity during the PSW and TSW between HS and TFA at fast speed. The PSW significant difference was associated with the shift observed in TFA VM minor burst as compared to the HS. The TSW significant difference was due to the heightened activity of HS VM to a greater extent compared to the TFA.

Four suprathreshold clusters were observed during the ES, MS, MSW, and TSW due to the heightened activity of TFA VL to a greater extent as compared to the HS.

BFLH significant differences occurred during the MS, TS, and ISW due to the higher activation of TFA as compared to the HS at fast speed. The difference in ISW could be due to the TFA BFLH activity to assist in knee flexion. No significant difference was observed in SEM between HS and TFA fast speed. No significant difference was observed between HS and TFA at fast speed.

A significant difference was observed during the TS prior to the second peak of TFA TA which was heightened to a greater extent as compared to the HS. One possible explanation is that TA contributed to dorsiflexion of the foot for foot clearance in transition between stance to swing phase.

GM showed three suprathreshold clusters in weighting acceptance to foot-flat, MS, and TS to PSW. GL illustrated two suprathreshold clusters in foot-flat and TS and TS to the whole swing phase. SOL showed two suprathreshold clusters in weighting acceptance to foot-flat, TS to the whole swing phase. The significant differences occurred during the ES and MS were due to the foot-flat activation and heightened activity of triceps surae in TFA as compared to the HS. The significant difference in TS was due to the HS peak presented earlier than the TFA. The TS to phase significant difference was due to the heightened activity of TFA triceps surae caused by co-contraction against quadriceps muscle in order to provide enough knee flexion during swing phase. Refer to Figure 3.76 for the comparison between HS and TFA during fast transient-state walking.

3.4.1.5 Comparing Individual Muscle Activities to the Literature

In general, in this chapter, the results presented for HS were in agreement with the previous literature to a great extent in terms of the major burst occurrence intervals [239,

288, 317]. However, discrepancies do exist, which are likely to be attributed to differences in methodology (e.g., signal processing and transient-state) and in subjects' selection (e.g., age and demographic). The following is a discussion of the similarities and differences in the results obtained from the present study and literature. It is worth mentioning, none of the previous studies considered the whole time-series or SPM as a means of comparison within- and between-subject.

The self-selected walking speed in TFA was lower than HS at each speed category which agrees with the literature [37, 235, 255, 256].

The results obtained from the present study were comparable to the literature even though the strides after gait initiation were considered (i.e., transient-state). Moreover, the muscle activation patterns of HS in the present study were comparable to the study conducted by [52] on HS during four steps from gait initiation as well as a study conducted by [96] during steady-state walking. In addition, the major and minor bursts occurred during transient-state gait are approximately within the same range of the previous findings [96, 118].

Previous studies reported [52, 62-64] HS TA contraction increased when walking speed increased, and TA coincided with the triceps surae deactivation during gait initiation which agreed with the results obtained in the present study.

Jaegers et al. [37, 64] found TFA BFLH activity in ISW was to assist the flexion of the knee which was also observed in TFA of present study at fast speed.

Wentink et al. [36] studied the differences in muscle activities of TFA and HS during gait. They reported the prolonged duration of plantarflexor and dorsiflexor of TFA IL as compared to control which agree with the muscle activities of TFA triceps surae obtained in the present study. However, the TFA TA in the present study was only significantly different in terms of magnitude and pattern as the duration of activation was not compared objectively in this study.

The major and minor bursts occurred in TFA IL of the present study are of comparable with the findings of the previous literature (Table 3.3) [36, 47].

Bae et al. [46] found that the hamstring and quadriceps muscle activity and co-activity of TFA IL were larger compared to the control during steady-state of gait. In the present study, significantly greater differences were observed in the TFA activities of VL and BFLH during slow walking (Figure 3.74), TFA activities of RF, VM, and BFLH during normal (Figure 3.75) and TFA activities of quadriceps and BFLH during fast (Figure 3.76) as compared to the HS. They also reported TA and triceps surae activities of TFA IL were significantly greater than HS which agrees with the results of this study across speeds (Figure 3.74, Figure 3.75 and Figure 3.76) [46].

3.5 Summary

The HD EMG is a reflection of both peripheral and central properties of the neuromuscular system. Therefore, the information from the brain, spinal cord, and muscular level are converged and extracted by means of a non-invasive approach, i.e., surface EMG. This study was carried out to investigate the HD EMG patterns of the HS and TFA IL across speeds. Generally, muscle activation patterns were similar. However, the magnitude was increased for both HS and TFA with increased transient-state walking speed. The muscle activity analysis was performed within- (across all speeds) and between-subject (between groups at each speed category) from biomechanics and robotic control perspectives. SPM 1D analysis was performed to consider the whole time-series (i.e., between 0% and 100% time). Significant differences occurred between muscle activities of HS and TFA at different regions of the GC especially in plantarflexor muscles during stance phase, indicating the TFA adjustment strategy to create large push off in the IL to compensate for the loss of muscle in PL during transient-state walking. These results have important implications for adjusting the rehabilitation strategy to focus on the muscles and the timing where the differences occurred in the GC. This may help therapists to reduce the TFA dependency of their IL. Consequently, decrease the risk of secondary physical conditions (e.g., osteoarthritis). The information may be useful for the prosthetic companies to build prostheses that incorporate information from the IL to improve the myoelectric control strategy.

3.6 Conclusion

The effect of speeds on both HS and TFA HD sensorimotor Modules and ankle and knee co-contraction muscles from biomechanical perspective showed significant differences, suggesting neuromuscular adaptation mechanism in both groups to satisfy the kinematic and kinetic demands of increasing transient-state walking speed.

The effect of speeds on HS individual muscle activities (robotic control perspective) showed significant differences at different regions of the GC, suggesting, walking at different speeds should be considered as a separate task. The effect of speeds on TFA individual muscle activities (robotic control perspective) showed significant differences in different regions of GC, except in SEM, TFL, and SOL. The information from these muscles could be used in the robotic perspective which reduces the control complexity of prosthetic devices across different speeds. In addition, the temporal features of these muscles would help to control the onset of stance and swing at different speeds (i.e., mid-level control).

The HD sensorimotor Modules comparison between HS and TFA showed significant differences in HD M2 at all speeds. The difference attributed to the TFA longer stance phase, heightened activity, prolonged duration and the need for larger push off of the HD M2 muscles to compensate for the lack of plantarflexor in the PL. The muscles contributed to the ankle co-contraction were significantly different at all speeds, suggesting compensatory mechanism required to stabilize TFA IL ankle joint during double support before PL enters the single limb support phase which is indicative of reduced stability during this time. Individual muscle activity showed no significant differences in SEM and TFL activity between HS and TFA at all speeds, suggesting a similar neuromotor mechanism underlying the motor control regulation of both groups. The significant difference in the muscles is mainly associated with the stance phase which could be due to the TFA effort to stabilize their joints and body weight during this time. Notwithstanding, the triceps surae showed to be significantly different during swing phase, indicating the importance of TFA plantarflexor after push off to propel the body forward and decelerate the ankle joint at the end of the swing phase.

Chapter 4

MODULAR MOTOR CONTROL IN TRANSFEMORAL AMPUTEES DURING TRANSIENT-STATE WALKING

4.1 Introduction

This Chapter is the extension of the previous research conducted on high dimensional (HD) EMG between healthy subjects (HS) and transfemoral amputees (TFA) during transient-state walking at different speeds. The main aim is to investigate changes in HS and TFA control strategy during transient-state walking at three different speeds (slow, normal, and fast) from a low dimensional motor module viewpoint. Muscle synergy analysis is performed on thirteen HS dominant leg and eleven TFA IL. Previous reports found that the kinematics, kinetics, and HD muscle activities change with increasing steady-state walking speed within the same group of homogenous subjects [88, 318, 319]. However, there have been no studies considering the transient-state walking in HS and TFA in terms of muscle synergies/module motor control. Muscle synergy analysis is performed by means of a mathematical technique known as concatenated non-negative matrix factorization (CNMF) to linearly decompose HD EMG activation patterns into two low dimensional components including time-varying activation coefficient profiles and spatially fixed muscle synergy vectors. This study is regarded as exploratory thereby two approaches were taken into account, namely biomechanics and robotic control to investigate *a priori* hypotheses. The biomechanics related hypotheses consider the covariance between inter-activation coefficient profiles whereas the robotic control related hypotheses account for individual activation coefficient profiles. Six hypotheses were tested to compare the effect of speed on activation coefficient profile of HS and TFA as well as to assess the differences between groups at each speed. Therefore, the within-subject analysis was performed for each group separately across speeds, and the between-subject analysis accounted for individual speed as a different task under the walking control.

4.2 Experimental Protocol

4.2.1 Methodology

The same subjects, data, and protocol have been used to those of chapter 3 (section 3.2.1, page 57).

4.3 Algorithm Description

CNMF was implemented as a mathematical technique to investigate the differences between muscle synergy components of the HS and TFA within- and between-subject.

4.3.1 Signal Processing

Prior to the muscle synergy analysis, HD EMG signals were processed implementing these subsequent steps: 1) filtering: raw EMG signals were bandpass filtered at a cut off frequency of 20-500 Hz with zero-lag Butterworth filter to remove motion artefacts and high-frequency noise from the signals; 2) Linear envelope: the muscle activation pattern was obtained by full-wave rectification and a low pass filter (zero lag 2nd order Butterworth at 6 Hz); 3) amplitude normalization: the data were normalized with respect to the peak processed EMG values obtained from all walking trials at different speeds. Therefore, all values of each muscle were ranged between zero and one. 4) time normalization: the data were then interpolated to 101 data points corresponding to the instrumented leg GC (for detailed information on signal processing refer to chapter 3, section 3.2.2) [77, 79, 84, 126, 312].

4.3.2 Non-Negative Matrix Factorization (NMF)

NMF is a multivariate statistical data analysis technique which linearly decomposes high dimensional EMG activation patterns into low dimensional subsets including time-varying activation referred to as C (known as activation coefficient profiles, activation coefficient, coefficients, neural commands, temporal components, motor primitives) and an independent spatially fixed matrix of weights referred to as S (known as muscle synergies, motor modules, modules, synergy vectors or weighting coefficients).

Activation coefficient profiles (C) are sets of basis functions that represent the timing of muscle synergies being active over time, i.e., GC [185, 190]. Muscle synergies (S) are scalar values which represent the relative weighting of each muscle within the corresponding synergy. Therefore, one synergy group or module consists of a muscle synergy vector and its corresponding activation coefficient profile [77, 84].

4.3.3 NMF Frameworks

Standard non-negative matrix factorization (NMF) is a multiplicative update rules-based algorithm to build two matrices of S and C [174, 218, 320]. Therefore, the basic formula for the NMF is (Equation 4.6):

$$A = S * C + E \quad (4.6)$$

Where A is an m -by- n initial matrix (m = number of muscles and n = number of time points), S is an m -by- k matrix (k = number of synergy groups), C is a k -by- n matrix and E is an m -by- n matrix. A is the original EMG signal which represents the normalized linear envelope signal, S is an independent of time which represents relative weighting of each muscle within each module, C is the time-varying component of the signal which represents recruitment of the muscle synergy over time and E is the residual ($A - S * C$) which represents an error matrix.

4.3.4 Concatenated Non-Negative Matrix Factorization (CNMF) Frameworks

CNMF approach is a new technique which concatenates A and a decomposition vector i.e., C such that the original matrix A^C is an n -by- m (n = number of subjects \times number of GCs \times 101 and m = number of muscles) and concatenated C , i.e., C^C is an n -by- k (k = number of synergy groups) whereas S is a k -by- m (fixed synergy) [92, 93, 95, 213, 230]. The objective function for CNMF is as follows (Equation 4.7)

$$J = \sum_{i=1}^{N_s} \frac{\|A_i^C - C_i^C S\|_F}{\|A_i^C\|_F} \quad (4.7)$$

Where $\|A_i^C\|_F$ represents Frobenius norm of a vector defined as $\sqrt{\text{tr}(AA^T)}$ (tr =matrix trace and A^T = matrix A conjugate transpose), C_i^C is a concatenated coefficient, S is a fixed synergy vector, and N_s is the number of subjects. In this thesis, CNMF has been implemented due to a priori hypothesis that accounts for the similarities in a population which can be considered as a model of a variation of homogeneous people rather than an individual (more details in chapter 6, section 4.3.6).

4.3.5 Justification for not Using Other Factorization Techniques

Apart from NMF or CNMF, other factorization techniques such as principal component analysis and independent component analysis can also be used. However, they require assumptions such as orthogonality and independency of parameters [78]. On the other hand, NMF or CNMF is more physiologically relevant because of the non-negative nature

of linear envelope data as well as muscles can only pull (exert a contracting force) rather than push which also explains the non-negative parts of the NMF or CNMF algorithm [218, 320]. Notwithstanding, it has been shown that the components of muscle synergy analysis obtained from the NMF (i.e., muscle synergy vector and activation coefficient profiles) are highly correlated to other decomposition methods [185, 190]. Greater generalizability of the results can be obtained from the CNMF/NMF because it is the most commonly used technique in prior literature.

4.3.6 Justification for Using CNMF Factorization Techniques over NMF

NMF has been used widely in the literature for static and dynamic activities [77, 79, 83, 91, 126, 213, 218]. However, repeatability issue is one of the main hurdles of implementing NMF. This is due to the inherent property of the NMF algorithms which are known to be convex in terms of either C or S [213, 320]. Therefore, NMF solver might not find a global minimum for C and S due to 1) scaling optimal C and S by an invertible matrix so that their errors remain the same, 2) the order switch of C and S indices, and 3) the optimization problem might not converge which results in unrepeatable solutions [92, 93, 213]. In addition, in CNMF, optimization variables are less due to the concatenation of the data (C : number of subjects \times (n-by-k), S : k-by-m) as opposed to NMF approach which is subject dependent thereby each subject will have (C : (n-by-k), S : (k-by-m)) variables. As a result of search space reduction in CNMF, the significant decrease can be perceived in the number of local minima as compared to NMF. One of the main advantages of CNMF is that the results obtained from S reflect the similarities in a population which can be considered as a model of a variation of homogeneous people rather than an individual. This also facilitates the comparison between populations in terms of biomechanics and robotic control. Therefore, CNMF has shown to be reliable and provides a more robust solution.

4.3.7 CNMF MATLAB Implementation

Random values of C and S were chosen (*rand* function in MATLAB) in order to initiate the CNMF. An *alternating least squares* algorithm was implemented to attain optimal C and S . These values must satisfy the Frobenius norm to minimize the error $J = \|A - CS\|_F$. To ensure the value is reliable, perturbation was introduced to the data. In order to find the final optimal solution of S and C , three iterations were performed for the whole framework. However, the error was not applied in the last iteration [92, 94, 213, 230].

4.3.8 Variance Accounted For (VAF)

The number of synergy groups needs to be determined in order to reconstruct the original signal. This is done by the changes in total Variance Accounted For (VAF) as a function of the number of muscle synergies [79, 84]. The most common technique is to vary the number of synergies based on the number of muscles minus one (i.e., 1-9) and select the lowest number of synergies that accounted for > 0.80 of VAF (grouped-muscle criterion) [136, 179, 214]. The other criterion is to check if the addition of the next synergy group will not increase VAF by more than 0.05 [91, 123]. Additionally, the goodness of fit between each muscle's reconstruction and the original signal at each speed is performed by means of the coefficient of determination and intra-class correlation (individual-muscle criterion).

VAF was defined according to [204], as the uncentered Pearson correlation coefficient between the reconstructed and the original EMG data (Equation 4.8).

$$VAF^c = (1 - \sum_{o=1}^n \sum_{p=1}^m e_{op}^2 / \sum_{o=1}^n \sum_{p=1}^m A_{op}^2) \times 100 \quad (4.8)$$

Where e is the error, i.e., $A - CS$, and the indices o and p represent the rows and the columns of the quantities e and A . The $VAF > 0.80$ has been accepted as a standard threshold for determining the appropriate number provided that an extra synergy improves the VAF for less than 0.05 [136, 179, 219]. The threshold for each muscle reconstruction quality was determined by either $R^2 > 0.6$ [204] or $ICC > 0.5$ [92-95] however; this criterion was not considered as the primary choice to determine the number of muscle synergies.

4.3.9 Synergy Output Normalization

The activation coefficient profile was normalized with respect to their maximum value. Each module was then scaled by the inverse of the normalization activation coefficient profile. Hence, the activation coefficient profile and muscle synergy vector are varied between 0 and 1 representing temporal modulation of muscle recruitment and amplitude information in arbitrary unit [136].

4.3.10 Functional Sorting

After determining the minimum number of synergy groups and normalizing the synergies components, functional sorting was implemented to resolve the large differences in contribution to the total data variability by rearranging the indices of synergy and coefficient of one group based on the other group or between the speeds of the same group [81, 84]. Arbitrary reference was chosen to sort muscle synergy based on the similarity of S and/or C values by means of maximum R^2 . The order switch of synergy components allows comparison to be made statistically between groups. In this study, HS were sorted based on speeds intra-subjectively, i.e., HS normal was used to sort

synergy indices of HS slow and HS fast. However, for TFA, two types of sorting were performed:

Sorting 1: The sorting was done pairwise based on HS with similar speed category. That is, the synergy indices from TFA on one speed has been sorted based on their counterpart HS with the same speed. i.e., TFA slow was sorted based on HS slow, TFA normal was sorted based on HS normal, and TFA fast was sorted based on HS fast.

Sorting 2: Consequently, the previously sorted TFA (based on HS) slow and fast were sorted based on TFA normal walking speed for intra-subjective comparison. i.e., TFA fast was sorted based on TFA normal, and TFA slow was sorted based on TFA Normal.

4.3.11 Correlation Analysis

The coefficient of determination (R^2) and intra-class correlation (ICC) was calculated between each muscle's reconstructed and original signal to identify similarity in magnitude and pattern, respectively. In addition, to assess the similarity of the concatenated C between trials/subjects, ICC based on two-way mixed models for average measurements with no interactions (ICC(C,k)) was applied. According to [222], $ICC < 0.5$, $0.5 < ICC$ and $R^2 < 0.75$, and ICC and $R^2 > 0.75$ imply low, moderate, and high correlation, respectively. The degree of similarity in spatially fixed synergy vectors of HS and TFA were compared in pairwise fashion within-and between-subject by means of R^2 .

4.3.12 Statistical Parametric Mapping

All activation coefficients were statistically evaluated over the GC since the hypothesis pertains to the whole times series rather than specific time points. Therefore, the scalar and qualitative analyses were not performed in this chapter. Muscle synergies consider inter-activation coefficient profiles covariance, however; the hypothesis may pertain to a specific coefficient and/or application. Here, statistical analyses were selected based on a *priori* null hypotheses made before the experiment including:

- 1) Non-directed null hypothesis (**biomechanics perspective**): There is no difference between all activation coefficient profiles of HS and TFA IL during gait at different speeds.
- 2) Non-directed null hypothesis (**robotic control perspective**): There is no difference between individual activation coefficient profiles of HS and TFA IL during gait at different speeds.

The biomechanics hypothesis considers the covariance of the inter-activation coefficient profile whereas the robotic control hypothesis involves individual activation coefficient comparison. The rationale behind the first hypothesis is that the CNS possibly

employs activation coefficient profiles to control neuro-modularity of muscle synergies simultaneously. In addition, even though these activations are distinct, there is some degree of similarity in the temporal characteristics of synergy components as well as some commonalities in muscles involved. However, in the robotic control perspective, which has application in the controlling of robotic devices for rehabilitation such as the clinical state of the art myoelectric prosthesis, individual muscle synergy, i.e., the activation coefficient becomes important, and comparison would be useful to distinguish between populations. In this chapter, six different null hypotheses were proposed based on biomechanics and robotic control perspectives before observing the data.

4.3.12.1 Within-Subject Hypotheses

- 1) Biomechanics null hypothesis 1: There is no effect of walking speeds on HS activation coefficient profiles during walking (paired Hotelling T^2).
- 2) Robotic control null hypothesis 2: There is no effect of walking speeds on HS individual activation coefficient profiles during walking (RM ANOVA).
- 3) Biomechanics null hypothesis 3: There is no effect of walking speeds on TFA activation coefficient profiles during walking (paired Hotelling T^2).
- 4) Robotic control null hypothesis 4: There is no effect of walking speeds on TFA individual activation coefficient profiles during walking (RM ANOVA).

4.3.12.2 Between-Subject Hypotheses

- 5) Biomechanics null hypothesis 5: There is no difference between HS and TFA activation coefficient profiles during walking at each speed category (Hotelling's T^2).
- 6) Robotic control null hypothesis 6: There is no difference between individual activation coefficient profiles of HS and TFA during walking at each speed (two-sample t-test).

To account for inter-activation coefficient profile covariance (biomechanics hypotheses), SPM paired Hotelling's T^2 (hypothesis 1 and 3), and SPM Hotelling's T^2 statistics (hypothesis 5) were used within- and between-subject, respectively. Furthermore, a pairwise comparison was made using a Bonferroni correction to correct for the alpha, due to the limited multivariate ANOVA functionality in the SPM, within each population between speeds to test the biomechanics null hypotheses, i.e., HS (Normal vs. Slow), HS (Fast vs. Normal) and HS (Fast vs. Slow). A similar approach was followed for the TFA within-subject. The coefficients were analysed as a 4-component vector-field $I = 4$ (number of synergy), $J = 24$ (total number of subjects HS and TFA), $Q = 100$ (i.e. HS = [13x100x4] and TFA = [11x100x4] at each speed).

Hotelling's T^2 is conceptually similar to the scalar two-sample t-test, but it is equivalent to vector fields of scalar values. The comparison was made between two populations with the same speed category (hypothesis 5), i.e., HS slow vs. TFA slow; HS normal vs. TFA normal and HS fast vs. TFA fast. The coefficients were analyzed as an I, J and Q stated in paired Hotelling's T^2 .

For the robotic control hypotheses, SPM RM ANOVA (hypothesis 2 and 4) and SPM two-sample t-test (hypothesis 6) were implemented within- and between-subject, respectively. For more information about the SPM statistical tests refer to the literature review (Chapter 2). All SPM statistics were implemented in MATLAB R2017 (Mathworks, Inc, Natick, MA).

4.4 Results

4.4.1 Analysis of Dimensionality

4.4.1.1 Within-Subject

The VAF comparison was performed for each group between speeds. The group-muscle criterion is to select the lowest number of synergies that accounted for > 0.80 , and the next synergy group will not increase VAF by more than 0.05.

HS VAF

Figure 4.1 shows VAF of HS during transient-state walking at different speeds. Four to seven synergy groups in slow and normal, and three to seven in fast met the group-muscle criterion ($< 80\%$). However, four synergies were selected as the optimal number of groups based on the 5% criterion for all speeds.

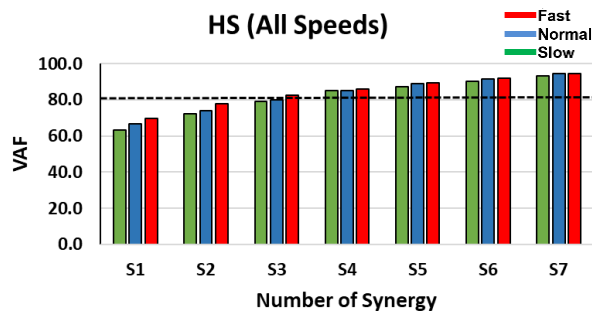


Figure 4.1: VAF comparison as a function of the number of synergies in HS at slow, normal and fast speeds.

TFA VAF

Figure 4.2 shows VAF of TFA during transient-state walking at different speeds. Three to seven synergy groups in slow and normal and two to seven in fast met the group-muscle criterion ($> 80\%$). However, four synergies were selected as the optimal number of groups based on the 5% criterion for all speeds.

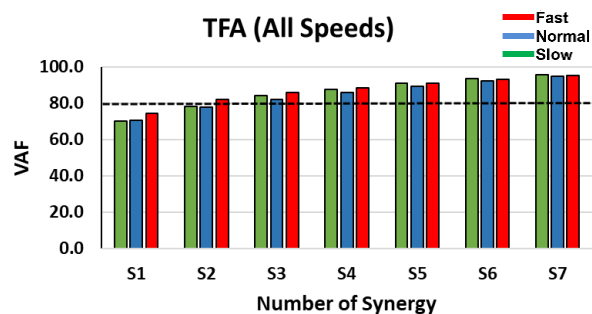


Figure 4.2: VAF comparison as a function of the number of synergies in TFA at slow, normal and fast speeds.

4.4.1.2 Between-Subject

The VAF comparison between groups was performed pairwise in terms of gait speed. The group-muscle criterion is to select the lowest number of synergies that accounted for > 0.80 .

HS vs.TFA (Slow)

Figure 4.3 illustrates HS and TFA analysis of dimensionality during slow walking where four modules accounted for 85 % and 88% of the total VAF, respectively. Three synergy groups were lower than the critical threshold in HS (79%) however, TFA showed a VAF value of 83%. Additional of a fifth synergy increased the HS VAF to 87% and TFA VAF to 90.9% which was less than the 5% criterion.

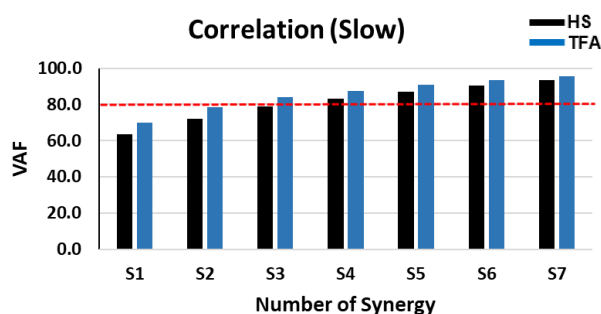


Figure 4.3: VAF comparison as a function of the number of synergy groups in HS and TFA at slow speed.

HS vs.TFA (Normal)

Figure 4.4 illustrates HS and TFA VAF values of 85% and 86% when four synergy groups were selected during normal walking, respectively. The third module was able to account for 79% and 81% of the original EMG variance in HS and TFA, respectively. An additional fifth synergy produced less than 5% improvement (HS = 89% and TFA = 89%).

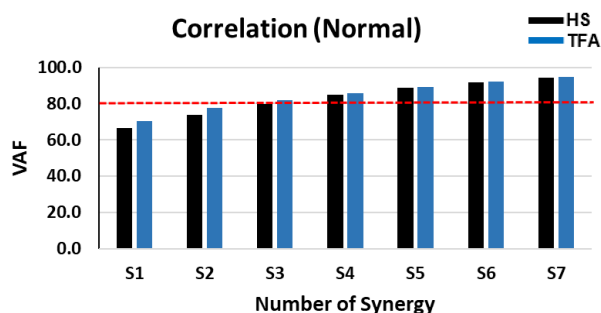


Figure 4.4: VAF comparison as a function of the number of synergy groups in HS and TFA at normal speed.

HS vs.TFA (Fast)

Figure 4.5 illustrates four modules could reproduce the original EMG data with a VAF value of 86% and 88% in HS and TFA during fast walking, respectively. However, the third synergy groups also passed the critical threshold in both groups and illustrated HS VAF of 82% and TFA VAF of 85%. Additional of a fifth synergy increased the VAF to 89% in HS and 91% in TFA which was less than the 5% criterion.

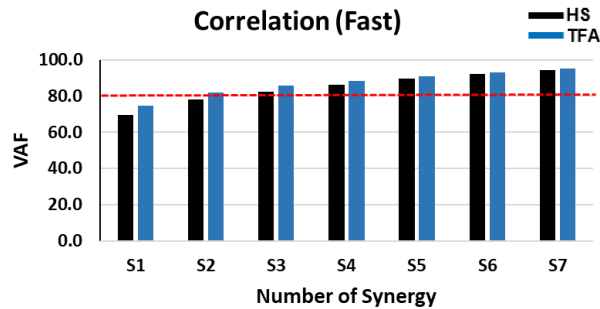


Figure 4.5: VAF comparison as a function of the number of synergy groups in HS and TFA at fast speed.

4.4.2 Correlation Analysis Using R^2 (Individual-Muscle Criterion)

R^2 was performed to assess how well the original muscle signal can be replicated by the individual muscle signal reconstruction. R^2 is a good statistical analysis that accounts for the magnitude of the signal and ranges from 0 (low correlation) to 1 (strong correlation).

4.4.2.1 Within-Subject

HS R^2

Figure 4.6 shows moderate to strong correlation between reconstructed and original signals in the HS while walking at three different speeds. The lowest and the highest correlation was observed in TFL (0.52) during slow and in VL (0.98) during normal walking, respectively.

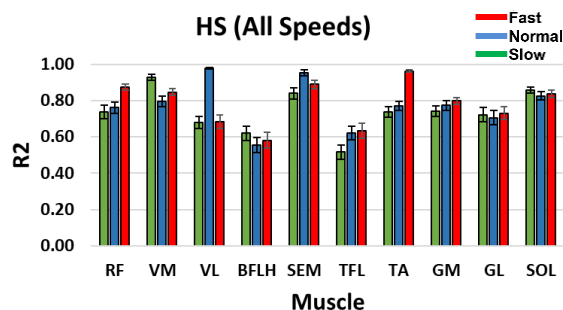


Figure 4.6 HS R^2 between the reconstructed and original muscle signal when four synergy groups were selected during slow, normal and fast speeds. Standard error bars indicate \pm one.

TFA R²

Figure 4.7 shows a correlation between the reconstructed and the original individual muscle signal in TFA at three different speeds. All muscles within their respective speeds showed moderate to high correlation. The lowest and the highest R² associated with SEM (0.53) and TA (0.98) during normal walking, respectively.

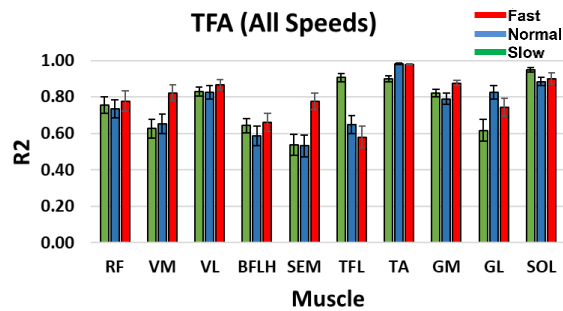


Figure 4.7: TFA R² between the reconstructed and original muscle signal when four synergy groups were selected during slow, normal and fast speeds. Standard error bars indicate \pm one.

4.4.2.2 Between-Subject

HS vs.TFA (Slow)

Figure 4.8 shows a reasonable correlation between the reconstructed individual muscle signal and the original signal in HS and TFA during slow transient-state walking. The lowest and the highest correlation in HS were found in TFL (0.52) and VM (0.93) whereas in TFA, SEM (0.54) and SOL (0.95), respectively.

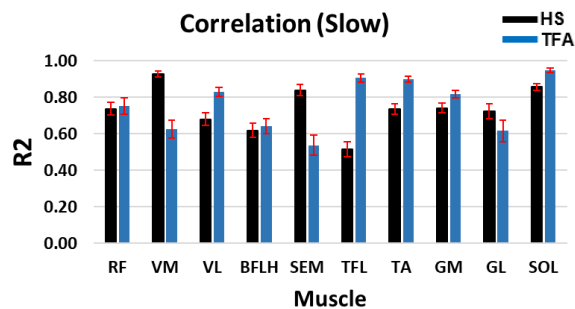


Figure 4.8: HS R² between the reconstructed and original muscle signal when four synergy groups were selected at slow speed. Standard error bars indicate \pm one.

HS vs.TFA (Normal)

Figure 4.9 shows moderate to strong correlation of the individual reconstructed muscle signal and the original signal during normal transient-state walking. HS lowest and highest correlation were observed in BFLH (0.56) and VL (0.98), respectively. In TFA, the lowest correlation was shown in SEM (0.53) and the highest in TA (0.98).

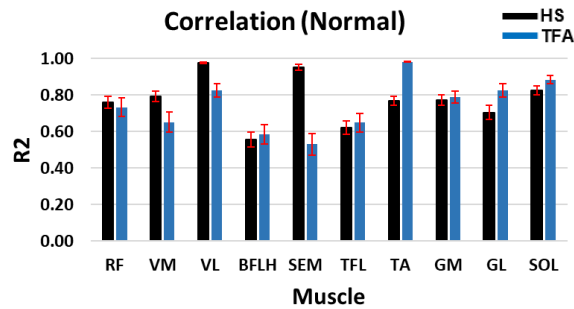


Figure 4.9: HS R^2 between the reconstructed and original muscle signal when four synergy groups were selected at normal speed. Standard error bars indicate \pm one.

HS vs. TFA (Fast)

Figure 4.10 shows moderate to high correlation between reconstructed and original muscle signals during fast transient-state walking. The lowest and the highest correlation in HS were found in BFLH (0.58) and TA (0.96) whereas in TFA, TFL (0.58) and TA (0.98) showed the lowest and the highest correlation, respectively.

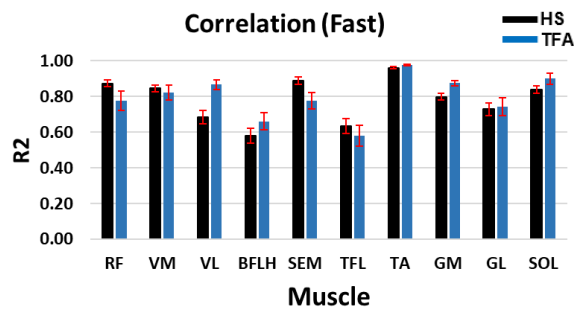


Figure 4.10: HS R^2 between the reconstructed and original muscle signal when four synergy groups were selected at fast speed. Standard error bars indicate \pm one.

4.4.3 Correlation Analysis Using ICC

As opposed to R^2 , ICC takes the signal pattern comparison into account and allows for multiple comparisons to be made. ICC was used for two purposes in this study: 1) to assess the similarities between reconstructed and original muscle EMG signal (within-subject and between-subject for individual-muscle criterion); and 2) to evaluate the repeatability of coefficients between trials/subjects.

4.4.3.1 Within-Subject

HS ICC

Figure 4.11 shows moderate to strong correlation between reconstructed and original signals in HS at three different speeds. The results agree with the HS R^2 .

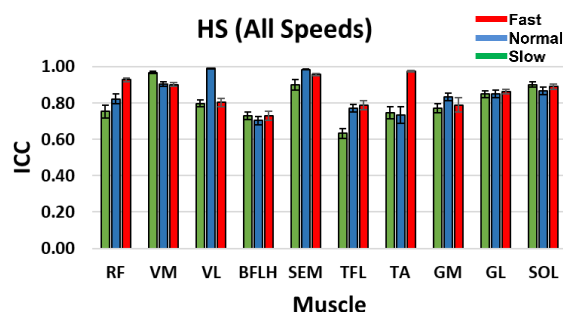


Figure 4.11: HS ICC between the reconstructed and original muscle signal when four synergy groups were selected during slow, normal and fast speeds. Standard error bars indicate \pm one.

TFA ICC

Figure 4.12 shows a correlation between the reconstructed and the original individual muscle signals in TFA at three different speeds. All muscles within their respective speeds showed moderate to high correlation. The results agree with the TFA R^2 .

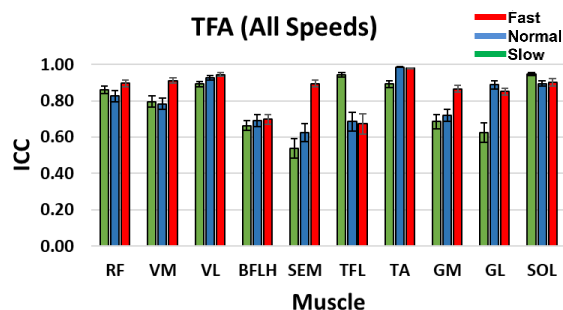


Figure 4.12: TFA ICC between the reconstructed and original muscle signal when four synergy groups were selected during slow, normal and fast speeds. Standard error bars indicate \pm one.

4.4.3.2 Between-Subject

HS vs.TFA (Slow)

In HS, the lowest and highest similarities between reconstructed and original signals were observed in TFL (0.52) and VM (0.93) respectively, whereas in TFA, SEM and SOL ICC showed the lowest and highest values of 0.54 and 0.95 respectively (Figure 4.13).

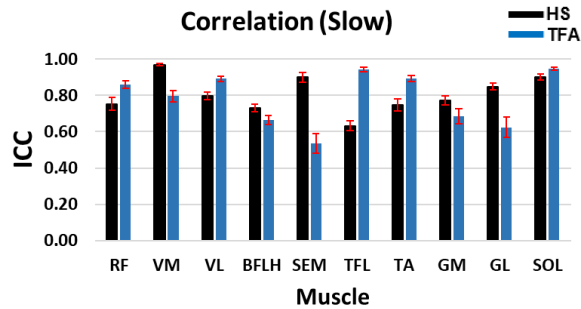


Figure 4.13: HS ICC between the reconstructed and original muscle signal when four synergy groups were selected at slow speed. Standard error bars indicate \pm one.

HS vs.TFA (Normal)

In HS, the lowest and highest similarities between reconstructed and original signals were observed in BFLH (0.53) and VL (0.98) respectively, whereas in TFA, SEM and TA ICC showed the lowest and highest values of 0.53 and 0.98 respectively (Figure 4.14).

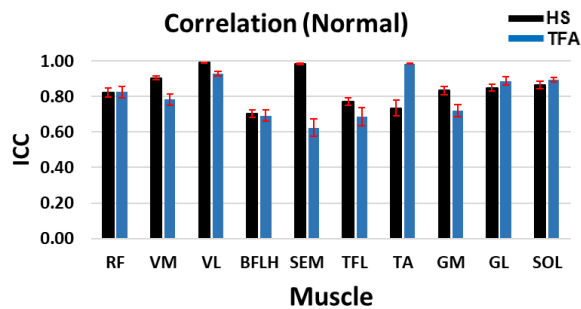


Figure 4.14: HS ICC between the reconstructed and original muscle signal when four synergy groups were selected at normal speed. Standard error bars indicate \pm one.

HS vs.TFA (Fast)

In HS, the lowest and highest similarities between reconstructed and original signals were observed in TA (0.96) and BFLH (0.58) respectively, whereas in TFA, TA and TFL ICC showed the lowest and highest values of 0.98 and 0.58 respectively (Figure 4.15).

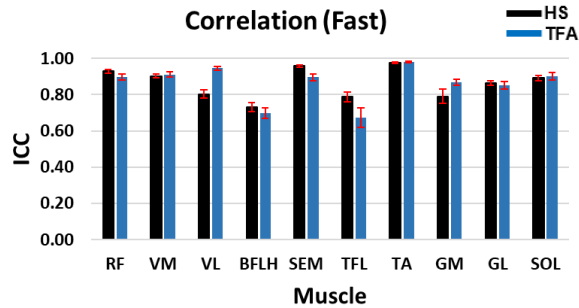


Figure 4.15: HS ICC between the reconstructed and original muscle signal when four synergy groups were selected at fast speed. Standard error bars indicate \pm one.

4.4.4 CNMF Activation Coefficient Profile Repeatability

4.4.4.1 Within-Subject

As shown in Table 4.1 and Table 4.2, In both groups, high repeatability (ICC > 0.75) was perceived as the ICC value for between trials/subjects similarities in each speed category was above 0.80 except in TFA C4 normal speed. ICC for TFA C4 showed to be 0.29, indicating poor repeatability (ICC < 0.5).

Table 4.1: HS activation coefficient profile repeatability between trials/subjects using ICC.

HS intra-class correlation				
	C1	C2	C3	C4
Slow	0.98	0.99	0.95	0.97
Normal	0.99	0.99	0.97	0.91
Fast	0.99	0.99	0.99	0.97

Table 4.2: TFA activation coefficient profile repeatability between trials/subjects using ICC.

TFA intra-class correlation				
	C1	C2	C3	C4
Slow	0.89	0.80	0.97	0.87
Normal	0.98	0.94	0.90	0.29
Fast	0.98	0.97	0.94	0.85

4.4.5 Muscle Synergy Analysis Description

4.4.5.1 Within-Subject

As shown in Figure 4.16 (A) and (B), the descriptive analysis of HS muscle synergy vectors (S1-S4) and activation coefficient profiles (C1-C4) was investigated during transient-state walking across speeds, respectively (summary of results in Table 4.3 to Table 4.6).

As shown in Figure 4.17 (A) and (B), the descriptive analysis of TFA muscle synergy vectors (S1-S4) and activation coefficient profiles (C1-C4) was investigated during transient-state walking across speeds, respectively (summary of results in Table 4.7 to Table 4.10)

HS Muscle Synergy Description

HS synergy 1 (S1) consisted of the activation of VM in slow (during ES and TSW), VM, TFL and TA in normal (during ES, ISW, and TSW) and TA in fast walking (during ES, ISW, and TSW) (Table 4.3). HS synergy 2 (S2) was associated with the forward propulsion subtask across speeds, in which plantarflexor muscles were primarily involved (Table 4.4). HS synergy 3 (S3) consisted of the activation of knee extensors in ES and TSW across speeds (Table 4.5). HS synergy 4 (S4) primary activated knee flexor in ES and transition from swing to stance phase across speeds (Table 4.6). HS muscle synergy description is based on Figure 4.16 (A) and (B).

TFA Muscle Synergy Description

TFA S1 was related to the recruitment of TFL in slow (during ES and TSW), SOL and TFL in normal (during ES-MS, TS, and TSW), and knee extensors in fast walking (during ES-MS) across speeds (Table 4.7). TFA S2 related to body support and forward propulsion, in which the plantarflexor muscles were primarily involved across speeds (Table 4.8). TFA S3 was related to the activation of the knee extensors during ES and TSW of slow and normal walking and SEM and VL during ES and MS-TSW of fast walking (Table 4.9). TFA S4 related to the leg swing as well as the transition from swing to stance, in which the dorsiflexor muscle was primarily involved across speeds (Table 4.10). TFA muscle synergy description is based on Figure 4.17 (A) and (B).

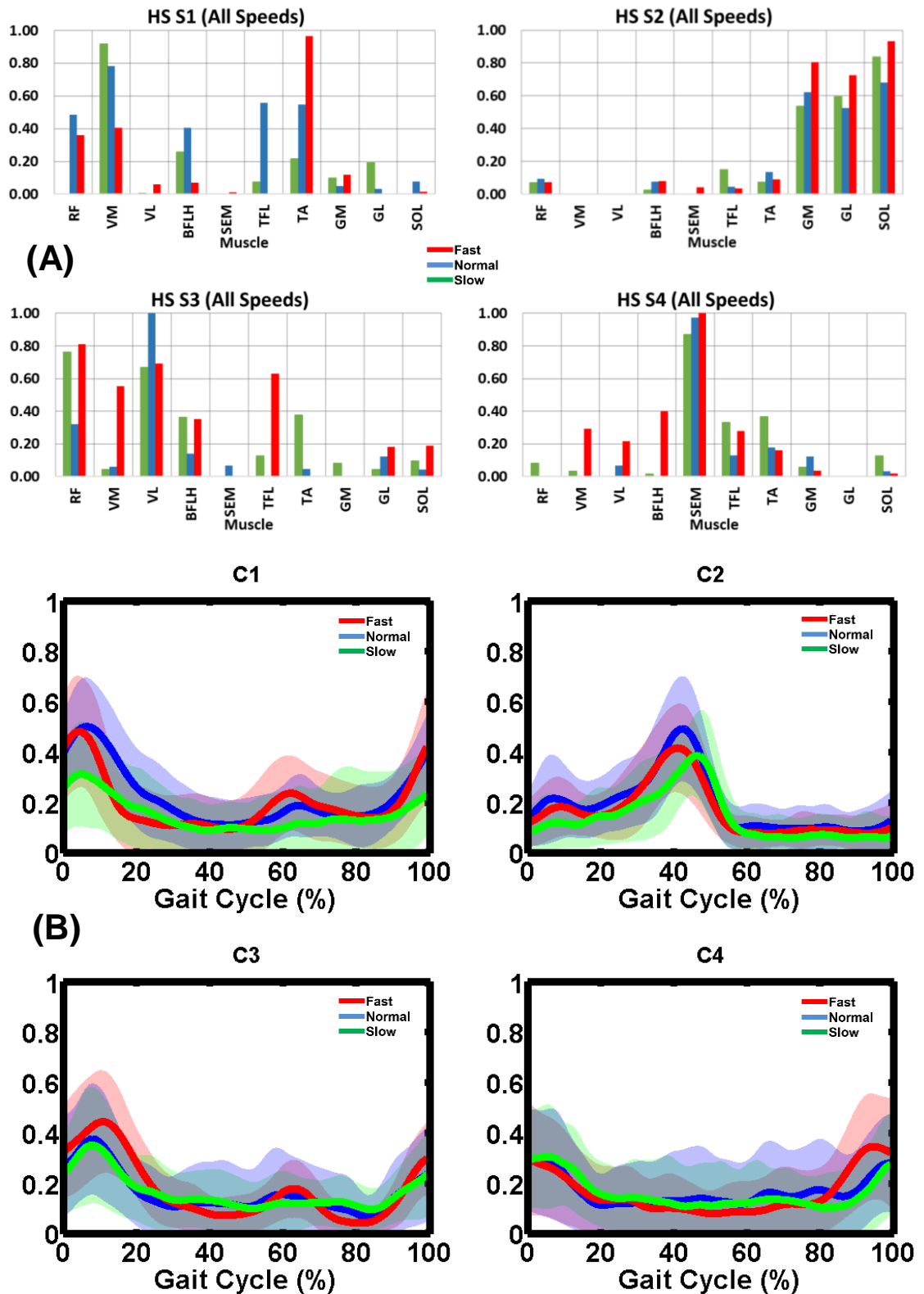


Figure 4.16: HS (A) muscle synergy vectors (S1-S4) and (B) activation coefficient profiles (C1-C4) during slow, normal and fast speeds. In (A), the bars represent muscle weightings within each synergy group. In (B), the thick lines represent the mean trajectory of activation coefficient profiles and the shaded area \pm one standard deviation from the mean.

Table 4.3: HS muscle weightings contribution and corresponding activation timing profile of S1 across speeds. Early, mid and terminal stance represent ES, MS, and TS; initial, mid and terminal swing represents ISW, MSW, and TSW; the whole stance and swing phase represents SP and SW respectively.

HS synergy 1 (All speeds)			
Module	Muscle		Activation
	<i>Primary*</i>	<i>Secondary*</i>	
Fast	TA	VM, RF, GM, BFLH, VL, SEM, SOL	IC-LR, ISW, TSW
Normal	VM, TFL, TA	RF, BFLH, SOL, GM, GL	IC-LR, ISW, TSW
Slow	VM	BFLH, TA, GL, GM, TFL, VL	IC-LR, TSW

* Muscle weighting: primary > 0.5, and secondary < 0.05

Table 4.4: HS muscle weightings contribution and corresponding activation timing profile of S2 across speeds.

HS synergy 2 (All speeds)			
Module	Muscle		Activation
	<i>Primary*</i>	<i>Secondary*</i>	
Fast	SOL, GM, GL	TA, BFLH, RF, SEM, TFL	TS
Normal	SOL, GM, GL	TA, RF, BFLH, TFL	TS
Slow	SOL, GL, GM	TFL, RF, TA, BFLH	TS

* Muscle weighting: primary > 0.5, and secondary < 0.05

Table 4.5: HS muscle weightings contribution and corresponding activation timing profile of S3 across speeds.

HS synergy 3 (All speeds)			
Module	Muscle		Activation
	<i>Primary*</i>	<i>Secondary*</i>	
Fast	RF, VL, TFL, VM	BFLH, SOL, VL	ES-MS, TSW
Normal	VL	RF, BFLH, GL, SEM, VM, TA, SOL	IC-LR, TSW
Slow	RF, VL	TA, BFLH, TFL, SOL, GM, GL, VM	IC-LR

* Muscle weighting: primary > 0.5, and secondary < 0.05

Table 4.6: HS muscle weightings contribution and corresponding activation timing profile of S4 across speeds.

HS synergy 4 (All speeds)			
Module	Muscle		Activation
	<i>Primary*</i>	<i>Secondary*</i>	
Fast	SEM	BFLH, VM, TFL, VL, TA, GM, SOL	IC-LR, MSW-TSW
Normal	SEM	TA, TFL, GM, VL, SOL	IC-LR, TSW
Slow	SEM	TA, TFL, SOL, RF, GM, VM, BFLH	IC-LR, TSW

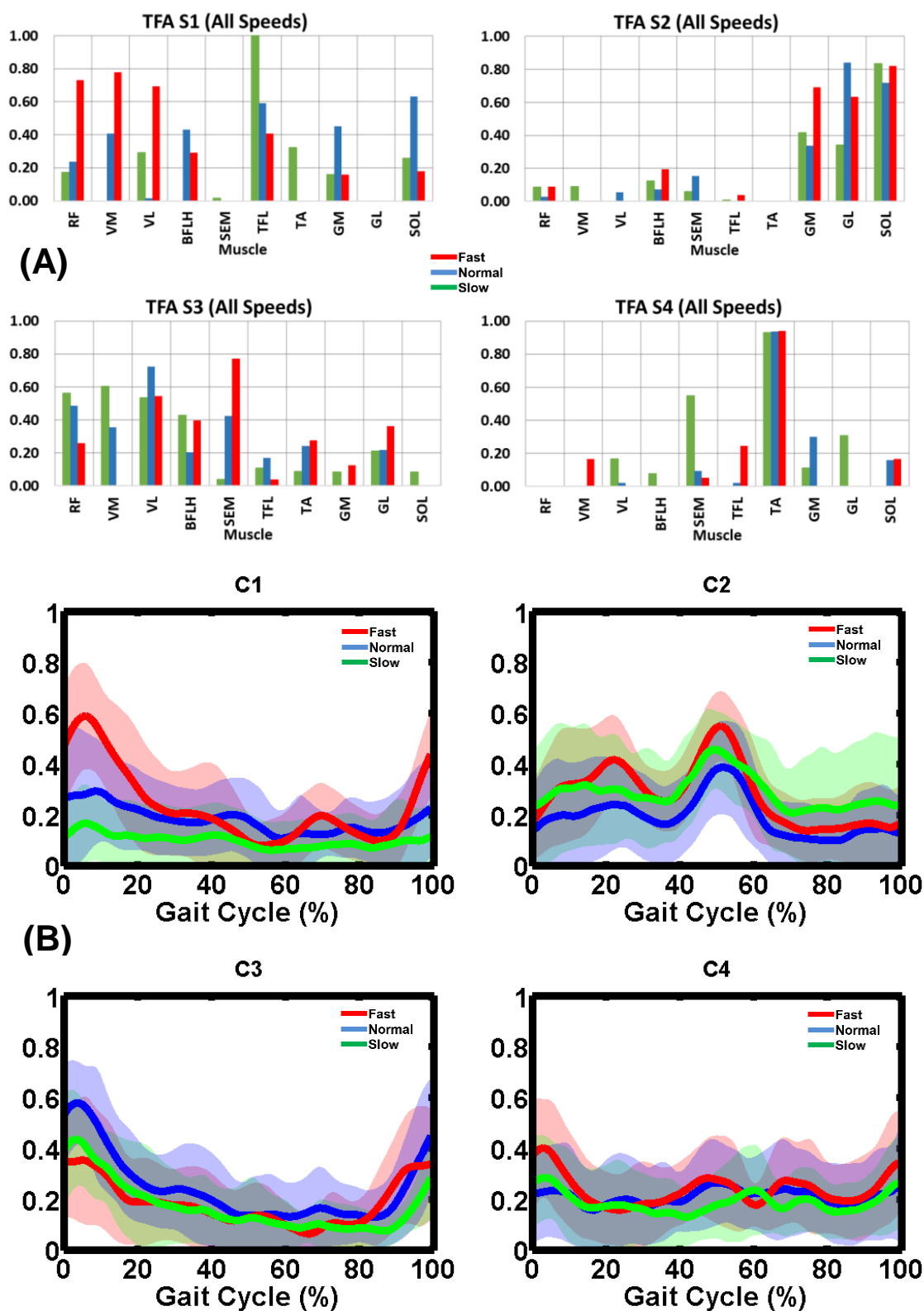


Figure 4.17: TFA (A) muscle synergy vectors (S1-S4) and (B) activation coefficient profiles (C1-C4) during slow, normal and fast speeds. In (A), the bars represent muscle weightings within each synergy group. In (B), the thick lines represent the mean trajectory of activation coefficient profiles and the shaded area \pm one standard deviation from the mean.

Table 4.7: TFA muscle weightings contribution and corresponding activation timing profile of S1 across speeds.

TFA synergy 1 (All speeds)			
Module	Muscle		Activation
	<i>Primary*</i>	<i>Secondary*</i>	
Fast	VM, RF, VL	TFL, BFLH, SOL, GM	ES, TSW
Normal	SOL, TFL	GM, BFLH, VM, RF, VL	ES*-MS, TS, TSW
Slow	TFL	TA, VL, SOL, RF, GM, SEM	IC-LR, MS

* Muscle weighting: primary > 0.5, and secondary < 0.05

Table 4.8: TFA muscle weightings contribution and corresponding activation timing profile of S2 across speeds.

TFA synergy 2 (All speeds)			
Module	Muscle		Activation
	<i>Primary</i>	<i>Secondary</i>	
Fast	SOL, GM, GL	BFLH, RF, TFL	MS, TS
Normal	GL, SOL	GM, SEM, BFLH, VL, RF	MS, TS
Slow	SOL	GM, GL, BFLH, RF, VM, SEM	MS, TS

* Muscle weighting: primary > 0.5, and secondary < 0.05

Table 4.9: TFA muscle weightings contribution and corresponding activation timing profile of S3 across speeds.

TFA synergy 3 (All speeds)			
Module	Muscle		Activation
	<i>Primary*</i>	<i>Secondary*</i>	
Fast	SEM, VL	BFLH, GL, TA, RF, GM, TFL	ES, MSW-TSW
Normal	VL	RF, SEM, VM, TA, GL, BFLH, TFL	IC-LR, TSW
Slow	VM, RF, VL	BFLH, GL, TFL, TA, GM, SOL, SEM	IC-LR, TSW

* Muscle weighting: primary > 0.5, and secondary < 0.05

Table 4.10: TFA muscle weightings contribution and corresponding activation timing profile of S4 across speeds.

TFA synergy 4 (All speeds)			
Module	Muscle		Activation
	<i>Primary*</i>	<i>Secondary*</i>	
Fast	TA	TFL, VM, SOL, SEM	IC-LR, TS, ISW, TSW
Normal	TA	GM, SOL, SEM, VL, TFL	IC-LR, TS-PSW-ISW, TSW
Slow	TA, SEM	GL, VL, GM, BFLH	IC-LR, PSW-ISW, TSW

* Muscle weighting: primary > 0.5, and secondary < 0.05

4.4.5.2 Between-Subject

Descriptive analysis was done between HS and TFA muscle synergy vectors (S1-S4) and activation coefficient profiles (C1-C4) during transient-state walking at each speed category.

HS Muscle Synergy Description (Slow)

In HS during slow walking, S1 showed a high activation of VM and to a lesser extent BFLH, TA and GL during ES (IC-LR) and TSW. S2 consisted of activity in TS primarily from SOL and a lesser activity from GM and GL. S3 was comprised primarily of activity in RF and VL and lower activation of TA, BFLH during ES. S4 was mainly composed of SEM activation as a primary muscle and TA, TFL, SOL, RF activations as secondary muscles during ES and TSW (Table 4.11 and Figure 4.18).

Table 4.11: HS muscle weightings contribution and activation timing profile within each corresponding module during slow speed.

HS (Slow)			
Module	Muscle		Activation
	Primary*	Secondary*	
S1	VM	BFLH, TA, GL, GM, TFL, VL	IC-LR, TSW
S2	SOL, GL, GM	TFL, RF, TA, BFLH	TS
S3	RF, VL	TA, BFLH, TFL, SOL, GM, GL, VM	IC-LR
S4	SEM	TA, TFL, SOL, RF, GM, VM, BFLH	IC-LR, TSW

* Muscle weighting: primary > 0.5, and secondary < 0.05

TFA Muscle Synergy Description (Slow)

In TFA during slow walking, S1 was composed of mainly TFL high activation and a lesser activity from TA, VL and SOL during ES and MS. S2 consisted of activity in MS and TS from SOL and to a lesser extent from GM and GL. S3 comprised primary activity in quadriceps and lower activations of BFLH and GL during ES, and TSW. S4 was mainly composed of TA and SEM activations as primary muscles and GL and VL activations as secondary muscles during ES, PSW-ISW, and TSW (Table 4.12 and Figure 4.18).

Table 4.12: TFA muscle weightings contribution and activation timing profile within each corresponding module during slow speed.

TFA (Slow)			
Module	Muscle		Activation
	Primary*	Secondary*	
S1	TFL	TA, VL, SOL, RF, GM, SEM	IC-LR, MS
S2	SOL	GM, GL, BFLH, RF, VM, SEM	MS, TS
S3	VM, RF, VL	BFLH, GL, TFL, TA, GM, SOL, SEM	IC-LR, TSW
S4	TA, SEM	GL, VL, GM, BFLH	IC-LR, PSW-ISW, TSW

* Muscle weighting: primary > 0.5, and secondary < 0.05

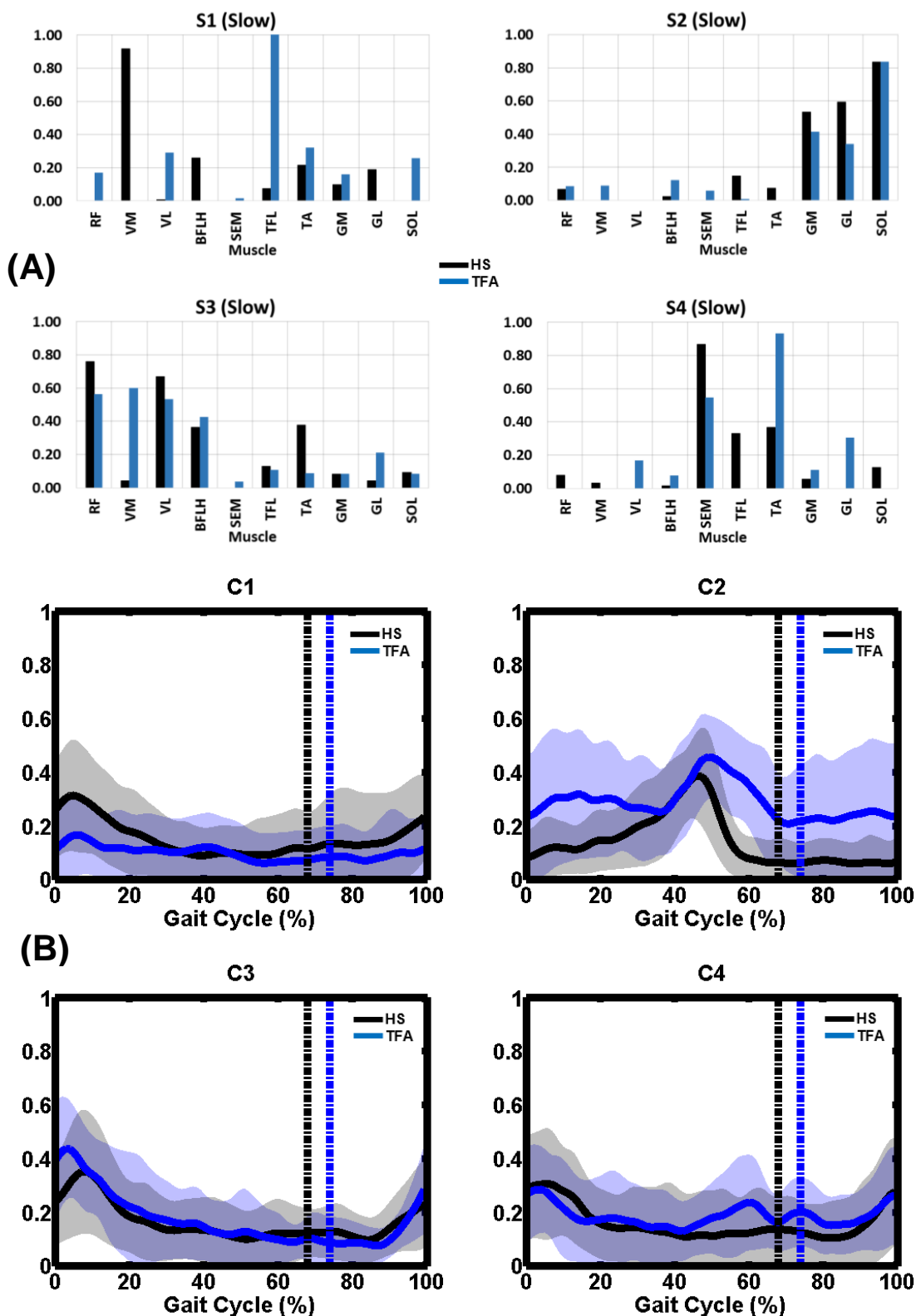
HS vs. TFA (Slow)

Figure 4.18: (A) muscle synergy vectors (S1-S4) and (B) activation coefficient profiles (C1-C4) for HS and TFA groups during slow speed. In (A), bars represent weighting of each muscle within each synergy group. In (B), thick lines represent the mean trajectory of the activation coefficient profiles and the shaded area \pm one standard deviation from the mean.

HS Muscle Synergy Description (Normal)

In HS during normal walking, S1 showed a high activation of VM, TFL, and TA as primary muscles and to a lesser extent RF and BFLH during ES, ISW, and TSW. S2 consisted of activity in TS primarily from triceps surae. S3 was comprised primarily of activity VL and lower activation of RF during ES and TSW. S4 was mainly composed of SEM activation as a primary muscle and TA, TFL and GM activations as secondary muscles during ES and TSW (Table 4.13 and Figure 4.19).

Table 4.13: HS muscle weightings contribution and activation timing profile within each corresponding module during normal speed.

Healthy (Normal)			
Module	Muscle		Activation
	<i>Primary*</i>	<i>Secondary*</i>	
S1	VM, TFL, TA	RF, BFLH, SOL, GM, GL	IC-LR, ISW, TSW
S2	SOL, GM, GL	TA, RF, BFLH, TFL	TS
S3	VL	RF, BFLH, GL, SEM, VM, TA, SOL	IC-LR, TSW
S4	SEM	TA, TFL, GM, VL, SOL	IC-LR, TSW

* Muscle weighting: primary > 0.5, and secondary < 0.05

TFA Muscle Synergy Description (Normal)

In TFA during normal walking, S1 was composed of mainly SOL and TFL high activations and a lesser activity from GM, BFLH, GL and TFL in ES to MS, TS as well as TSW. S2 consisted of activity in MS and TS from GL and SOL, and to a lesser extent from GM. S3 comprised primary activity in VL and lower activations of RF, SEM, VM, TA, GL, and BFLH during ES and TSW. S4 was mainly composed of TA activation as a primary muscle and GM, SOL and SEM activations as secondary muscles during ES, TS to PSW, ISW, and TSW (Table 4.14 and Figure 4.19).

Table 4.14: TFA muscle weightings contribution and activation timing profile within each corresponding module during normal speed.

Transfemoral (Normal)			
Module	Muscle		Activation
	<i>Primary*</i>	<i>Secondary*</i>	
S1	SOL, TFL	GM, BFLH, VM, RF, VL	ES-MS, TS, TSW
S2	GL, SOL	GM, SEM, BFLH, VL, RF	MS, TS
S3	VL	RF, SEM, VM, TA, GL, BFLH, TFL	IC-LR, TSW
S4	TA	GM, SOL, SEM, VL, TFL	IC-LR, TS-PSW, ISW, TSW

* Muscle weighting: primary > 0.5, and secondary < 0.05

HS vs. TFA (Normal)

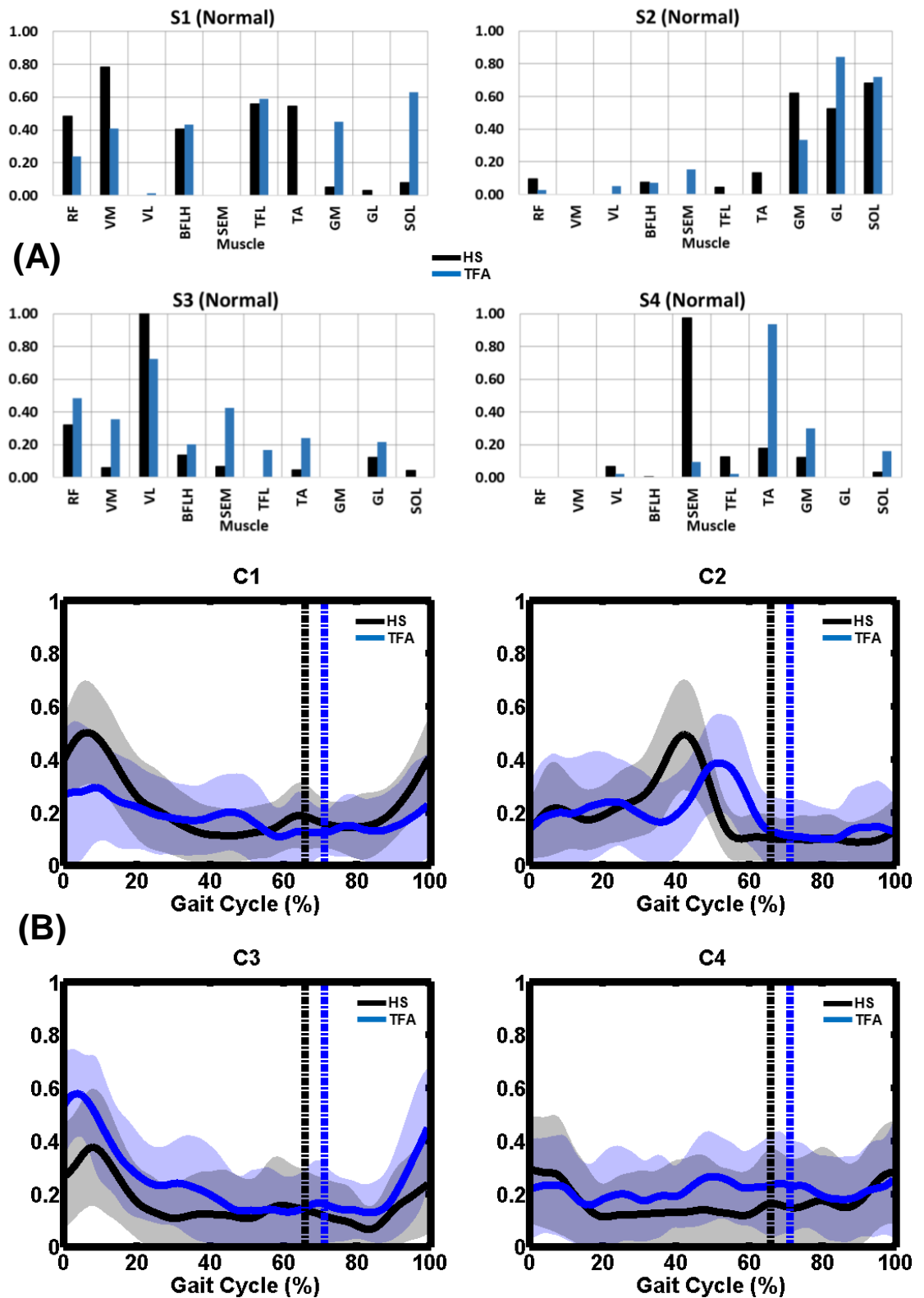


Figure 4.19: (A) muscle synergy vectors (S1-S4) and (B) activation coefficient profiles (C1-C4) for HS and TFA groups during normal speed. In (A), bars represent weighting of each muscle within each synergy group. In (B), thick lines represent the mean trajectory of the activation coefficient profiles and the shaded area \pm one standard deviation from the mean.

HS Muscle Synergy Description (Fast)

In HS during fast walking, S1 showed a high activation of TA and to a lesser extent VM and RF during ES, ISW, and TSW. S2 consisted of activity in TS primarily from triceps surae. S3 was comprised primarily of activity RF, Vasti and TFL and a lesser activity of BFLH during ES to MS and TSW. S4 was mainly composed of SEM activation as a primary muscle and BFLH, Vasti and TFL activations as secondary muscles during ES and MSW to TSW (Table 4.15 and Figure 4.20).

Table 4.15: HS muscle weightings contribution and activation timing profile within each corresponding module during fast speed.

Healthy (Fast)			
Module	Muscle		Activation
	<i>Primary*</i>	<i>Secondary*</i>	
S1	TA	VM, RF, GM, BFLH, VL, SEM, SOL	IC-LR, ISW, TSW
S2	SOL, GM, GL	TA, BFLH, RF, SEM, TFL	TS
S3	RF, VL, TFL, VM	BFLH, SOL, VL	ES-MS, TSW
S4	SEM	BFLH, VM, TFL, VL, TA, GM, SOL	IC-LR, MSW-TSW

* Muscle weighting: primary > 0.5, and secondary < 0.05

TFA Muscle Synergy Description (Fast)

In TFA during fast walking, S1 was composed of mainly TA high activation and a lesser activity from TFL during ES, TS, ISW, and TSW. S2 consisted of activity in MS and TS from triceps surae and to a lesser extent from BFLH. S3 comprised primary activity in quadriceps and lower activations of TFL and BFLH during ES and TSW. S4 was mainly composed of SEM and VL activations as primary muscles and BFLH, GL, TA and RF activations as secondary muscles during ES, MSW to TSW (Table 4.16 and Figure 4.20).

Table 4.16: TFA muscle weightings contribution and activation timing profile within each corresponding module during fast speed.

Transfemoral (Fast)			
Module	Muscle		Activation
	<i>Primary*</i>	<i>Secondary*</i>	
S1	TA	TFL, VM, SOL, SEM	IC-LR, TS, ISW, TSW
S2	SOL, GM, GL	BFLH, RF, TFL	MS, TS
S3	VM, RF, VL	TFL, BFLH, SOL, GM	ES, TSW
S4	SEM, VL	BFLH, GL, TA, RF, GM, TFL	ES, MSW-TSW

* Muscle weighting: primary > 0.5, and secondary < 0.05

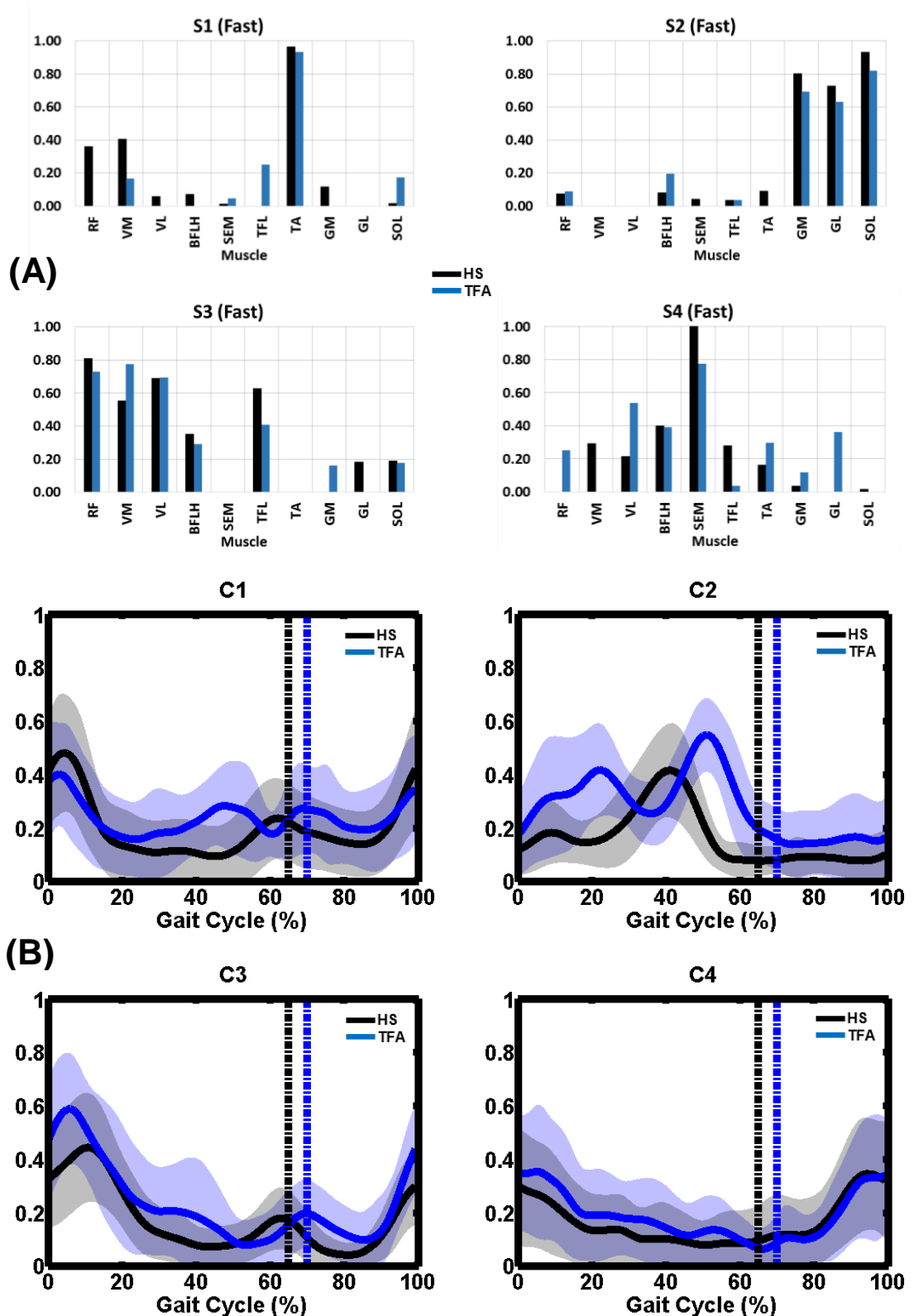
HS vs. TFA (Fast)

Figure 4.20: (A) muscle synergy vectors (S1-S4) and (B) activation coefficient profiles (C1-C4) for HS and TFA groups during fast speed. In (A), bars represent weighting of each muscle within each synergy group. In (B), thick lines represent the mean trajectory of the activation coefficient profiles and the shaded area \pm one standard deviation from the mean.

4.4.6 Module Contribution

The contribution of each module has been calculated with respect to the total synergies contribution at each speed category (Figure 4.21).

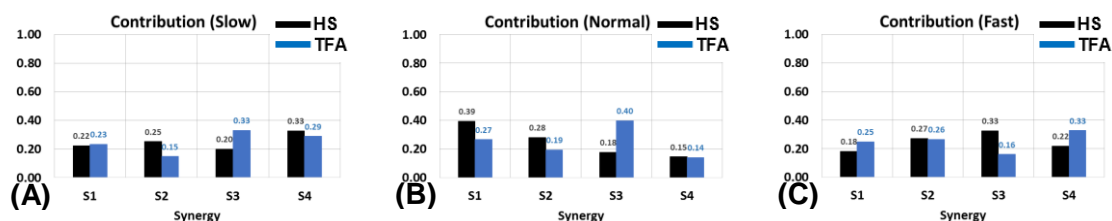


Figure 4.21: Individual synergy group contribution with respect to the total contribution between HS and TFA at (A) slow, (B) normal and (C) fast.

Table 4.17 shows the functional muscle group corresponded to the highest and lowest contributed module. In slow gait, S4 (mainly related to knee flexors) for HS and S3 (mainly activated knee extensors) for TFA had the highest contribution. However, the contribution of S3 (mainly activated knee extensor) and S2 (mainly activated plantarflexors) for HS and TFA were the lowest, respectively. In walking, the highest and lowest module contribution of HS belonged to S1 (mainly activated knee extensors) and S4 (mainly activated knee flexors) whereas, in TFA, S3 (mainly activated knee extensors) and S4 showed (mainly activated dorsiflexor) the highest and lowest contribution, respectively. In fast gait, the highest and lowest module contribution of HS was observed in S3 (mainly activated knee extensor) and S1 (mainly activated dorsiflexor) however, S4 (Mainly activated knee flexors) had the highest and S3 (mainly activated knee extensors) the lowest module contribution in TFA.

Table 4.17: Highest and lowest muscle synergy group contribution and corresponding muscle group association.

	<u>Highest</u>		<u>Lowest</u>	
	HS	TFA	HS	TFA
Slow	S4 (Knee flexors)	S3 (knee extensors)	S3 (knee extensors)	S2 (plantarflexors)
Normal	S1 (knee extensors)	S3 (knee extensors)	S4 (knee flexors)	S4 (dorsiflexor)
Fast	S3 (knee extensors)	S4 (knee flexors)	S1 (dorsiflexor)	S3 (knee extensors)

4.4.7 Statistical Analyses (Spatially Fixed Muscle Synergies)

R^2 was calculated intra-subjectively between speeds as a pairwise analysis to investigate the correlation between two muscle synergies.

4.4.7.1 Within-Subject

Speed Dependence of the HS Muscle Synergy Vectors

The goodness of fit between HS normal-slow speed showed moderate to strong correlation between modules. The correlation between HS normal-slow speed showed low (S3), moderate (S1, S4), and strong correlation (S2) between synergy groups. The comparison between HS slow-fast speed showed a low correlation in S1, the moderate correlation in S3 and S4, and strong correlation in S2.

As shown in Table 4.18, HS normal-slow R^2 showed moderate (S1 and S3) and strong (S2 and S4) correlations between muscle synergies. Comparison between modules of normal and fast illustrated low (S3), moderate (S1) and strong (S2 and S4) correlations. The results obtained from muscle synergies of HS during fast-slow gait exhibited low (S1), moderate (S3) and strong (S2 and S4) correlations. The average module goodness of fit for each muscle synergy across speeds illustrated a moderate correlation of S1 (0.43) and S3 (0.45), as well as a strong correlation of S2 (0.92) and S4 (0.79). Overall average R^2 of all four modules combined (S1-S4) in pairwise speed comparison showed strong ($R^2_{Average} = 0.75$), moderate ($R^2_{Average} = 0.56$) and moderate ($R^2_{Average} = 0.63$) in slow-normal, normal-fast and fast-slow walking, respectively.

Table 4.18: R^2 values for four muscle synergies in HS at different speeds; The module average obtained column wise represents the average correlation of each module with respect to all paired-wise speed comparison. The overall average value obtained row-wise represents the average correlation of all muscle synergies with respect to each pair-wise speed comparison.

	S1	S2	S3	S4	Overall Average
Normal vs. Slow	0.6	0.95	0.57	0.89	0.75
Normal vs. Fast	0.53	0.88	0.12	0.71	0.56
Fast vs. Slow	0.17	0.94	0.66	0.76	0.63
Module Average	0.43	0.92	0.45	0.79	

Speed Dependence of the TFA Muscle Synergy Vectors/Modules

As shown in Table 4.19, TFA normal-slow R^2 showed a low correlation of S1, moderate correlation of S4 and a strong correlation of S2 and S3. The comparison between modules of normal and fast illustrated low (S1), moderate (S3) and strong (S2 and S4) correlations. The correlation between TFA fast-slow R^2 revealed low (S1 and S3),

moderate (S4) and strong (S2) relationship between muscle synergies. The module average goodness of fit for each muscle synergy across speeds illustrated low correlation for S1 (0.04), moderate correlation of S3 (0.53) and S4 (0.65) as well as a strong correlation for S2 (0.83). Overall average R^2 of all four modules combined (S1-S4) showed low correlation between fast-slow ($R^2_{Average} = 0.40$) and moderate correlation between normal-slow ($R^2_{Average} = 0.53$) and normal-fast ($R^2_{Average} = 0.61$) gait.

Table 4.19: R^2 values for four muscle synergies in TFA at different speeds; Refer to Table 4.18 for the meaning of the module average and the overall average.

	S1	S2	S3	S4	<i>Overall Average</i>
Normal vs. Slow	0	0.78	0.72	0.61	0.53
Normal vs. Fast	0.13	0.83	0.66	0.83	0.61
Fast vs. Slow	0	0.89	0.2	0.5	0.40
Module Average	0.04	0.83	0.53	0.65	

4.4.7.2 Between-Subject (Muscle Synergy Vector)

HS vs. TFA (Slow)

The muscle synergies comparison between HS and TFA showed a poor correlation of S1 and S4, moderate correlation of S3 and a strong correlation of S2 during slow walking (Table 4.20).

HS vs. TFA (Normal)

In normal walking, the differences between modules illustrated S1 and S4 poor, S3 moderate and S2 strong correlation (Table 4.20).

HS vs. TFA (Fast)

Moderate (S4) to strong (S1, S2, and S3) correlations were observed between HS and TFA during fast walking (Table 4.20).

Table 4.20: The comparison between HS and TFA at each speed by means of R^2 .

R^2	S1	S2	S3	S4
Slow	0.00	0.91	0.63	0.33
Normal	0.41	0.80	0.66	0.00
Fast	0.76	0.97	0.92	0.63

4.4.8 Statistical Analyses (Activation Coefficient Profile)

4.4.8.1 Within-Subject (Biomechanics Perspective)

Due to the limitations of SPM, repeated-measures MANOVA could not be performed. In addition, the design of this study is regarded as exploratory which searches for the effect of speeds on temporal components of muscle synergies in each group separately. Therefore, paired Hotelling's T^2 for hypothesis 1 and 3 were implemented using a Bonferroni correction across three speeds. SPM vector field analysis was performed pairwise between speeds. The threshold was corrected for the Bonferroni threshold of 0.02.

Speed Dependence of the HS Activation Coefficient Profile

As shown in Figure 4.22, no significant differences were found in C (fast-normal) and C (fast-slow). In normal-slow speed comparison, HS C was significantly greater at 0-13% ($p < 0.001$), 38-39% ($p = 0.041$), 61-69% ($p < 0.001$), 92-93% ($p = 0.030$) and 97-100% ($p = 0.011$). Therefore, null hypothesis 1 was rejected as a significant difference was observed in coefficients of HS.

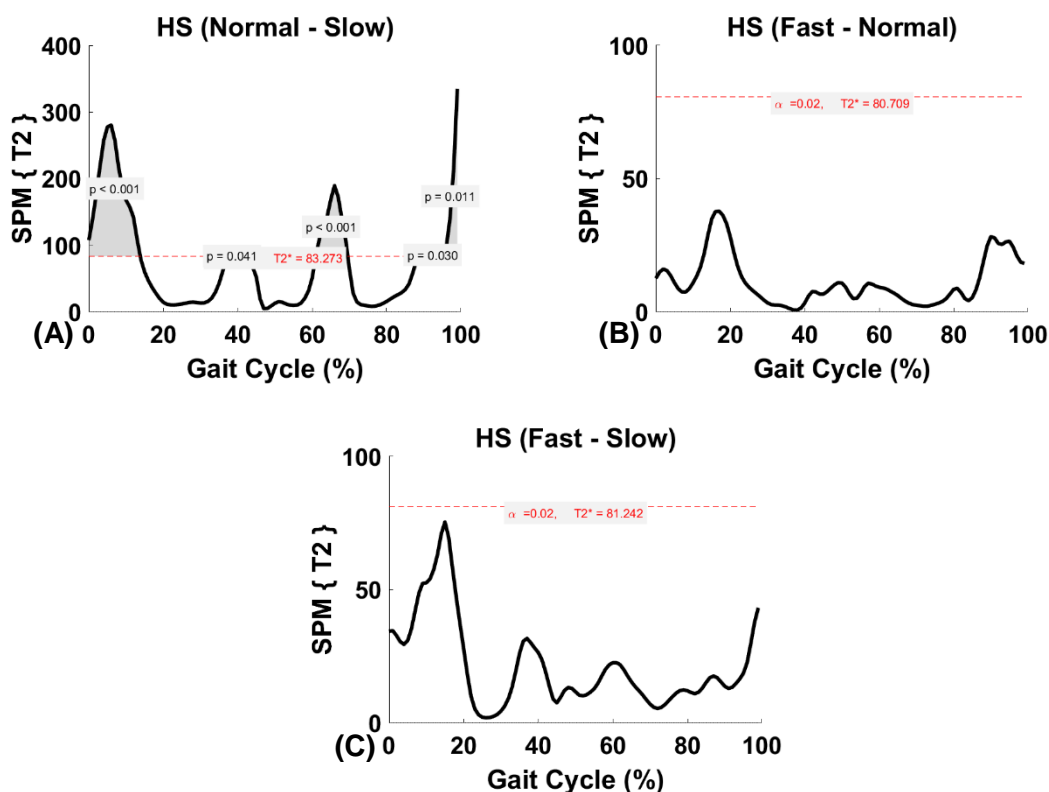


Figure 4.22: HS post hoc SPM vector field results (paired Hotelling's T^2 test) depicting significant differences between speeds. The red dashed lines indicate critical thresholds of $T2^* = 83.273$, 80.709 and 81.242 for (A), (B), and (C), respectively. Suprathreshold clusters are shown in grey where $p < 0.02$.

Speed Dependence of the TFA Activation Coefficient Profile

As shown in Figure 4.23, no significant differences were found in C (fast-normal). In normal-slow and fast-slow speed comparison, TFA C was significantly greater at 0-2% ($p=0.049$) and 95-100% ($p=0.002$), respectively. Therefore, null hypothesis 3 was rejected as a significant difference was observed in coefficients of TFA.

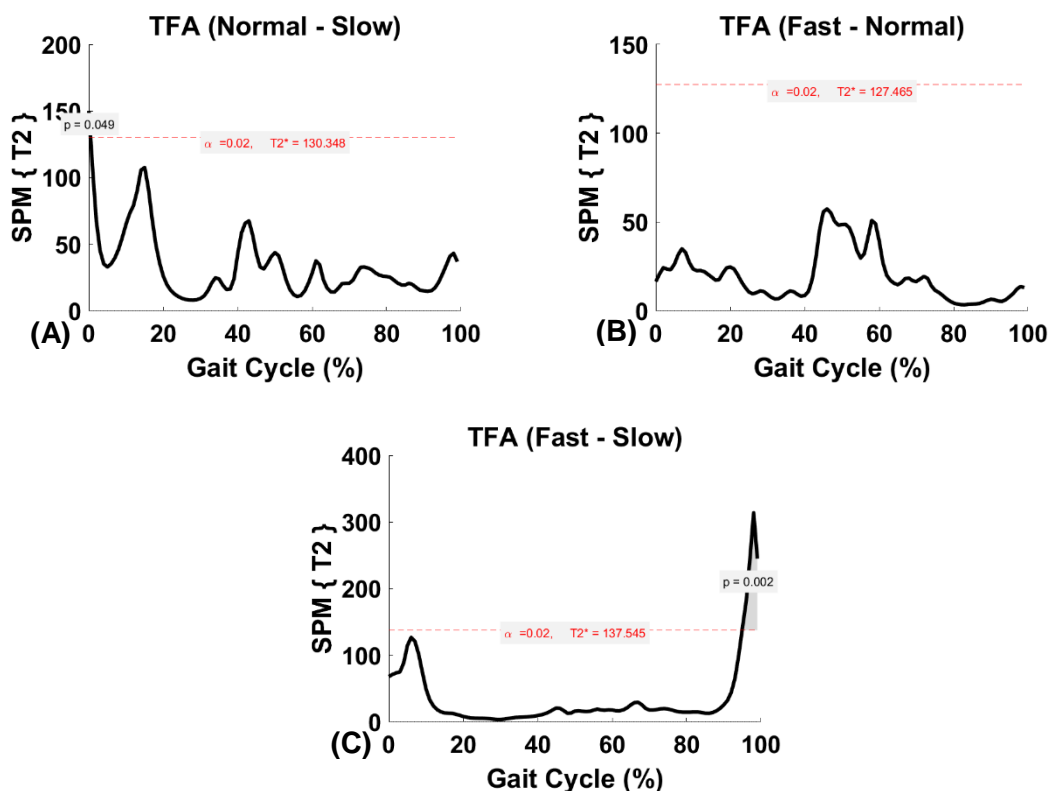


Figure 4.23: TFA post hoc SPM vector field results (paired Hotelling's T2 test) depicting significant differences between speeds. The red dashed lines indicate critical thresholds of $T2^* = 130.348$, 127.465 and 137.54 for (A), (B), and (C), respectively. Suprathreshold clusters are shown in grey where $p < 0.02$.

4.4.8.2 Within-Subject (Robotic Control Perspective)

A *priori* hypothesis in robotic control approach was to investigate the effect of speeds on individual activation coefficient profiles during gait in each group separately. Therefore, one-way repeated-measures ANOVA (represented as a black trajectory in Figure 4.24) was implemented to investigate the within-subject F statistics for hypothesis 2 and 4. It is worth mentioning that one-way ANOVA was performed between-subject for demonstration (represented as a red trajectory in Figure 4.24) however, this is not an appropriate test since the same subjects performed transient-state walking at different speeds. Moreover, the between-subject analysis yields a small F value because between-subject variability is large relative to between-condition variability. The within-subject analysis yields a large F value because paired effects are large relative to paired variability. Post hoc analysis was done to investigate further the differences between

speeds. Multiple post hoc paired or two sample t-test increases the chances of making a type I error (false positive). Therefore, alpha was corrected according to the number of comparisons made to decrease the likelihood of a type I error, to increase the critical threshold, and to ensure the false positive error rate is appropriate for the number of comparisons made. In this case, a Bonferroni threshold of $p = 0.017$ was adopted for the three walking speeds to retain a family-wise error of $\alpha = 0.05$ which was then used for inference calculation.

Speed Dependence of the HS Activation Coefficient Profile

As shown in Figure 4.24, statistically significant differences occurred in HS C1 across different speeds. Three suprathreshold clusters were found at 6-18% ($p=0.002$), 56-64% ($p=0.008$) and 98-100% ($p=0.047$) GC intra-subjectively. The between-subject analysis showed one significant statistical region (11-17%) which peaked at 14% GC. Since significant differences were found in the ANOVA within-subject, post hoc paired t-test was conducted in pairwise fashion between speeds, respectively (Figure 4.25).

As shown in Figure 4.26, SPM analysis revealed two suprathreshold clusters between three speeds in C2 intra-subjectively at approximately 2-8% ($p=0.012$) and 34-44% ($p=0.001$) GC. No significant differences were found between-subject. Post hoc paired t-test showed significant differences between normal-slow at 36-44% ($p=0.001$) and fast-slow at 35-41% ($p=0.003$) GC (Figure 4.27).

As shown in Figure 4.28, SPM vector field analysis found a highly significant difference in C3 within-subject. One suprathreshold cluster was found at 12-21% GC ($p=0.002$). SPM failed to find any significance between-subject. Post hoc paired t-test was conducted between speeds where significant differences occurred in fast-normal at 15-20% GC ($p=0.012$) and fast-slow at 15-19% GC ($p=0.008$) (Figure 4.29).

As shown in Figure 4.30, the significant difference was found in C4 at 88-93% GC ($p=0.027$) within-subject but none between-subject. No differences were found in post hoc analyses within-subject even though the main SPM analysis showed one suprathreshold cluster. It is noteworthy that the null hypothesis was answered completely by the RM ANOVA (Figure 4.31).

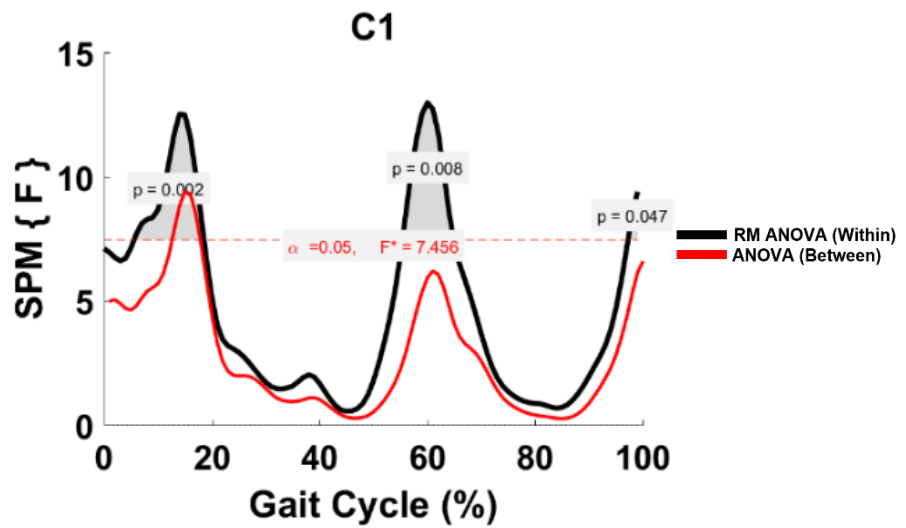
HS C1

Figure 4.24: HS C1 parametric RM ANOVA within- and between-subjects, depicting significant differences between speeds. The horizontal red dotted line indicates the critical threshold of 7.46. Suprathreshold clusters are shown in grey where $p < 0.05$.

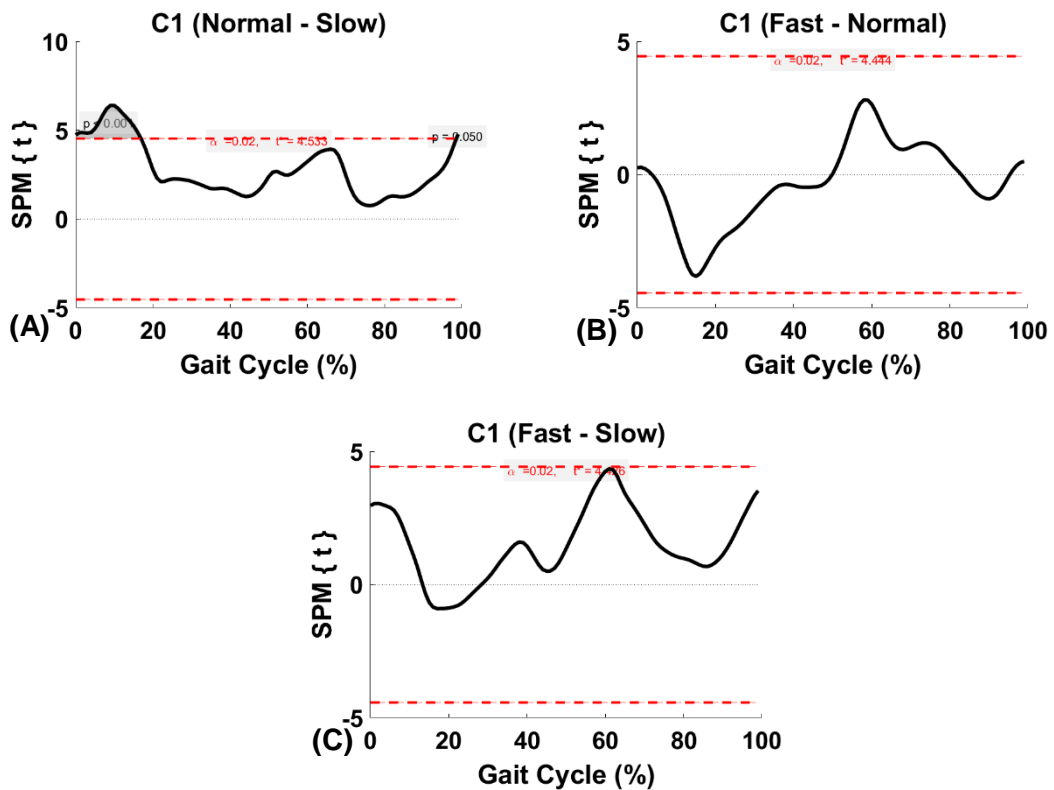


Figure 4.25: HS C1 within-subject post hoc paired t statistic between pairs of walking speeds. The red dashed lines indicate critical thresholds of $t^* = 4.53$, 4.44 and 4.43 for (A), (B), and (C), respectively. Suprathreshold clusters are shown in grey where $p < 0.02$.

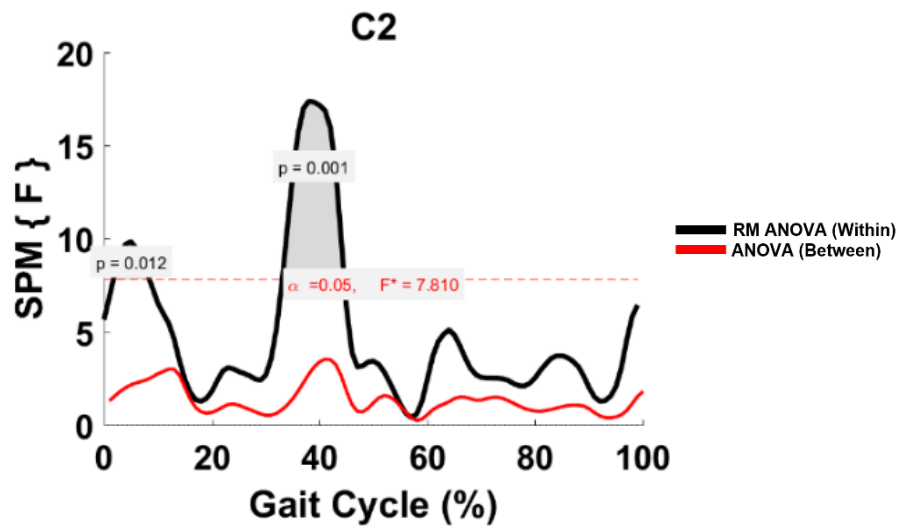
HS C2

Figure 4.26: HS C2 parametric RM ANOVA within- and between-subjects, depicting significant differences between speeds. The horizontal red dotted line indicates the critical RFT threshold of 7.81. Suprathreshold clusters are shown in grey where $p < 0.05$.

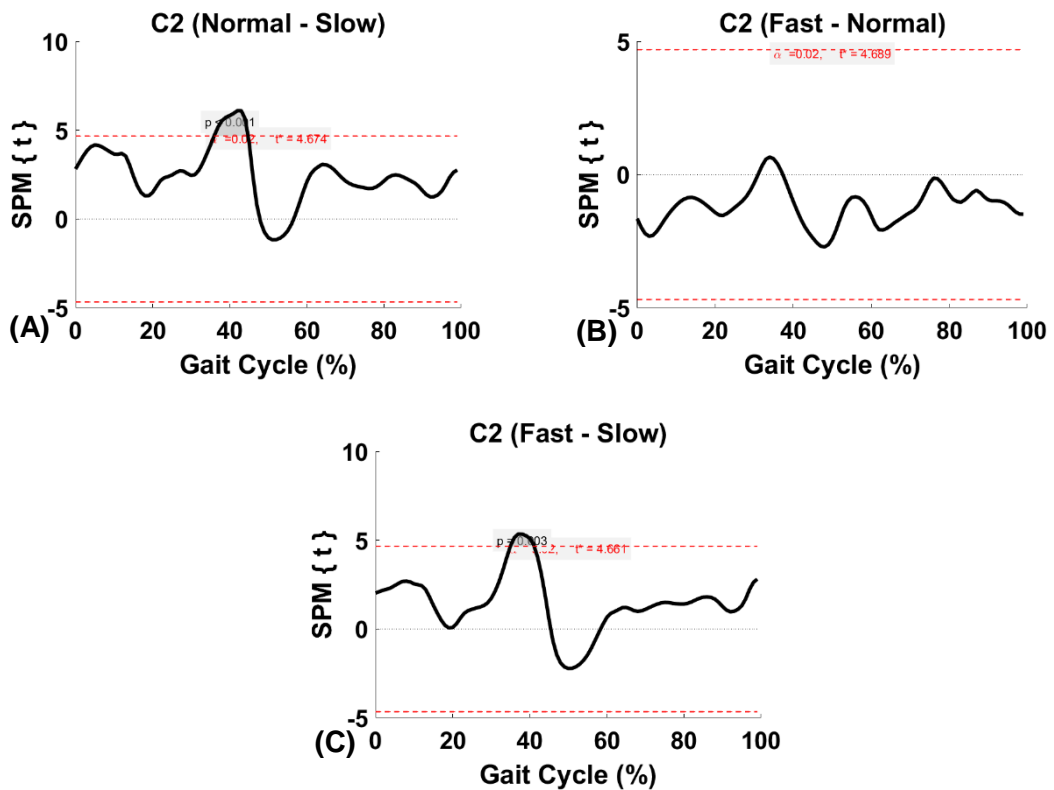


Figure 4.27: HS C2 within-subject post hoc paired t statistic between pairs of walking speeds. The red dashed lines indicate critical thresholds of $t^* = 4.67$, 4.70 and 4.66 for (A), (B) and (C), respectively. Suprathreshold clusters are shown in grey where $p < 0.02$.

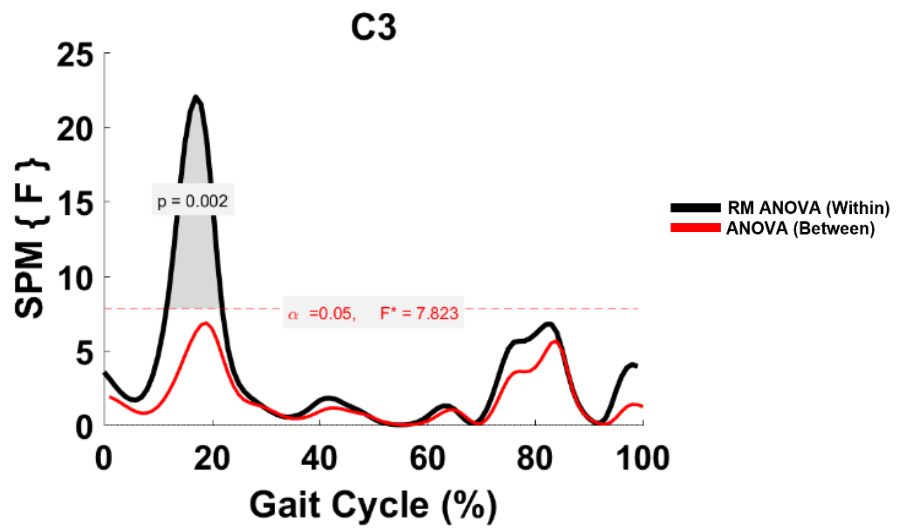
HS C3

Figure 4.28: HS C3 parametric RM ANOVA within- and between-subjects, depicting significant differences between speeds. The horizontal red dotted line indicates the critical threshold of 7.82. Suprathreshold clusters are shown in grey where $p < 0.05$.

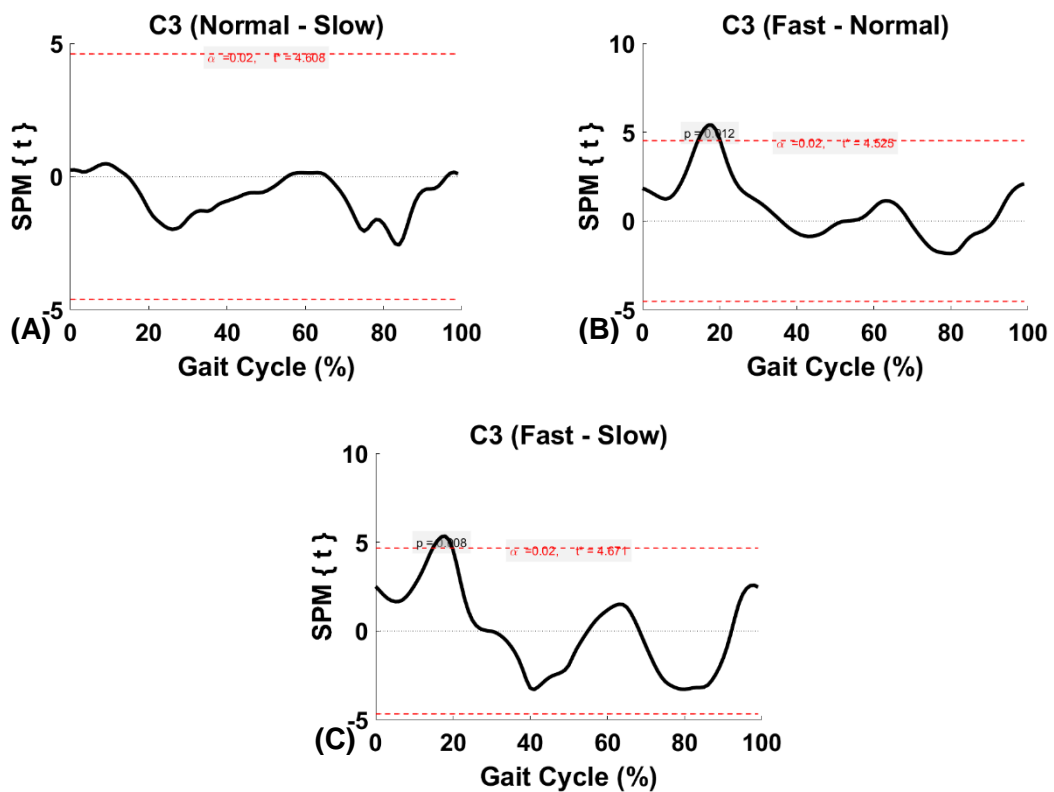


Figure 4.29: HS C3 within-subject post hoc paired t statistic between pairs of walking speeds. The red dashed lines indicate critical thresholds of $t^* = 4.61$, 4.53 and 4.67 for (A), (B), and (C), respectively. Suprathreshold clusters are shown in grey where $p < 0.02$.

HS C4

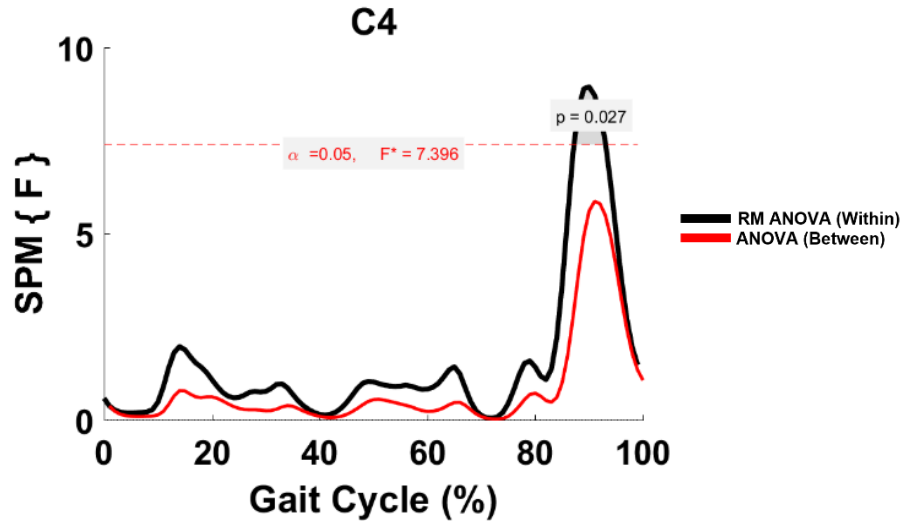


Figure 4.30: HS C4 parametric RM ANOVA within- and between-subjects, depicting significant differences between speeds. The horizontal red dotted line indicates the critical threshold of 7.4. Suprathreshold clusters are shown in grey where $p < 0.05$.

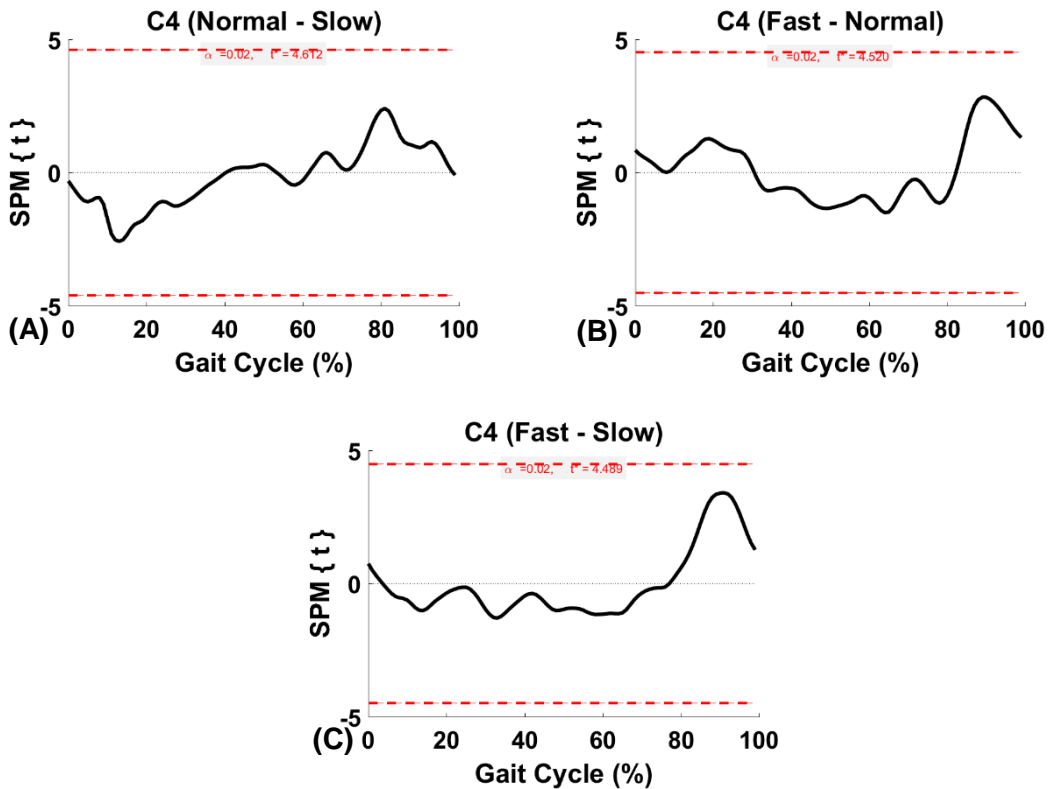


Figure 4.31: HS C4 within-subject post hoc paired t statistic between pairs of walking speeds. The red dashed lines indicate critical thresholds of $t^* = 4.61$, 4.52 and 4.49 for (A), (B), and (C), respectively. Suprathreshold clusters are shown in grey where $p < 0.02$.

Speed Dependence of the TFA Activation Coefficient Profile

As shown in Figure 4.32, main SPM analysis found significant differences in TFA C1 between three different speeds. Two suprathreshold clusters were found at 0-19% ($p=0.0$) and 94-100% ($p=0.27$) GC. Post hoc paired t-test was conducted pairwise between speeds which revealed C1 was significantly different between fast-normal at 0-8% ($p=0.001$) as well as fast-slow at 0-14% ($p=0.0$) and 95-100% ($p=0.014$) GC (Figure 4.33).

As shown in Figure 4.34, SPM analysis revealed three suprathreshold clusters across speeds in C2 within-subject at 19% ($p=0.049$), 44-53% ($p=0.006$) and 68% (0.05). No significant differences were found between-subject. Post hoc paired t-test showed a significant difference between fast-normal at 45-49% ($p=0.010$) GC (Figure 4.35).

As shown in Figure 4.36, SPM analysis showed no significant in TFA C3 across speeds.

As shown in Figure 4.37, SPM analysis showed the statistically significant difference in C4 within-subject across speeds. One suprathreshold cluster occurred at 42-47% ($p=0.014$). No significant differences were found between-subject. Post hoc paired t-test showed a significant difference between fast-slow at 42-45% ($p=0.013$) GC (Figure 4.38).

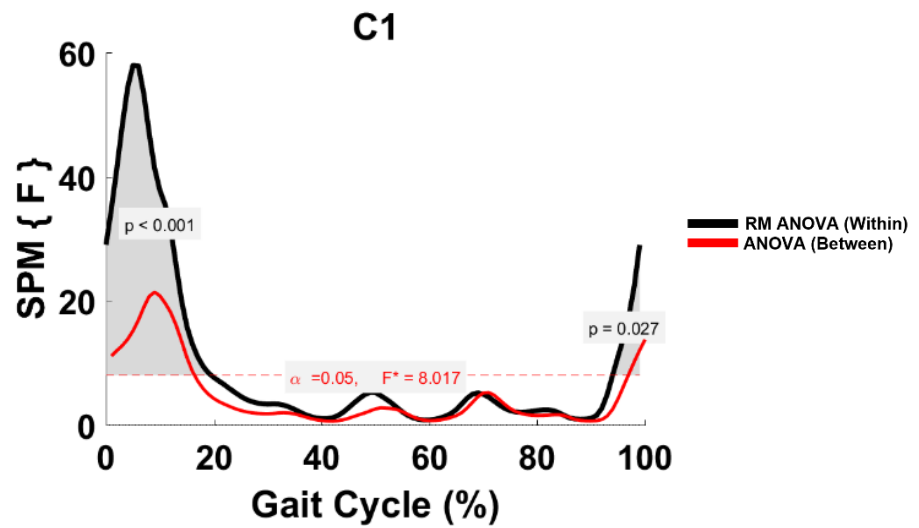
TFA C1

Figure 4.32: TFA C1 parametric RM ANOVA within- and between-subjects, depicting significant differences between speeds. The horizontal red dotted line indicates the critical threshold of 8.02. Suprathreshold clusters are shown in grey where $p < 0.05$.

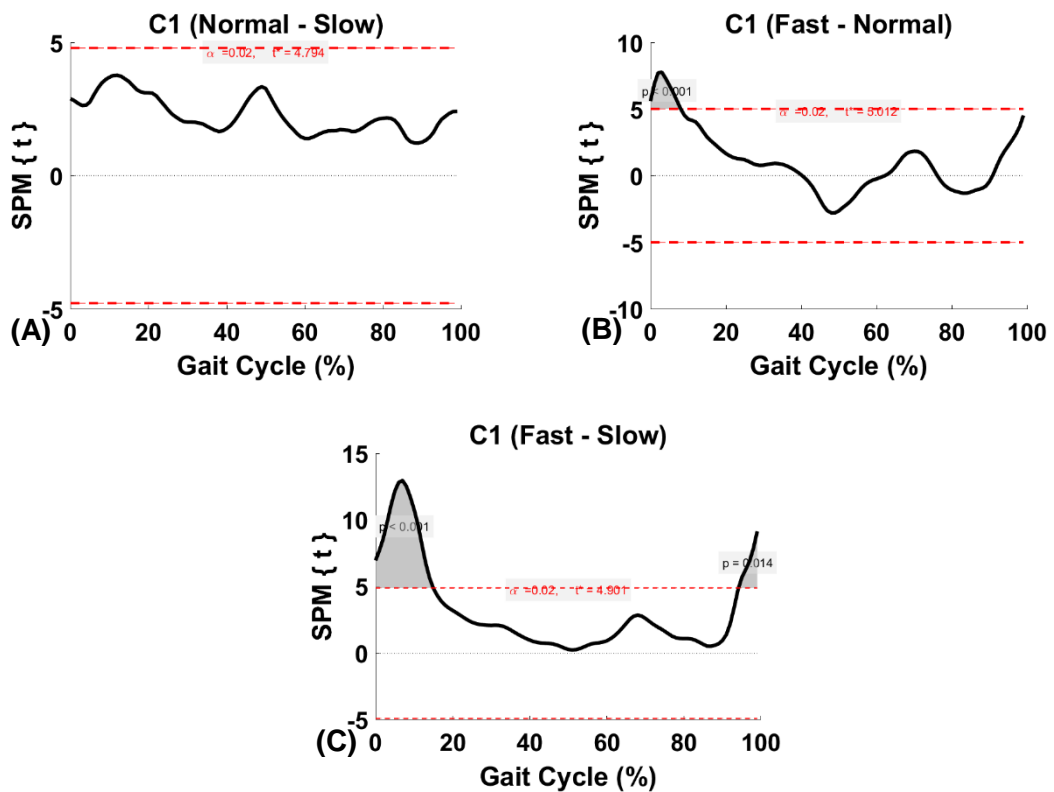


Figure 4.33: TFA C1 within-subject post hoc paired t statistic between pairs of walking speeds. The red dashed lines indicate critical thresholds of $t^* = 4.79$, 5.01 and 4.9 for (A), (B), and (C), respectively. Suprathreshold clusters are shown in grey where $p < 0.02$.

TFA C2

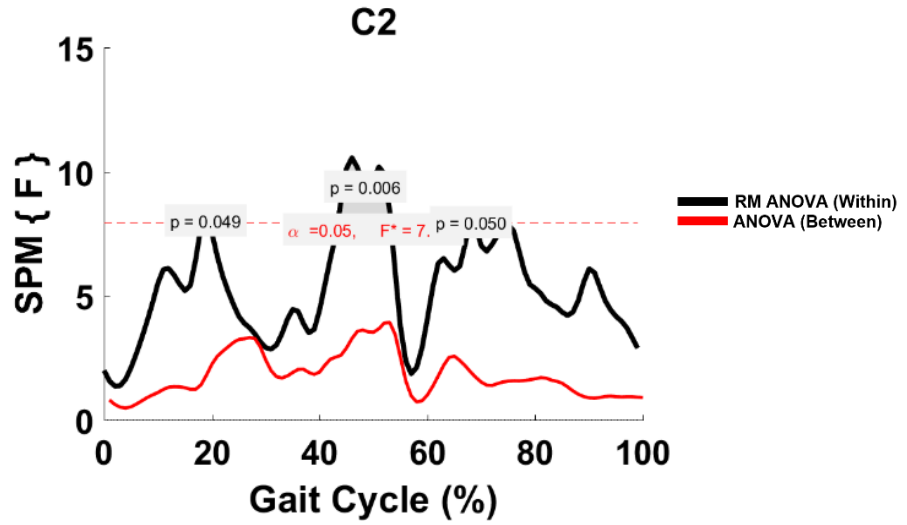


Figure 4.34: TFA C2 parametric RM ANOVA within- and between-subjects, depicting significant differences between speeds. The horizontal red dotted line indicates the critical threshold of 7.89. Suprathreshold clusters are shown in grey where $p < 0.05$.

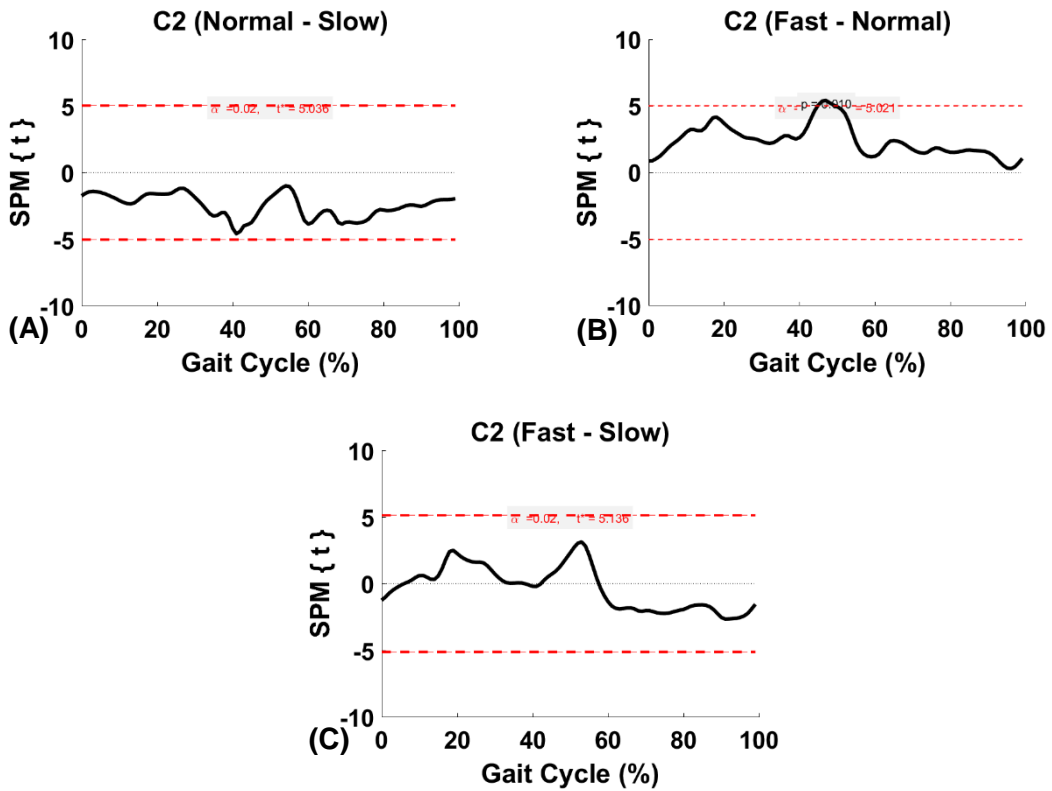


Figure 4.35: TFA C2 within-subject post hoc paired t statistic between pairs of walking speeds. The red dashed lines indicate critical thresholds of $t^* = 5.04$, 5.02 and 5.14 for (A), (B), and (C), respectively. Suprathreshold clusters are shown in grey where $p < 0.02$.

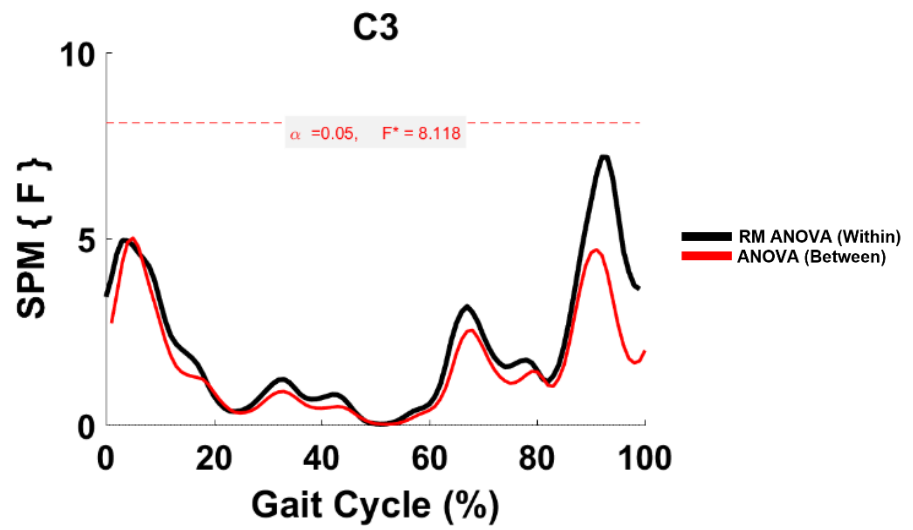
TFA C3

Figure 4.36: TFA C3 parametric RM ANOVA within- and between-subjects, depicting significant differences between speeds. The horizontal red dotted line indicates the critical threshold of 8.12. Suprathreshold clusters are shown in grey where $p < 0.05$.

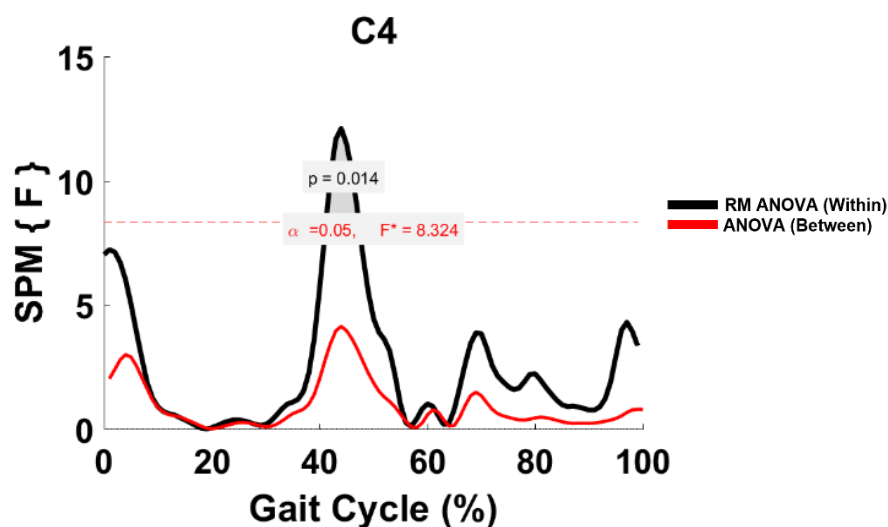
TFA C4

Figure 4.37: TFA C4 parametric RM ANOVA within- and between-subjects, depicting significant differences between speeds. The horizontal red dotted line indicates the critical threshold of 8.32. Suprathreshold clusters are shown in grey where $p < 0.05$.

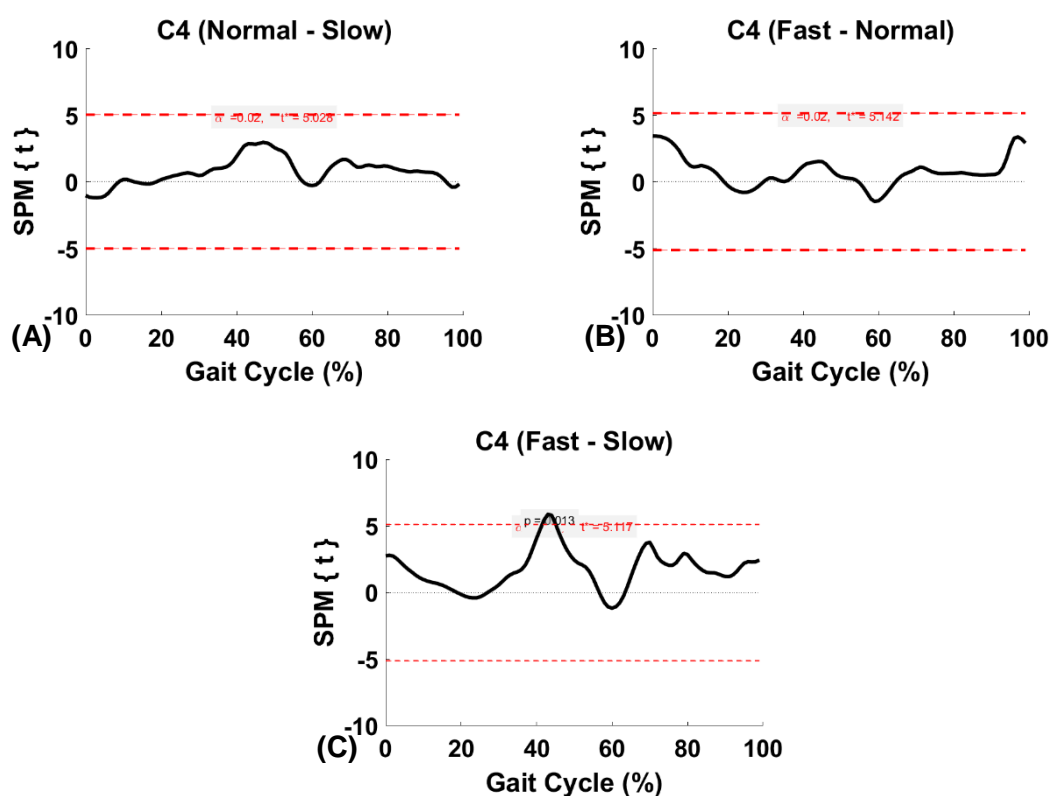


Figure 4.38: TFA C4 within-subject post hoc paired t statistic between pairs of walking speeds. The red dashed lines indicate critical thresholds of $t^* = 5.03, 5.14$ and 5.12 for (A), (B), and (C), respectively. Suprathreshold clusters are shown in grey where $p < 0.02$.

4.4.8.3 Between-Subject (Biomechanics Perspective)

A *priori* hypothesis accounted for individual speed as a different task under the walking control between-subject. Therefore, the effect of groups on individual activation coefficient profiles during walking was compared at each speed category. Consequently, Hotelling's T^2 was implemented for hypothesis 5. The post hoc test was considered if the main analysis showed significant level. The threshold was corrected for the sidak corrected threshold of 0.01 for four individual *C* comparison to retaining a Type I family-wise error rate of $\alpha = 0.05$. Table 4.21 shows where significant differences occurred in the main (Hotelling T^2) and post hoc (two-sample t-test) analyses between-subject. Refer to section HS vs. TFA (slow), HS vs. TFA (Normal) and HS vs. TFA (Fast) for more details.

Table 4.21: Summary of the suprathreshold clusters obtained from the main test (SPM Hotelling's T^2) and post hoc test (SPM two-sample t-test) between HS and TFA at each speed category (biomechanics perspective)

	Hotelling T^2	Post hoc two-sample t-test			
	$P < 0.05$	$P < 0.0127$			
	<i>C</i>	<i>C1</i>	<i>C2</i>	<i>C3</i>	<i>C4</i>
Slow	[0-3], [54-61]	NA	[53-64]	NA	NA
Normal	[2-5], [53-59]	NA	[38-43] [53-59]	[0-5]	NA
Fast	[49-58]	[44-45]	[18-24], [49-60]	NA	NA

HS vs. TFA (Slow)

As shown in Figure 4.39, SPM vector field found two suprathreshold clusters indicating significant differences between HS and TFA at 0-3% and 54-61% during slow speed gait. Identically, smooth random 1D data would produce clusters of this breadth with a probability of $p=0.038$ and $p=0.009$. Therefore, the null hypothesis was rejected as significant differences were observed between HS and TFA.

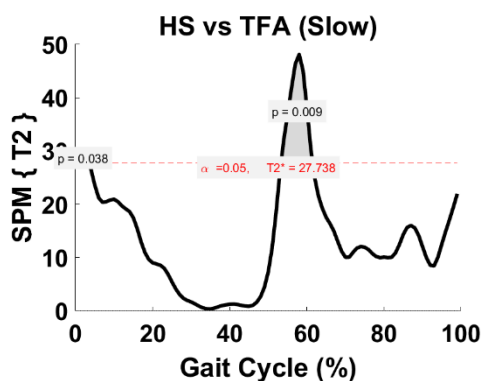


Figure 4.39: SPM vector field result (Hotelling's T^2) depicting HS vs. TFA differences at slow speed. The red dashed line indicates critical threshold of $T^2^*=27.738$. Suprathreshold clusters are shown in grey where $p<0.05$.

As shown in Figure 4.40, no significant differences were found in C1, C3, and C4. TFA C2 was significantly greater than HS C2 at 53-64% ($p=0.002$).

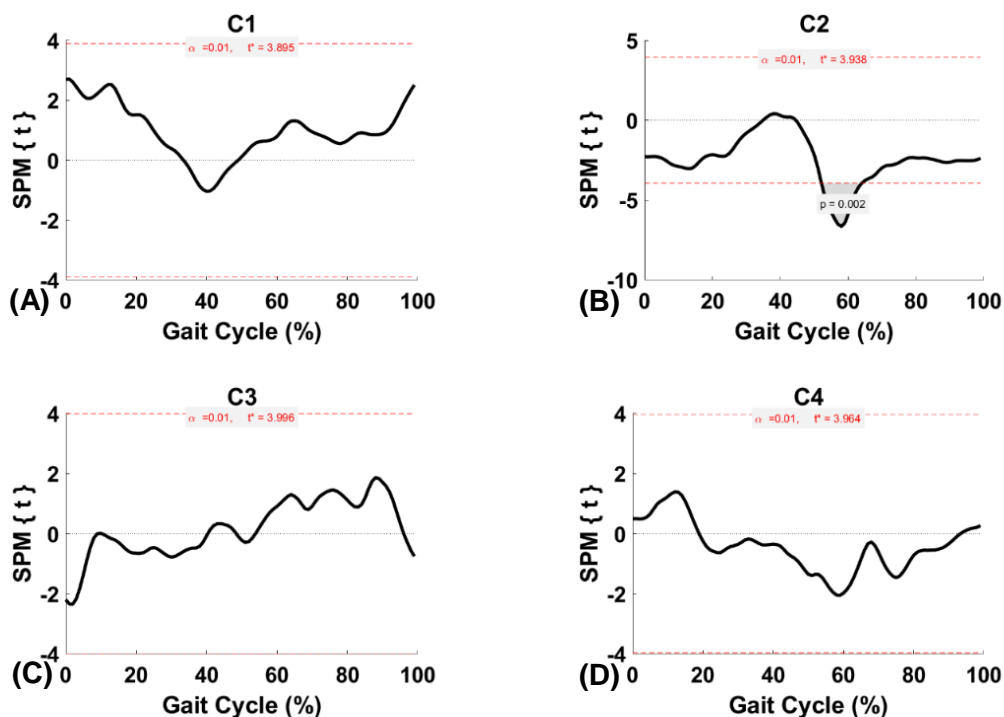


Figure 4.40: Post hoc two sample SPM t-test results comparing HS versus TFA at slow speeds for individual C. Red dashed line indicates critical threshold ((A): $t^*C1=3.895$, (B): $t^*C2=3.938$, (C): $t^*C3=3.996$, and (D): $t^*C4=3.964$). Suprathreshold clusters are shown in grey where $p<0.01$.

HS vs. TFA (Normal)

As shown in Figure 4.41, SPM vector field found two suprathreshold clusters indicating significant differences between HS and TFA at 2-5% and 53-59% during normal speed gait. Identically, smooth random 1D data would produce clusters of this breadth with a probability of $p=0.030$. and $p=0.013$. Therefore, the null hypothesis was rejected as significant differences were observed between HS and TFA.

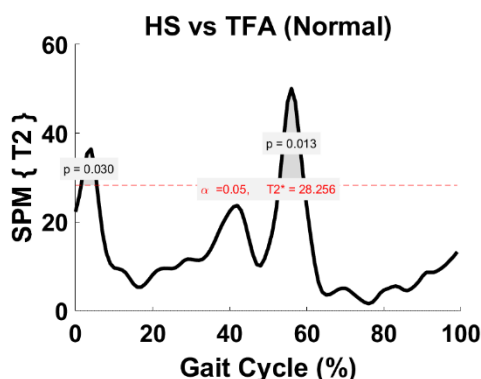


Figure 4.41: SPM vector field result (Hotelling's T^2) depicting HS vs. TFA differences at normal speed. The red dashed line indicates critical threshold of $T^2^*=28.256$. Suprathreshold clusters are shown in grey where $p<0.05$.

As shown in Figure 4.42, no significant differences were found in C1 and C4. TFA C2 was significantly greater than HS C2 at 53-59% ($p=0.023$) whereas HS revealed a statistically significant difference at 38-43% ($p=0.014$). TFA C4 was significantly greater than HS C4 at 0-5% ($p=0.022$).

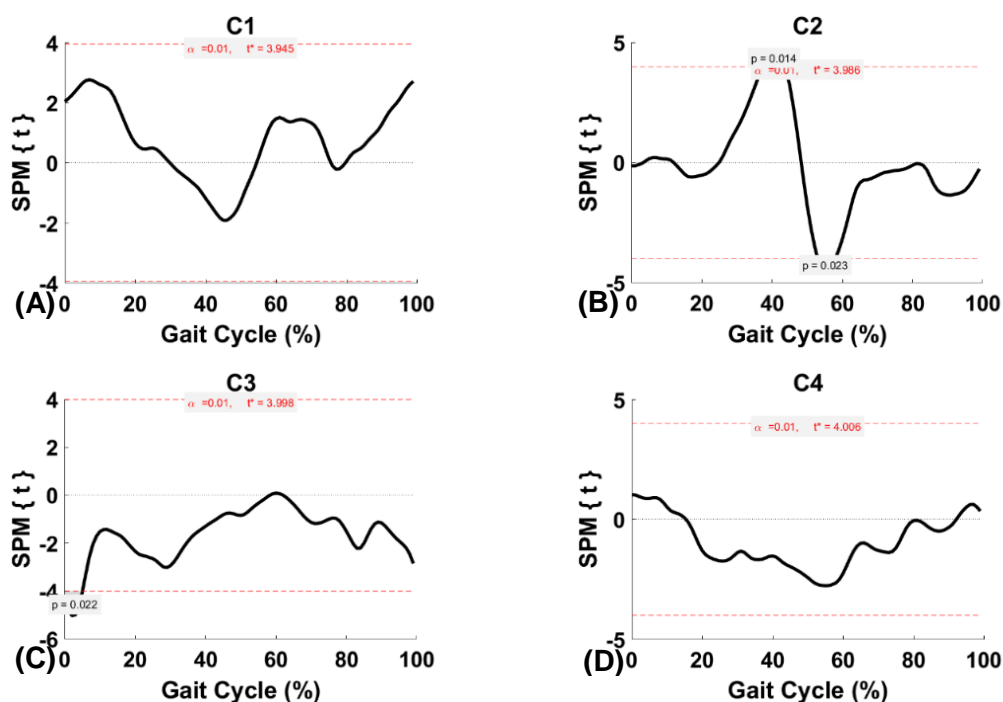


Figure 4.42: Post hoc two sample SPM t-test results comparing HS versus TFA at normal speeds for individual C. Red dashed line indicates critical threshold ((A): $t^*C1=3.945$, (B): $t^*C2=3.986$, (C): $t^*C3=3.998$, and (D): $t^*C4=4.006$). Suprathreshold clusters are shown in grey where $p<0.01$.

HS vs. TFA (Fast)

As shown in Figure 4.43, SPM vector field found one suprathreshold cluster indicating a significant difference between HS and TFA at 48-58% during fast speed gait. Identically, smooth random 1D data would produce clusters of this breadth with a probability of $p=0.003$. Therefore, the null hypothesis was rejected as significant differences were observed between HS and TFA.

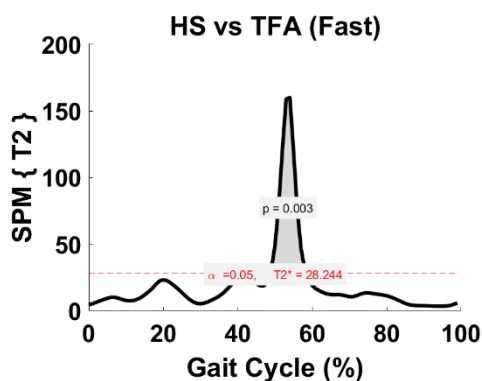


Figure 4.43: SPM vector field result (Hotelling's T^2) depicting HS vs. TFA differences at fast speed. The red dashed line indicates critical threshold of $T2^*=28.244$. Suprathreshold clusters are shown in grey where $p<0.05$.

As shown in Figure 4.44, no significant differences were found in C3 and C4. TFA C1 was significantly greater than HS C1 at 44-45% ($p=0.048$). TFA C2 was significantly greater than HS C2 at 18-24% ($p=0.014$) and 49-60% ($p=0.001$).

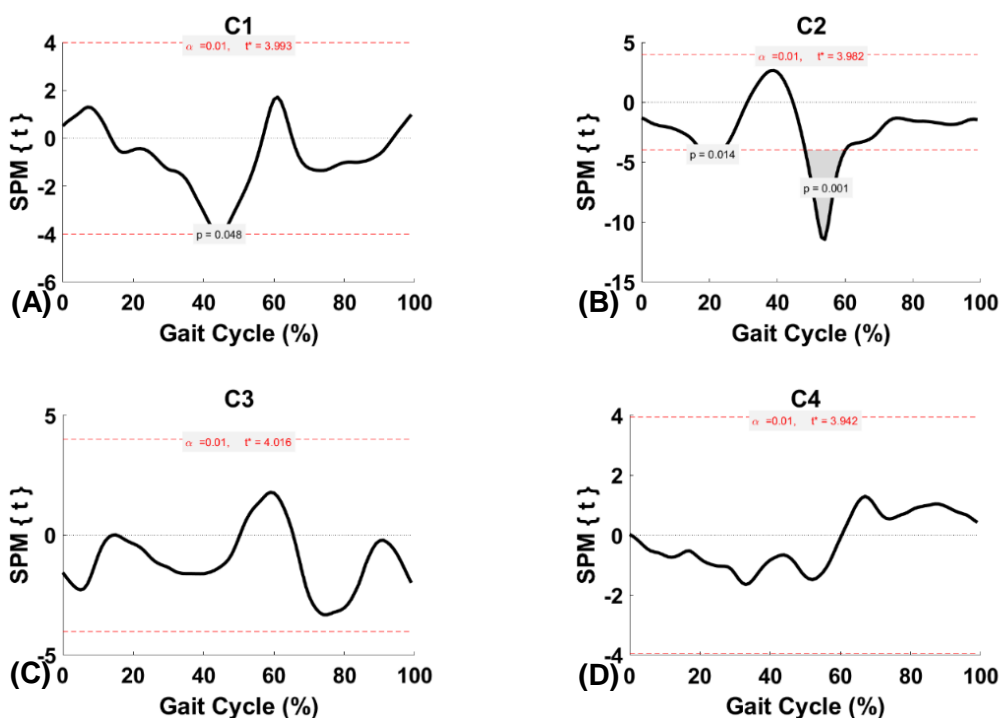


Figure 4.44: Post hoc two sample SPM t-test results comparing HS versus TFA at fast speeds for individual C. Red dashed line indicates critical threshold ((A): $t^*C1=3.993$, (B): $t^*C2=3.982$, (C): $t^*C3=4.016$, and (D): $t^*C4=3.942$). Suprathreshold clusters are shown in grey where $p<0.01$.

4.4.8.4 Between-Subject (Control Perspective)

A *priori* hypothesis accounted for individual speed as a different task under the walking control between-subject. Consequently, SPM two-sample t-test ($\alpha=0.05$) was implemented for hypothesis 6. Table 4.22 shows where significant differences occurred in the main analysis (two-sample t-test) between-subject. Refer to section HS vs. TFA (slow), HS vs. TFA (Normal) and HS vs. TFA (Fast) for more details.

Table 4.22: Summary of the suprathreshold clusters obtained from the SPM two-sample t-test between HS and TFA at each speed category (control perspective).

P < 0.05				
	C1	C2	C3	C4
Slow	[0-14], [97-100]	[0-27], [50-100]	[0-3]	[58-60]
Normal	[0-15], [43-48], [93-100]	[33-46], [50-62]	[0-8], [20-34], [95-100]	[50-57]
Fast	[37-53]	[4-29], [36-40], [46-72], [86-94]	[0-8], [31-43], [69-84], [97-100]	NA

HS vs. TFA (Slow)

As shown in Figure 4.45, HS C1 was significantly greater than TFA C1 at 0-14% ($p=0.001$) and 97-100% ($p=0.045$) time at slow speed. TFA C2 was significantly greater than HS C2 at 0-27% ($p=0.001$) and 50-100% ($p=0.001$). For C3, one suprathreshold occurred at 0-3% ($p=0.035$) where TFA was significantly different from HS. TFA C4 was significantly greater than HS C4 at 58-60% ($p=0.038$). Therefore, the null hypothesis was rejected in all activation coefficient profiles at slow speed.

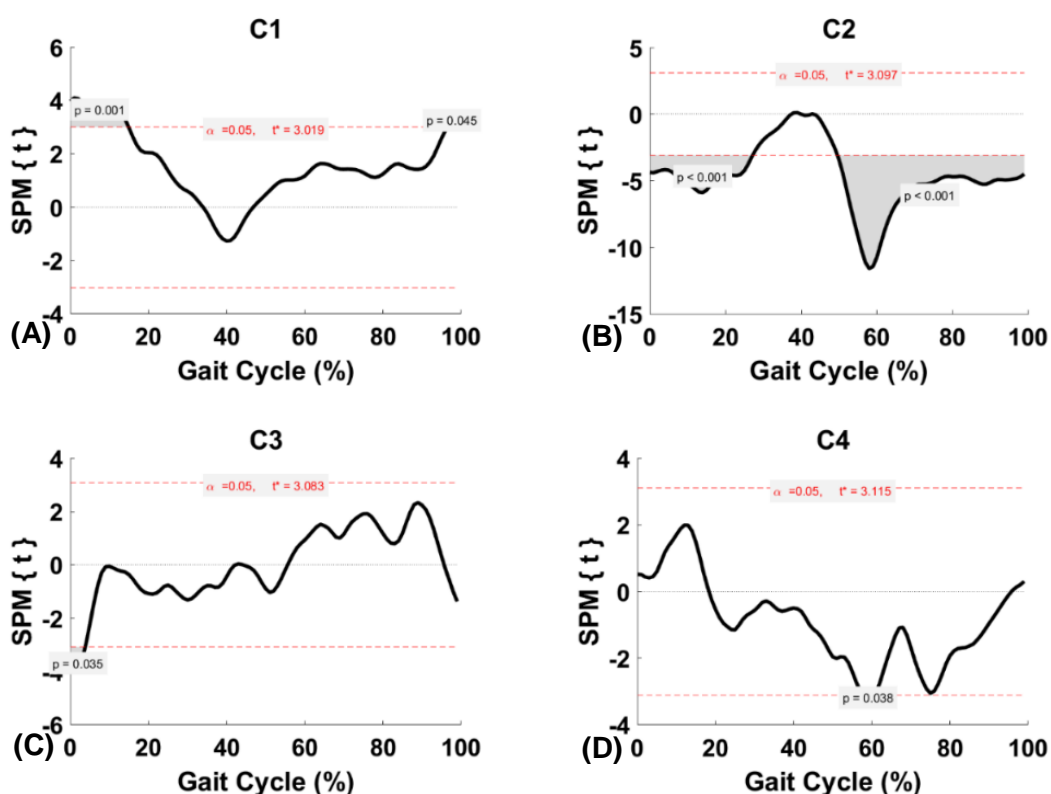


Figure 4.45: A statistical inference curve indicating a significant relationship between HS C and TFA C at slow speed. Red dashed line indicates critical threshold ((A): $t^*C1=3.019$, (B): $t^*C2=3.097$, (C): $t^*C3=3.083$, and (D): $t^*C4=3.115$). The period where the critical threshold is exceeded depicted as grey ($p < 0.05$).

HS vs. TFA (Normal)

As shown in Figure 4.46, HS C1 was significantly greater than TFA C1 at 0-15% ($p=0.001$) and 93-100% ($p=0.021$) where as TFA revealed a statistically significant difference at 43-48% ($p=0.023$). Two suprathreshold clusters were found in C2 at 33-46% ($p=0.0$) and 50-62% ($p=0.001$) indicating greater significance in HS and TFA, respectively. For C3, three suprathreshold clusters were found at 0-8% ($p=0.01$), 20-34% ($p=0.0$) and 95-100% ($p=0.030$) where TFA was significantly different than HS. TFA C4 was significantly greater than HS C4 at 50-57% ($p=0.006$). Therefore, the null hypothesis was rejected in all activation coefficient profiles at normal speed.

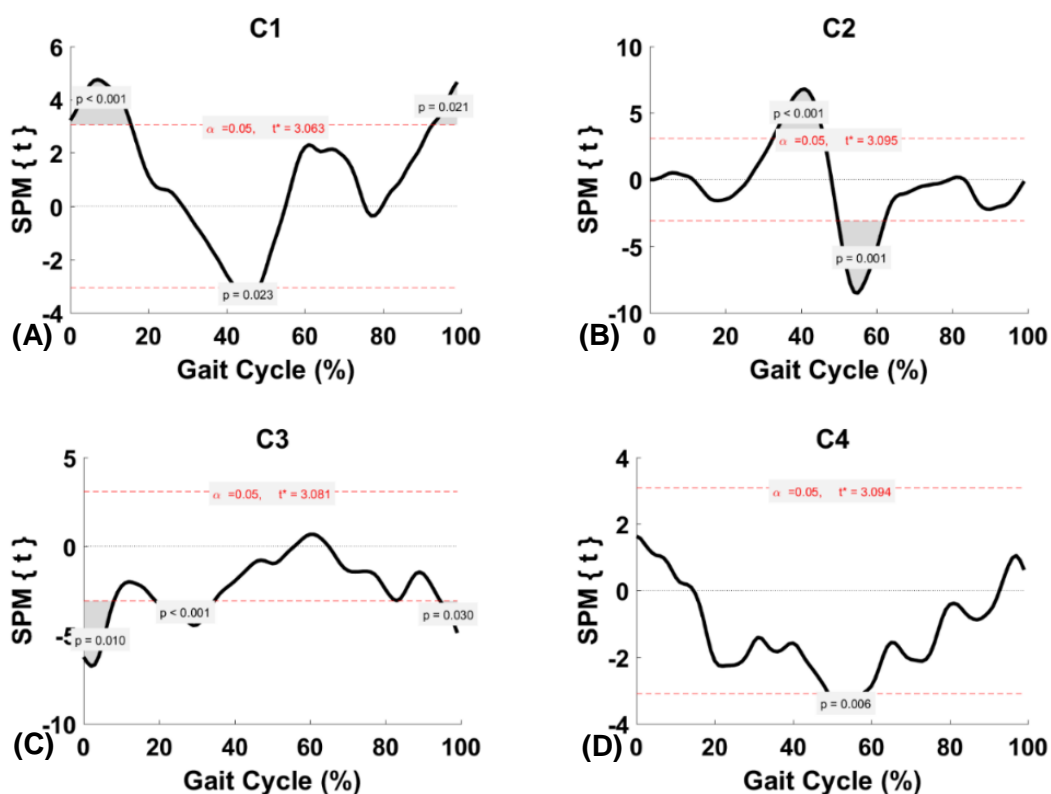


Figure 4.46: A statistical inference curve indicating a significant relationship between HS C and TFA C at normal speed. Red dashed line indicates critical threshold ((A): $t^*C1=3.063$, (B): $t^*C2=3.095$, (C): $t^*C3=3.081$, and (D): $t^*C4=3.094$). The period where the critical threshold is exceeded depicted as grey ($p < 0.05$).

HS vs. TFA (Fast)

As shown in Figure 4.47, TFA C1 was significantly greater than HS C1 at 37-53% ($p=0.0$). TFA C2 was significantly greater than HS C2 at 4-29% ($p=0.0$), 46-72% ($p=0.0$) and 86-94% ($p=0.006$) whereas HS revealed a statistically significant difference at 36-40% ($p=0.025$). Four suprathreshold clusters were found in C3 at 0-8% ($p=0.009$) and 31-43% ($p=0.001$), 69-84% ($p=0.0$), 97-100% ($p=0.044$) indicating greater significance in TFA as compared to the HS. No significant difference was found in C4.

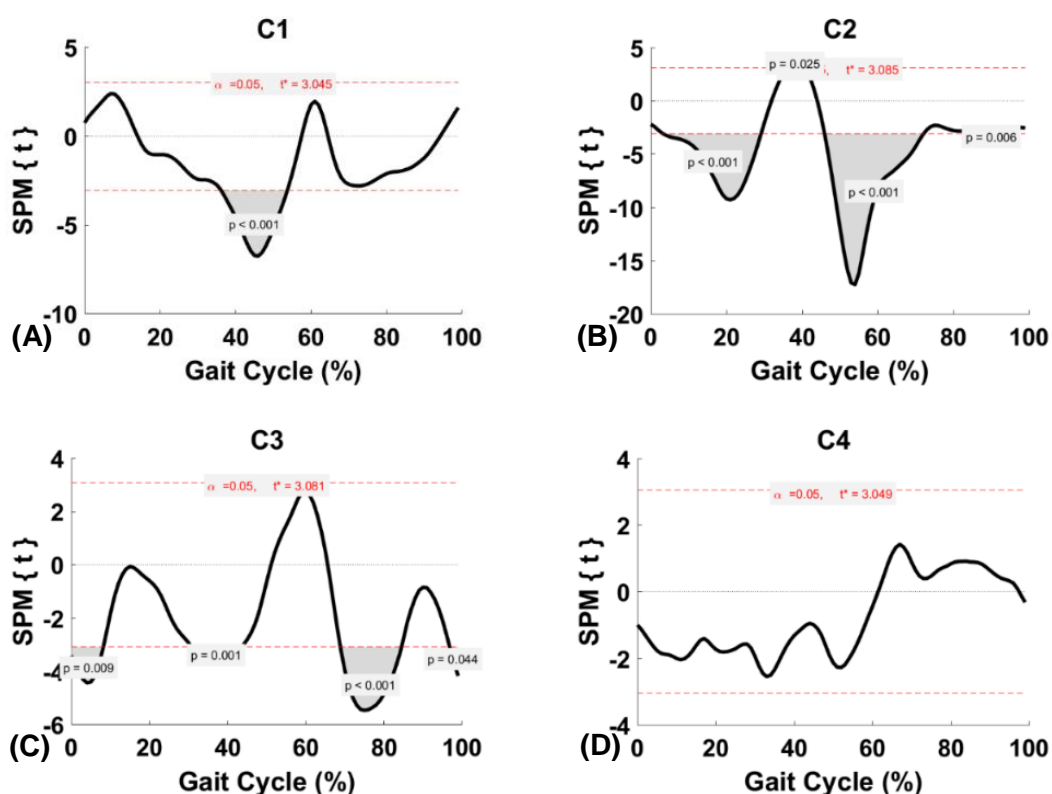


Figure 4.47: A statistical inference curve indicating a significant relationship between HS C and TFA C at fast speed. Red dashed line indicates critical threshold ((A): $t^*C1=3.045$, (B): $t^*C2=3.085$, (C): $t^*C3=3.081$, and (D): $t^*C4=3.049$). The period where the critical threshold is exceeded depicted as grey ($p < 0.05$).

4.5 Discussions

4.5.1 Analysis of dimensionality (VAF)

As described in the result section, the number of muscle synergy groupings was determined according to the literature ($k = 4$) [77, 81, 84, 91-93, 95, 204, 230]. The HS data illustrated that four modules are an optimal number to match the reconstructed and original EMG in slow, normal and fast transient-state walking condition which accounted for the VAF of 85%, 85%, and 86%, respectively. Similarly, four modules were selected for the TFA in slow, normal, fast transient-state walking which accounted for a VAF of 88%, 86% and 88%, respectively. In both groups, higher VAF using five synergies were obtained. However, four synergies were believed to provide more distinct synergy groups of muscle EMG contents. Moreover, since both VAF values were higher than 80% and the difference between them was not more than 5%, four synergies was chosen for both healthy and amputee groups.

The similarity in the number of modules suggests that complexity of muscles recruitment by the CNS is analogous in both groups. At the level of muscle synergy dimensionality, the results are comparable to the previous studies [92, 93, 230] on TTA which represents strategy implemented by the CNS does not change with the level of amputation. TFA and TTA results in terms of synergistic strategies are in disagreement with other pathological groups such as post-stroke patients [91] but in favor of joint injury groups such as anterior cruciate ligament deficiency patients [126]. Therefore, level of amputation and variation in speeds seem to not have any impacts on the CNS control complexity for the number of module recruitment. However, a larger sample size of TFA and TTA should be considered (i.e., distal, proximal) to generalize this statement.

4.5.2 Correlation Analysis (Individual-Muscle Criterion)

The goodness of fit for every individual muscle was calculated by implementing R^2 (Figure 4.8, Figure 4.9 and Figure 4.10) and ICC (Figure 4.13, Figure 4.14 and Figure 4.15) between the original and reconstructed data. The results revealed a reasonable correlation, suggesting magnitude and pattern similarities between the results obtained from $C \times S$ (reconstructed signal) and A (original signal) which met the individual-muscle criterion.

4.5.3 CNMF Activation Coefficient Profile Repeatability

ICC was also used to assess the repeatability and between trials/subjects similarity of activation coefficients. This is a crucial step as CNMF fixes an unknown S and allows C to be varied. Therefore, an approach such as ICC is required to be able to compare the pattern of the signals between all subjects rather than pairwise comparison using a

reference subject. A high correlation was observed in both populations across speeds. However, TFA C4 showed poor repeatability (high inter-subject variability), indicating differences in patterns of coefficients between trials/subjects in normal speed. However, ICC does not highlight to which phase this variability is associated with. One possible explanation is S4 comprised of primary activity of TA which contributed to the slowing down the leg in the early and late swing, ease of foot clearance. Therefore, the instability in TFA PL (due to the feeling of insecurity) during the weighting acceptance before IL starts swinging may be a factor contributing to the inconsistency in shape of C4 between trials/subjects. In addition, due to the presence of triceps surae during weighting acceptance, TA co-contracts to stabilize the ankle joint which may lead to discrepancies in TFA C4 (Table 4.2). Furthermore, previous research has shown high inter-subject variability in the TA activity during walking [76, 321].

Lastly, one may be able to explain this from a psychological point of view. TFA are used to performing normal walking. However, the slow and fast walking (especially in transient-state) would be a challenging task for them. Therefore, they will be more careful and adopt a more cautious gait pattern when performing gait at other speeds than the comfortable, self-selected normal speed. The higher cognitive load may reduce the variability in muscle activities [322].

4.5.4 Module Contribution

Module contribution is a good indicator of overall muscular contributions which this may be useful in therapies to tailor the rehabilitation plan to focus on primary muscles within a particular module.

4.5.5 Within-Subject (Synergy/Module Comparison)

Previous reports illustrated similarity in the construction of muscle synergies of HS at different walking speeds which contradicts the motor modules obtained from HS in the present study across transient-state walking speeds [77, 83, 91, 218]. Furthermore, Gui and Zhang [218] showed similar motor modules across speeds with modest changes in the timing of coefficients of the non-disabled subjects to satisfy the kinematic and kinetic requirements of different steady-state walking speeds. However, others found different muscle synergies are recruited as the result of a change in steady-state walking speeds and locomotion modes which agrees with the findings of the present study [170, 248, 249].

Generally, a reasonable correlation was observed in the majority of the HS muscle synergies, indicating shared modular motor control between subjects across different walking speeds. The lowest correlation between normal-fast ($S3=0.12$) and fast-slow ($S1=0.17$) was directly associated with the primary muscle weighting suggesting a

difference in the weighting contributions of the knee extensor and ankle dorsiflexor muscles rather than completely different muscle groups recruitment (Table 4.18). Although gait in the present study is performed as a transient-state walking, some of the HS modules are comparable to the literature (i.e., S2 and S3) [77, 79, 83, 91, 126, 218].

TFA R^2 results revealed poor (S1), moderate (S3 and S4) and strong (S2) correlations across paired-speeds comparisons (i.e., module average). The primary muscle weighing in S1 is different across speeds which led to poor correlation. On the contrary, analogous muscle group in S2 resulted in a strong correlation between speeds. The lowest correlation in S1 (0) and S3 (0.2) between fast-slow walking was due to the difference in weighting ratio (Table 4.19). The difference could be attributed to the significant change of speeds which resulted in neuromuscular modulation at the transition from stance to swing phase and body support phase of the GC [218].

4.5.6 Between-Subject (Synergy/Module Comparison)

The lowest correlations were observed in S1 and S4 during slow and normal walking speeds, respectively. The strongest correlation was perceived in S2 during slow and fast walking speeds, respectively. By investigating the results further, it can be perceived that primary muscle weightings have significant impacts on the total correlation results. Significant changes in TFA IL muscle adaptation could be due to the inadequate proprioceptive feedback, weight-bearing deficiency in PL and prosthesis type [46, 92-95]. As a result, changes in motor modules occurs. In addition, each of the TFA tends to develop their own ambulation patterns because of the rehabilitation training, level of amputation, the reason for amputation, and age which may cause neuromuscular modulation between amputees themselves and HS. Most importantly, the gait in this chapter was performed as a transient-state walking which may lead to inconsistency in muscle recruitments, change in the duration of activity, difference in magnitude of the burst of both groups as well as postural instability in TFA.

4.5.6.1 Motor Modules Comparison with Literature

The muscle synergy components extracted in this study were compared to the literature. It is worth mentioning in this chapter; the transient-state walking was carried out across three different self-initiated and self-selected speeds for both HS and TFA. Therefore, the comparison was made based on the available literature on the steady-state of the gait. [84] studied the influence of data structure on the motor synergies during treadmill walking, and [77] carried out forward dynamics simulation using muscle synergy components. In the present study, the modules extracted from HS during fast transient-state walking matches well with 4 of their modules in both studies. In addition, in the study conducted by [91], the differences between motor modules of HS and post-stroke

patients were identified. The same number of synergy groups and similar modules were observed to those of the HS during fast transient-state walking in the present study.

A study carried out by [77] showed five muscle activation modules was sufficient to generate forward dynamics simulation of gait and their associations with biomechanical subtasks of walking. The study reported, knee and hip extensors contribute to body support in early stance while acting to decelerate forward motion (Module 1), plantarflexors contribute to loading and propulsion in late stance (Module 2), dorsiflexor and hip flexor muscles contribute to deceleration of the leg in early and late swing as well as trunk stabilization throughout swing phase (Module 3), knee flexors decelerates the leg in late swing (Module 4) and hip flexors contribute to acceleration of the leg forward in pre- and early swing (Module 5) [77]. In the present study, in slow walking, HS S3, S2, and S4 correspond to Module 1, Module 2 and Module 4 of [77], respectively. In HS during normal walking, S2 and S4 corresponded to Module 2 and Module 4 of [77], respectively. In HS during fast walking; S3, S2, S1 and S4 corresponded to Module 1, Module 2, Module 3 and Module 4 of [77], respectively. The difference between literature [77] and present study with regards to S1 (primary: VM) during slow walking as well as S1 (primary muscle: VM, TFL, and TA) and S3 (primary muscle: VL) during normal walking seemed to be affected by the synergy analysis methods, task performed (steady-state vs. transient-state), number and choice of muscles included, and difference in speed.

The neuromuscular modulation between muscle synergies of HS across speeds agreed with the study conducted by [249], suggesting a change in speeds lead to recruitment of different spinal locomotor networks.

In conclusion, the results obtained from the HS during fast transient-state walking in the present study corresponded well with the normal steady-state walking in the previous reports [77, 84, 91, 126].

4.5.7 Statistical Analyses (Activation Coefficient Profile)

4.5.7.1 Within-Subject (Biomechanics Perspective)

Speed Dependence of the HS and TFA Activation Coefficient Profile

The null hypotheses regarding the effect of speeds on activation coefficient of HS (hypothesis 1) and TFA (hypothesis 3) were not supported, suggesting adaptation strategy implemented by the CNS to fulfill the task-dependent requirements of transient-state walking at different speeds.

The post hoc paired Hotelling's T2 test illustrated suprathreshold clusters in HS during body support, foot-flat, and transition from stance to swing phase as well as a

swing to stance phase in the comparison between normal-slow speed (Figure 4.22). TFA showed to be significantly different in weighting acceptance between normal-slow and in the transition from PL to IL at the end of IL swing phase between fast-slow (Figure 4.23).

The difference could be related to the kinematic and kinetic demands of different speeds which led to different intensity in magnitude and time lag in activation timing in both groups across speeds. Previous reports indicated small changes in the epoch where the peak activation coefficient occurred across speeds during steady-state walking which is in contradiction to the findings in the present study [170, 185]. However, [109] concluded the activation coefficient is flexibly controlled by the CNS in the regulation of walking speed which agrees with the present findings.

4.5.7.2 Within-Subject (Robotic Control Perspective)

Speed Dependence of the HS and TFA Activation Coefficient Profile

SPM RM ANOVA analysis showed that the null hypothesis was not supported as significant differences were found in all the HS coefficients across speeds (hypothesis 2). The reason for those coefficients, whose associated muscle synergies were reasonably correlated, to be statistically significant could be due to the CNS adaptation strategy to increase the intensity of activation coefficient profile to satisfy the kinematic and kinetic requirements of different speeds. This does not necessarily mean that as speed increases only the intensity of activation coefficient profiles would increase because muscle synergy analysis depends on two factors C and S (Equation 4.7). Thereby, increase in muscle synergy vectors ratio can also be perceived. On the other hand, those activation coefficient profiles associated with the poor muscle synergies correlation between speeds, have different activation timing, patterns, and magnitudes.

HS C4 post hoc SPM t-values did not reach the Bonferroni significant threshold of ($p=0.02$). The discrepancy between the main RM ANOVA C4 and post hoc paired t-test might be due to the Bonferroni threshold. Bonferroni post hoc analyses are approximate and conservative to avoid type I error. Different post hoc procedures are required to yield a precise probabilistic agreement between the main analysis (RM ANOVA) and post hoc results. It is worth mentioning, in general, post hoc analyses are considered as approximate explanations for the main results where differences occurred. Conclusions must not be drawn about the post hoc test which disagrees with the main SPM results. Therefore, the null hypothesis was rejected as there is a significant difference between the HS C4 within-subject at different speeds (Figure 4.30 and Figure 4.31).

SPM RM ANOVA analysis showed a significant difference in TFA C1, C2 and C4 across speeds (hypothesis 4). The post hoc TFA C1 between fast-normal and between

fast-slow showed significant differences in ES and TSW. The muscle synergy comparison (i.e., S1 fast-normal and S1 fast-slow) showed to be poorly correlated with R^2 of 0.13 and 0, respectively. The primary muscles in TFA C1 between slow (mainly activated TFL), normal (mainly activated SOL) and fast (mainly activated RF) were different. One could suggest the significant differences in activation timing between speeds are due to the different group of muscles recruitment thereby each module contributed to different biomechanical subtasks (Figure 4.32 and Figure 4.33).

Although a high correlation was observed between S2 across speeds (pair-wise speed comparison), TFA C2 (mainly activated plantarflexor) showed to be significantly different in MS, TS, and ISW between fast and normal speed. Since the same set of muscles were recruited across speeds, the reason for the discrepancy between the speeds may due to the higher activation and intensity required for the plantarflexor muscles of the IL to stabilize the ankle joint during single support stance phase and generate larger push off in TS with increased speed. This is evident from the significant difference that occurred during fast gait as compared to normal gait (Figure 4.34 and Figure 4.35).

TFA C4 (mainly activated TA) was found significantly different in MS between fast and slow speed walking. The activation of SEM was coordinated with TA in S4 at slow walking in which a moderate correlation (0.5) was observed compared to fast walking. The higher magnitude of the second peak in the stance phase of fast walking (suprathreshold cluster) occurred before the second peak in slow walking. This could be due to the kinematic and kinetic demands which altered TA activation timing (Figure 4.37 and Figure 4.38).

Interestingly, TFA C3 showed no significant differences between speeds. The same group of muscles (SEM and VL) associated with S3 across speeds, except at fast speed. Observing the mean difference t-trajectory, one could observe the black line at the end of swing phase is very close to the critical threshold (Figure 4.36). The results indicate no adaptation strategy is required to augment the intensity of the temporal component. The results agree with the effect of speeds in HD EMG activity of SEM where no significant differences were found suggesting the low dimensional and high dimensional temporal component would be the same for this muscle (chapter 3).

4.5.7.3 Comparison of Activation Coefficient Profile with Literature

The results of the present study appear to conflict with the previous reports as they suggested a small increase in activation coefficient timing at different walking speeds [77, 83, 91, 218]. It is worth mentioning that none of the studies conducted in muscle synergies considered the whole time-series as a means of comparison (i.e., using 1D SPM). This could be attributed to the fact that discrete points in the traditional statistical analysis (i.e., scalar) may result in a different interpretation. Therefore, one should consider the time normalized *C* waveforms especially when there is no *a priori* hypothesis pertains to the point of interest [225, 226]. In addition, the present study did not consider the steady-state walking as opposed to the studies conducted in the literature [77, 79, 82, 84, 91-93, 95, 126, 136, 179, 217, 218, 221, 230, 323]. In summary, the difference could be attributed to the difference in muscle synergy methodological consideration, state of walking (steady-state vs. transient-state), number and choice of muscles included, and the difference in speed.

4.5.7.4 Between-Subject (Biomechanics Perspective)

Since the biomechanics hypothesis does not pertain to a specific *C* and time point, inter-activation coefficient profiles covariance and time dependency have been considered into statistical testing whilst maintaining a constant error rate of α , respectively. The main SPM analysis rejected the null hypothesis across all speeds (hypothesis 5).

In slow walking, two suprathreshold clusters exceeded the critical threshold in weighting acceptance and TS between groups. Post hoc analysis showed C2 was significantly greater in TFA as higher peak and forward shift of the main burst was observed. This could be due to the compensatory strategy implemented by the CNS to stabilize the IL joints during weighting acceptance, to generate larger push off during the TS and to compensate for the lack of push off in PL (Figure 4.39 and Figure 4.40).

In normal walking, two suprathreshold clusters were found in the vector field analysis result in weighting acceptance and TS between groups. The post hoc t-test illustrated significant differences in C2 and C3. TFA C3 (mainly related to knee extensor muscles) is significantly different from HS in ES, suggesting necessities of IL higher activation for body support at the transition from PL to IL. The post hoc C2 result of significant difference at normal speed is comparable to the post hoc C2 at slow speed with the difference that another suprathreshold occurred at the peak activation of HS C2 instant. The possible explanation for the difference between HS and TFA at normal speed is because of the TFA feeling of insecurity which led to a longer stance phase of the IL compared to the HS, which agreed with other studies [35, 67, 71, 72]. Therefore, a forward shift in the activation can be observed (Figure 4.41 and Figure 4.42).

In fast walking, one suprathreshold cluster was observed in the main analysis during the TS. Post hoc analysis showed significant differences in the TFA C1 during the MS and TFA C2 during the TS. The TFA C1 peak in MS of the GC was significantly greater as compared to the HS C1. However, since the result does not agree with higher-level analyses (main analysis), MS significant difference was rejected. Similar to the slow and normal speeds, a significant difference occurred during the TS between groups which could be due to the higher TFA IL push off required to compensate for the PL lack of push off as compared to the HS (Figure 4.43 and Figure 4.44).

4.5.7.5 Between-Subject (Robotic Control Perspective)

The null hypothesis 6 that there would be no difference in individual activation coefficient profiles between HS and TFA during transient-state walking at different speeds was supported in C4 (mainly activated SEM) during fast.

Generally, larger variation (represented as a blue shaded cloud) was observed in TFA coefficients as compared to the HS across speeds. One of the main possible reasons for neuromuscular compensation in TFA could be associated with the lack of proprioceptive feedback from PL and type of prostheses (e.g., mechanically passive and SACH foot) which fails to provide sufficient push off to move the body forward. This results in a higher GRF and greater mechanical work on both IL and PL [21, 24].

The TFA C2, which activated plantarflexor muscles, demonstrated two prominent peaks during the ES to MS and TS across speeds. These peaks were heightened and shifted forward in the GC as compared to the HS at all speeds (except 2nd peak of TFA C2 normal speed) (Figure 4.45, Figure 4.46 and Figure 4.47). In addition, TFA C3 (activated knee extensors primarily) showed higher peaks at the ES as compared to the HS across speeds. Consequently, SPM two-sample t-test showed TFA C2, and C3 were statistically significantly different than those of HS at the aforementioned regions. The difference could be due to the efforts of TFA to stabilize their joints and body weight during the single support phase and to provide push off in late stance to propel the body forward. Along the same line in HD EMG analysis, TFA plantarflexor muscle showed earlier and prolonged activation (chapter 3, Figure 3.3). The comparison between groups in C4 illustrated there were common drives in SEM as the SPM results showed no significant difference in the temporal component. In addition, the muscle synergy showed a reasonable correlation between the two groups indicating a similar neural strategy for Module 4 at fast speed (Figure 4.47). Along the same lines of observed results, the SEM muscle activity showed the similarity between groups in high dimensional level at all speeds. In general, neuromuscular compensation in TFA could be associated with the type of prostheses (e.g., mechanically passive) which fails to provide sufficient push off

to move the body forward. This results in a higher GRF and greater mechanical work on both IL and PL.

4.6 Summary

The study presented CNMF as a robust algorithm which facilitates the comparison of muscle synergy analysis between populations by keeping synergies fixed between subjects. Four modules were able to account for more than 85% of the variability in the original signals for each group. Total module contribution was calculated in which lowest and highest synergy were determined. A high correlation was perceived between individual muscle's reconstructed and original signals by means of R^2 and ICC. Prior to the comparison of the muscle synergy components within- and between-subject, functional sorting was done. The strong correlation in muscle synergy implies the same group of muscles is controlled by the CNS synergistically. Primary muscles in each module had a significant impact on the correlation results. Generally, a reasonable correlation was observed in muscle synergies of HS indicating shared motor modules within group across different gait speeds. On the contrary, higher variation was found in TFA muscle synergies correlations. The between-subject muscle synergy comparison showed variability in correlation results between HS and TFA across speeds. The coefficient analysis was done within- (across all speeds) and between-subject (between each speed category) from biomechanics and robotic control perspectives. SPM 1D analysis was performed to consider the whole time-series (i.e., between 0% and 100% time). The intra-subject comparison was considered to investigate modulation in activation coefficient of muscle synergies across speeds. It was revealed that muscle synergies were dependent on the walking speeds as significant differences were observed in activation coefficient profile at different epochs of GC for HS and TFA. This suggests the adaptation strategy by the CNS to satisfy kinematic and kinetic demands of different transient-state walking speeds. Therefore, it was crucial to investigate the influence of walking speeds within the homogenous population as a separate analysis to constructively distinguish the changes in motor modules of each group. Inter-subject activation coefficient comparison showed significant differences between HS and TFA at different regions of the GC especially during stance phase, indicating the compensatory strategy for stabilization of the TFA IL joints. The findings in this study aid to tailor the therapies to improve the quality of movement of amputees as well as providing useful information for the development of the new generation of prostheses (synergy-based control frame).

4.7 Conclusion

Both HS and TFA illustrated that four synergies are an optimal number of groups to match the reconstructed and original EMG at all speeds. This suggests that complexity of muscles recruitment by the CNS is analogous in both groups. Therefore, there is no compensatory adjustment in TFA.

Reasonable correlation in muscle synergies of HS was observed across different speeds, indicating that the CNS activates the same groups of muscles synergistically. The low correlation was directly associated with the primary muscle weighting suggesting a difference in the weighting contributions of the knee extensor and ankle dorsiflexor muscles rather than recruitment of different muscle groups. The highest correlation in TFA was observed between plantarflexor muscles at different speeds. The low correlation between TFA muscle synergies across speeds could be attributed to the significant change of speeds which resulted in neuromuscular modulations at the transition from stance to swing phase and body support phase of the GC.

The low correlation between HS and TFA muscle synergies could be due to the ambulation pattern, inadequate proprioceptive feedback, weight-bearing deficiency in PL, type of prostheses, and level of amputation which may cause neuromuscular modulation between amputees themselves and HS.

The effect of speeds on activation coefficient profiles of both HS and TFA were compared from biomechanics perspective in which significant differences were found, suggesting adaptation strategy implemented by the CNS to fulfill the task-dependent requirements of transient-state walking at different speeds. The difference could be related to the kinematic and kinetic demands of different speeds which led to different intensity in magnitude and time lag of activation timing for both groups across speeds.

The effect of speeds on individual activation coefficient profiles of HS and TFA (robotic control) showed significant differences (except TFA C3), indicating the CNS strategy to increase the intensity of activation coefficient profile to satisfy the kinematic and kinetic requirements of different speeds. No significant differences were found in TFA C3, suggesting no adaptation strategy is required to augment the intensity of the temporal component.

Significant differences were observed in activation coefficient profiles (biomechanics approach) between HS and TFA at each speed category. A common significant difference (i.e., suprathreshold cluster) occurred between both groups during the TS at all speeds which could be due to the higher TFA IL push off required to compensate for the PL lack of push off as compared to the HS.

Individual activation coefficient profile (robotic control approach) showed no significant differences in C4 at fast speed between HS and TFA which shows common drives in SEM. The significant difference in the other activation coefficient profiles mainly associated with the stance phase which could be due to the TFA effort to stabilize their joints and body weight during this time. The significant differences in C2 were in late stance and PSW and epochs of swing phase which shows the importance of TFA plantarflexor after push off to propel the body forward and to control the ankle during swing phase.

Chapter 5

MODULAR MOTOR CONTROL IN TRANSTIBIAL AMPUTEE DURING STEADY-STATE WALKING

5.1 Introduction

This chapter presents the implementation of concatenated non-negative matrix factorization (CNMF) algorithm developed in the previous chapter on a new set of data and walking condition. Muscle synergy analysis is performed on a transtibial amputee (TTA) to investigate the modular motor control in steady-state walking (i.e., after transient-state), accounting for the intact leg (IL) and prosthetic leg (PL), and modulating the number of muscles. The study is carried out with four healthy subjects (HS), and one TTA during ramp ascending (RA), ramp descending (RD) and steady-state walking. However, in this chapter, only modular motor control comparison between HS and TTA during steady-state walking is presented (publications related to the RA and RD are presented in Appendix E). Previous literature reported on TTA high dimensional (HD) EMG activities across a range of speeds during steady-state walking. However, to the best of the author's knowledge, no studies are available in the literature to use muscle synergy analysis in TTA during steady-state walking.

5.2 Experimental Protocol

5.2.1 Methodology

The pilot study involved participation of four active HS (mean (SD): age 21.3 (0.4) years, weight 72.2 (5.9) kg, height 175.7 (6.0) cm) and one active elderly TTA (age: 76; weight: 69.3 kg; height: 185.1 cm) during steady-state walking (Appendix C, Table C.1, Table C.2 and Table C.3 show the anthropometric characteristics of HS and TTA, and details of prosthesis used by the TTA, respectively). The HS and TTA were free of any lower limb injury, any skin condition or neurodegenerative disease except the amputation of the TTA PL. All subjects wore their own daily shoes. Noraxon surface EMG electrodes (Telemyo, Noraxon, Scottsdale, USA) were used to collect electrical signals unilaterally from HS dominant leg and TTA IL and PL (PL) during LGW (Figure 5.1 (A)). EMG system consists of a 2400R receiver in which 10 channels were used to record from 6 upper knee muscles and 4 shank muscles. LGW was performed on a 10-meter walkway at the self-selected speed. Two AMTI force plates (Advanced Medical Technology Inc,

Massachusetts, USA) were installed in the middle of the walkway. The subjects performed at least 5 strides to reach the steady-state walking. Gait cycles were extracted using the kinetic information obtained from these force plates. Moreover, four foot-switches located at (1) heel, (2) 1st metatarsal, (3) 5th metatarsal (4) toe to detect heel strikes and TO outside the force plates (Figure 5.1 (B)). In addition, an ultrasound scanner (LogiQ e, GE Healthcare, USA) was utilized by an experienced sports medicine doctor to attach the surface EMG electrodes to the belly of ten muscles (Figure 5.1 (C) and (D)).

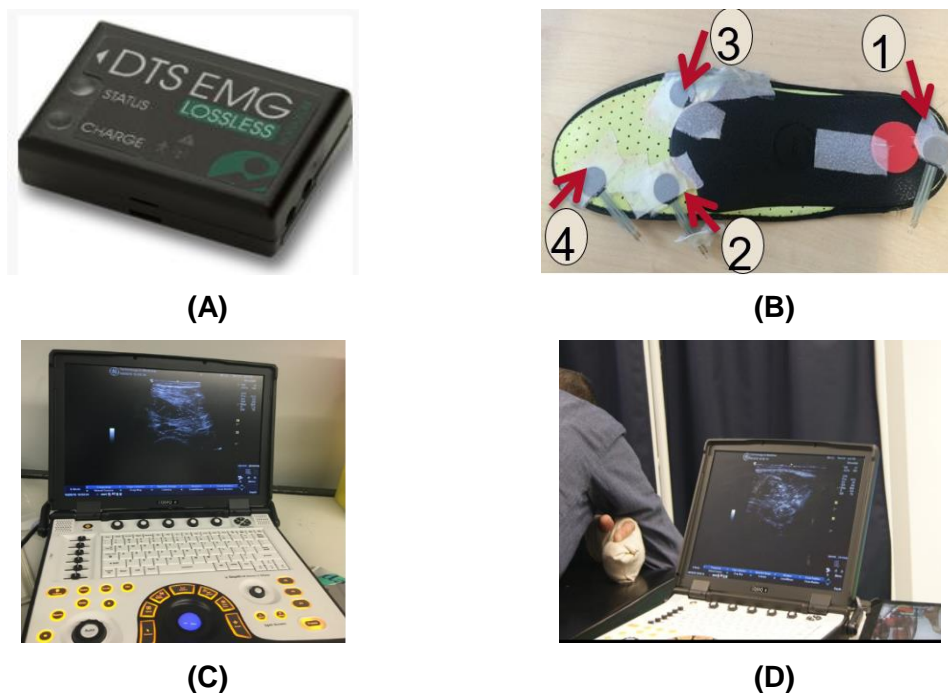


Figure 5.1: Experimental setup: (A) surface EMG, (B) foot switches location; 1: Heel; 2 & 3: 1st & 5th Metatarsal; 4: Toe, (C) ultrasound scanner, and (D) muscle view using ultrasound

Among the recorded muscles, six were from upper knee muscles (UKN) including rectus femoris (RF), and vasti (i.e. vastus medialis (VM) and vastus lateralis (VL)), biceps femoris long head (BFLH), gluteus medius (GMED), tensor fascia latae (TFL) and four was from below knee including; tibialis anterior (TA) and triceps surae (i.e. gastrocnemius medialis (GM) and gastrocnemius lateralis (GL), soleus (SOL)). The captured information sampled at 1500 Hz and amplified by a gain of 1000. The data were displayed on a computer with a visual feedback program called Qualisys Track Manager [324]. The TTA had used his prosthesis for a long period of time. An information sheet containing the research background, description of the experiments and consequences of participating were given to each subject and consent form was signed by all participants prior to the experiment. University of Leeds Ethical Review Board approved all experimental procedures in this study. Figure 5.2 and Figure 5.3 show attachment of surface EMG on HS dominant leg and TTA IL and PL, respectively.

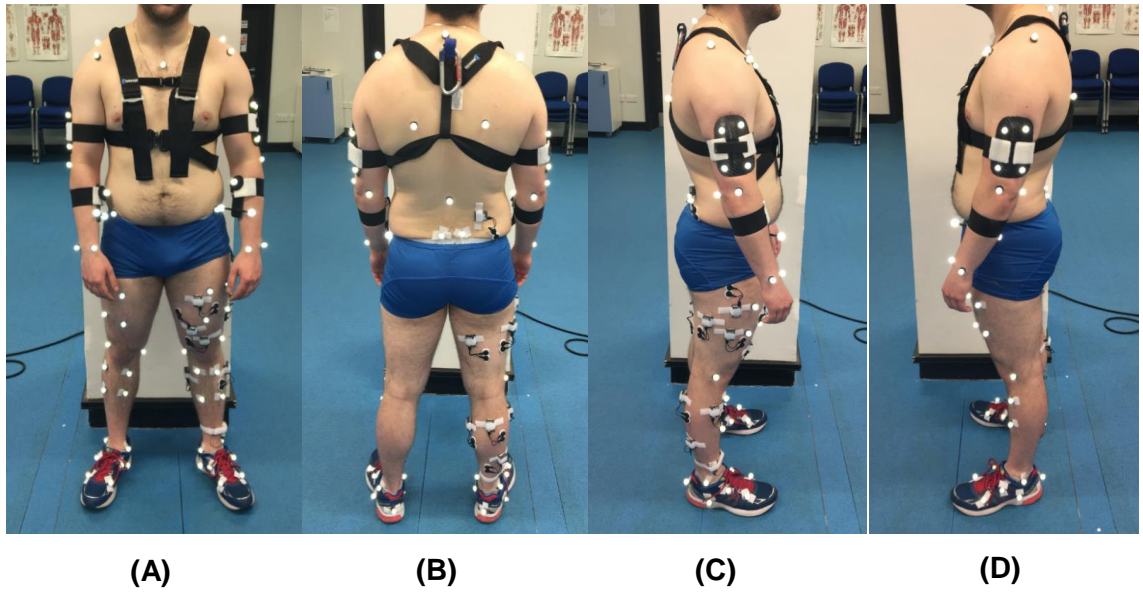


Figure 5.2 EMG and reflective markers attachments on HS. (A) front dominant leg, (B) back dominant leg, (C) side dominant leg, (D) side non-dominant leg.

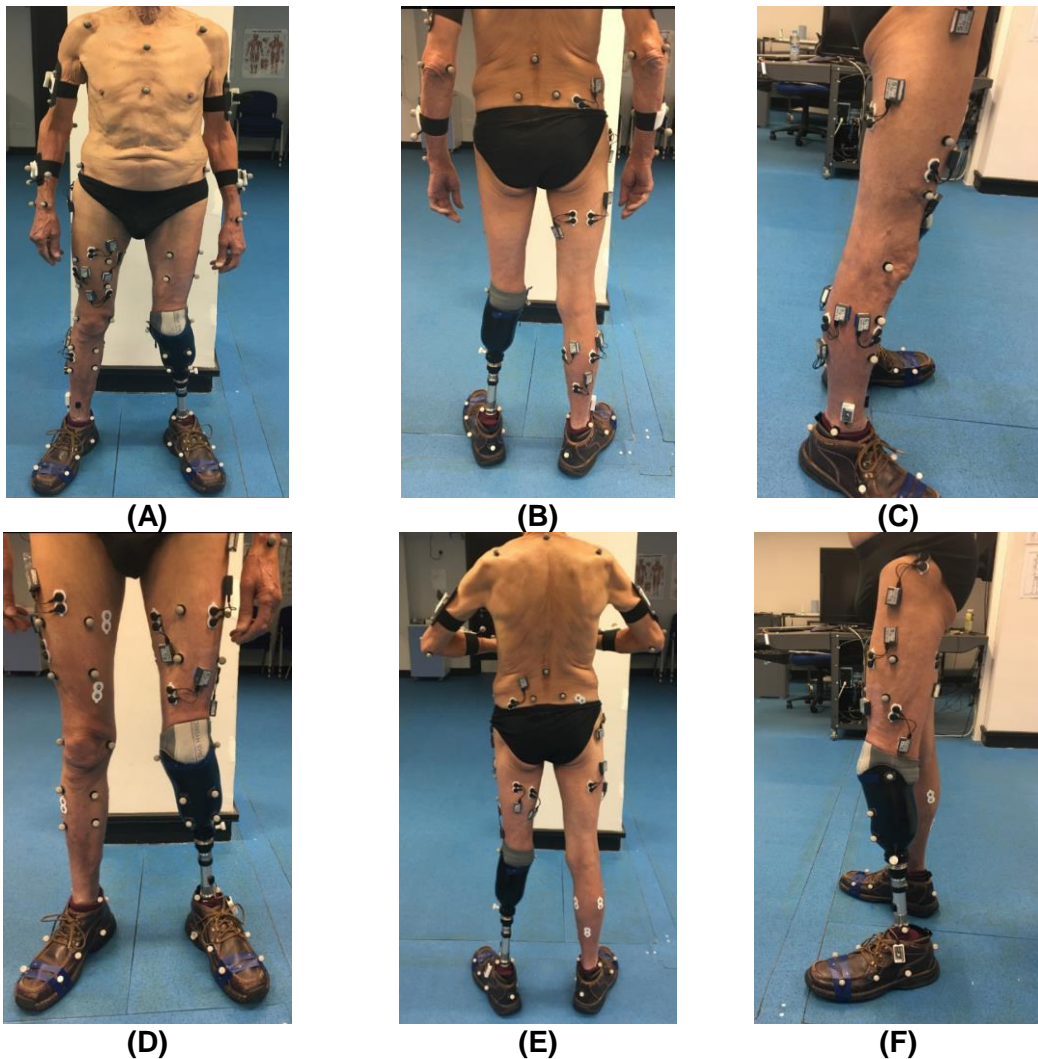
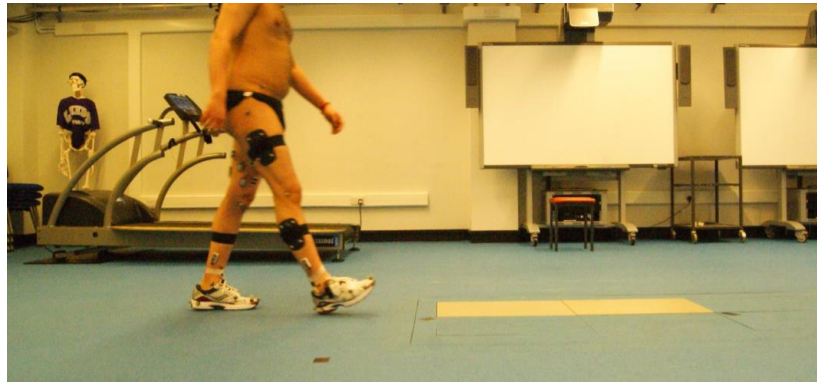


Figure 5.3: EMG and reflective markers attachments on TTA IL and PL. (A) front IL, (B) posterior IL, (C) side IL, (D) front PL, (E) posterior PL and (F) side PL.

After all EMG electrodes were attached to the belly of the muscles, the subjects were asked to familiarize themselves with a walkway in the lab. Based on the protocol, HS and TTA performed at least six trials for each activity and were asked to hit their dominant leg, IL, and PL on the force plate, respectively. The trajectories from reflective markers placed on the instrumented foot (calcaneus and 1st metatarsal) as well as the foot switches on heel and toe were used to identify the GC.

Subjects were given 10 minutes break between each activity to avoid fatigue. Figure 5.4 shows subjects performing steady-state walking.



(A)



(B)

Figure 5.4: (A) HS and (B) TTA walking (length: 10 m; Inclination: 0° pathway)

5.3 Algorithm Description for Muscle Synergy Analysis

5.3.1 Signal Processing

A MATLAB script (Mathworks, Inc, Natick, MA) processed all data. A bandpass filter (zero-lag Butterworth filter with a cut off frequency of 20-500 Hz) was used to remove motion artifacts and high frequency noise from the signals. In order to obtain the muscle activation pattern (linear envelope), full wave rectification and a low-pass filter (a zero-lag 2nd order Butterworth at 6 Hz) were performed. The data were normalized to the maximum peak value obtained from each muscle overall selected GCs. Therefore, all values of each muscle were ranged between zero and one. The data were then interpolated to 101 data points corresponding to the instrumented leg GC.

5.3.2 Concatenated Non-Negative Matrix Factorization (CNMF)

Concatenated non-negative matrix factorization (CNMF) approach was implemented to linearly decompose the concatenated data into a linear combination of activation coefficient profile (C) and muscle synergy vector (S) [92, 213]. The norm-2 length of S was constrained to be 1 to minimize the indeterminacy of the factorization. A matrix A^c ($n \times m$) was created to combine and concatenate the surface EMG data, where n represents the number of subjects \times number of GCs \times 101 and m accounts for the number of muscles. The results of CNMF populated: (1) the concatenated coefficient ($C^c = n \times k$) and (2) the fixed muscle synergy ($S = k \times m$), where k represents the number of synergy groups. The summation of the product of muscle weightings in all the synergies and their corresponding coefficients provides the reconstructed signals.

5.3.3 CNMF Frameworks

Random values of C and S were chosen (*rand* function in MATLAB) in order to initiate the CNMF. An *alternating least squares* algorithm was implemented to attain optimal C and S . These values must satisfy the Frobenius norm to minimize the error $J = \|A - CS\|_F$. To ensure the value is reliable, perturbation was introduced to the data. In order to find the final optimal solution of S and C , three iterations were performed for the whole framework. However, the error was not applied in the last iteration [92, 213].

5.3.4 Variance Accounted For (VAF)

In order to find the appropriate number of muscle synergy groups in HS and TTA groups and adequately reconstruct the original signals, concatenated variance accounted for (VAF) was calculated. The VAF > 0.80 has been accepted as a standard threshold for determining the appropriate number provided that an extra synergy improves the VAF for less than 0.05 [136, 179].

5.3.5 Functional Sorting

The functional sorting was performed because each group might use muscle synergies differently and subsequently to facilitate inter-subjective comparison. This method resolves the large differences in contribution to the total data variability by rearranging the indices of synergy and coefficient of one group based on the other group. The sorting in most cases was done by choosing the HS synergy and coefficient vectors as a reference to sort the TTA results. For TTA within-subject comparison, TTA IL was selected as the reference to sort the synergy components of PL. To rearrange the synergy and coefficient vectors coefficient of determination was used.

5.3.6 Correlation Analysis

Coefficient of determination (R^2) was used to investigate the goodness of fit between the reconstruction signal ($C * S$) and original signal (A). In addition, Intra-class correlation (ICC) was performed to investigate the reconstruction quality of each muscle intra-subjectively by assessing the shape and pattern of the reconstructed signal. Two-way mixed models for average measurements with no interactions (ICC(C,k)) were used. According to [222], $ICC < 0.5$, $0.5 < ICC$ and $R^2 < 0.75$, and ICC and $R^2 > 0.75$ imply low, moderate, and high correlation, respectively. Spatially fixed synergy vectors were compared pairwise between legs by means of R^2 .

5.3.7 Statistical Parametric Mapping (SPM)

Temporal components of muscle synergy analysis (i.e., activation coefficient profiles) were compared inter-subjectively (SPM two-sample t-test) between two groups as well as intra-subjectively between TTA IL and PL (SPM paired t-test).

The null hypothesis was presented in four different cases between HS dominant leg, TTA IL, and TTA PL during steady-state walking only accounting for individual activation coefficient profiles:

Case 1) HS dominant leg versus amputee's IL (10 muscles);

Null hypothesis Case 1: There is no difference between individual activation coefficient profiles of HS dominant leg and TTA IL during normal steady-state walking (two-sample t-test)

Case 2) HS UKN versus amputee's UKN IL (6 muscles);

Null hypothesis Case 2: There is no difference between individual activation coefficient profiles of HS UKN dominant leg and TTA UKN IL during normal steady-state walking (two-sample t-test)

Case 3) HS UKN versus amputee's UKN PL (6 muscles);

Null hypothesis Case 3: There is no difference between individual activation coefficient profiles of HS UKN dominant leg and TTA UKN PL during normal steady-state walking (two-sample t-test)

Case 4) amputee's UKN IL versus amputee's UKN PL (6 muscles):

Null hypothesis Case 4: There is no difference between individual activation coefficient profiles of TTA UKN IL and TTA UKN PL during normal steady-state walking (paired t-test).

5.4 Results

Muscle synergy analysis was performed between HS and TTA during LGW, RD and RA activities. Similarly, the comparison between synergy components of HS and TFA was made during LGW. In this chapter, only the results between HS and TTA during normal steady-state walking were presented. For other activities, refer to the publications lists.

5.4.1 Variance Accounted For (VAF)

The similarity of reconstructed and original signals was calculated by the VAF. The total VAF showed to be higher than 0.8 when four (*case 1*) and three (*cases 2-4*) synergy groups were chosen. In *cases 2-4*, three synergy groups satisfied the VAF criteria. shows changes in a number of synergy groups in all four *cases* by means of VAF (Figure 5.5).

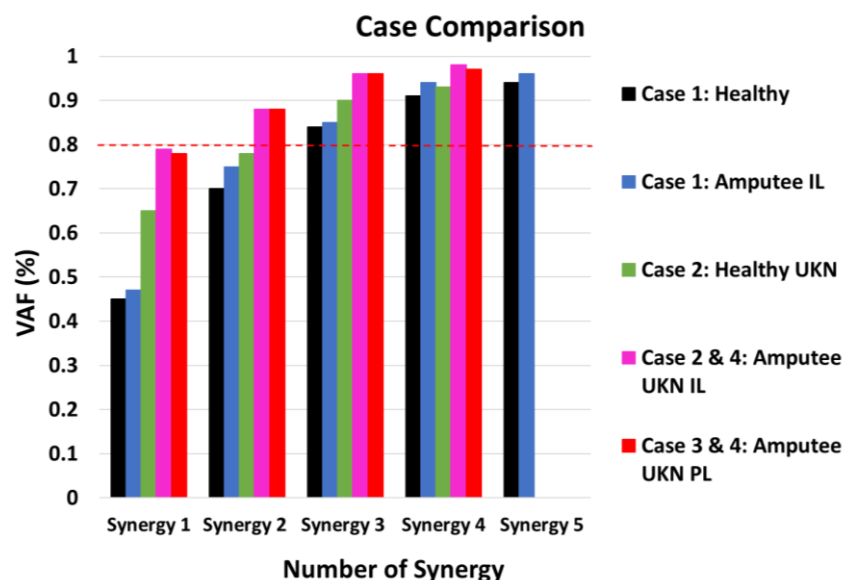


Figure 5.5: VAF comparison as a function of the number of synergies in cases 1-4.

5.4.2 Intra-class Correlation (ICC)

An individual muscle signal reconstruction showed a reasonable correlation to the original signal in all four cases (Figure 5.6). The lowest and highest ICC illustrated in RF

(case 2: healthy) and TA (case 1: amputee) with a correlation value of 0.31 and 0.99, respectively.

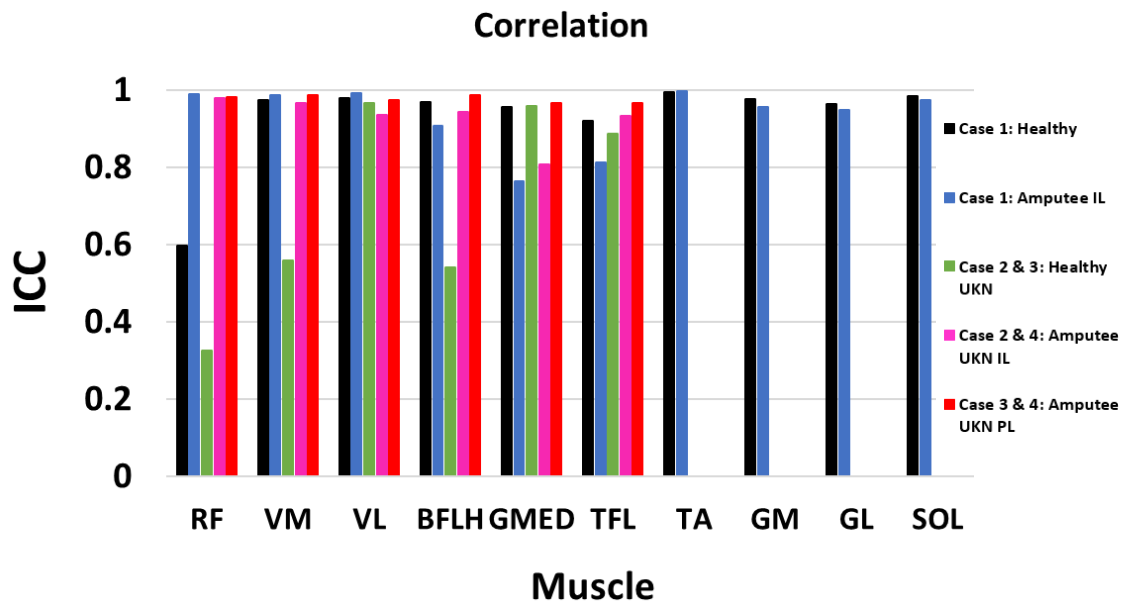


Figure 5.6: ICC of reconstructed signals compared to the original signal for each muscle in cases 1-4.

5.4.3 Muscle Synergy Analysis Description

Figure 5.7 (A) and (B) show muscle synergy vectors (S1-S4) and activation coefficient profiles (C1-C4) of cases 1-4, respectively. The muscle synergy is divided into two muscle groups based on their weighting; primary > 0.5 and secondary < 0.5 (Figure 5.7 (A)). The subsequent section is the interpretation of each case.

It is worth noting, functional sorting in this study was performed choosing HS synergy components as references to sort the amputee's results (cases 1-3). However, in case 4, amputee's IL was chosen as a reference to sort amputee's PL.

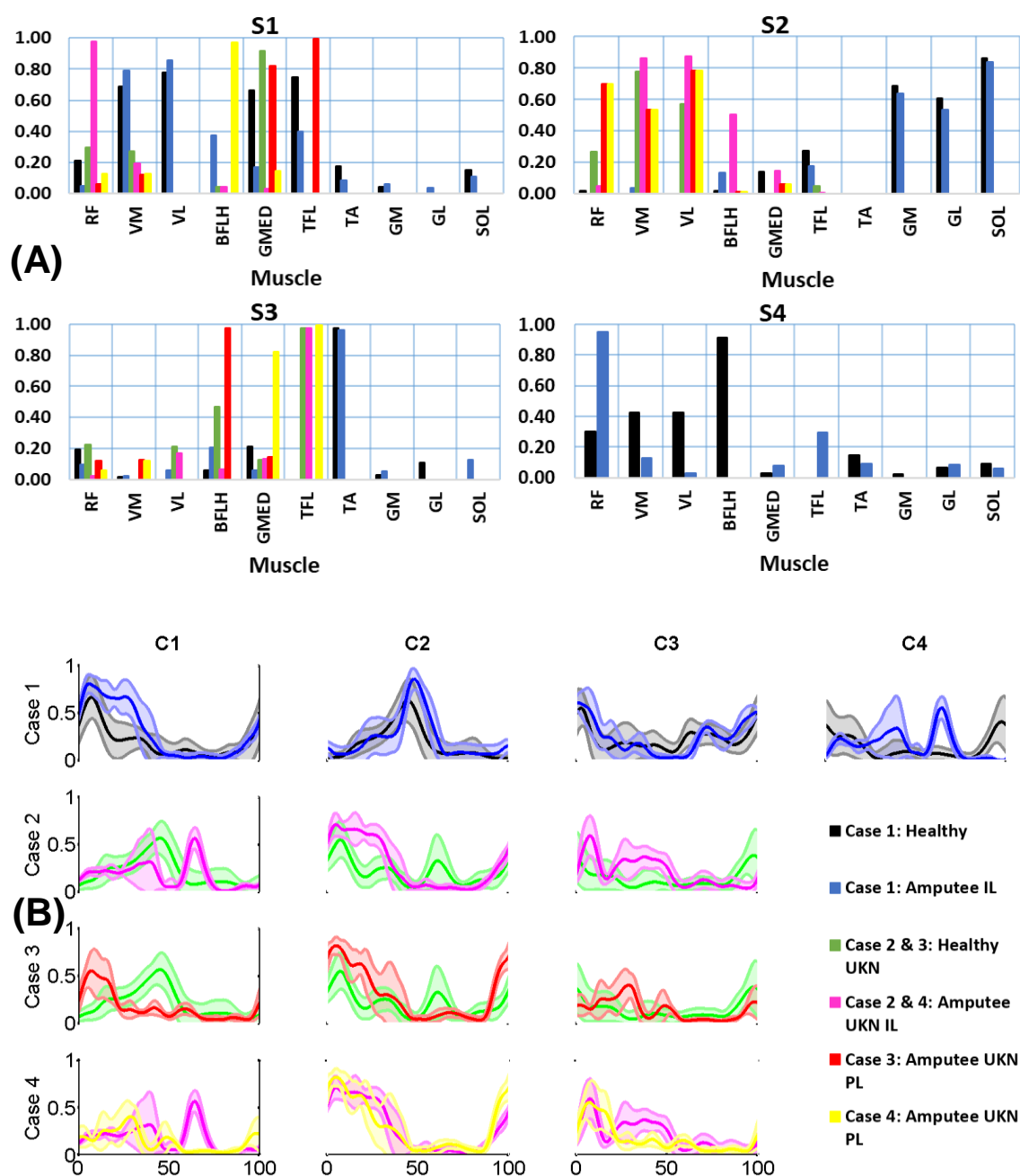


Figure 5.7: (A) Muscle weighting within each synergy and (B) activation coefficient profiles of cases 1-4.

Case 1: In HS, synergy 1 (S1) showed a high activation of vasti, TFL and GMED muscles as well as a lesser activity of RF, SOL, and TA during the ES and TSW. Synergy 2 (S2) consisted of primarily triceps surae muscles and to a lesser extent TFL and GMED during the MS-TS. Synergy 3 (S3) composed of primarily TA activation, and GMED and RF as secondary muscles during the ES and ISW and TSW. Synergy 4 (S4) comprised of BFLH as primary and vasti, RF and TA as secondary muscles during the ES and TSW (Table 5.1).

Table 5.1: Muscle weightings contribution and activation timing profile within each corresponding module (case 1: HS dominant leg).

Case 1: HS Dominant Leg			
Module	Muscle		Activation
	<i>Primary*</i>	<i>Secondary*</i>	
S1	Vasti, TFL, GMED	RF, SOL, TA	ES, TSW
S2	Triceps surae	TFL, GMED	MS, TS
S3	TA	GMED, RF, GL	ES, ISW, TSW
S4	BFLH	Vasti, RF, TA, SOL	ES, TSW

* Muscle weighting: primary > 0.5, and secondary < 0.05

Case 1: In amputee's IL, S1 was composed of mainly vasti high activation and lower activation of TFL, BFLH GMED, SOL, and TA during the ES-MS and TSW. S2 consisted of triceps surae and to lesser extent TFL and BFLH during the MS-TS. S3 composed of primarily TA muscle during the ES-MS and whole swing phase. S4 consisted of RF as a primary with the highest activation along with a lesser activity of TFL, VM, and TA as secondary muscles during the ES-MS and ISW (Table 5.2).

Table 5.2: Muscle weightings contribution and activation timing profile within each corresponding module (case 1: TTA IL).

Case 1: TTA IL			
Module	Muscle		Activation
	<i>Primary*</i>	<i>Secondary*</i>	
S1	Vasti, TFL, BFLH	GMED, SOL, TA	ES, MS, TSW
S2	Triceps surae	TFL, BFLH	MS, TS
S3	TA	BFLH, SOL, RF	ES, MS, TSW
S4	RF	TFL, VM, TA	ES, MS, ISW

* Muscle weighting: primary > 0.5, and secondary < 0.05

Case 2 and 3: In HS UKN, S1 showed a high activation of GMED and lesser activity of RF, VM, and BFLH during the MS-TS. S2 consisted of mainly vasti muscles and to a lesser extent RF and TFL muscles during ES-MS and ISW. S3 composed of high activation of TFL, and lower activation of BFLH, VL, RF, and GMED during ES-MS and TSW (Table 5.3).

Table 5.3: Muscle weightings contribution and activation timing profile within each corresponding module (case 2 & 3: HS UKN).

Case 2 & 3: HS UKN			
Module	Muscle		Activation
	<i>Primary*</i>	<i>Secondary*</i>	
S1	GMED	RF, VM, BFLH	MS, TS
S2	Vasti	RF, TFL	MS, TS, ISW
S3	TFL	BFLH, VL, RF, GMED	ES, MS, TSW

* Muscle weighting: primary > 0.5, and secondary < 0.05

Case 2 and 4: In amputee's UKN IL, S1 was comprised of primarily RF high activation and lower activation of VM during the stance phase and ISW. S2 consisted of mainly

vasti and BFLH muscles and lesser activity of GMED and RF during ES-MS stance and TSW. S3 showed a high activation of TFL as primary muscle and low activation of VL, GMED, and BFLH as secondary muscles during the whole stance phase (SP) (Table 5.4).

Table 5.4: Muscle weightings contribution and activation timing profile within each corresponding module (case 2 & 4: TTA UKN IL).

Case 2 & 4: TTA UKN IL			
Module	Muscle		Activation
	Primary*	Secondary*	
S1	RF	VM	SP, ISW
S2	Vasti, BFLH	GMED, RF	ES, MS, TSW
S3	TFL	VL, GMED, BFLH	SP

* Muscle weighting: primary > 0.5, and secondary < 0.05

Case 3: In amputee's UKN PL, S1 showed a high activation of TFL and GMED muscles and to a lesser extent VM and RF muscles during the ES. S2 consisted of mainly vasti and RF muscles as primary and lower activation of GMED during ES-MS and TSW. S3 was composed of primarily BFLH muscle and lesser activity of GMED, VM, and RF as secondary muscles during the whole stance phase and TSW (Table 5.5).

Table 5.5: Muscle weightings contribution and activation timing profile within each corresponding module (case 3: TTA UKN PL).

Case 3: TTA UKN PL			
Module	Muscle		Activation
	Primary*	Secondary*	
S1	TFL, GMED	VM, RF	ES
S2	Vasti, RF	GMED	ES, MS, TSW
S3	BFLH	GMED, VM, RF	SP, TSW

* Muscle weighting: primary > 0.5, and secondary < 0.05

Case 4: The interpretation of TTA UKN PL is similar to the case 3 but the order of synergy group 1 and 3 switches because the functional sorting was done based on TTA UKN IL (Table 5.6).

Table 5.6: Muscle weightings contribution and activation timing profile within each corresponding module (case 4: TTA UKN PL).

Case 4: TTA UKN PL			
Module	Muscle		Activation
	Primary*	Secondary*	
S1	BFLH	GMED, VM, RF	SP, TSW
S2	Vasti, RF	GMED	ES, MS, TSW
S3	TFL, GMED	VM, RF	ES

* Muscle weighting: primary > 0.5, and secondary < 0.05

5.4.4 TTA Muscle Synergy Comparison with TFA

Figure 5.8 illustrates the comparison between muscle synergies of TTA during normal steady-state walking and TFA during transient-state walking across different speeds (the description is presented in chapter 6, section 6.3).

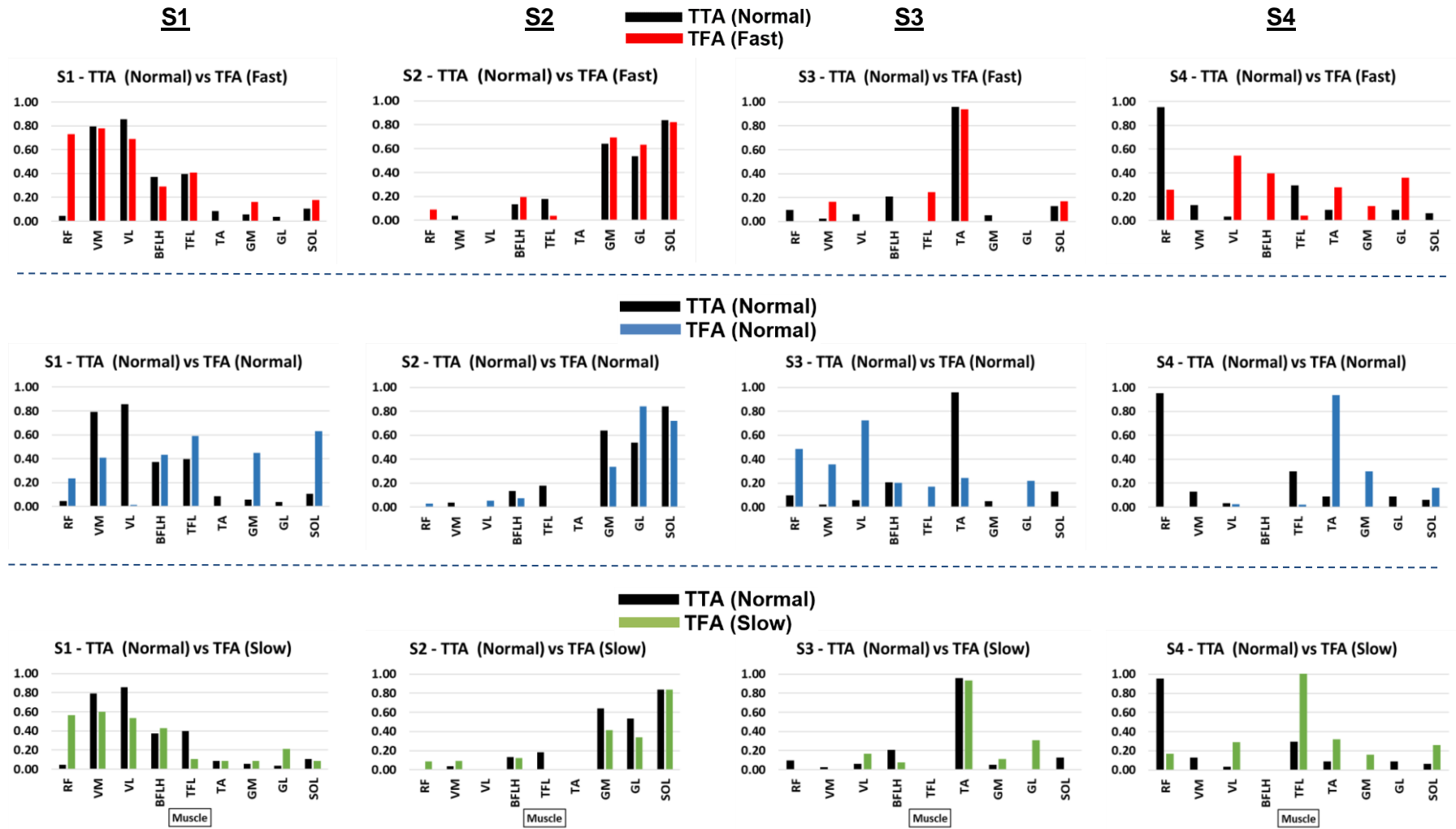


Figure 5.8: Comparison between muscle synergies of TTA and TFA.

5.4.5 Statistical Analyses (Spatially Fixed Muscle Synergies)

To assess the differences in the muscle synergies of each case, R^2 was performed.

5.4.5.1 Correlation Analysis using R^2

Table 5.7 shows muscle synergies correlation in all cases. In case 1, the highest and lowest correlation occurred in S2 and S4, respectively. Case 2 showed a low, moderate and strong correlation in S1, S2, and S3 between the two groups, respectively. In case 3, low correlation of S1 and S3 and moderate correlation of S2 were observed. In case 4, S1 showed low correlation, but S2 and S3 revealed moderate correlation.

Table 5.7: Muscle synergy comparison in case 1-4 using R^2 . NA indicates not applicable.

	S1	S2	S3	S4
Case 1	0.74	0.97	0.92	0
Case 2	0	0.57	0.84	NA
Case 3	0	0.70	0	NA
Case 4	0	0.57	0.48	NA

5.4.6 Statistical Analyses (Activation Coefficient Profile)

In the SPM analysis, the t-value is zero when there is no difference between the mean activation coefficient profiles of the two groups. When it is positive; meaning $C_{HS} > C_{TTA}$ and when it is negative; vice versa. The critical value is calculated through inference based on random field theory. If the t-curve exceeds the threshold (red line), then this shows the statistically significant difference in activation coefficient profile.

Case 1: The statistically significant difference between HS and TTA C1 occurred at 15-32% ($p < 0.001$) GC. This is where the t-trajectory passed Critical thresholds (t^*) and cluster-level probability values was less than 0.05. In C2, three suprathreshold clusters were obtained at 0-2% ($p = 0.042$), 49-55% ($p = 0.008$) and 94-100% ($p = 0.018$) GC. In C3, the significant differences occurred in only one region GC (57-62% ($p = 0.008$)). C4 showed the highest percentage where the t-trajectory passed the threshold (25-34% ($p < 0.001$), 58-71% ($p < 0.001$), and 88-97% ($p < 0.001$)) indicating the major difference between the two groups (Figure 5.9).

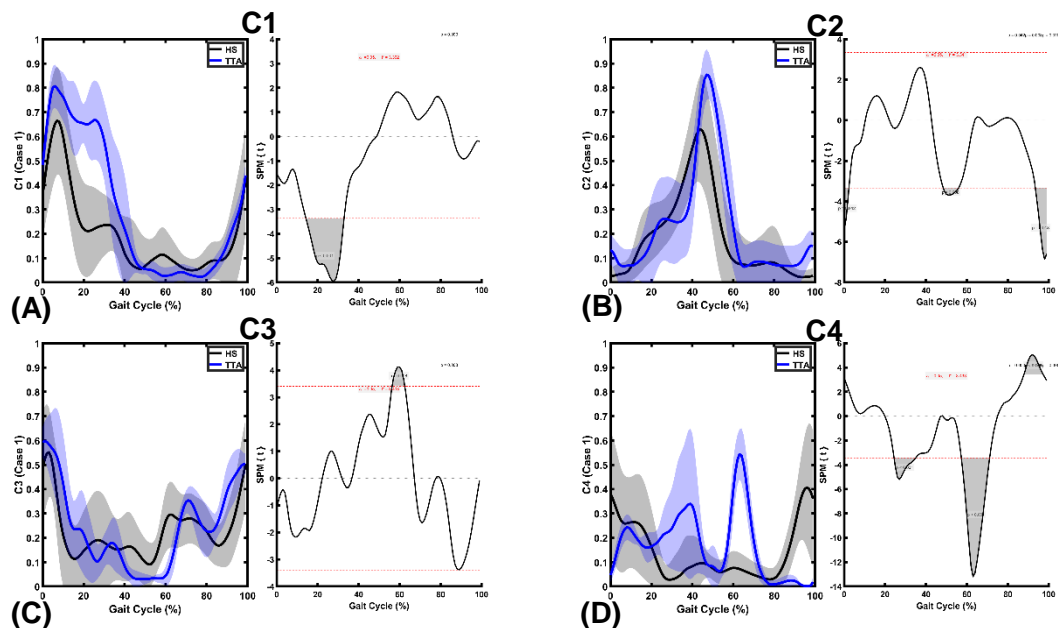


Figure 5.9: A statistical inference curve indicating a significant relationship between HS C and TTA IL C (case 1) at normal speed. Red dashed line indicates critical threshold ((A): $t^*C1=3.362$, (B): $t^*C2=3.341$, (C): $t^*C3=3.408$, (D): $t^*C4=3.433$). The period where the critical threshold is exceeded depicted as grey ($p<0.05$).

Case 2: The statistically significant difference in C1 occurred at 42-51% ($p=0.001$) and 60-68% ($p=0.002$) GC. In C2, two suprathreshold clusters were found where the significant difference between the two groups illustrated at 0-2% ($p=0.037$) and 12-31% ($p<0.001$) GC. C3 showed the highest number of clusters where the differences occurred at 6-11% ($p=0.013$), 23-50% ($p<0.001$) and 89-95% ($p=0.008$) GC (Figure 5.10).

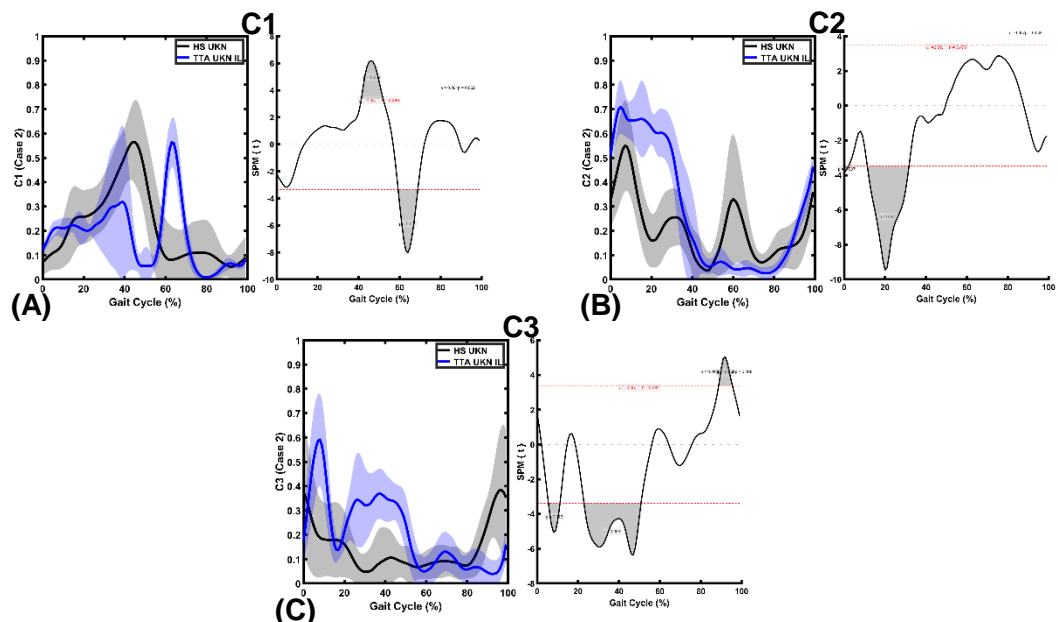


Figure 5.10: A statistical inference curve indicating a significant relationship between HS UKN C and TTA UKN IL C (case 2) at normal speed. Red dashed line indicates critical threshold ((A): $t^*C1=3.360$, (B): $t^*C2=3.473$, (C): $t^*C3=3.384$). The period where the critical threshold is exceeded depicted as grey ($p<0.05$).

Case 3: In C1, the suprathreshold occurred at 0-13% ($p<0.001$) and 29-51% ($p<0.001$) of GC. C2 revealed statistically significant differences at 0-5% ($p=0.003$), 13-24%

($p < 0.001$) and 90-100% ($p < 0.001$) GC. Two clusters were found in C3 at 24-33% ($p < 0.001$) and 90-91% ($p = 0.045$) GC (Figure 5.11).

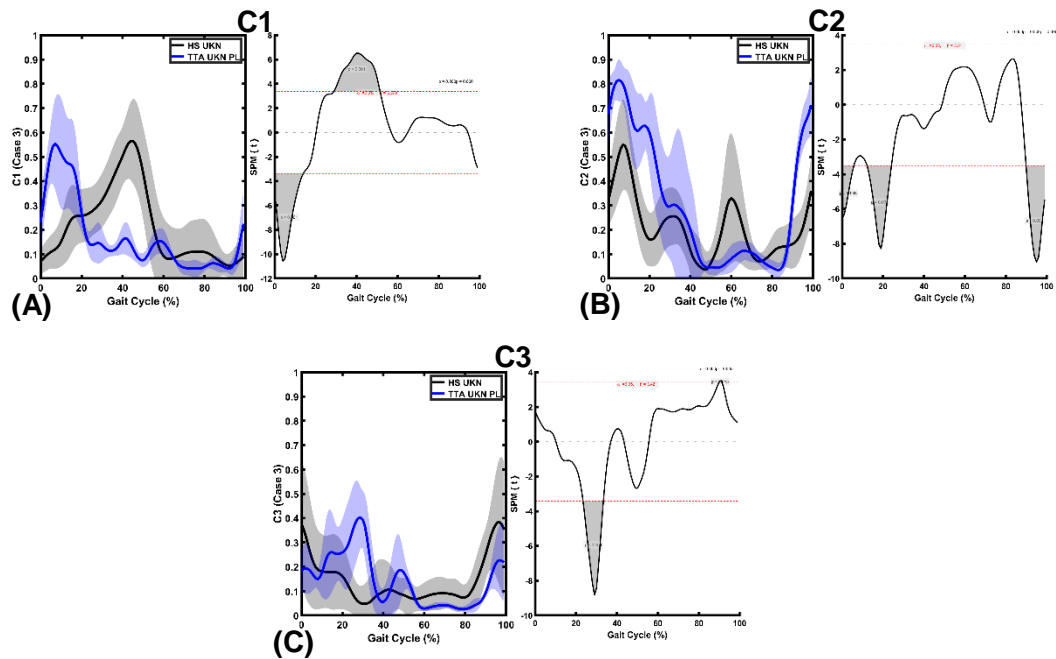


Figure 5.11: A statistical inference curve indicating a significant relationship between HS UKN C and TTA UKN PL C (case 3) at normal speed. Red dashed line indicates critical threshold ((A): $t^*C1=3.379$, (B): $t^*C2=3.511$, (C): $t^*C3=3.421$). The period where the critical threshold is exceeded depicted as grey ($p < 0.05$).

Case 4: In C1, the significant difference occurred at 59-69% ($p < 0.001$) GC. In C2, the suprathreshold resulted in significant difference PL at 92-98% ($p < 0.001$) GC. Two clusters were found in C3 at 34-38% ($p = 0.004$) and 44-48% ($p = 0.005$) GC (Figure 5.12).

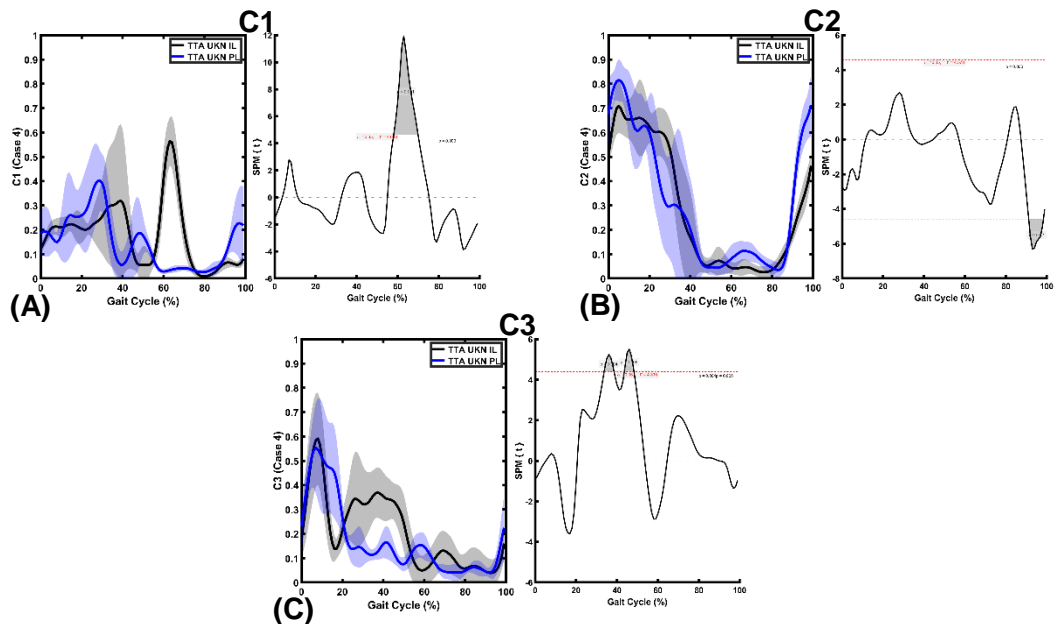


Figure 5.12: A statistical inference curve indicating a significant relationship between TTA UKN IL C and TTA UKN PL C (case 4) at normal speed. Red dashed line indicates critical threshold ((A): $t^*C1=4.633$, (B): $t^*C2=4.578$, (C): $t^*C3=4.395$). The period where the critical threshold is exceeded depicted as grey ($p < 0.05$).

Table 5.8 shows the summary of regions where statistically significant differences (t curve passed the t-critical values) occurred in all four cases during steady-state gait (Figure 5.9 to Figure 5.12).

Table 5.8: Summary of the suprathreshold clusters of case 1-4 occurred during the GC. Early, mid and terminal stance represent ES, MS, and TS; initial, mid and terminal swing represents ISW, MSW, and TSW, respectively.

<i>P < 0.05</i>				
	C1	C2	C3	C4
Case 1	MS*	ES*, TS*, TSW*	TS	MS*, ISW*, TSW
Case 2	TS, ISW*	ES*, MS*	ES*, MS-TS*, TSW	NA
Case 3	ES*, MS-TS	ES*, MS*, TSW*	MS*, TSW	NA
Case 4	ISW	TSW*	MS, TS	NA

* indicates the region where TTA is significantly greater than HS within the respective case.

5.5 Discussion

In this chapter, the differences between the synergy components of the HS and TTA were investigated during self-selected steady-state walking. The VAF results revealed a similar number of synergies between the two groups in all cases. This indicates the complexity acquired by the CNS to control the muscles of both groups in each case is similar, in agreement with other studies which analyzed the TFA (Chapter 4) and ACL deficiency patients [95, 126] and in contrast with the paretic (post-stroke) subjects study [91]. The increase in the number of synergy groups resulted in a higher VAF. However, the optimal number was chosen based on the VAF criteria. In addition, it was checked if the optimal group number provided better distinct synergy groups and physiological relevance of muscle EMG contents. There were observable differences in modular motor control dimension depending on the number of muscles included in the analysis. Cases 2-4 in which only thigh muscles were involved, three synergy groups were able to account for more than 90% of the variation in the original signals. This result is in agreement with the concept that the number and choices of muscles have an impact on the modular motor control dimensionality [209].

In order to compare the muscle synergy vectors of all cases, R^2 was performed. In case 1, triceps surae had the highest weightings in S2, indicating a strong correlation between HS and TTA. However, S4 showed the lowest correlation due to the difference in the primary muscle of the HS (related to the BFLH activation) and TTA (related to the RF activation). The weighting of the primary muscle showed to have a significant effect

on the synergies correlation between the two groups. In case 2 and 4, TTA UKN IL S2 showed knee extensors as well as a knee flexor as primary muscles with higher weighing compared to the HS UKN and TTA UKN PL, respectively. The presence of the two agonist and antagonist muscles in one muscle synergy group shows higher co-contraction at the knee of IL as compared to the PL and HS. This is indicative of reduced stability during the stance phase. Previous reports suggested co-contraction of BFLH and VAS of PL in ES. However, they only considered the high dimensional muscle activity patterns rather than motor modules in TTA [28, 34]. Along similar lines of the observed results in SPM, C2 showed significant differences in ES and MS in case 2 (Figure 5.10) as well as statistical differences at the transition from swing to stance phase in case 4 (Figure 5.12). The lowest correlation was found in case 3 in which S1 and S3 showed no common primary muscles. The low correlation could be attributed to the fact that significantly higher activities of the TTA UKN PL were reported in the literature as compared to the HS UKN [28]. Therefore, the compensation from the UKN PL could be caused by the fact that TTA tried to stabilize the knee joint especially at the transition from swing to stance and at the single limb support phase GC (the grey area in C1 and C3 of Figure 5.11). The highest correlation was found in case 1 where the first three synergy groups (S1-S3) had the strongest correlation between HS dominant leg and TTA IL. R^2 in case 4 showed a moderate correlation of S2 and S3 and a low correlation of S1 between amputee's UKN IL and UKN PL. In S1, a different group of muscles was recruited, and the low correlation of S1 could be due to the fact that higher activation in BFLH of PL during braking and lower activation in swing phase were expected than that of IL, as reported in [28]. The high correlation (case 1: S1, S2, and S3; case 2: S3, case 3: S2) between muscle synergies suggesting the CNS synergistically activates the same group of muscles in both groups. The low to moderate correlation between some synergy groups (case 1: S4; case 2: S1 and S2; case 3: S1 and S3; case 4: S1-S3) are indicative of alteration in muscle synergies which could be due to the weight bearing deficiency and inadequate proprioceptive feedback of the PL as well as type of prosthesis (mechanically passive).

The results of the t-test in SPM showed activation of the two groups, regardless of a high correlation in S, could be significantly different in some regions GC, i.e., all null hypotheses were not supported. As an example, case 1 showed amputee's C1 and C2 were significantly different from HS although a high correlation of 0.74 and 0.97 was perceived between S of the two groups. The largest significant differences have been observed in case 1 (C4), case 2 (C3), case 3 (C1) and case 4 (C1). This indicated that the activation coefficient profile controlling the muscle synergy was not similar in terms of timing and level of activation (intensity) at multiple regions GC between groups of all cases. One of the possible reasons for the differences between groups in all cases is

TTA effort to stabilize his joints and body weight during the single limb support phase, at the transition from stance to swing phase and swing to stance phase.

The neuromuscular compensation in TTA could be associated with the type of prostheses (e.g., stiffness) which fails to provide sufficient push off to move the body forward. This results in a higher GRF and greater mechanical work on both IL and PL [21]. Furthermore, the physiological modifications of the CNS and different strategy deployed by elderly to manage the age-related modifications of the human neuromusculoskeletal system have been reported in the prior literature [58, 304] which may have affected the synergy outcomes. In addition, sarcopenia (loss of muscle strength and volume) could play a major role in modifying the muscle activation of elderly TTA.

It is not easy to draw a far-reaching conclusion from one elderly TTA, and further investigation on a larger pool of subjects is needed to be able to generalize the interpretation of the present study. Therefore, the potential limitations of this chapter were the low number of participants and the age difference between them. In addition, each activation coefficient profile was compared separately (robotic control perspective). Thus the covariance between the temporal components of muscle synergy was not considered in this study.

5.6 Summary

In this study, muscle synergy analysis was used to elicit neuromuscular changes in TTA. It was revealed that TTA CNS complexity to recruit muscles is analogous to those of non-amputees. In each case, the primary muscle(s) had a significant impact on the level of muscle synergy vectors correlation. The results of activation coefficient profile suggested that amputee's IL and PL were significantly different when compared together and to the HS. These findings could provide useful information to therapists to tailor rehabilitation methods in TTA. Also, this study will help the prosthetic companies to develop synergy-based control prostheses.

5.7 Conclusion

Four synergies in case 1 and three synergies in cases 2 and 3 were found during normal steady-state walking. This indicates the complexity acquired by the CNS to control the muscles of both groups in each case is similar.

The fewer number of muscles in cases 2-4 showed one less synergy group as compared to case 1, indicating the number and choices of muscles have an impact on the modular motor control dimensionality.

The high correlation between muscle synergies suggests the CNS synergistically activates the same group of muscles in both groups. The low to moderate correlations between some synergy groups are indicative of an alteration in muscle synergies which could be due to the weight bearing deficiency and inadequate proprioceptive feedback of the PL as well as the type of prosthesis (mechanically passive).

Significant differences were observed in individual activation coefficient profiles between groups in cases 1-4 which indicate the changes in timing and level of activation (i.e., intensity) in multiple regions of the GC. This could be due to the TTA effort to stabilize their joints and body weight during the single support phase, at the transition from stance to swing phase and swing to stance phase.

Chapter 6

COMMON DISCUSSIONS

6.1 Introduction

This chapter is divided into three main sections. The first section is speculation on the commonalities/differences in the statistically significant differences between high dimensional (HD) sensorimotor Modules (M1-M4) and low dimensional activation coefficient profiles (C1-C4) of healthy subjects (HS) and transfemoral amputees (TFA) across different walking speeds. In addition, commonalities/differences between transtibial amputee (TTA) and TFA muscle synergies are investigated. The second section provides the rationale behind investigating the muscle coordination from high level and low level analysis, separating group and speed, implementing statistical parametric mapping (SPM) instead of traditional statistical analysis, using both multivariate and univariate as a means of biomechanics and robotic control comparison, not using other factorization techniques, using concatenated non-negative matrix factorization (CNMF) instead of non-negative matrix factorization (NMF). The third part presents the implications of using the outcomes of this research in clinics and robotic control.

6.2 Comparison Between HD Sensorimotor Modules and HS Low Dimensional Temporal Component of Muscle Synergy

The commonalities/differences in suprathreshold clusters (i.e., statistically significant differences) occurred between the HD sensorimotor Modules (M1-M4), and low dimensional activation coefficient profiles (C1-C4) in each population during transient-state walking at different speeds were investigated.

6.2.1 HS HD Sensorimotor Modules vs. HS Low Dimensional Activation Coefficient Profiles (Within-Subject)

HS HD M1 vs. HS C3

HS HD M1 (Figure 3.7) and HS C3 (Figure 4.28) (mainly related to activation of knee extensor muscles) contributed to weight acceptance at heel contact in early stance. A common suprathreshold cluster was observed during the MS between the HD

sensorimotor Module and low dimensional activation coefficient profile with increased transient-state walking speed.

HS HD M2 vs. HS C2

HS HD M2 (Figure 3.8) and HS C2 (Figure 4.26) (mainly related to activation of ankle plantarflexors) contributed to body support and forward propulsion in late stance. A common suprathreshold cluster was observed during the TS between the HD sensorimotor Module and low dimensional activation coefficient profile with increased transient-state walking speed.

HS HD M3 vs. HS C1

HS HD M3 (Figure 3.9) and HS C1 (Figure 4.24) (mainly related to activation of ankle dorsiflexor and hip flexors) contributed to foot lift-off in early- to mid-swing. Common suprathreshold clusters were observed during the MS, PSW-ISW, and TSW between the HD sensorimotor Module and low dimensional activation coefficient profile with increased transient-state walking speed.

HS HD M4 vs. HS C4

HS HD M4 (Figure 3.10) and HS C4 (Figure 4.30) (mainly related to activation of hamstrings) contributed to deceleration of the leg in late swing in preparation for heel contact and then stabilizes the pelvis after initial contact. A common suprathreshold cluster was observed during the TSW between the HD sensorimotor Module and low dimensional activation coefficient profile with increased transient-state walking speed.

6.2.2 TFA HD Sensorimotor Modules vs. TFA Low Dimensional Activation Coefficient Profiles (Within-Subject)

TFA HD M1 vs. TFA C3

Both TFA HD M1 (Figure 3.13) and TFA C3 (Figure 4.36) mainly involved knee extensor muscles activation at the beginning of the stance period. No common suprathreshold cluster was observed between the HD sensorimotor Module and low dimensional activation coefficient profile with increased transient-state walking speed as TFA C3 showed no significant difference.

TFA HD M2 vs. TFA C2

Both TFA HD M2 (Figure 3.14) and TFA C2 (Figure 4.34) mainly involved plantarflexor muscles activation which contributed to both body support and propulsion. A common suprathreshold cluster was observed during the TS between the HD sensorimotor

Module and low dimensional activation coefficient profile with increased transient-state walking speed.

TFA HD M3 vs. TFA C1

TFA HD M3 (Figure 3.15) involved dorsiflexor, and hip flexor muscle activation and TFA C1 (Figure 4.32) involved hip abductor and knee extensor activation. Although there are similarities in the occurrence of the suprathreshold clusters in TFA HD M3 and TFA C1 (low dimensional modular motor control) during the ES and TSW, the primary muscles comprised HD Modules, and low dimensional muscle synergies were different to a great extent. One possible explanation for commonalities between the HD and low dimensional modules is the major activation burst that occurred almost at the same time. The change in speeds reflects the magnitude of these bursts which happened to be the same in both cases. It is noteworthy that the changes in muscle recruitments may be due to the overloading of the IL as compared to the HS [21, 23].

TFA HD M4 vs. TFA C4

TFA HD M4 (Figure 3.16) involved hamstrings activation and TFA C4 (Figure 4.37) mainly activated the dorsiflexor muscle. No Common suprathreshold cluster was observed between the HD sensorimotor Module and low dimensional activation coefficient profile with increased transient-state walking speed. Since the muscles included in the HD and low dimensional are different, the significant difference in the temporal component is also different, and there are no commonalities between both analysis.

In summary, the commonalities in significant differences were speculated between the HS HD sensorimotor Modules (HD M1-M4) and temporal components (C1-C4) from muscle synergy analysis in response to increasing transient-state walking speeds. In HS, the HD Modules and low dimensional activation coefficient profiles partially agreed in terms of the epochs where the significant differences occurred in the gait cycle. There are some differences which can be due to the computation methodology and several assumptions which have been made to calculate muscle synergy components. In addition, the differences may also arise from the physiological factors including the effect of local sensory feedback, descending and ascending pathways and proprioceptive feedback. Previous reports have shown that the activation coefficient profiles are relatively stable across subjects in spite of the fact that inter-individual variability is higher in the HD EMG [312, 325].

The commonalities in significant differences between TFA HD sensorimotor Modules (HD M1-M4) and activation coefficient profiles (C1-C4) from muscle synergy analysis have been observed in one module mainly related to activation of plantarflexor

muscles (TFA HD M2 vs. TFA C2). No commonalities found in other HD Modules and associated lower dimensional counterparts could be attributed to the fact that the muscles involved in the former were different from the latter. Other factors associated with the computational analysis and physiological aspects as mentioned above may also contribute to the differences.

It is worth noting that the comparison between HD Modules and low dimensional activation coefficient profiles is simple speculation from the results obtained using SPM. Therefore, objective analyses must be performed for generalization of the outcomes.

6.3 Motor Modules Comparison between TTA and TFA

Mehryar et al. [92, 93, 230] investigated the modular motor control in one transtibial amputee during several activities of daily living. They reported a reasonable correlation between the HS and TTA during the slope walking, however, in normal steady-state walking, a poor correlation was observed in S4 (mainly activity of RF in TTA) as compared to the HS [92, 94].

Four synergy groups explained the variability in the EMG (VAF > 80%) signals of HS, TTA and TFA during walking at different walking states (i.e., transient and steady) and speeds (slow, normal, fast), indicating that different walking states, variation in speeds, and level of amputation do not have any impacts on the CNS control complexity.

In spite of certain variability between the synergy vectors of TTA normal steady-state walking and TFA fast transient-state walking, it was speculated, three of TTA modules corresponded to the TFA modules (S1, S2, and S3) (Figure 5.8). S1 was mainly loaded by knee extensor and hip extensor muscles (VM, VL, and BFLH), S2 was mainly loaded by plantarflexor muscles (SOL, GM, and GL), S3 was mainly loaded by the ankle dorsiflexor (TA). A low correlation was observed in S4 between TTA (mainly activated knee extensor and hip abductor in ES, MS, and ISW) and TFA (mainly activated knee flexor in ES and MS-TSW). The difference in choice of the muscles included (SEM excluded in TTA and GMED excluded in TFA), walking state (steady vs. transient), level of amputation (below knee vs. above knee), prosthesis type (ESR vs. SACH) and small sample size (1 subject vs. 11 subjects) may have led to differences in the results. Therefore, a larger pool of homogenous amputees with a similar prosthesis is required to be able to generalize the interpretation of this study.

6.4 Applicability of This Study

6.4.1 Clinical Implications

It is not possible to directly measure neural activity thereby; muscle activation signals are recorded through surface EMG. The behavioral output is the result of force generated by the muscle activity which in turn is the reflection of the motoneuron activity [329]. Therefore, recording electrical activity from the muscles has been the focus of many studies to identify neural behavior. However, the high dimensional muscle activation alone would not provide adequate information about functional deficits as a higher variation of muscle activity has been reported in individuals with pathology [246]. Computational analyses have been developed to help in this context. Information about muscle synergies provides valuable clinical implications of the neural structure underlying the motor behaviors, functional outcomes of muscle activation and how they alter in pathologies and after rehabilitation [192].

Muscle synergies could be used for identifying the degree to which the amputation has led to an alteration in descending neural pathways [246, 330]. Therefore, the number of muscle synergies is a good indicator of the CNS complexity in controlling the lower extremity after limb loss. Furthermore, this type of analysis is a potential means for identification of the degrees of impairment, gait asymmetry, level of amputation and effect of prosthesis types and setting.

The significant differences in activation coefficient profiles between HS and lower limb amputees provide valuable information on biomechanical subtasks that have been affected in terms of magnitude and/or morphology. Therefore, the focus of rehabilitation could be on those muscles contributing to the associated biomechanical subtasks.

Despite no change in the number of muscle synergies grouping between HS and lower limb amputees, spatially fixed synergy vector results showed changes in some of the muscle synergy recruitment of the lower limb amputees which could be the reflection of the ascending and proprioceptive feedback due to the type and mechanical properties of the prosthesis.

The structure of the existing muscle synergies can be subject to change, or even new muscle synergies could be developed if proper training programme is implemented [331]. Therefore, muscle synergies could elucidate the changes in muscle activation pattern, recruitment, number and structure after a rehabilitation course has been completed for the lower limb amputees.

The muscle synergy analysis could indicate the presence of co-contraction at ankle and knee joints based on the weighting of the muscles (i.e., synergy vector) and

the timing of occurrence (i.e., activation coefficient profiles). Along similar lines of the observed results in HD EMG, the significant differences occurred in muscles involved in co-contraction of ankle and knee may provide valuable information on the epochs in the GC where larger stability is required as speed changes and as a comparison between-populations. Furthermore, the co-contraction can significantly change the internal forces being applied to the joint which may have an indication of secondary physical conditions in lower limb amputees such as osteoarthritis [330]. Therefore, it may be possible to recognize the progression of the degenerative disease by investigating muscle coordination by means of HD EMG and low dimensional muscle synergies.

Finally, since factors such as type, level, and reason of amputation as well as age influence the rehabilitation strategy, muscle synergy would be an effective tool to evaluate the therapy results, to assess the effect of rehabilitation, and to alter treatments.

6.4.2 Robotic Control Implications

Lack of robust control strategy has limited the application of robotic devices in rehabilitation and prostheses. Current assistive technologies are still quite limited in interacting physically with human body mostly because they do not operate according to the same principles. Even though there are several sensor modalities which could be used for extracting neural information, surface EMG is the key to existing robotic-aided prostheses for intuitive control [332].

6.4.2.1 Clinical State of the Art (Direct Control)

The use of muscle activation signal to control prostheses known as myoelectric control is the clinical state of the art. Surface EMG is recorded from two muscle groups (agonist or antagonist). The patients could control these two group of muscles independently, so the electrical activity of one muscle is associated with the task (e.g., flexion); and the electrical activity of the antagonist is used to control the other DOF (e.g., extension). The user can act in one DOF and in some clinical systems it is possible to switch between the DOF with some prefix (e.g., co-contracting of the two muscles) to switch the state machine, and the same control is applied for the other DOF (e.g., internal/external rotation). This approach is very simple for control, and it has the advantage of being very robust. However, the limitations of this system are not being able to simultaneously control multiple DOF as well as limited recovery of the functionality.

6.4.2.2 Model-free Approaches

The temporal information from HD EMG can be used in machine learning to estimate a numerical function that maps between biomechanical variables (i.e., EMG and joint angles or EMG and moments) as well as to detect locomotion tasks (i.e., activity

recognition). In this context, the number of EMG signals recorded from different sites transform into a two-dimensional feature space and a system which is usually a supervised machine learning classifier decides, based on the position in the feature space, which task the patients want to activate. The most frequent pattern recognition techniques used in previous studies are the artificial neural network (classification), and linear and/or nonlinear regression. The former has been implemented in human performing ADLs to approximate joint moments and joint angles [333]. The latter was deployed in an approximation of the EMG and hand kinematics [334, 335] and wrist angles [334, 336, 337]. Even though using machine learning techniques in multi-joints and multi-degrees of freedom upper limb prostheses has shown superior and more natural control (i.e., no direct association of each signal with each DOF is required) as compared to the commercialized prosthetic devices, there are some demerits using this type of approaches including: 1) model-free based approaches are regarded as black box because they do not give an insight into neuro mechanics process (i.e., no explicit equation used) [338], 2) they are good at training but not good at extrapolating (i.e., novel condition may not be generalizable with the previous training condition) [333, 339, 340], 3) classic overfitting problem (i.e., lack of generalization if a complex relationship exists between the input variables which cannot be explained by a single macroscopic nonlinear transfer function (e.g., including many HD EMG signals as an input)), 4) not able to directly understand underlying mechanics of the input parameters (e.g., not able to know how population of neurons contributes to accelerating the joint just because all the transformations are summarized by regression equation) 5) they are limited to execution of simple movements (i.e., arm and hand functions and only validated in laboratory settings) [338], 6) there have been a very limited translation into the market and consequently to the patients, and 7) lack of robustness (i.e., this system works well in the restricted laboratory condition).

In order to overcome some of these limitations and have a more natural control (i.e., simultaneous control), the synergistic approach can be used. Furthermore, the abundance and multi-muscle activation increase the dimensionality and complexity of robotic devices control. A prosthesis controlled by a large number of muscles signals could be susceptible to the artifacts and sensor noise during locomotion tasks. This limits the utility of myoelectric control. Muscle synergy analysis has been implemented to reduce the complexity of the HD muscle activation thus decrease in complexity of control strategy. That is, taking the HD EMG to calculate set of low dimensional activation coefficient profiles which are the signals that are sent by the spinal cord circuits and then they are transmitted to the motor neuron pools to generate the muscle electrical signals.

It has been shown in the previous research that upper limb amputees are capable of controlling mechanical prosthetic hand simultaneously and proportionally (i.e., meaning that the user can control the speed of each DOF independently and simultaneously) using a synergistic controller [329, 332]. However, there is still lack of robustness in synergistic machine learning approaches.

6.4.2.3 Neuro-mechanical Modeling (Model-based Approach)

Even though recent advancements in lower limb prostheses have shown improvement in fall prevention and mobility, the commercialized prostheses are still inferior in terms of modulation and viscoelastic forces as well as they do not provide positive net energy during demanding ADLs as compared to their biological counterparts [341]. As a result, metabolic energy consumption is much higher in lower limb amputees when performing different tasks across different grades and speeds or transitioning across locomotion tasks. Furthermore, higher dependency on the IL would lead to the secondary physical conditions such as osteoarthritis [21, 269, 270, 323].

The bio-inspired approach can be implemented to provide a new paradigm for controlling artificial limbs and create a better solution for replacing natural motor function in an individual with amputation. Neuro-mechanical modeling allows converting neural information into estimates of mechanical output [136, 338]. That is, the neuromuscular information can be recorded using EMG from amputees' lower limb. The mechanical model will use forward dynamics simulation to understand how muscle activates, generate forces and accelerates specific degrees of freedom in the IL. The mechanical forces predicted from the IL muscles are projected on to the amputated limb to predict the joint torque that is needed to actuate the prosthesis (echo-control strategy). In this context, electrophysiological information can be used to control individual muscle-tendon units in a subject-specific model of the musculoskeletal system.

In the model-based approach, the biomechanical model constrains the space of the potential solution. Thereby, the muscle activations will generate the command that is biomechanically relevant otherwise the model would not recognize the non-relevant task as a physiological activation, so it does not translate it into action. As a result, the system becomes much more robust as compared to the data-driven model (model-free approach). The downside is more information is required to be put into the system because of the need to build the musculoskeletal model. In addition, model-based approaches allow estimating the internal forces which cannot be measured directly without invasive methods as well as the possibility of estimating amputee-prosthesis interaction. One of these important forces is the knee medial compartment force which has shown to associate with the knee osteoarthrosis [323, 342]. Consequently, this

approach would help to develop rehabilitation strategy to alleviate the force on medial knee compartment by designing better prostheses.

6.4.2.4 Mid-level Control

Other use of HD EMG and temporal components of muscle synergies (i.e., activation coefficient profiles) could be in the implementation of the mid-level control to investigate the occurrence of the important events/phases in the GC [35, 343]. The detection of the events/phases could potentially be used in the development of the control systems for lower limb prostheses to switch between states based on events/phases [344, 345]. Knowing the time intervals of the event/phase and the electromechanical delay naturally occurring (10 – 80 milli-seconds) (i.e., the mechanical force produced after the onset of activity detection) allow enough time to predict the intended movement/phase/state and modulate the prosthesis based on the detection of the events/phases.

6.4.2.5 Mimicking Healthy Subjects Control

Lastly, the significant differences observed from the SPM results of HD muscle activities and low dimensional activation coefficient profiles between HS and lower limb amputees allow identifying where the functional deficits or overloading may occur. Therefore, the necessary interventions could be applied at the onset of affected regions (similar to the technological interventions used in the powered and semi-active prostheses or utility of functional electrical stimulation to overcome the deficit). In this way, the mimicked healthy neuromuscular information could be deployed to control prosthetic devices in order to replicate the HS performance.

6.5 Summary

The commonalities of significant differences between the HD sensorimotor Modules and low dimensional activation coefficient profiles of HS and TFA were speculated. In addition, the comparison between TTA and TFA muscle synergy vectors were discussed. The justification behind the study of muscle coordination and selection of methodological analyses from the choice of signals to statistical analysis and choice of the algorithm has been explained. The possibilities of using the findings of this research in clinics and neurorehabilitation robotic-aided prostheses were also presented.

6.6 Conclusion

The differences in suprathreshold clusters occurred between the HD sensorimotor Modules and low dimensional activation coefficient profiles in each population could be due to the computational analysis (i.e., CNMF) and physiological aspects (i.e., the effect

of local sensory feedback, descending and ascending pathways and proprioceptive feedback).

The same number of synergy groups (=4) found in HS, TFA and TTA indicates analogous complexity implemented by the CNS which does not depend on the state of the GC (transient vs. steady), speed (slow, normal and fast), and level of amputation (below knee vs. above knee).

The differences in muscle synergies of the TTA and TFA could be due to the difference in choice of the muscles included, walking state, level of amputation, prosthesis type, and small sample size.

Chapter 7

SUMMARY, CONCLUSIONS, LIMITATIONS AND FUTURE WORK

7.1 Summary and Assessment of Research Objectives

The changes in the neuromuscular behavior of the lower limb amputees during ADLs have been receiving widespread attention over the past few years in order to improve quality of their life [16, 26-28, 34, 36-38, 46, 48, 50, 66, 73]. The consequence of lower limb amputations has been discussed in the previous research from the kinematics and kinetics viewpoint [20, 21]. However, this thesis focuses on the lower limb amputees' neuromuscular coordination function by investigating the HD EMG and low dimensional motor modules from biomechanics and robotic control perspectives.

In chapter 1, a set of research aims, and objectives were outlined. The aims of the current research were to examine the HD EMG and low dimensional motor modules across transient-state walking speeds to identify the adjustment and compensatory strategies in HS dominant leg and TFA IL from biomechanics and robotic control perspectives. In addition, the low dimensional motor modules were examined between HS and TTA during steady-state walking to identify neuromuscular changes in TTA IL and PL adapted by the TTA IL and PL. This section evaluates the research objectives and the results found in this work.

- To investigate the differences in temporal characteristics of HD sensorimotor Modules and all muscles that contribute to the co-contraction of ankle and knee joints (biomechanics perspective) as well as individual muscle activations (robotic control perspective) for both HS and TFA in response to increasing transient-state walking speeds (within-subject HD EMG).

Biomechanics: This is reported in chapter 3. The effect of speeds on HS and TFA muscle activities were compared from the biomechanics perspective. Significant differences were observed in all of the HD sensorimotor Modules (M1 to M4) and muscles contributed to the co-contraction of the ankle and knee at different regions of the GC, suggesting neuromuscular adaptation mechanism in both groups to satisfy the kinematic and kinetic demands of increasing transient-state walking speed.

Robotic control: This is reported in chapter 3. The effect of speeds showed that while HS individual muscle activities (robotic control approach) were statistically significant at

different regions of the GC, TFA did not show significant differences in all muscles including SEM, TFL, and SOL. The information from these muscles could be used in the robotic perspective which reduces the mid-level control complexity for event detection.

- To investigate the differences in temporal characteristics of HD sensorimotor Modules and all muscles that contribute to the co-contraction of ankle and knee joints (biomechanics perspective) as well as individual muscle activations (robotic control perspective) between HS and TFA during transient-state walking at different speeds (slow, normal, and fast) (between-subject HD EMG).

Biomechanics: This is reported in chapter 3. The biomechanics approach has shown that HD M2 is significantly different in late stance between HS and TFA at slow, normal and fast walking speeds. On the other hand, no significant difference was found in HD M1, M3, and M4. The muscles contributed to the ankle co-contraction were significantly different at the transition from stance to swing phase at all speeds. In addition, both HD M2 and ankle co-contraction muscles were statistically significant in MS at fast speed.

Robotic control: This is reported in chapter 3. At slow transient-state walking, significant differences were observed in VL, BFLH, TFL, TA, GM, GL and SOL between HS and TFA. At normal transient-state walking, significant differences were observed in RF, VM, BFLH, TA, GM, GL, SOL. At fast transient-state walking, significant differences were observed in RF, VM, VL, BFLH, TA, GM, GL, SOL. The results showed SEM and TFL were similar between HS and TFA at different speeds, suggesting an analogous neuromotor mechanism for controlling those muscles.

- To develop a reliable and robust algorithm for muscle synergy analysis which accounts for the whole population rather than an individual subject.

This is reported in chapter 4. CNMF was written in MATLAB to calculate muscle synergies/motor modules from HD EMG data. Two components of muscle synergy analysis are a time-varying component (activation coefficient profile) representing recruitment of the muscle synergy over time and spatially fixed muscle synergy vectors (i.e., muscle synergy vectors, modules) representing relative weighting of each muscle within each module.

- To examine the changes in complexity of control strategy implemented by the CNS of HS and TFA with increasing transient-state walking speed.

This is reported in chapter 4. The number of synergy groups reflects the complexity of the neuromuscular system which was determined by means of VAF. The criteria were to select the lowest number of synergies that accounted for > 0.80 of VAF and to check if the addition of the next synergy group will not increase VAF by more than 0.05. Both HS

and TFA showed to have four synergy groups during transient-state walking at all speeds.

- To assess whether the recruitment of spatially fixed muscle synergy vectors changes in HS and TFA with increases in transient-state walking speeds.

This is reported in chapter 4. Generally, a reasonable correlation was observed in the majority of the HS muscle synergies across speeds. The low correlation mainly related to the knee extensor and ankle dorsiflexor muscles synergy groups. The TFA high correlation was observed in S2 across speeds. In both groups, the low correlation was mainly related to the primary muscles weighting contributions rather than recruitment of different functionally related muscles.

- To assess whether muscle synergies change between HS and TFA at each speed.

This is reported in chapter 4. The lowest correlations were observed in S1 and S4 during slow and normal walking speeds, respectively. The strongest correlation was perceived in S2 during slow and fast walking speeds, respectively.

- To investigate the differences in low dimensional temporal components of muscle synergy (i.e., activation coefficient profiles) of HS and TFA from biomechanics and robotic control perspectives in response to increasing transient-state walking speeds (within-subject activation coefficient profile).

Biomechanics: This is reported in chapter 4. The effect of speeds on the covariance between the activation coefficient profiles of HS and TFA were compared (within-subject). HS showed significant differences during body support, foot-flat, and transition from stance to swing phase as well as swing to stance phase. TFA showed to be significantly different in weighting acceptance between and in the transition from PL to IL at the end of IL swing phase.

Robotic control: This is reported in chapter 4. The effect of speeds on individual activation coefficient profiles of HS and TFA were compared (between-subject). HS showed significant differences in all the activation coefficient profiles at different regions of GC. TFA showed to be significantly different in TFA C1, C2, and C4.

- To investigate the differences in low dimensional temporal components of muscle synergy (i.e., activation coefficient profiles) between HS and TFA from biomechanics and robotic control perspectives during transient-state walking at each speed category (between-subject activation coefficient profile).

Biomechanics: This is reported in chapter 4. The biomechanics approach has shown that the activation coefficient profiles commonly were significantly different in late stance

between HS and TFA at slow, normal and fast as well as in weight-bearing phase at slow and normal speeds.

Robotic control: This is reported in chapter 4. The robotic control approach showed significant differences in individual activation coefficient profiles between HS and TFA at different regions of the GC at all speeds (except C4 fast speed). Most significant differences occurred during the stance phase.

- To compare the changes in complexity of control strategy implemented by the CNS between HS and TTA during steady-state walking.

This is presented in chapter 5. The optimal number of synergy groups were calculated by means of VAF. The results revealed four synergy groups for case 1 and three synergy groups for cases 2-4.

- To determine whether muscle synergy complexity changes with respect to the number of recorded muscles.

This is reported in chapter 5. Cases 2-4 represent the upper knee muscles of HS, TTA IL and TTA PL in which the results showed one fewer synergy groups as compared to the case 1 which consists of upper knee and shank muscles.

- To assess whether muscle recruitment of spatially fixed muscle synergies changes among HS dominant leg, TTA IL, and TTA PL.

This is reported in chapter 5. The highest correlation was observed in case 1: S1, S2, and S3; case 2: S3, case 3: S2 and the low and moderate correlation was found in case 1: S4; case 2: S1 and S2; case 3: S1 and S3; case 4: S1-S3.

- To investigate the differences in low dimensional temporal components of muscle synergy (i.e., activation coefficient profiles) among HS dominant leg, TTA IL, and TTA PL during normal steady-state walking (between-subject activation coefficient profile).

This is reported in chapter 5. Significant differences were observed in individual activation coefficient profiles in cases 1-4 at different regions of the GC. The largest significant differences have been observed in case 1 (C4), case 2 (C3), case 3 (C1) and case 4 (C1).

- To assess commonalities/differences in the statistically significant differences between HD sensorimotor Modules and low dimensional activation coefficient profiles of HS and TFA across speeds.

This is reported in chapter 6. In HS, the HD Modules (HD M1-M4) and low dimensional activation coefficient profiles (C1-C4) partially agreed in terms of the epochs where the

significant differences occurred in the GC across different speeds. In TFA, only the HD sensorimotor M2 showed commonalities with the low dimensional activation coefficient profile 2 (C2) in terms of the epochs where the significant differences occurred in the GC across different speeds.

- To assess the commonalities/differences between TTA and TFA muscle synergies.

This is reported in chapter 6. Four synergy groups explained the variability in the EMG (VAF > 80%) signals of HS, TTA, and TFA during walking at different walking states (i.e., transient and steady) and speeds (slow, normal, and fast). In spite of certain variability between the synergy vectors of TTA normal steady-state walking and TFA fast transient-state walking, it was speculated that three of TTA modules corresponded to the TFA modules (S1, S2, and S3).

7.2 Conclusions

1. The effect of speeds on both HS and TFA HD sensorimotor Modules and ankle and knee co-contraction muscles from biomechanical perspective showed significant differences, suggesting neuromuscular adaptation mechanism in both groups to satisfy the kinematic and kinetic demands of increasing transient-state walking speed.
2. The effect of speeds on HS individual muscle activities (robotic control perspective) showed significant differences at different regions of the GC, suggesting, walking at different speeds should be considered as a separate task.
3. The effect of speeds on TFA individual muscle activities (robotic control perspective) showed significant differences in different regions of GC, except in SEM, TFL, and SOL. The information from these muscles could be used in the robotic perspective which reduces the control complexity of prosthetic devices across different speeds. In addition, the temporal features of these muscles would help to control the onset of stance and swing at different speeds (i.e., mid-level control).
4. The HD sensorimotor Modules comparison between HS and TFA showed significant differences in HD M2 at all speeds. The difference attributed to the TFA longer stance phase, heightened activity, prolonged duration and the need for larger push off of the HD M2 muscles to compensate for the lack of plantarflexor in the PL. The muscles contributed to the ankle co-contraction were significantly different at all speeds, suggesting compensatory mechanism required to stabilize TFA IL ankle joint during double support before PL enters

the single limb support phase which is indicative of reduced stability during this time.

5. Individual muscle activity showed no significant differences in SEM and TFL activity between HS and TFA at all speeds, suggesting a similar neuromotor mechanism underlying the motor control regulation of both groups. The significant difference in the muscles is mainly associated with the stance phase which could be due to the TFA effort to stabilize their joints and body weight during this time. Notwithstanding, the triceps surae showed to be significantly different during swing phase, indicating the importance of TFA plantarflexor after push off to propel the body forward and decelerate the ankle joint at the end of the swing phase.
6. Both HS and TFA illustrated that four synergies are an optimal number of groups to match the reconstructed and original EMG at all speeds. This suggests that complexity of muscles recruitment by the CNS is analogous in both groups. Therefore, there is no compensatory adjustment in TFA.
7. Reasonable correlation in muscle synergies of HS was observed across different speeds, indicating that the CNS activates the same groups of muscles synergistically. The low correlation was directly associated with the primary muscle weighting suggesting a difference in the weighting contributions of the knee extensor and ankle dorsiflexor muscles rather than recruitment of different muscle groups. The highest correlation in TFA was observed between plantarflexor muscles at different speeds. The low correlation between TFA muscle synergies across speeds could be attributed to the significant change of speeds which resulted in neuromuscular modulations at the transition from stance to swing phase and body support phase of the GC.
8. The low correlation between HS and TFA muscle synergies could be due to the ambulation pattern, inadequate proprioceptive feedback, weight-bearing deficiency in PL, type of prostheses, and level of amputation which may cause neuromuscular modulation between amputees themselves and HS.
9. The effect of speeds on activation coefficient profiles of both HS and TFA were compared from biomechanics perspective in which significant differences were found, suggesting adaptation strategy implemented by the CNS to fulfill the task-dependent requirements of transient-state walking at different speeds. The difference could be related to the kinematic and kinetic demands of different speeds which led to different intensity in magnitude and time lag of activation timing for both groups across speeds.
10. The effect of speeds on individual activation coefficient profiles of HS and TFA (robotic control) showed significant differences (except TFA C3), indicating the

CNS strategy to increase the intensity of activation coefficient profile to satisfy the kinematic and kinetic requirements of different speeds. No significant differences were found in TFA C3, suggesting no adaptation strategy is required to augment the intensity of the temporal component.

11. Significant differences were observed in activation coefficient profiles (biomechanics approach) between HS and TFA at each speed category. A common significant difference (i.e., suprathreshold cluster) occurred between both groups during the TS at all speeds which could be due to the higher TFA IL push off required to compensate for the PL lack of push off as compared to the HS.
12. Individual activation coefficient profile (robotic control approach) showed no significant differences in C4 at fast speed between HS and TFA which shows common drives in SEM. The significant difference in the other activation coefficient profiles mainly associated with the stance phase which could be due to the TFA effort to stabilize their joints and body weight during this time. The significant differences in C2 were in late stance and PSW and epochs of swing phase which shows the importance of TFA plantarflexor after push off to propel the body forward and to control the ankle during swing phase.
13. Four synergies in case 1 and three synergies in cases 2 and 3 were found during normal steady-state walking. This indicates the complexity acquired by the CNS to control the muscles of both groups in each case is similar.
14. The fewer number of muscles in cases 2-4 showed one less synergy group as compared to case 1, indicating the number and choices of muscles have an impact on the modular motor control dimensionality.
15. The high correlation between muscle synergies suggests the CNS synergistically activates the same group of muscles in both groups. The low to moderate correlations between some synergy groups are indicative of an alteration in muscle synergies which could be due to the weight bearing deficiency and inadequate proprioceptive feedback of the PL as well as the type of prosthesis (mechanically passive).
16. Significant differences were observed in individual activation coefficient profiles between groups in cases 1-4 which indicate the changes in timing and level of activation (i.e., intensity) in multiple regions of the GC. This could be due to the TTA effort to stabilize their joints and body weight during the single support phase, at the transition from stance to swing phase and swing to stance phase.
17. The differences in suprathreshold clusters occurred between the HD sensorimotor Modules and low dimensional activation coefficient profiles in each population could be due to the computational analysis (i.e., CNMF) and

physiological aspects (i.e., the effect of local sensory feedback, descending and ascending pathways and proprioceptive feedback).

18. The same number of synergy groups (=4) found in HS, TFA and TTA indicates analogous complexity implemented by the CNS which does not depend on the state of the GC (transient vs. steady), speed (slow, normal and fast), and level of amputation (below knee vs. above knee).
19. The differences in muscle synergies of the TTA and TFA could be due to the difference in choice of the muscles included, walking state, level of amputation, prosthesis type, and small sample size.

7.3 Limitations

1. The focus of this thesis was on the transient (chapter 3 and 4) and steady-state (chapter 5) walking. For the better understanding of how CNS recruit muscles in the lower limb amputees during gait, it is crucial to investigate the neuromuscular modulation in other states of walking as well as other activities of daily living.
2. Due to space limitation, only one gait per recording was extracted such that the intact and prosthetic leg hit the force plates. As a result, at least three separate trials were picked for data analyses. One may consider consecutive cycles, before entering to the steady-state, within the same trial to investigate step by step variability. Notwithstanding, [84] reported, the number of step cycles did not impact the modularity dimension.
3. Only ten muscles have been included in this study for all groups. In the literature, the number varies from 8 to 31 muscles during gait [82, 91, 190, 209]. As reported by [209], the number of muscles has an impact on the neuromuscular results. Therefore, the results may have varied if more muscles were included in the study.
4. Only superficial muscles were included in the present study. Prior research focused on the effect of deeper muscles during activities of daily livings. However, it has been shown that the number of synergies is invariant when compared to synergies extracted only from superficial muscles [82].
5. Due to the use of prosthetic strap by some of the amputees, GMED was not recorded for all of the TFA. Hence, it was removed from the analysis. Had GMED activity been included in the muscle synergy analysis; it most likely would have appeared as the primary muscle contributing to TFA S3 across different speeds.
6. Had two-way MANOVA been performed for the biomechanics hypotheses, it most likely would have yielded similar results to those that were produced by the Hotelling's T² tests. However, it is important to note; the results may not be

exactly the same for the reason that multivariate tests use different types of corrections as compared to the Bonferroni correction used in this thesis.

7. The differences between the results of the main vector field and the post hoc scalar analyses could be due to the inter-component covariance. Therefore, the post hoc analyses are meant to qualify the original hypotheses provided they do not disagree with higher-level analyses. Where differences occurred, one must not draw the conclusion that disagrees with the main results.
8. Finally, a larger pool of homogenous amputees with a similar prosthesis is required to be able to generalize the results of this study. The mean age (55) of TFA was larger than that of HS (41), and only one TTA participated in this thesis (78). Literature has shown that a higher variation in muscle activities may be the result of aging which has an impact on spinal cord level and walking speeds [58, 312]. Therefore age-matched groups would be ideal for such comparison.

7.4 Future Work

1. In chapter 3 and 4 transient-state and in chapter 5 steady-state walking were considered. For a better understanding of the neuromuscular modulation in TFA and TTA, it is crucial to consider the other states of gait such as gait initiation and gait termination.
2. Due to space limitation, only one gait per recording was extracted from each trial. One may consider the same trial to investigate step by step variability.
3. Recording from a higher number of muscles (i.e., superficial and deep) certainly help to elucidate the motor control behavior and the existence of additional muscle synergies corresponded to the deeper muscles in lower limb amputees.
4. The methodology implemented in this thesis was based on the global muscle synergy analysis (i.e., time domain) in which linear envelope of signals was input to the algorithm. Another approach to investigating the neuro structure underlying the muscle activation is to extract spectral properties (i.e., time-frequency domain). This has been proposed by Frere [79], to distinguish between descriptive and prescriptive analysis.
5. Chapters 3 and 4 focused on the TFA IL. Future work should also investigate the muscle activities and muscle synergies extracted from the PL to identify the differences from the biomechanical and robotic control perspectives.
6. Further experimental validation needs to be carried out due to the low number of amputees involved in this study. Chapter 5 only included one transtibial amputee. Therefore, one must not generalize the results for all amputees.

7. The exact level of amputation in the TFA subjects was not known. This information would have been useful to categorize the amputees into different groups and to understand the differences between them. Notwithstanding, the same number of muscle synergy groups between TTA and TFA groups illustrated muscle synergies do not depend on the level of amputation. Prosthetics components and stiffness were not controlled in this study. Future research should focus on the relationship between the prosthetic setting adjustment, level of amputation, and neuromuscular results.
8. The next step in muscle synergy analysis is the possibility of using HS motor modules to describe the muscle activation pattern of TFA accurately.
9. Future work should focus on the compensatory mechanism of lower limb amputees performing other ADLs such as ramp ascending/descending, stair ascending/descending that are more biomechanically challenging.
10. A larger pool of homogenous amputees with a similar prosthesis is required to be able to generalize the results of this study. The mean age (55) of TFA was larger than that of HS (41). Literature has shown a higher variation in muscle activities may be the result of aging which has an impact on spinal cord level and walking speeds [58, 312]. Therefore age-matched groups would be ideal for such comparison.
11. One of the main future works is to use the information obtained from HD EMG and low dimensional modular motor control (robotic control perspective) in mid-level control to detect important events occurring in the gait cycle. The temporal information in muscle synergies can be used in the detection of the high-level control in activity recognition.
12. Future research should focus on the comparison between the experimental EMG and the muscle activation obtained from the multi-body dynamics simulation which provides an inside into changes in the muscle forces and stress around the joints affected by the secondary physical conditions (knee and hip OA). Therefore, modifications in gait and orthopedic interventions (laterally wedged shoes and valgus braces) can be used to alleviate such impacts to the joints [323].
13. Future research could focus on the integration of the EMG and multi-body dynamics simulation (e.g., a combination of the linear envelope and moments) in order to better understand the mechanical behavior of muscle-tendon units which could not be concluded only from the EMG studies [261].
14. The information from the HD EMG and low dimensional modular motor control can be used in the bio-inspired approach to provide a new paradigm for controlling artificial limbs and create a better solution for replacing natural motor

function in the individual with amputation. The future research should establish neuromechanical modeling which allows converting neural information into estimates of mechanical output. The mechanical model will use forward dynamics simulation to understand how muscle activates, generates forces and accelerates specific degrees of freedom in the intact leg. The mechanical forces predicted from the intact leg muscles are projected on to the amputated limb to predict the joint torque that is needed to actuate the prosthesis. In this context, electrophysiological information can be used to control individual muscle-tendon units in a subject-specific model of the musculoskeletal system.

REFERENCES

1. Amputation. 2018 [cited 2018 05/04/2018]; Available from: <http://cirrie.buffalo.edu/encyclopedia/en/article/251/>.
2. Stewart, C., *Lower Limb Amputation* 2008.
3. Zhang, X., et al., *On Design and Implementation of Neural-Machine Interface for Artificial Legs*. Ieee Transactions on Industrial Informatics, 2012. **8**(2): p. 418-429.
4. Potter, B.K. and C.R. Scoville, *Amputation is not isolated: an overview of the US Army Amputee Patient Care Program and associated amputee injuries*. JAAOS-Journal of the American Academy of Orthopaedic Surgeons, 2006. **14**(10): p. S188-S190.
5. Holman, N., R. Young, and W. Jeffcoate, *Variation in the recorded incidence of amputation of the lower limb in England*. Diabetologia, 2012. **55**(7): p. 1919-1925.
6. Boyle, J.P., et al., *Projection of the year 2050 burden of diabetes in the US adult population: dynamic modeling of incidence, mortality, and prediabetes prevalence*. Popul Health Metr, 2010. **8**: p. 29.
7. Versluys, R., et al. *From conventional prosthetic feet to bionic feet: a review study*. in *Biomedical Robotics and Biomechanics, 2008. BioRob 2008. 2nd IEEE RAS & EMBS International Conference on*. 2008. IEEE.
8. Awad, M.I.M.H., *A novel biomechatronic above knee prosthetic device based on dynamic coupling effect*. 2012, University of Leeds.
9. Perry, J. and J.R. Davids, *Gait analysis: normal and pathological function*. Journal of Pediatric Orthopaedics, 1992. **12**(6): p. 815.
10. Ambrozic, L., et al., *CYBERLEGS: A user-oriented robotic transfemoral prosthesis with whole-body awareness control*. IEEE Robotics & Automation Magazine, 2014. **21**(4): p. 82-93.
11. Saxena, S. and P. Mukhopadhyay, *EMG operated electronic artificial-leg controller*. Medical and Biological Engineering and Computing, 1977. **15**(5): p. 553-557.
12. Horn, G., *Electro-control: an EMG-controlled A/K prosthesis*. Medical and biological engineering, 1972. **10**(1): p. 61-73.
13. Hoover, C.D., G.D. Fulk, and K.B. Fite, *The design and initial experimental validation of an active myoelectric transfemoral prosthesis*. Journal of Medical Devices, 2012. **6**(1): p. 011005.
14. Au, S., M. Berniker, and H. Herr, *Powered ankle-foot prosthesis to assist level-ground and stair-descent gaits*. Neural Networks, 2008. **21**(4): p. 654-666.
15. Huang, H., T.A. Kuiken, and R.D. Lipschutz, *A strategy for identifying locomotion modes using surface electromyography*. Biomedical Engineering, IEEE Transactions on, 2009. **56**(1): p. 65-73.
16. Peeraer, L., B. Aeyels, and G. Van der Perre, *Development of EMG-based mode and intent recognition algorithms for a computer-controlled above-knee prosthesis*. Journal of biomedical engineering, 1990. **12**(3): p. 178-182.
17. Meng, M., et al. *Automatic recognition of gait mode from EMG signals of lower limb*. in *Industrial Mechatronics and Automation (ICIMA), 2010 2nd International Conference on*. 2010. IEEE.

18. Englehart, K. and B. Hudgins, *A robust, real-time control scheme for multifunction myoelectric control*. Biomedical Engineering, IEEE Transactions on, 2003. **50**(7): p. 848-854.
19. Ajiboye, A.B. and R.F. Weir, *A heuristic fuzzy logic approach to EMG pattern recognition for multifunctional prosthesis control*. Neural Systems and Rehabilitation Engineering, IEEE Transactions on, 2005. **13**(3): p. 280-291.
20. Robert Gailey PhD, P., *Review of secondary physical conditions associated with lower-limb amputation and long-term prosthesis use*. Journal of rehabilitation research and development, 2008. **45**(1): p. 15.
21. Miller, R.H., et al., *Medial knee joint contact force in the intact limb during walking in recently ambulatory service members with unilateral limb loss: a cross-sectional study*. PeerJ, 2017. **5**: p. e2960.
22. Kellgren, J. and J. Lawrence, *Radiological assessment of osteo-arthritis*. Annals of the rheumatic diseases, 1957. **16**(4): p. 494.
23. Kulkarni, J., et al., *Chronic low back pain in traumatic lower limb amputees*. Clinical rehabilitation, 2005. **19**(1): p. 81-86.
24. Esposito, E.R., J.M.A. Whitehead, and J.M. Wilken, *Sound limb loading in individuals with unilateral transfemoral amputation across a range of walking velocities*. Clinical Biomechanics, 2015. **30**(10): p. 1049-1055.
25. Liikavainio, T., et al., *Gait and muscle activation changes in men with knee osteoarthritis*. The Knee, 2010. **17**(1): p. 69-76.
26. Culham, E., M. Peat, and E. Newell, *Below-knee amputation: a comparison of the effect of the SACH foot and single axis foot on electromyographic patterns during locomotion*. Prosthetics and Orthotics International, 1986. **10**(1): p. 15-22.
27. Czerniecki, J.M., *Rehabilitation in limb deficiency. 1. Gait and motion analysis*. Archives of physical medicine and rehabilitation, 1996. **77**(3): p. S3-S8.
28. Fey, N.P., A. Silverman, and R. Neptune, *The influence of increasing steady-state walking speed on muscle activity in below-knee amputees*. Journal of electromyography and Kinesiology, 2010. **20**(1): p. 155-161.
29. Isakov, E., O. Keren, and N. Benjuya, *Trans-tibial amputee gait: Time-distance parameters and EMG activity*. Prosthetics and Orthotics International, 2000. **24**(3): p. 216-220.
30. Perry, J. and S. Shanfield, *Efficiency of dynamic elastic response prosthetic feet*. Journal of rehabilitation research and development, 1993. **30**(1): p. 137.
31. Pinzur, M.S., M. Asselmeier, and D. Smith, *Dynamic electromyography in active and limited walking below-knee amputees*. Orthopedics, 1991. **14**(5): p. 535-538.
32. Rietman, J., K. Postema, and J. Geertzen, *Gait analysis in prosthetics: opinions, ideas and conclusions*. Prosthetics and orthotics international, 2002. **26**(1): p. 50-57.
33. Torburn, L., et al., *Below-knee amputee gait with dynamic elastic response prosthetic feet: a pilot study*. Journal of Rehabilitation Research and Development, 1990. **27**(4): p. 369.
34. Winter, D.A. and S.E. Sienko, *Biomechanics of below-knee amputee gait*. Journal of biomechanics, 1988. **21**(5): p. 361-367.
35. Wentink, E., et al., *Intention detection of gait initiation using EMG and kinematic data*. Gait & posture, 2013. **37**(2): p. 223-228.

36. Wentink, E.C., et al., *Comparison of muscle activity patterns of transfemoral amputees and control subjects during walking*. Journal of neuroengineering and rehabilitation, 2013. **10**(1): p. 87.
37. Jaegers, S.M., J.H. Arendzen, and H.J. de Jongh, *An electromyographic study of the hip muscles of transfemoral amputees in walking*. Clinical orthopaedics and related research, 1996. **328**: p. 119-128.
38. Huang, S. and D.P. Ferris, *Muscle activation patterns during walking from transtibial amputees recorded within the residual limb-prosthetic interface*. J Neuroeng Rehabil, 2012. **9**(55): p. 1-16.
39. Prinsen, E.C., M.J. Nederhand, and J.S. Rietman, *Adaptation strategies of the lower extremities of patients with a transtibial or transfemoral amputation during level walking: a systematic review*. Archives of physical medicine and rehabilitation, 2011. **92**(8): p. 1311-1325.
40. Hong, J.H. and M.S. Mun, *Relationship between socket pressure and EMG of two muscles in trans-femoral stumps during gait*. Prosthetics and orthotics international, 2005. **29**(1): p. 59-72.
41. Donath, M., *Proportional EMG control for above knee protheses*. 1974, Massachusetts Institute of Technology.
42. Aeyels, B., et al. *An EMG-based finite state approach for a microcomputer-controlled above-knee prosthesis*. in *Engineering in Medicine and Biology Society, 1995., IEEE 17th Annual Conference*. 1995. IEEE.
43. Huang, H., et al., *Continuous locomotion-mode identification for prosthetic legs based on neuromuscular-mechanical fusion*. Biomedical Engineering, IEEE Transactions on, 2011. **58**(10): p. 2867-2875.
44. Ha, K.H., H.A. Varol, and M. Goldfarb, *Volitional control of a prosthetic knee using surface electromyography*. Biomedical Engineering, IEEE Transactions on, 2011. **58**(1): p. 144-151.
45. Wu, S.-K., G. Waycaster, and X. Shen, *Electromyography-based control of active above-knee protheses*. Control Engineering Practice, 2011. **19**(8): p. 875-882.
46. Bae, T.S., et al., *Dynamic analysis of above-knee amputee gait*. Clinical Biomechanics, 2007. **22**(5): p. 557-566.
47. Cerqueira, A.S.O.d., et al., *Ground reaction force and electromyographic activity of transfemoral amputee gait: a case series*. Revista Brasileira de Cineantropometria & Desempenho Humano, 2013. **15**(1): p. 16-26.
48. Cooper, J., et al., *Trunk kinematics and trunk muscle EMG activity during five functional locomotor types*. Canadian Journal of Occupational Therapy, 1989. **56**(3): p. 120-127.
49. Hargrove, L.J., et al., *Toward the Development of a Neural Interface for Lower Limb Prosthesis Control*, in *2009 Annual International Conference of the Ieee Engineering in Medicine and Biology Society, Vols 1-20*. 2009, Ieee: New York. p. 2111-2114.
50. Hargrove, L.J., et al., *Robotic leg control with EMG decoding in an amputee with nerve transfers*. N Engl J Med, 2013. **369**(13): p. 1237-42.
51. Tokuno, C.D., et al., *Postural and movement adaptations by individuals with a unilateral below-knee amputation during gait initiation*. Gait & posture, 2003. **18**(3): p. 158-169.
52. Park, S., et al., *Kinematics, kinetics and muscle activities of the lower extremity during the first four steps from gait initiation to the steady-state walking*. Journal of Mechanical Science and Technology, 2009. **23**(1): p. 204-211.

53. Mickelborough, J., et al., *Muscle activity during gait initiation in normal elderly people*. *Gait & posture*, 2004. **19**(1): p. 50-57.
54. Mbourou, G.A., Y. Lajoie, and N. Teasdale, *Step length variability at gait initiation in elderly fallers and non-fallers, and young adults*. *Gerontology*, 2003. **49**(1): p. 21-26.
55. Wong, C.K., S.T. Chihuri, and G. Li, *Risk of fall-related injury in people with lower limb amputations: a prospective cohort study*. *Journal of rehabilitation medicine*, 2016. **48**(1): p. 80-85.
56. Vanicek, N., et al., *Gait patterns in transtibial amputee fallers vs. non-fallers: Biomechanical differences during level walking*. *Gait & Posture*, 2009. **29**(3): p. 415-420.
57. Gailey, R. and C.R. Clark, *Physical therapy management of adult lower-limb amputees*. *Atlas of limb prosthetics: surgical, prosthetic and rehabilitation principles*. 2th edition, Bowker JH, Michael JW. St. Louis, editors. Baltimore: Mosby Yearbook, 1992: p. 569-97.
58. Monaco, V., A. Ghionzoli, and S. Micera, *Age-related modifications of muscle synergies and spinal cord activity during locomotion*. *Journal of neurophysiology*, 2010. **104**(4): p. 2092-2102.
59. Hausdorff, J.M., *Gait variability: methods, modeling and meaning*. *Journal of neuroengineering and rehabilitation*, 2005. **2**(1): p. 19.
60. Bus, S.A. and A. de Lange, *A comparison of the 1-step, 2-step, and 3-step protocols for obtaining barefoot plantar pressure data in the diabetic neuropathic foot*. *Clinical biomechanics*, 2005. **20**(9): p. 892-899.
61. Carlsöö, S., *The initiation of walking*. *Cells Tissues Organs*, 1966. **65**(1-3): p. 1-9.
62. Cook, T. and B. Cozzens, *Human Solutions for Locomotion III. the Initiation of Gait*, in *Neural control of locomotion*. 1976, Springer. p. 65-76.
63. Crenna, P. and C. Frigo, *A motor programme for the initiation of forward-oriented movements in humans*. *The Journal of physiology*, 1991. **437**(1): p. 635-653.
64. Elble, R.J., et al., *The initiation of normal walking*. *Movement Disorders*, 1994. **9**(2): p. 139-146.
65. Herman, R., et al., *Control of postural reactions in man: the initiation of gait*, in *Control of posture and locomotion*. 1973, Springer. p. 363-388.
66. Mann, R.A., et al., *The initiation of gait*. *The Journal of bone and joint surgery. American volume*, 1979. **61**(2): p. 232-239.
67. Michel, V. and R. Chong, *The strategies to regulate and to modulate the propulsive forces during gait initiation in lower limb amputees*. *Experimental brain research*, 2004. **158**(3): p. 356-365.
68. Polcyn, A.F., et al., *Age-related changes in the initiation of gait: degradation of central mechanisms for momentum generation*. *Archives of physical medicine and rehabilitation*, 1998. **79**(12): p. 1582-1589.
69. Nissan, M., *The initiation of gait in lower limb amputees: some related data*. *Journal of rehabilitation research and development*, 1991. **28**(2): p. 1.
70. Rossi, S.A., W. Doyle, and H.B. Skinner, *Gait initiation of persons with below-knee amputation: the characterization and comparison of force profiles*. *Journal of rehabilitation research and development*, 1995. **32**(2): p. 120.
71. Vrieling, A.H., et al., *Gait initiation in lower limb amputees*. *Gait & posture*, 2008. **27**(3): p. 423-430.

72. van Keeken, H.G., et al., *Controlling propulsive forces in gait initiation in transfemoral amputees*. Journal of biomechanical engineering, 2008. **130**(1): p. 011002.
73. Wentink, E.C., et al., *Detection of the onset of gait initiation using kinematic sensors and EMG in transfemoral amputees*. Gait & Posture, 2014. **39**(1): p. 391-396.
74. Lee, D.D. and H.S. Seung, *Learning the parts of objects by non-negative matrix factorization*. Nature, 1999. **401**(6755): p. 788-91.
75. Tresch, M.C., V.C. Cheung, and A. d'Avella, *Matrix factorization algorithms for the identification of muscle synergies: evaluation on simulated and experimental data sets*. Journal of neurophysiology, 2006. **95**(4): p. 2199-2212.
76. Hug, F., *Can muscle coordination be precisely studied by surface electromyography?* Journal of electromyography and kinesiology, 2011. **21**(1): p. 1-12.
77. Neptune, R.R., D.J. Clark, and S.A. Kautz, *Modular control of human walking: a simulation study*. Journal of biomechanics, 2009. **42**(9): p. 1282-1287.
78. Ting, L.H. and S.A. Chvatal, *Decomposing muscle activity in motor tasks*. Motor Control Theories, Experiments and Applications. Oxf. Univ. Press, New York, 2010: p. 102v-138.
79. Frère, J., *Spectral properties of multiple myoelectric signals: New insights into the neural origin of muscle synergies*. Neuroscience, 2017. **355**: p. 22-35.
80. d'Avella, A., P. Saltiel, and E. Bizzi, *Combinations of muscle synergies in the construction of a natural motor behavior*. Nature neuroscience, 2003. **6**(3): p. 300.
81. Torres-Oviedo, G. and L.H. Ting, *Muscle synergies characterizing human postural responses*. Journal of neurophysiology, 2007. **98**(4): p. 2144-2156.
82. Saito, A., et al., *Similarity of muscle synergies extracted from the lower limb including the deep muscles between level and uphill treadmill walking*. Gait & posture, 2018. **59**: p. 134-139.
83. Gonzalez-Vargas, J., et al., *A predictive model of muscle excitations based on muscle modularity for a large repertoire of human locomotion conditions*. Frontiers in computational neuroscience, 2015. **9**.
84. Oliveira, A.S., et al., *Motor modules of human locomotion: influence of EMG averaging, concatenation, and number of step cycles*. Frontiers in human neuroscience, 2014. **8**.
85. Chvatal, S.A. and L.H. Ting, *Common muscle synergies for balance and walking*. Frontiers in computational neuroscience, 2013. **7**: p. 48.
86. Oliveira, A., et al., *Fast changes in direction during human locomotion are executed by impulsive activation of motor modules*. Neuroscience, 2013. **228**: p. 283-293.
87. Zelik, K.E., et al., *Can modular strategies simplify neural control of multidirectional human locomotion?* Journal of neurophysiology, 2014. **111**(8): p. 1686-1702.
88. Rodriguez, K.L., et al., *Persons with Parkinson's disease exhibit decreased neuromuscular complexity during gait*. Clinical neurophysiology, 2013. **124**(7): p. 1390-1397.
89. Danner, S.M., et al., *Human spinal locomotor control is based on flexibly organized burst generators*. Brain, 2015. **138**(3): p. 577-588.

90. Steele, K.M., A. Rozumalski, and M.H. Schwartz, *Muscle synergies and complexity of neuromuscular control during gait in cerebral palsy*. *Developmental Medicine & Child Neurology*, 2015. **57**(12): p. 1176-1182.
91. Clark, D.J., et al., *Merging of healthy motor modules predicts reduced locomotor performance and muscle coordination complexity post-stroke*. *Journal of neurophysiology*, 2009. **103**(2): p. 844-857.
92. Mehryar, P., et al. *Muscle synergy analysis in transtibial amputee during ramp ascending activity*. in *Engineering in Medicine and Biology Society (EMBC), 2016 IEEE 38th Annual International Conference of the*. 2016. IEEE.
93. Mehryar, P., et al. *Changes in synergy of transtibial amputee during gait: A pilot study*. in *Biomedical & Health Informatics (BHI), 2017 IEEE EMBS International Conference on*. 2017. IEEE.
94. Mehryar, P., M.S. Shourijeh, and A.A. Dehghani-Sanij. *Muscle synergy analysis in transtibial amputee during ramp descending activity*. in *International Conference on NeuroRehabilitation*. 2016. Segovia, Spain: Springer.
95. Mehryar, P., et al., *Do activation & synergy of above knee amputees' intact leg change?*, in *School and Symposium on Advanced Neurorehabilitation (SSNR2017)*. 2017: Baiona, Spain.
96. Winter, D.A., *Biomechanics and motor control of human gait: normal, elderly and pathological*. 1991.
97. Line. *Human Body*. 2014 [cited 2014; Available from: <http://www.healthline.com/human-body-maps/leg#seoBlock>.
98. Bones, L. 2018 [cited 2018 25/04/2018]; Available from: <http://www.clipartkid.com/leg-bones-fQ03QE-clipart/>.
99. Florimond, V., *Basics of surface electromyography applied to physical rehabilitation and biomechanics*. Montreal, Canada: Thought Technology Ltd, 2009.
100. Rowe, P., B. Durward, and G. Baer, *Functional human movement: measurement and analysis*. 1999: Butterworth-Heinemann.
101. Bernstein, N., *The co-ordination and regulation of movements*. The co-ordination and regulation of movements, 1966.
102. Whittle, M.W., *Chapter 2 - Normal gait*, in *Gait Analysis (Fourth Edition)*. 2007, Butterworth-Heinemann: Edinburgh. p. 47-100.
103. splint, S., *Shin splints biomechanics*. 2011.
104. Whittle, M.W., *Gait analysis: an introduction*. 2003.
105. Berger, N. and S. Fishman, *Lower-limb Prosthetics*. 1997: Prosthetic-Orthotic Publications.
106. Nissan, M. and M. Whittle, *Initiation of gait in normal subjects: a preliminary study*. *Journal of biomedical engineering*, 1990. **12**(2): p. 165-171.
107. Breniere, Y. and M. Do, *When and how does steady state gait movement induced from upright posture begin?* *Journal of biomechanics*, 1986. **19**(12): p. 1035-1040.
108. Miller, C.A. and M.C. Verstraete, *Determination of the step duration of gait initiation using a mechanical energy analysis*. *Journal of Biomechanics*, 1996. **29**(9): p. 1195-1199.
109. Kibushi, B., et al., *Speed-dependent modulation of muscle activity based on muscle synergies during treadmill walking*. *Frontiers in Human Neuroscience*, 2018. **12**: p. 4.

110. Muro-De-La-Herran, A., B. Garcia-Zapirain, and A. Mendez-Zorrilla, *Gait analysis methods: An overview of wearable and non-wearable systems, highlighting clinical applications*. *Sensors*, 2014. **14**(2): p. 3362-3394.
111. Farina, D., R. Merletti, and R.M. Enoka, *The extraction of neural strategies from the surface EMG*. *Journal of applied physiology*, 2004. **96**(4): p. 1486-1495.
112. Frigo, C. and R. Shiavi, *Applications in movement and gait analysis*. *Electromyography: physiology, engineering and noninvasive applications*, 2004: p. 381-397.
113. Lau, B.G., *An intelligent prosthetic hand using hybrid actuation and myoelectric control*. 2009, The University of Leeds.
114. Mann, R.A. and J. Hagy, *Biomechanics of walking, running, and sprinting*. *The American journal of sports medicine*, 1980. **8**(5): p. 345-350.
115. Adler, N., et al., *Electromyography of the vastus medialis oblique and vasti in normal subjects during gait*. *Electromyography and clinical neurophysiology*, 1983. **23**(7): p. 643.
116. Guth, V., F. Abbink, and H. Theysohn, *Electromyographic investigations on gait. Methods and applications in orthopaedics*. *Electromyography and clinical neurophysiology*, 1979. **19**(4): p. 305.
117. Winter, D.A., *Biomechanics and motor control of human movement*. 2009: John Wiley & Sons.
118. Winter, D. and H. Yack, *EMG profiles during normal human walking: stride-to-stride and inter-subject variability*. *Electroencephalography and clinical neurophysiology*, 1987. **67**(5): p. 402-411.
119. Kleissen, R.F., *Effects of electromyographic processing methods on computer-averaged surface electromyographic profiles for the gluteus medius muscle*. *Physical therapy*, 1990. **70**(11): p. 716-722.
120. Shiavi, R., C. Frigo, and A. Pedotti, *Electromyographic signals during gait: criteria for envelope filtering and number of strides*. *Medical and Biological Engineering and Computing*, 1998. **36**(2): p. 171-178.
121. Hug, F. and S. Dorel, *Electromyographic analysis of pedaling: a review*. *Journal of Electromyography and Kinesiology*, 2009. **19**(2): p. 182-198.
122. Shiavi, R. and N. Green, *Ensemble averaging of locomotor electromyographic patterns using interpolation*. *Medical and Biological Engineering and Computing*, 1983. **21**(5): p. 573-578.
123. Banks, C.L., et al., *Methodological choices in muscle synergy analysis impact differentiation of physiological characteristics following stroke*. *Frontiers in Computational Neuroscience*, 2017. **11**: p. 78.
124. Bruce, E., M. Goldman, and J. Mead, *A digital computer technique for analyzing respiratory muscle EMG's*. *Journal of Applied Physiology*, 1977. **43**(3): p. 551-556.
125. Murray, M., et al., *Kinematic and EMG patterns during slow, free, and fast walking*. *Journal of Orthopaedic Research*, 1984. **2**(3): p. 272-280.
126. Serrancolí, G., J.C. Monllau, and J.M. Font-Llagunes, *Analysis of muscle synergies and activation–deactivation patterns in subjects with anterior cruciate ligament deficiency during walking*. *Clinical Biomechanics*, 2016. **31**: p. 65-73.
127. Hof, A. and J. Van Den Berg, *Linearity between the weighted sum of the EMGs of the human triceps surae and the total torque*. *Journal of biomechanics*, 1977. **10**(9): p. 529-539.
128. Komi, P., *Relationship between muscle tension, EMG and velocity of contraction under concentric and eccentric work*, in *New Concepts of the*

- Motor Unit, Neuromuscular Disorders, Electromyographic Kinesiology*. 1973, Karger Publishers. p. 596-606.
129. Maton, B., *Motor unit differentiation and integrated surface EMG in voluntary isometric contraction*. European journal of applied physiology and occupational physiology, 1976. **35**(2): p. 149-157.
 130. De Jong, R., *Relation between electromyogram and isometric twitch tension in human muscle*. Arch Phys Med Rehabil, 1967. **48**: p. 539-542.
 131. Bouisset, S. and F. Goubel, *Integrated electromyographical activity and muscle work*. journal of Applied Physiology, 1973. **35**(5): p. 695-702.
 132. Dubo, H., et al., *Electromyographic temporal analysis of gait: normal human locomotion*. Archives of physical medicine and rehabilitation, 1976. **57**(9): p. 415-420.
 133. MIRKA, G.A., *The quantification of EMG normalization error*. Ergonomics, 1991. **34**(3): p. 343-352.
 134. Burden, A. and R. Bartlett, *Normalisation of EMG amplitude: an evaluation and comparison of old and new methods*. Medical Engineering and Physics, 1999. **21**(4): p. 247-257.
 135. Clarys, J.P. and J. Cabri, *Electromyography and the study of sports movements: a review*. Journal of sports sciences, 1993. **11**(5): p. 379-448.
 136. Sartori, M., et al., *A musculoskeletal model of human locomotion driven by a low dimensional set of impulsive excitation primitives*. Frontiers in computational neuroscience, 2013. **7**.
 137. Ryan, M.M. and R.J. Gregor, *EMG profiles of lower extremity muscles during cycling at constant workload and cadence*. Journal of Electromyography and Kinesiology, 1992. **2**(2): p. 69-80.
 138. Nashner, L., A. Shumway-Cook, and O. Marin, *Stance posture control in select groups of children with cerebral palsy: deficits in sensory organization and muscular coordination*. Experimental Brain Research, 1983. **49**(3): p. 393-409.
 139. Badke, M.B. and P.W. Duncan, *Patterns of rapid motor responses during postural adjustments when standing in healthy subjects and hemiplegic patients*. Physical therapy, 1983. **63**(1): p. 13-20.
 140. Barrett, G., H. Shibasaki, and R. Neshige, *A computer-assisted method for averaging movement-related cortical potentials with respect to EMG onset*. Electroencephalography and Clinical Neurophysiology, 1985. **60**(3): p. 276-281.
 141. Walter, C.B., *Temporal quantification of electromyography with reference to motor control research*. Human Movement Science, 1984. **3**(1-2): p. 155-162.
 142. Dobie, R.A. and M.J. Wilson, *Objective response detection in the frequency domain*. Electroencephalography and Clinical Neurophysiology/Evoked Potentials Section, 1993. **88**(6): p. 516-524.
 143. Di Fabio, R.P., *Reliability of computerized surface electromyography for determining the onset of muscle activity*. Physical therapy, 1987. **67**(1): p. 43-48.
 144. Staude, G. and W. Wolf, *Objective motor response onset detection in surface myoelectric signals*. Medical Engineering and Physics, 1999. **21**(6): p. 449-467.
 145. Thexton, A., *A randomisation method for discriminating between signal and noise in recordings of rhythmic electromyographic activity*. Journal of neuroscience methods, 1996. **66**(2): p. 93-98.

146. Hodges, P.W. and B.H. Bui, *A comparison of computer-based methods for the determination of onset of muscle contraction using electromyography*. *Electroencephalography and Clinical Neurophysiology/Electromyography and Motor Control*, 1996. **101**(6): p. 511-519.
147. Staude, G.H., *Precise onset detection of human motor responses using a whitening filter and the log-likelihood-ratio test*. *IEEE Transactions on Biomedical Engineering*, 2001. **48**(11): p. 1292-1305.
148. Hedman, L., et al., *Electromyographic analysis of postural responses during standing leg flexion in adults with hemiparesis*. *Electroencephalography and Clinical Neurophysiology/Electromyography and Motor Control*, 1997. **105**(2): p. 149-155.
149. Connemann, B., et al., *A fully automated system for the evaluation of masseter silent periods*. *Clinical Neurophysiology*, 1997. **105**(1): p. 53-57.
150. Bonato, P., T. D'Alessio, and M. Knaflitz, *A statistical method for the measurement of muscle activation intervals from surface myoelectric signal during gait*. *IEEE Transactions on Biomedical Engineering*, 1998. **45**(3): p. 287-299.
151. Van Putten, J. *EMG onset determination using a maximum likelihood method*. in *[Engineering in Medicine and Biology, 1999. 21st Annual Conference and the 1999 Annual Fall Meeting of the Biomedical Engineering Society] BMES/EMBS Conference, 1999. Proceedings of the First Joint*. 1999. IEEE.
152. Khalil, M. and J. Duchêne, *Uterine EMG analysis: a dynamic approach for change detection and classification*. *IEEE Transactions on Biomedical Engineering*, 2000. **47**(6): p. 748-756.
153. Merlo, A., D. Farina, and R. Merletti, *A fast and reliable technique for muscle activity detection from surface EMG signals*. *IEEE Transactions on Biomedical Engineering*, 2003. **50**(3): p. 316-323.
154. Li, X. and A.S. Aruin. *Muscle activity onset time detection using teager-kaiser energy operator*. in *Engineering in Medicine and Biology Society, 2005. IEEE-EMBS 2005. 27th Annual International Conference of the*. 2005. IEEE.
155. Farina, D., et al., *Surface EMG crosstalk evaluated from experimental recordings and simulated signals Reflections on crosstalk interpretation, quantification and reduction*. *Methods Archive*, 2004. **43**(1): p. 30-35.
156. De Luca, C.J. and R. Merletti, *Surface myoelectric signal cross-talk among muscles of the leg*. *Electroencephalography and clinical neurophysiology*, 1988. **69**(6): p. 568-575.
157. Farina, D., et al., *Surface EMG crosstalk between knee extensor muscles: experimental and model results*. *Muscle & nerve*, 2002. **26**(5): p. 681-695.
158. Lowery, M.M., N.S. Stoykov, and T.A. Kuiken, *A simulation study to examine the use of cross-correlation as an estimate of surface EMG cross talk*. *Journal of Applied Physiology*, 2003. **94**(4): p. 1324-1334.
159. Campanini, I., et al., *Effect of electrode location on EMG signal envelope in leg muscles during gait*. *Journal of Electromyography and Kinesiology*, 2007. **17**(4): p. 515-526.
160. Winter, D., A. Fuglevand, and S. Archer, *Crosstalk in surface electromyography: theoretical and practical estimates*. *Journal of Electromyography and Kinesiology*, 1994. **4**(1): p. 15-26.

161. Lowery, M.M., N.S. Stoykov, and T.A. Kuiken, *Independence of myoelectric control signals examined using a surface EMG model*. IEEE Transactions on Biomedical Engineering, 2003. **50**(6): p. 789-793.
162. Van Vugt, J. and J. Van Dijk, *A convenient method to reduce crosstalk in surface EMG*. Clinical Neurophysiology, 2001. **112**(4): p. 583-592.
163. Hermens, H.J., et al., *Development of recommendations for SEMG sensors and sensor placement procedures*. Journal of electromyography and Kinesiology, 2000. **10**(5): p. 361-374.
164. Day, S.J. and M. Hulliger, *Experimental simulation of cat electromyogram: evidence for algebraic summation of motor-unit action-potential trains*. Journal of Neurophysiology, 2001. **86**(5): p. 2144-2158.
165. Keenan, K.G., et al., *Influence of amplitude cancellation on the simulated surface electromyogram*. Journal of Applied Physiology, 2005. **98**(1): p. 120-131.
166. Chanaud, C., C. Pratt, and G. Loeb, *Functionally complex muscles of the cat hindlimb*. Experimental brain research, 1991. **85**(2): p. 300-313.
167. Holtermann, A., K. Roeleveld, and J.S. Karlsson, *Inhomogeneities in muscle activation reveal motor unit recruitment*. Journal of Electromyography and Kinesiology, 2005. **15**(2): p. 131-137.
168. Mesin, L., et al., *Effect of spatial filtering on crosstalk reduction in surface EMG recordings*. Medical Engineering and Physics, 2009. **31**(3): p. 374-383.
169. Farina, D., *Interpretation of the surface electromyogram in dynamic contractions*. Exercise and sport sciences reviews, 2006. **34**(3): p. 121-127.
170. Ivanenko, Y.P., R.E. Poppele, and F. Lacquaniti, *Five basic muscle activation patterns account for muscle activity during human locomotion*. The Journal of physiology, 2004. **556**(1): p. 267-282.
171. Davis, B.L. and C.L. Vaughan, *Phasic behavior of EMG signals during gait: use of multivariate statistics*. Journal of Electromyography and Kinesiology, 1993. **3**(1): p. 51-60.
172. Olree, K.S. and C.L. Vaughan, *Fundamental patterns of bilateral muscle activity in human locomotion*. Biological cybernetics, 1995. **73**(5): p. 409-414.
173. Cheung, V.C., et al., *Central and sensory contributions to the activation and organization of muscle synergies during natural motor behaviors*. Journal of Neuroscience, 2005. **25**(27): p. 6419-6434.
174. Ting, L.H. and J.M. Macpherson, *A limited set of muscle synergies for force control during a postural task*. Journal of neurophysiology, 2005. **93**(1): p. 609-613.
175. Bizzi, E. and V.C. Cheung, *The neural origin of muscle synergies*. Frontiers in computational neuroscience, 2013. **7**.
176. Lacquaniti, F., Y.P. Ivanenko, and M. Zago, *Patterned control of human locomotion*. The Journal of physiology, 2012. **590**(10): p. 2189-2199.
177. Overduin, S.A., et al., *Modulation of muscle synergy recruitment in primate grasping*. Journal of Neuroscience, 2008. **28**(4): p. 880-892.
178. Duysens, J., F. De Groote, and I. Jonkers, *The flexion synergy, mother of all synergies and father of new models of gait*. Frontiers in computational neuroscience, 2013. **7**: p. 14.
179. Gizzi, L., et al., *Impulses of activation but not motor modules are preserved in the locomotion of subacute stroke patients*. Journal of Neurophysiology, 2011. **106**(1): p. 202-210.

180. Allen, J.L., et al., *Increased neuromuscular consistency in gait and balance after partnered, dance-based rehabilitation in Parkinson's disease*. Journal of Neurophysiology, 2017. **118**(1): p. 363-373.
181. Coscia, M., et al., *Muscle synergies and spinal maps are sensitive to the asymmetry induced by a unilateral stroke*. Journal of neuroengineering and rehabilitation, 2015. **12**(1): p. 39.
182. Hashiguchi, Y., et al., *Merging and fractionation of muscle synergy indicate the recovery process in patients with hemiplegia: the first study of patients after subacute stroke*. Neural plasticity, 2016. **2016**.
183. Kautz, S.A., et al., *Comparison of motor control deficits during treadmill and overground walking poststroke*. Neurorehabilitation and neural repair, 2011. **25**(8): p. 756-765.
184. Chau, T., *A review of analytical techniques for gait data. Part 1: Fuzzy, statistical and fractal methods*. Gait Posture, 2001. **13**(1): p. 49-66.
185. Cappellini, G., et al., *Motor patterns in human walking and running*. Journal of neurophysiology, 2006. **95**(6): p. 3426-3437.
186. Hart, C.B. and S.F. Giszter, *Modular premotor drives and unit bursts as primitives for frog motor behaviors*. J Neurosci, 2004. **24**(22): p. 5269-82.
187. Bell, A.J. and T.J. Sejnowski, *An information-maximization approach to blind separation and blind deconvolution*. Neural computation, 1995. **7**(6): p. 1129-1159.
188. Tresch, M.C., P. Saltiel, and E. Bizzi, *The construction of movement by the spinal cord*. Nature neuroscience, 1999. **2**(2): p. 162-167.
189. Devarajan, K. and V.C. Cheung, *On nonnegative matrix factorization algorithms for signal-dependent noise with application to electromyography data*. Neural computation, 2014. **26**(6): p. 1128-1168.
190. Ivanenko, Y.P., et al., *Coordination of locomotion with voluntary movements in humans*. Journal of Neuroscience, 2005. **25**(31): p. 7238-7253.
191. Santuz, A., et al., *On the Methodological Implications of Extracting Muscle Synergies from Human Locomotion*. Int J Neural Syst, 2017. **27**(5): p. 1750007.
192. Hug, F., et al., *Smoothing of electromyographic signals can influence the number of extracted muscle synergies*. Clin Neurophysiol, 2012. **123**(9): p. 1895-6.
193. Devaprakash, D., et al., *The influence of digital filter type, amplitude normalisation method, and co-contraction algorithm on clinically relevant surface electromyography data during clinical movement assessments*. Journal of Electromyography and Kinesiology, 2016. **31**: p. 126-135.
194. De Luca, C.J., et al., *Filtering the surface EMG signal: Movement artifact and baseline noise contamination*. Journal of biomechanics, 2010. **43**(8): p. 1573-1579.
195. Routson, R.L., S.A. Kautz, and R.R. Neptune, *Modular organization across changing task demands in healthy and poststroke gait*. Physiological reports, 2014. **2**(6).
196. Bowden, M.G., D.J. Clark, and S.A. Kautz, *Evaluation of abnormal synergy patterns poststroke: relationship of the Fugl-Meyer Assessment to hemiparetic locomotion*. Neurorehabilitation and neural repair, 2010. **24**(4): p. 328-337.
197. Torres-Oviedo, G. and L.H. Ting, *Subject-specific muscle synergies in human balance control are consistent across different biomechanical contexts*. Journal of neurophysiology, 2010. **103**(6): p. 3084-3098.

198. Sawers, A., J.L. Allen, and L.H. Ting, *Long-term training modifies the modular structure and organization of walking balance control*. Journal of neurophysiology, 2015. **114**(6): p. 3359-3373.
199. van der Krogt, M.M., et al., *The effect of EMG processing choices on muscle synergies before and after BoNT-A treatment in cerebral palsy*. 2016.
200. Merletti, R. and P. Di Torino, *Standards for reporting EMG data*. J Electromyogr Kinesiol, 1999. **9**(1): p. 3-4.
201. Shuman, B.R., M.H. Schwartz, and K.M. Steele, *Electromyography Data Processing Impacts Muscle Synergies during Gait for Unimpaired Children and Children with Cerebral Palsy*. Frontiers in computational neuroscience, 2017. **11**: p. 50.
202. Muceli, S., et al., *Identifying representative synergy matrices for describing muscular activation patterns during multidirectional reaching in the horizontal plane*. Journal of neurophysiology, 2010. **103**(3): p. 1532-1542.
203. Cheung, V.C., A. d'Avella, and E. Bizzi, *Adjustments of motor pattern for load compensation via modulated activations of muscle synergies during natural behaviors*. Journal of neurophysiology, 2009. **101**(3): p. 1235-1257.
204. Torres-Oviedo, G., J.M. Macpherson, and L.H. Ting, *Muscle synergy organization is robust across a variety of postural perturbations*. Journal of neurophysiology, 2006. **96**(3): p. 1530-1546.
205. Berger, D.J., et al., *Differences in adaptation rates after virtual surgeries provide direct evidence for modularity*. Journal of Neuroscience, 2013. **33**(30): p. 12384-12394.
206. Walter, J.P., et al., *Muscle synergies may improve optimization prediction of knee contact forces during walking*. Journal of biomechanical engineering, 2014. **136**(2): p. 021031.
207. Cheung, V.C., et al., *Stability of muscle synergies for voluntary actions after cortical stroke in humans*. Proceedings of the National Academy of Sciences, 2009. **106**(46): p. 19563-19568.
208. Roh, J., et al., *Alterations in upper limb muscle synergy structure in chronic stroke survivors*. J Neurophysiol, 2013. **109**(3): p. 768-81.
209. Steele, K.M., M.C. Tresch, and E.J. Perreault, *The number and choice of muscles impact the results of muscle synergy analyses*. Frontiers in computational neuroscience, 2013. **7**.
210. Nordez, A. and F. Hug, *Muscle shear elastic modulus measured using supersonic shear imaging is highly related to muscle activity level*. Journal of applied physiology, 2010. **108**(5): p. 1389-1394.
211. Routson, R.L., et al., *The influence of locomotor rehabilitation on module quality and post-stroke hemiparetic walking performance*. Gait Posture, 2013. **38**(3): p. 511-7.
212. Hayes, H.B., et al., *Neuromuscular constraints on muscle coordination during overground walking in persons with chronic incomplete spinal cord injury*. Clinical Neurophysiology, 2014. **125**(10): p. 2024-2035.
213. Shourijeh, M.S., T.E. Flaxman, and D.L. Benoit, *An approach for improving repeatability and reliability of non-negative matrix factorization for muscle synergy analysis*. Journal of Electromyography and Kinesiology, 2016. **26**: p. 36-43.
214. Gizzi, L., et al., *Motor modules in robot-aided walking*. Journal of neuroengineering and rehabilitation, 2012. **9**(1): p. 76.

215. Chvatal, S.A. and L.H. Ting, *Voluntary and reactive recruitment of locomotor muscle synergies during perturbed walking*. Journal of Neuroscience, 2012. **32**(35): p. 12237-12250.
216. Barroso, F.O., et al., *Shared muscle synergies in human walking and cycling*. Journal of neurophysiology, 2014. **112**(8): p. 1984-1998.
217. De Groot, F., I. Jonkers, and J. Duysens, *Task constraints and minimization of muscle effort result in a small number of muscle synergies during gait*. Frontiers in computational neuroscience, 2014. **8**.
218. Gui, K. and D. Zhang, *Influence of locomotion speed on biomechanical subtask and muscle synergy*. Journal of Electromyography and Kinesiology, 2016. **30**: p. 209-215.
219. Frère, J. and F. Hug, *Between-subject variability of muscle synergies during a complex motor skill*. Frontiers in computational Neuroscience, 2012. **6**.
220. d'Avella, A. and E. Bizzi, *Shared and specific muscle synergies in natural motor behaviors*. Proceedings of the National Academy of Sciences of the United States of America, 2005. **102**(8): p. 3076-3081.
221. Hagio, S., M. Fukuda, and M. Kouzaki, *Identification of muscle synergies associated with gait transition in humans*. Frontiers in human neuroscience, 2015. **9**.
222. Portney, L. and M. Watkins, *Foundations of clinical research: application to practice*. Stamford, USA: Appleton & Lange, 1993.
223. Safavynia, S.A. and L.H. Ting, *Task-level feedback can explain temporal recruitment of spatially fixed muscle synergies throughout postural perturbations*. Journal of neurophysiology, 2011. **107**(1): p. 159-177.
224. Dominici, N., et al., *Locomotor primitives in newborn babies and their development*. Science, 2011. **334**(6058): p. 997-999.
225. Pataky, T.C., M.A. Robinson, and J. Vanrenterghem, *Vector field statistical analysis of kinematic and force trajectories*. Journal of Biomechanics, 2013. **46**(14): p. 2394-2401.
226. Robinson, M.A., J. Vanrenterghem, and T.C. Pataky, *Statistical Parametric Mapping (SPM) for alpha-based statistical analyses of multi-muscle EMG time-series*. Journal of Electromyography and Kinesiology, 2015. **25**(1): p. 14-19.
227. Penny, W.D., et al., *Statistical parametric mapping: the analysis of functional brain images*. 2011: Elsevier.
228. Pataky, T.C., M.A. Robinson, and J. Vanrenterghem, *A computational framework for estimating statistical power and planning hypothesis-driven experiments involving one-dimensional biomechanical continua*. Journal of biomechanics, 2017.
229. Adler, R.J. and J.E. Taylor, *Random fields and geometry*. 2009: Springer Science & Business Media.
230. Mehryar, P., M.S. Shourijeh, and A.A. Dehghani-Sanij, *Muscle synergy analysis in transtibial amputee during ramp descending activity*, in *Converging Clinical and Engineering Research on Neurorehabilitation II*. October 2016, Springer. p. 945-949.
231. Winter, D.A., *Energy generation and absorption at the ankle and knee during fast, natural, and slow cadences*. Clinical orthopaedics and related research, 1983(175): p. 147-154.
232. Loudon, J.K., M. Swift, and S. Bell, *The clinical orthopedic assessment guide*. 2008: Human Kinetics.

233. Shultz, S., P. Houglum, and D. Perrin, *Examination of Musculoskeletal Injuries with Web Resource*. 2015: Human Kinetics.
234. Berke, G., et al., *Transfemoral Amputation: The Basics and Beyond*. 2008: Prosthetics Research Study.
235. Nolan, L. and A. Lees, *The functional demands on the intact limb during walking for active trans-femoral and trans-tibial amputees*. Prosthetics and orthotics international, 2000. **24**(2): p. 117-125.
236. Den Otter, A., et al., *Speed related changes in muscle activity from normal to very slow walking speeds*. Gait & posture, 2004. **19**(3): p. 270-278.
237. Franz, J.R. and R. Kram, *The effects of grade and speed on leg muscle activations during walking*. Gait & posture, 2012. **35**(1): p. 143-147.
238. Hof, A., et al., *Speed dependence of averaged EMG profiles in walking*. Gait & posture, 2002. **16**(1): p. 78-86.
239. Nilsson, J., A. Thorstensson, and J. HALBERTSMA, *Changes in leg movements and muscle activity with speed of locomotion and mode of progression in humans*. Acta Physiologica, 1985. **123**(4): p. 457-475.
240. Yang, J.F. and D.A. Winter, *Surface EMG profiles during different walking cadences in humans*. Electroencephalography and clinical Neurophysiology, 1985. **60**(6): p. 485-491.
241. Duysens, J., et al., *Selective activation of human soleus or gastrocnemius in reflex responses during walking and running*. Experimental Brain Research, 1991. **87**(1): p. 193-204.
242. Neptune, R., S. Kautz, and F. Zajac, *Contributions of the individual ankle plantar flexors to support, forward progression and swing initiation during walking*. Journal of biomechanics, 2001. **34**(11): p. 1387-1398.
243. Delp, S.L., D.A. Ringwelski, and N.C. Carroll, *Transfer of the rectus femoris: effects of transfer site on moment arms about the knee and hip*. Journal of biomechanics, 1994. **27**(10): p. 1201-1211.
244. Shiavi, R., H. Bugle, and T. Limbird, *Electromyographic gait assessment, Part 1: Adult EMG profiles and walking speed*. Journal of rehabilitation research and development, 1987. **24**(2): p. 13-23.
245. Nene, A., R. Mayagoitia, and P. Veltink, *Assessment of rectus femoris function during initial swing phase*. Gait & posture, 1999. **9**(1): p. 1-9.
246. Safavynia, S., G. Torres-Oviedo, and L. Ting, *Muscle synergies: implications for clinical evaluation and rehabilitation of movement*. Topics in spinal cord injury rehabilitation, 2011. **17**(1): p. 16-24.
247. Ivanenko, Y., et al., *Spatiotemporal organization of α -motoneuron activity in the human spinal cord during different gaits and gait transitions*. European Journal of Neuroscience, 2008. **27**(12): p. 3351-3368.
248. McGowan, C.P., et al., *Modular control of human walking: adaptations to altered mechanical demands*. Journal of biomechanics, 2010. **43**(3): p. 412-419.
249. Yokoyama, H., et al., *Distinct sets of locomotor modules control the speed and modes of human locomotion*. Scientific reports, 2016. **6**: p. 36275.
250. Types, A. *Different types of Amputations*. 2018 [cited 2018 01/05/2018]; Available from: http://www.nccs.com.sg/pbcation/CU/vol3_05/p7.htm.
251. Database, N.A.S., *The amputee statistical database for the United Kingdom 2006/07*. 2009.
252. Ziegler-Graham, K., et al., *Estimating the prevalence of limb loss in the United States: 2005 to 2050*. Archives of physical medicine and rehabilitation, 2008. **89**(3): p. 422-429.

253. Nolan, L., et al., *Adjustments in gait symmetry with walking speed in transfemoral and trans-tibial amputees*. *Gait & posture*, 2003. **17**(2): p. 142-151.
254. Sanderson, D.J. and P.E. Martin, *Lower extremity kinematic and kinetic adaptations in unilateral below-knee amputees during walking*. *Gait & posture*, 1997. **6**(2): p. 126-136.
255. Jaegers, S.M., J.H. Arendzen, and H.J. de Jongh, *Prosthetic gait of unilateral transfemoral amputees: a kinematic study*. *Archives of physical medicine and rehabilitation*, 1995. **76**(8): p. 736-743.
256. Seroussi, R.E., et al., *Mechanical work adaptations of above-knee amputee ambulation*. *Archives of physical medicine and rehabilitation*, 1996. **77**(11): p. 1209-1214.
257. Hurley, G., et al., *The role of the contralateral limb in below-knee amputee gait*. *Prosthetics and orthotics international*, 1990. **14**(1): p. 33-42.
258. Kelly, K.M., W. Doyle, and H.B. Skinner, *The relationship between gait parameters and pain in persons with transtibial amputation: a preliminary report*. *Journal of rehabilitation research and development*, 1998. **35**(2): p. 231.
259. Awad, M., et al. *Estimation of actuation system parameters for lower limb prostheses*. in *Mechatronics (MECATRONICS)/17th International Conference on Research and Education in Mechatronics (REM), 2016 11th France-Japan & 9th Europe-Asia Congress on*. 2016. IEEE.
260. Waters, R., et al., *Energy cost of walking of amputees: the influence of level of amputation*. *J Bone Joint Surg Am*, 1976. **58**(1): p. 42-46.
261. Powers, C.M., S. Rao, and J. Perry, *Knee kinetics in trans-tibial amputee gait*. *Gait & Posture*, 1998. **8**(1): p. 1-7.
262. Vanicek, N.K., *Biomechanical and psychological factors that distinguish fallers from non-fallers: a comparative study of transtibial amputees and able bodied individuals*. 2009, University of Hull.
263. Powers, C.M., et al., *Influence of prosthetic foot design on sound limb loading in adults with unilateral below-knee amputations*. *Archives of physical medicine and rehabilitation*, 1994. **75**(7): p. 825-829.
264. Menard, M.R., et al., *Comparative biomechanical analysis of energy-storing prosthetic feet*. *Archives of physical medicine and rehabilitation*, 1992. **73**(5): p. 451-458.
265. Beyaert, C., et al., *Compensatory mechanism involving the knee joint of the intact limb during gait in unilateral below-knee amputees*. *Gait & Posture*. **28**(2): p. 278-284.
266. Dillon, C.F., et al., *Prevalence of knee osteoarthritis in the United States: arthritis data from the Third National Health and Nutrition Examination Survey 1991-94*. *The Journal of rheumatology*, 2006. **33**(11): p. 2271-2279.
267. Murphy, L., et al., *Lifetime risk of symptomatic knee osteoarthritis*. *Arthritis Care & Research*, 2008. **59**(9): p. 1207-1213.
268. Dearborn, J., C. Eakin, and H. Skinner, *Medial compartment arthrosis of the knee*. *American journal of orthopedics (Belle Mead, NJ)*, 1996. **25**(1): p. 18-26.
269. Struyf, P.A., et al., *The prevalence of osteoarthritis of the intact hip and knee among traumatic leg amputees*. *Archives of physical medicine and rehabilitation*, 2009. **90**(3): p. 440-446.
270. Norvell, D.C., et al., *The prevalence of knee pain and symptomatic knee osteoarthritis among veteran traumatic amputees and nonamputees*. *Archives of physical medicine and rehabilitation*, 2005. **86**(3): p. 487-493.

271. Cheung, V.C., et al., *Muscle synergy patterns as physiological markers of motor cortical damage*. Proceedings of the National Academy of Sciences, 2012. **109**(36): p. 14652-14656.
272. Michael, J.W., *Modern prosthetic knee mechanisms*. Clinical Orthopaedics and Related Research®, 1999. **361**: p. 39-47.
273. Kapp, S., et al., *Lower limb prosthetics*. Pasquina PF, Cooper RA. Care of the combat amputee. Washington, DC: Borden Institute, 2009: p. 553-80.
274. Näder, M. and H. Näder, *Otto Bock Prostheses Compendium: Prostheses for Lower Limbs*. Schiele & SchoN GmbH, Berlin, 1993.
275. Torrealba, R.R., G. Fernández-López, and J.C. Grieco, *Towards the development of knee prostheses: review of current researches*. Kybernetes, 2008. **37**(9/10): p. 1561-1576.
276. Popovic, D. and L. Schwirtlich, *Belgrade active A/K prosthesis*. Electrophysiological Kinesiology, 1988: p. 337-343.
277. Dietl, H. and H. Bargehr, *The Application of Electronics in Prosthetics for Lower Extremities*. MEDIZINISCH ORTHOPADISCHE TECHNIK, 1997. **117**: p. 31-35.
278. Radcliffe, C., *Four-bar linkage prosthetic knee mechanisms: kinematics, alignment and prescription criteria*. Prosthetics and orthotics international, 1994. **18**(3): p. 159-173.
279. Blumentritt, S., et al., *Design principles, biomechanical data and clinical experience with a polycentric knee offering controlled stance phase knee flexion: A preliminary report*. JPO: Journal of Prosthetics and Orthotics, 1997. **9**(1): p. 18-24.
280. Borjian, R., *Design, modeling, and control of an active prosthetic knee*. 2008, University of Waterloo.
281. Dupes, B. *Prosthetic Knee Systems*. [cited 2018 02/05/2018]; Available from: <http://www.amputee-coalition.org/easyread/military-instep/knees-ez.html>.
282. Hafner, B.J., et al., *Evaluation of function, performance, and preference as transfemoral amputees transition from mechanical to microprocessor control of the prosthetic knee*. Archives of physical medicine and rehabilitation, 2007. **88**(2): p. 207-217.
283. Waycaster, G.C., *Design of a powered above knee prosthesis using pneumatic artificial muscles*. 2010: The University of Alabama.
284. SM, E.C.M.-V., *Agonist-antagonist active knee prosthesis: A preliminary study in level-ground walking*. Journal of rehabilitation research and development, 2009. **46**(3): p. 361.
285. Robinson, D.W., et al. *Series elastic actuator development for a biomimetic walking robot*. in *Advanced Intelligent Mechatronics, 1999. Proceedings. 1999 IEEE/ASME International Conference on*. 1999. IEEE.
286. Lambrecht, B.G. and H. Kazerooni. *Design of a semi-active knee prosthesis*. in *Robotics and Automation, 2009. ICRA'09. IEEE International Conference on*. 2009. IEEE.
287. Klute, G., et al. *Lower limb amputee activity unaffected by shock-absorbing pylon or C-leg knee*. in *The International Society of Biomechanics XXth Congress*. 2005.
288. Basmajian, J.V. and C. De Luca, *Muscles alive*. Muscles alive: their functions revealed by electromyography, 1985. **278**: p. 126.
289. Dietz, V., D. Schmidtbleicher, and J. Noth, *Neuronal mechanisms of human locomotion*. journal of Neurophysiology, 1979. **42**(5): p. 1212-1222.

290. Grillner, S., *Locomotion in vertebrates: central mechanisms and reflex interaction*. Physiological reviews, 1975. **55**(2): p. 247-304.
291. Tucker, M.R., et al., *Control strategies for active lower extremity prosthetics and orthotics: a review*. Journal of neuroengineering and rehabilitation, 2015. **12**(1): p. 1.
292. Sup, F., A. Bohara, and M. Goldfarb, *Design and control of a powered transfemoral prosthesis*. The International journal of robotics research, 2008. **27**(2): p. 263-273.
293. Varol, H.A., F. Sup, and M. Goldfarb, *Multiclass real-time intent recognition of a powered lower limb prosthesis*. IEEE Transactions on Biomedical Engineering, 2010. **57**(3): p. 542-551.
294. Hargrove, L.J., et al., *Non-weight-bearing neural control of a powered transfemoral prosthesis*. Journal of neuroengineering and rehabilitation, 2013. **10**(1): p. 62.
295. Young, A.J., et al. *Classifying the intent of novel users during human locomotion using powered lower limb prostheses*. in *Neural engineering (NER), 2013 6th international IEEE/EMBS conference on*. 2013. IEEE.
296. Stegeman, D. and H. Hermens, *Standards for surface electromyography: The European project Surface EMG for non-invasive assessment of muscles (SENIAM)*. Enschede: Roessingh Research and Development, 2007: p. 108-12.
297. Kuiken, T.A., et al., *Targeted muscle reinnervation for real-time myoelectric control of multifunction artificial arms*. Jama, 2009. **301**(6): p. 619-628.
298. Zecca, M., et al., *Control of multifunctional prosthetic hands by processing the electromyographic signal*. Critical Reviews™ in Biomedical Engineering, 2002. **30**(4-6).
299. Rose, W., *Electromyogram analysis*. Mathematics and Signal Processing for Biomechanics, 2014.
300. Gribble, P.L. and D.J. Ostry, *Compensation for interaction torques during single-and multijoint limb movement*. Journal of neurophysiology, 1999. **82**(5): p. 2310-2326.
301. DeVita, P. and T. Hortobagyi, *Age causes a redistribution of joint torques and powers during gait*. Journal of applied physiology, 2000. **88**(5): p. 1804-1811.
302. Benjuya, N., I. Melzer, and J. Kaplanski, *Aging-induced shifts from a reliance on sensory input to muscle cocontraction during balanced standing*. The Journals of Gerontology Series A: Biological Sciences and Medical Sciences, 2004. **59**(2): p. M166-M171.
303. Manchester, D., et al., *Visual, vestibular and somatosensory contributions to balance control in the older adult*. Journal of Gerontology, 1989. **44**(4): p. M118-M127.
304. Schmitz, A., et al., *Differences in lower-extremity muscular activation during walking between healthy older and young adults*. Journal of Electromyography and Kinesiology, 2009. **19**(6): p. 1085-1091.
305. Englehart, K., B. Hudgin, and P.A. Parker, *A wavelet-based continuous classification scheme for multifunction myoelectric control*. Biomedical Engineering, IEEE Transactions on, 2001. **48**(3): p. 302-311.
306. Hudgins, B., P. Parker, and R.N. Scott, *A new strategy for multifunction myoelectric control*. Biomedical Engineering, IEEE Transactions on, 1993. **40**(1): p. 82-94.

307. Hoover, C.D., G.D. Fulk, and K.B. Fite, *Stair ascent with a powered transfemoral prosthesis under direct myoelectric control*. *Mechatronics, IEEE/ASME Transactions on*, 2013. **18**(3): p. 1191-1200.
308. Ha, K.H., H.A. Varol, and M. Goldfarb. *Myoelectric control of a powered knee prosthesis for volitional movement during non-weight-bearing activities*. in *Conference proceedings:... Annual International Conference of the IEEE Engineering in Medicine and Biology Society. IEEE Engineering in Medicine and Biology Society. Annual Conference*. 2009.
309. Ha, K.H., H.A. Varol, and M. Goldfarb. *Myoelectric control of a powered knee prosthesis for volitional movement during non-weight-bearing activities*. in *Engineering in Medicine and Biology Society (EMBC), 2010 Annual International Conference of the IEEE*. 2010. IEEE.
310. GRILLNER, S. and P. ZANGGER, *The effect of dorsal root transection on the efferent motor pattern in the cat's hindlimb during locomotion*. *Acta Physiologica*, 1984. **120**(3): p. 393-405.
311. Pedotti, A., *A study of motor coordination and neuromuscular activities in human locomotion*. *Biological cybernetics*, 1977. **26**(1): p. 53-62.
312. Ivanenko, Y.P., R.E. Poppele, and F. Lacquaniti, *Motor control programs and walking*. *The Neuroscientist*, 2006. **12**(4): p. 339-348.
313. Shik, M.L., *Action of the brainstem locomotor region on spinal stepping generators via propriospinal pathways*. *Spinal Cord Reconstruction*, 1983: p. 421-434.
314. Bauby, C.E. and A.D. Kuo, *Active control of lateral balance in human walking*. *Journal of biomechanics*, 2000. **33**(11): p. 1433-1440.
315. Neptune, R.R., K. Sasaki, and S.A. Kautz, *The effect of walking speed on muscle function and mechanical energetics*. *Gait & posture*, 2008. **28**(1): p. 135-143.
316. Van Hedel, H., L. Tomatis, and R. Müller, *Modulation of leg muscle activity and gait kinematics by walking speed and bodyweight unloading*. *Gait & posture*, 2006. **24**(1): p. 35-45.
317. Herman, R., et al., *Human solutions for locomotion*, in *Neural control of locomotion*. 1976, Springer. p. 13-49.
318. Balasubramanian, C.K., et al., *Relationship between step length asymmetry and walking performance in subjects with chronic hemiparesis*. *Archives of physical medicine and rehabilitation*, 2007. **88**(1): p. 43-49.
319. Martino, G., et al., *Locomotor patterns in cerebellar ataxia*. *Journal of neurophysiology*, 2014. **112**(11): p. 2810-2821.
320. Lee, D.D. and H.S. Seung. *Algorithms for non-negative matrix factorization*. in *Advances in neural information processing systems*. 2001.
321. Guidetti, L., G. Rivellini, and F. Figura, *EMG patterns during running: intra- and inter-individual variability*. *Journal of Electromyography and Kinesiology*, 1996. **6**(1): p. 37-48.
322. Miall, R.C., *Walking the walk*. *Nature neuroscience*, 2007. **10**(8): p. 940.
323. Mehryar, P., et al., *Changes in knee joint kinetics of transfemoral amputee's intact leg: An osteoarthritis indication?* *Gait & Posture*, 2017. **57**: p. 151-152.
324. NORAXON, *Surface EMG*. 2014.
325. Wilbourn, A.J. and M.J. Aminoff, *AAEM minimonograph 32: the electrodiagnostic examination in patients with radiculopathies*. *Muscle & nerve*, 1998. **21**(12): p. 1612-1631.
326. Jeannerod, M., *The neural and behavioural organization of goal-directed movements*. 1988: Clarendon Press/Oxford University Press.

327. Pierrot-Deseilligny, E. and D. Burke, *The circuitry of the human spinal cord: its role in motor control and movement disorders*. 2005: Cambridge University Press.
328. De Luca, C., *Control properties of motor units*. Journal of Experimental Biology, 1985. **115**(1): p. 125-136.
329. Farina, D. and F. Negro, *Accessing the neural drive to muscle and translation to neurorehabilitation technologies*. IEEE Reviews in Biomedical Engineering, 2012. **5**: p. 3-14.
330. Ting, L.H., et al., *Review and perspective: neuromechanical considerations for predicting muscle activation patterns for movement*. International journal for numerical methods in biomedical engineering, 2012. **28**(10): p. 1003-1014.
331. Taborri, J., et al., *Feasibility of Muscle Synergy Outcomes in Clinics, Robotics, and Sports: A Systematic Review*. Applied Bionics and Biomechanics, 2018. **2018**.
332. Farina, D. and O. Aszmann, *Bionic limbs: clinical reality and academic promises*. Science translational medicine, 2014. **6**(257): p. 257ps12-257ps12.
333. Sepulveda, F., D.M. Wells, and C.L. Vaughan, *A neural network representation of electromyography and joint dynamics in human gait*. Journal of biomechanics, 1993. **26**(2): p. 101-109.
334. Jiang, N., et al., *EMG-based simultaneous and proportional estimation of wrist/hand kinematics in uni-lateral trans-radial amputees*. Journal of neuroengineering and rehabilitation, 2012. **9**(1): p. 42.
335. Ngeo, J.G., T. Tamei, and T. Shibata, *Continuous and simultaneous estimation of finger kinematics using inputs from an EMG-to-muscle activation model*. Journal of neuroengineering and rehabilitation, 2014. **11**(1): p. 122.
336. Hahne, J.M., et al., *Linear and nonlinear regression techniques for simultaneous and proportional myoelectric control*. IEEE Transactions on Neural Systems and Rehabilitation Engineering, 2014. **22**(2): p. 269-279.
337. Farina, D., et al., *The extraction of neural information from the surface EMG for the control of upper-limb prostheses: emerging avenues and challenges*. IEEE Transactions on Neural Systems and Rehabilitation Engineering, 2014. **22**(4): p. 797-809.
338. Sartori, M., D.G. Llyod, and D. Farina, *Neural data-driven musculoskeletal modeling for personalized neurorehabilitation technologies*. IEEE Transactions on Biomedical Engineering, 2016. **63**(5): p. 879-893.
339. Wang, L. and T.S. Buchanan, *Prediction of joint moments using a neural network model of muscle activations from EMG signals*. IEEE Transactions on Neural Systems and Rehabilitation Engineering, 2002. **10**(1): p. 30-37.
340. Naeem, U.J. and C. Xiong, *Neural-Genetic Model for Muscle Force Estimation Based on EMG Signal*. Communications in Information Science and Management Engineering, 2013. **3**(6): p. 301.
341. Caputo, J.M. and S.H. Collins, *A universal ankle-foot prosthesis emulator for human locomotion experiments*. Journal of biomechanical engineering, 2014. **136**(3): p. 035002.
342. Kutzner, I., et al., *Loading of the knee joint during activities of daily living measured in vivo in five subjects*. Journal of biomechanics, 2010. **43**(11): p. 2164-2173.

343. Mehryar, P., et al. *Investigation of Above Knee Muscles for Event Detection using Surface Electromyography*. in *MEIbioeng15*. 2015. Leeds.
344. Maqbool, H.F., et al. *Towards intelligent lower limb prostheses with activity recognition*. in *Conference Towards Autonomous Robotic Systems*. 2015. Springer.
345. Zakria, M., et al. *Heuristic based gait event detection for human lower limb movement*. in *Biomedical & Health Informatics (BHI), 2017 IEEE EMBS International Conference on*. 2017. IEEE.
346. TarniȚă, D., *Wearable sensors used for human gait analysis*. *Rom J Morphol Embryol*, 2016. **57**(2): p. 373-382.
347. Rueterbories, J., et al., *Methods for gait event detection and analysis in ambulatory systems*. *Medical Engineering and Physics*, 2010. **32**(6): p. 545-552.
348. Martino, G., et al., *Neuromuscular adjustments of gait associated with unstable conditions*. *Journal of neurophysiology*, 2015. **114**(5): p. 2867-2882.
349. Ferrante, S., et al., *A personalized multi-channel FES controller based on muscle synergies to support gait rehabilitation after stroke*. *Frontiers in neuroscience*, 2016. **10**: p. 425.
350. Fox, E.J., et al., *Modular control of varied locomotor tasks in children with incomplete spinal cord injuries*. *Journal of neurophysiology*, 2013. **110**(6): p. 1415-1425.
351. Knee, S.A.H. 2018 [cited 2018 02/05/2018]; Available from: <http://www.heritage-medical.com/hydraulic-prosthetic-knees/single-axis-hydraulic-knee/>.
352. hydraulic, K.P.p.k.w. 2018 [cited 2018 02/05/2018]; Available from: <http://www.blatchford.co.uk/endolite/kx06/>.
353. Bradley, D. and D.W. Russell, *Mechatronics in action*. 2010: Springer.
354. Knee, P., 2018.
355. Feet. [cited 19/03/2018 19/03/2018]; Available from: <https://www.ossur.com/prosthetic-solutions/products/dynamic-solutions/proprio-foot>.
356. Huang, H., et al., *Design of a robust EMG sensing interface for pattern classification*. *Journal of neural engineering*, 2010. **7**(5): p. 056005.
357. Zhang, F. and H. Huang, *Source Selection for Real-time User Intent Recognition towards Volitional Control of Artificial Legs*. *IEEE journal of biomedical and health informatics*, 2013. **17**(5): p. 907-914.
358. Spanias, J.A., E.J. Perreault, and L.J. Hargrove, *Detection of and Compensation for EMG Disturbances for Powered Lower Limb Prosthesis Control*. *Neural Systems and Rehabilitation Engineering, IEEE Transactions on*, 2015. **PP**(99): p. 1-1.

APPENDICIES

Appendix A Literature Review Supplements

Appendix B Chapter 3 Supplements

Appendix C Chapter 5 Supplements

Appendix D Ethical Approval

Appendix E List of Publications and Awards

E.1 Publications from this Thesis (P. Mehryar, main author)

E.2 Related Publications (P. Mehryar, co-author)

E.3 Awards

Appendix A

Literature Review Supplements

The ankle, knee and hip muscles and the moments they can generate.

Table A.1: Ankle muscles and corresponding movements (adapted from [99]).

Movement	Dorsiflexion	Plantarflexion
Involved Muscles	Extensor digitorum longus Extensor hallucis longus Peroneus tertius Tibialis anterior	Flexor digitorum longus Flexor hallucis longus Gastrocnemius Peroneus brevis Peroneus longus Plantaris Soleus Tibialis posterior
Movement	Eversion	Inversion
Involved Muscles	Extensor digitorum longus Peroneus brevis Peroneus longus Peroneus tertius	Flexor digitorum longus Tibialis anterior Tibialis posterior

Table A.2: Knee muscles and corresponding movements (adapted from [99]).

Movement	Flexion	Extension
Involved Muscles	Biceps femoris Gastrocnemius Gracilis Popliteus Sartorius Semimembranosus Semitendinosus	Rectus femoris Vastus intermedius Vastus lateralis Vastus medialis
Movement	Medial Rotation	Lateral Rotation
Involved Muscles	Gracilis Popliteus Sartorius Semimembranosus Semitendinosus	Biceps femoris

Table A.3: Hip muscles and corresponding movements (adapted from [99]).

Movement	Flexion	Extension
Involved Muscles	Adductor brevis Adductor longus Iliacus Pectineus Psoas major Rectus femoris Sartorius Tensor Fascia latae	Adductor magnus Biceps femoris Gluteus maximum Semimembranosus Semitendinosus
Movement	Abduction	Adduction
Involved Muscles	Gemellus inferior Gemellus Superior Gluteus maximus Gluteus medius Gluteus minimus Piriformis Tensor fascia latae	Adductor brevis Adductor longus Adductor magnus Biceps femoris Gluteus maximus Gracilis Pectineus Psoas major
Movement	Medial rotation	Lateral rotation
Involved Muscles	Gluteus medius Gluteus minimus Tensor fascia latae	Adductor brevis Adductor longus Adductor magnus Biceps femoris Gemellus inferior Gemellus superior Gluteus maximus Gluteus medius Obturator externus Obturator internus Piriformis Quadratus femoris Sartorius

Table A.4: Ambulatory measurement devices. Compiled from [9, 104, 110, 117, 346].

No	Device	Type	Brief Details	Example
1	Electromyography	Ambulatory	Record muscle activation	Surface & invasive electrodes
2	Electrogoniometer	Ambulatory	Measure kinematics angular information	Potentiometer, Flexible strain gauges,
3	Camera (Motion Capture System)	Stationary	Consists of infrared cameras. Record from active or passive markers placed on anatomical positions to measure kinematic data of joints and body segments	Vicon Motion Camera, Qualisys Track Manage
4	Force Platform	Stationary	Consists of an array of load cells and measure the kinetic data (ground reaction force)	Kistler, AMTI
5	Video Tape	Stationary	Record movement from different angles and used for qualitative observation of the locomotion tasks	Any video recorder
6	Pressure Sensor Mats	Stationary/ Ambulatory	measure kinetic data using mapping pressure distribution	Force sensitive resistor, Pressure map Pedar-X, Tekscan,
7	Foot-switch	Ambulatory	Consists of resistors which identifies the events occurring during locomotion tasks	Force sensitive resistor, Microswitch
8	Gyroscope	Ambulatory	Used to record the kinematic data such as angular velocities	Uni axis, Multi axis
9	Accelerometer	Ambulatory	Used to record linear acceleration and static tilt angles	Uni axis, Multi axis
10	Ultrasound	Ambulatory	Used to record spatial (distance) parameters such as step length, stride length	Ultrasonic sensor (HCSR04)

Table A.5: Comparison between gait analysis systems. Compiled from [110, 346, 347].

System Type	Advantages	Disadvantages
Stationary	better repeatability and reproducibility, High precision, no restriction on power consumption, less external interference,	expensive, heavy, large in size, restricted to use indoor environments (lab-based)
Ambulatory	small size, Portability, long-term monitoring, lightweight, inexpensive, indoor/outdoor applications,	Susceptible to noise and interference of external factors, limited battery duration, limited gait parameters can be analyzed

Table A.6: Summary of the studies on lower limb surface EMG, filtration techniques used on HS and TFA during ADLs.

No	Activity	Muscle	Filtration	Linear Envelope
[307]	SA	RF, VL, VM, BF, SEM	2 nd order Butterworth HPF = 20 LPF = 450	2 nd order Butterworth LPF= 2.5
[309]	Nonweight bearing activity	QUAD and HAM	1 st order Butterworth HPF = 20	1 st order Butterworth LPF= 2
[35]	LGW, STD, postural sway	GMAX, GMED, TFL, RF, VL, BFLH, TA, GM, SOL	2 nd order Butterworth HPF = 20	2 nd order Butterworth LPF = 9
[37]	LGW	SAR, RF, TFL, BFLH, SEM, SEMIM, ADL, ADM, GR	NM	3 rd order LPF = 25
[47]	LGW	VL, BFLH, TA, GL	NM	2 nd order Butterworth LPF = 5

Table A.7: Factors impact surface EMG. Compiled from [111, 155, 157].

Detection system	Impedance, Inter-electrode distance, electrode size and shape, placement of the electrodes on the muscles, position of the sensors with respect to the fiber orientation, Spatial filter for signal detection
Geometrical	Movement of the muscles with respect to the electrodes, shortening of muscle fiber
Physical	Tissue conductivity, cross talk from other muscles
Physiological Fiber membrane properties	Average muscle fiber conduction velocity, intracellular action potentials shape, Distribution of conduction velocities of the fibers within the motor units, Distribution of motor unit conduction velocities
Nonphysiological Anatomic	Thickness of subcutaneous fat, shape of volume conductor, fibers length, distribution of the end plate and tendon junctions within the motor unit, amount of cross talk from adjacent muscles, tissue conductivity, number and distribution of fibers in the motor unit territories, distribution of the motor unit territories in muscle, size of the motor unit territories, volume conductor shape, Tissue inhomogeneities, Spread of the innervation zones and tendon regions among motor units, variety of pinnation angle
Motor unit properties	Synchronization of motor unit, discharge rate coefficient of variation and statistics, Distribution of motor unit discharge rates, Number of recruited motor units

Table A.8: Literature review on muscle synergies during ADLs.

No	Activity	Muscle	Filtration (Hz)	Linear Envelope (Hz)	VAF Threshold (%)	No. Synergy Groups
[198]	LGW, narrow beam-walking, wide beam-walking,	TA, PERL, MG, SOL, VM, VL, BFLH, SEM, GMAX, GMED, RF, TFL, ADM, RAB, EO, ERE	3 rd order Butterworth (HPF = 35)	3 rd order Butterworth (LPF = 40)	90	HS = 4-6
[109]	Treadmill walking	GM, GL, SOL, TA, VL, RF, BFLH, TFL, ADDL, GMED, GMAX, ERE	4 th order Butterworth (HPF = 40)	4 th order Butterworth (LPF = 10)	90%	HS = 4-5
[216]	LGW, cycling	GMED, RF, VL, BFLH, SEM, GM, SOL, TA	3 rd order Butterworth (HPF = 20)	3 rd order Butterworth (LPF = 10)	90	HS = 4
[217]	LGW	TA, SOL, GM, VL, RF, BFLH, GMED, SEMIM,	4 th order Butterworth (HPF = 10 LPF = 50)	NA RMS (100 ms window)	90	HS = 4
[218]	Treadmill walking (different speeds)	TA, SOL, GM, VL, RF, BFLH, GMED, SEM,	4 th order Butterworth (HPF = 20 LPF = 450)	2 nd order Butterworth (LPF = 5)	90	HS = 4
[185]	LGW, RN	TA, FDB, GL, SOL, PERL, VL, VM, RF, SAR, BFLH, SEM, ADDL, TFL,	NM (HPF = 20 LPF = 450)	NM (LPF = 10)	NM	HS = 5

		GMAX, GMED, EO, IO, LD, IL, RAS, ERE				
[215]	LGW (slow and normal), perturbed LGW	VAS, RF, REAB, BFLH, SEM, ADM, ERE, EXOB, VM, TA, GM, GL, SOL, PERL, TFL, GMED	NM (HPF = 35)	NM (LPF = 40)	85	HS = 6
[91]	LGW at (different speeds)	TA, SOL, GM, VM, RF, SEM, BFLH, GMED	4 th order Butterworth (HPF = 40)	4 th order Butterworth (LPF = 4)	90%	Stroke = 2-4 HS = 4
[79]	LGW (fast and normal)	TA, SOL, GL, GM, VL, RF, VM, BFLH, SEM, TFL, GMAX	4 th order Butterworth (HPF = 20 LPF = 450)	2 nd order Butterworth (LPF = 5)	90	HS = 5
[221]	LGW, RN, transition LGW to RN and vice versa	SOL, GM, GL, TA, RF, VL, VM, BFLH, BFSH, GMED, GMAX	4 th order Butterworth (HPF = 100)	NM (LPF = 15)	95	Transition = 9
[77]	LGW	TA, SOL, GM, VM, RF, SEM, BFLH, GMED	4 th order Butterworth (HPF = 40)	4 th order Butterworth (LPF = 4)	90%	HS = 4-5
[214]	LGW (different speeds), LGW (with body weight support)	TA, SOL, GM, VL, RF, BFLH, RAB, ERE	4 th order Butterworth (HPF = 20 LPF = 400)	4 th order Butterworth (LPF = 10)	80%	HS = 4 Robotic aided device = 4
[83]	Treadmill (different speeds and slopes)	TA, SOL, PERL, VL, VM, RF, SAR, ADM, ADDL, GMED, TFL, GLAT, GMED, BFLH, SEMIM, GMAX	4 th order Butterworth (HPF = 30 LPF = 300)	2 nd order Butterworth (LPF = 3)	85	HS = 4

[82]	Treadmill LGW (different speeds), RA	VI, VM, RF, BFLH, SEM, ADM, ADDL, GM, TA,	NM (HPF = 20 LPF = 450)	4 th order Butterworth (LPF = 9)	90	HS = 4
[136]	FW, RN, SS, CO	TA, SOL, PERL, VL, VM, RF, SAR, ADM, ADDL, GMED, TFL, GLAT, GMED, BFLH, SEM, GMAX	NM (HPF = 30 LPF = 450)	NM (LPF = 6)	80	HS = 5
[84]	Treadmill walking	TA, GM, GL, SOL, VL, VM, RF, BFLH, SEM, GMAX	NM (HPF = 20 LPF = 500)	NM (LPF = 10)	90	HS = 5
[87]	WF, WB, WL, WR, SIP	ERE, GMAX, GMED, VM, VL, RF, BFLH, BFSH, SEM, SAR, IP, ADDL, ADM, TFL, GM, GL, SOL, TA, PERL, PERB, EHB, EDB, FDB, EHL, FHL, FDL	3 rd order Butterworth (HPF = 30)	4 th order Butterworth (LPF = 10)	90	HS = 5-8
[86]	Cutting manoeuvres, RN	TA, PER, SOL, GM, VM, VL, RF, BFLH, SEM, ADM, ADDL, GMED, GMAX, TFL, ERE, RAB, EO	2 nd order Butterworth (HPF = 10 LPF = 500)	NM (LPF = 10)	80	HS = 5
[126]	LGW	TA, SOL, GL, GMAX, RF, VL, SEM, EDL	NM	2 nd order Butterworth (LPF = 6)	90	ACL = 5 HS 5

[206]	LGW	BFLH, SEMIM, GM, GL, TFL, VL, RF, SAR, GR, SOL, TA, PERL, ADM	4 th order Butterworth (HPF = 30)	4 th order Butterworth (LPF = 6)	95	Knee replacement = 5
[348]	Walking on slippery ground, narrow bean	TA, GM, GL, SOL, PERL, VL, VM, RF, BFLH, SEM, TFL, GMED	3 rd order Butterworth (HPF = 20 LPF = 450)	4 th order Butterworth (LPF = 10)	90	cerebellar ataxic = 4 HS = 4
[180]	LGW, postural tasks after Dance (tango) rehab	RAB, EO, ERE, GMED, TFL, BFLH, RF, VM, GASTMED, GASTLAT, SOL, PERL, TA,	NM (HPF = 35)	NM (LPF = 40)	85, 90, 95	Parkinson = 4
[88]	Treadmill walking	SOL, GM, TA, VM, RF, SEM, BFLH, GMED	4 th order Butterworth (HPF = 35)	4 th order Butterworth (LPF = 7)	95	Parkinson = 3-5 HS = 3-6
[211]	LGW (different speeds)	TA, SOL, GM, VM, RF, SEM, BFLH, GMED	4 th order Butterworth (HPF = 40)	4 th order Butterworth (LPF = 4)	90	Post-stroke = (2-4) HS = 4
[58]	LGW (different speeds)	PERL, GL, SOL, RF, VM, TA, BFLH, SEM, ADDL, TFL, GMAX, GMED	NM	4 th order Butterworth (LPF = 15)	90	Elderly = 5 HS = 5
[216]	LGW	ERE, GMA, GMED, TFL, ADDL, RF, VL, BFLH, GM, SOL, TA	4 th order Butterworth (HPF = 20)	4 th order Butterworth (LPF = 5)	90	Paretic = 3 – 4 Non-paretic = 3 - 5
[181]	Treadmill walking (different speeds)	PERL, GL, SOL, TA, RF, VM, BF, SEM, ADDL, TFL, GMA, GMED	NM	4 th order Butterworth (LPF = 10)	Eval > 0.5	Paretic = 4 Non-paretic = 4 HS = 5

[349]	LGW and Treadmill	GMAX, RF, VM, SEM, BFLH, GM, TA	3 rd order Butterworth (HPF = 40 LPF = 400)	3 rd order Butterworth (LPF = 5)	90	Paretic = 3 Paretic after FES = 4 HS = 4
[179]	6-meter long LGW	TA, GM, SOL, VL, RF, BFLH, GMAX, RAB. ERE. LD, BB, TB, AD, UT, ST, SPL,	4 th order Butterworth (HPF = 20 LPF = 400)	4 th order Butterworth (LPF = 10)	80	Paretic = 4 Non-paretic = 4 HS = 4
[182]	LGW	TA, GL, SOL, GMED, RF, VM, BFLH, SEM	NM (HPF = 20 LPF = 250)	NM (LPF = 10)	90	Sub-acute = 2-5 After rehab = 2 - 5
[183]	LGW, Treadmill (normal, fast)	TA, SOL, GM, VM, RF, SEM, BFLH, GMED	4 th order Butterworth (HPF = 40)	4 th order Butterworth (LPF = 4)	90	Paretic LGW & treadmill = 2 HS LGW & treadmill = 4
[212]	LGW	TA, GM, GL, SOL, VL, VM, RF, SEM, BFLH, GMED, GMAX, TFL, SAR, ADM	4 th order Butterworth (HPF = 30)	4 th order Butterworth (LPF = 4)	90	ISCIs = 4 HS = 6
[350]	LGW, treadmill	TA, GM, VM, RF, SEM, GM,	4 th order Butterworth (HPF = 30)	4 th order Butterworth (LPF = 4)	90	ISCIs LGW = 2 ISCIs Treadmill = 4 HS LGW & treadmill = 4
[201]	LGW (different speeds)	GMED, BFLH, SEM, VL, RF, GL, SOL, TA	4 th order Butterworth (HPF = 40)	4 th order Butterworth (LPF = 4)	90	CP = changes with speeds (2-5)

						HS = changes with speeds (2-5)
[90]	LGW	RF, SEM, BFLH, GM, TA	NM (HPF = 20 LPF = 400)	NM (LPF = 10)	90	CP = 1-2 HS = 3
<p>gastrocnemius medialis (GM), gastrocnemius lateralis (GL), soleus (SOL), tibialis anterior (TA), vastus lateralis (VL), vastus internus (VI), vastus medialis (VM), rectus femoris (RF), sartorius (SAR), and vastus externus (VE), external oblique (EO), internal oblique (IO), biceps femoris long head (BFLH), biceps femoris short head (BFSH), semimembranosus (SEMIM), semitendinosus (SEM), tensor fasciae latae (TFL), adductor longus (ADDL), adductor magnus (ADM), gracilis (GR), gluteus medius (GMED), gluteus maximus (GMAX), iliopsoas (IP), erector spinae (ERE), rectus abdominis (RAB), peroneus longus (PERL), peroneus brevis (PERB), extensor hallucis brevis (EHB), extensor digitorum brevis (EDB), flexor digitorum brevis (FDBError! Bookmark not defined.), extensor hallucis longus (EHL), flexor hallucis longus (FHL), flexor digitorum longus (FDL), latissimus dorsi (LD), biceps brachii (BB), triceps brachii (TB), anterior deltoid (AD), upper trapezius (UT), sternocleidomastoideus (ST), splenius capitis (SPL), quadriceps (QUAD), hamstrings (HAM), rectus abdominis superior portion (RAS),</p> <p>steady-state level ground walking (LGW), running (RN), sidestepping (SS), and crossover (CO), walking forward (WF), walking backward (WB), walking leftward (WL), walking rightward (WR), stepping in place (SIP), rehabilitation (Rehab), prosthetic leg (PL), intact leg (IL), finite impulse response (FIR), root mean square (RMS), eigenvalue (Eval), functional electrical stimulation (FES), incomplete spinal cord injuries (ISCIs),</p>						

Table A.9: Key statistical output variables

alpha	the user-specified Type I error rate (default: 0.05)
nClusters	number of threshold surviving clusters
clusters	cell array containing cluster properties
df	degrees of freedom
H0rejects	null hypothesis rejection decision
P_set	the probability than smooth, random Gaussian 1D data would produce C upcrossings with a minimum width of K; by definition $p_{\text{set}} \leq \alpha$; p_{set} and p (below) are identical if there is only one upcrossing ($C=1$)
P	a list of probability values, one for each threshold-surviving cluster; the probability than smooth, random Gaussian 1D data would produce an upcrossing with a width of K; by definition each $p \leq \alpha$
z	the 1D test statistic continuum (or “test statistic field” or “test statistic trajectory”)
zstar	the critical Random Field Theory threshold

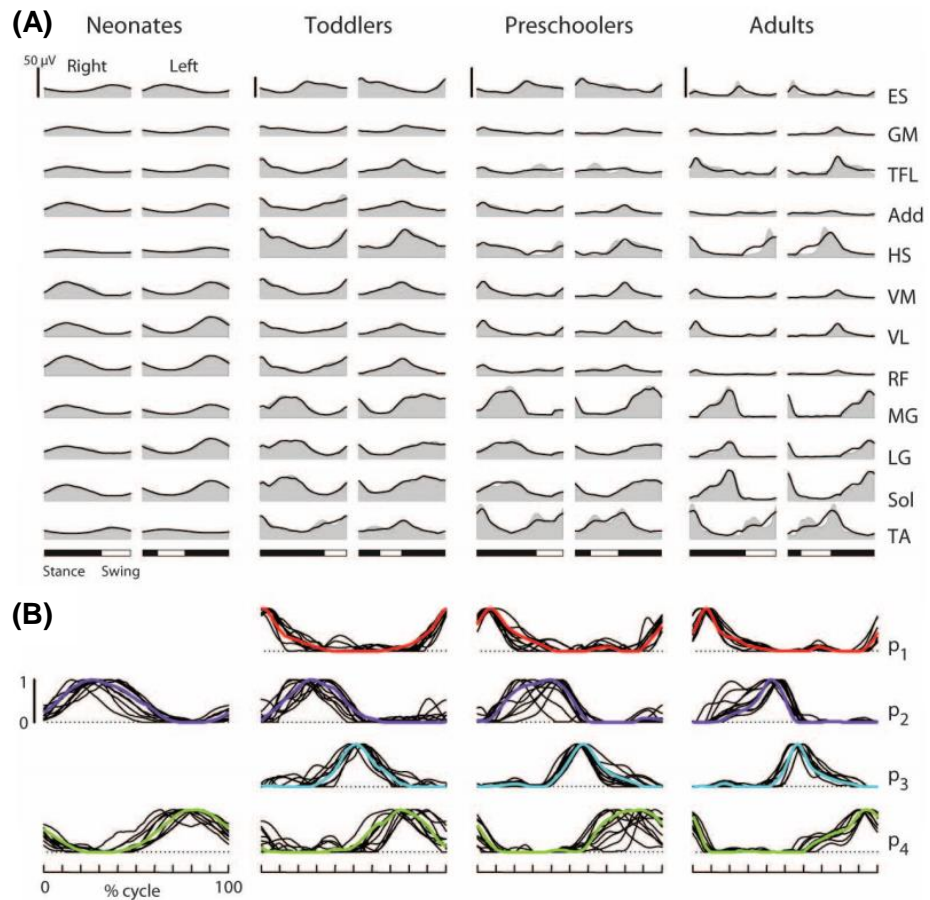


Figure A.1: (A) Ensemble average EMG profiles of neonates, toddlers, preschoolers and adults for both legs during the GC. (B) Activation coefficient profiles extracted from the ensemble EMG average (adapted from [224]).



Figure A.2: Examples of mechanically passive lower limb prostheses (adapted from [275, 280]).



Figure A.3: Examples of Mechanically passive prostheses. (A) Single-axis knee with hydraulic cylinder [351], and (B) KX06: Polycentric prosthetic knee with hydraulic [352].



(A) Blatchford's IP (B) Endolite Adaptive (C) Otto Bock C-Leg (D) Ossur Rheo Knee

Figure A.4: Examples of microprocessor lower limb prostheses (adapted from [353]).



(A) 1st generation 2006-07

(B) 2nd generation 2009-10

Figure A.5: Commercially available power knee prostheses (adapted from [354]).

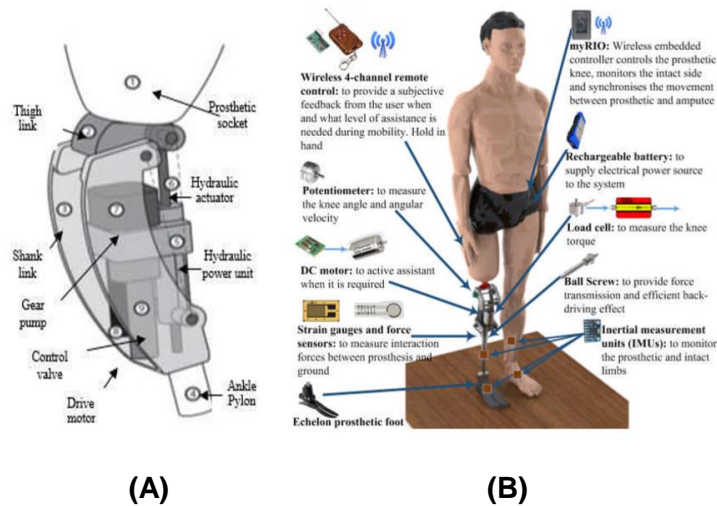


Figure A.6: Semi-active lower limb prosthetic device. (A) Adapted from [286] (B) University of Leeds prosthetic device (adapted from [8]).

Table A.10 Some of the most commercially available prostheses.

Name	Year	Company	Type of sensors	Actuation Methodology
C-Leg	1997	Otto Bock	Knee angle sensor, tube adapter with moment sensor	Motor controlled hydraulic valve and cylinder
IP and IP+	1998	Blatchford/Endolite	Speed sensor and knee angle sensor	Motor controlled pneumatic valve and cylinder
Smart Adaptive	2005	Blatchford/Endolite	Gyroscope, force sensor, and knee angle sensor	Combination of pneumatic and hydraulic actuators
RHEO	2005	Ossur	Force sensor and knee angle sensor	magnetorheolic fluid actuator
Orion	2011	Blatchford/Endolite	IMU, force sensor, and knee angle sensor	Combination of pneumatic and hydraulic actuators
Genium	2011	Otto Bock	IMU (six DOF), knee angle sensor and knee torque sensor	Motor controlled hydraulic valve and cylinder
1 st Generation Power Knee™	2006 - 2007	Ossur	Force sensors, pressure sensors, knee angle sensor, speed sensor and instrumented plantar orthosis connected to the intact leg	Ball screw and brushless DC motor
AgonistAntagonist Knee	2008	Biomechatronics Group (MIT)	Force sensor, ankle angle sensor, and motor displacement sensor	Pair of SEA in parallel and in an agonist-antagonist arrangement
Vanderbilt Prosthesis	2006 - 2012	Vanderbilt University	Knee and angle sensor, load cell, moment sensor and some EMG sensors	Pneumatic cylinder Brushless DC motor



(A) SACH



(B) Vari-Flex



(C) PROPRIO

Figure A.7: Prosthetic foot examples (adapted from [355]).

Table A.11: Summary of the EMG signals and classifiers implemented for predicting intended control output in lower limb prostheses.

Ref	Subjects		Sensor	Placement	Activity	Type of Classifiers	Results
	HS	TFA					
[16]	12	1	EMG, FSR	RF, ADDL, GMAX, GMED, TFL, HAM	LGW, RA, RD	Finite state	
[15]	8	2	EMG, FSR, MoCap	GMAX, GMED, SAR, RF, VL, VM, GR, BFLH, SEM, BFSH, TA, PERL, GL, GM, SOL, EDL	LGW, O, SA, SD, turning	LDA	80-95% (offline)
[356]	5	1	EMG, FSR, MoCap	GMA, GME, SAR, RF, VL, VM, GRA, BFL, SEM, BFS, ADM	LGW, O, SA, SD	LDA	90% (offline)
[309]	0	3	EMG	HAM, QUAD	STG	QDA	(real time)
[294]	6	6	EMG	SEM, SAR, TFL, ADM, GRA, VM, RF, VL, BFL	Knee F/E, Ankle PF/DF, Femoral and Tibial rotation	LDA	90% (real time)
[3]	1	1	EMG, pressure sensors	gluteal, thigh	STG, STD	LDA	(real time)

Table A.11: Summary of the EMG signals and classifiers implemented for predicting intended control output in lower limb prostheses.

[43]	0	5	EMG, GRF, IMU	SAR, RF, VL, VM, GR, BFL, SEM, BFSH, ADM	LGW, O SA, SD, RA, RD	Fusion-based SVM	99% in stance phase and 95% in swing phase
[357]	0	4	EMG GRF, IMU MoCap	RF, VL, VM, TFL, BFLH, SEM, BFSH ADM	LGW, SA, SD, RA, RD, STG & STD	Nonlinear SVM	95%
[35]	10	0	EMG IMU, FSR	GMAX, ERE TFL, RF, GMED, VL, BFLH	LGW, postural sway	Based on muscle activity	NA
[358]	0	8	EMG, Mechanical sensors	SEM, GR, BFLH, TFL, RF, VL, VM, SAR, ADM,	LGW	LDA	NA
<p>force sensitive resistor: FSR, inertial measurement unit: IMU, mechanical sensors: load cell, pressure insoles and IMU, MoCap: motion capture, level ground walking: LGW, walking over obstacle: O, stair ascending: SA, stair descending: SD, ramp ascending: RA, ramp descending: RD, sitting: STG, standing: STD, jumping: JMP, running: RN, flexion/extension: F/E, plantarflexion/dorsiflexion: PF/DF, linear discriminant analysis: LDA, support vector machine: SVM, quadratic discriminant analysis: QDA</p>							

Appendix B

Chapter 3 Supplements

Table B.1: Demographic data of HS.

Subject	Gender	Age	Height (cm)	Weight (Kg)	Health Status
HS-01	Male	22	174.5	67.6	Good
HS -02	Male	24	178	91.8	Good
HS -03	Male	25	174	74.6	Good
HS -04	Male	25	177	77.3	Good
HS -05	Male	59	173	88	Good
HS -06	Male	50	179	92.8	Good
HS -07	Male	39	175	88.6	Good
HS -08	Male	57	172.5	81.5	Good
HS -09	Male	50	166	75	Good
HS -10	Male	61	176	56	Good
HS -11	Male	54	172	92	Good
HS -12	Male	33	174	92	Good
HS -13	Male	34	173	100	Good
Mean (SD)		41 (14)	174.2 (3.1)	82.9 (11.8)	

Table B.2: Demographic data of TFA.

Subject	Gender	Age	Height (cm)	Weight (Kg)	Side of Amputation (L/R)
TFA -1	Male	48	168	88	RIGHT
TFA -2	Male	51	168	59	LEFT
TFA -3	Male	48	179	76.7	RIGHT
TFA -4	Male	55	165	68.8	RIGHT
TFA -5	Male	61	163	50.4	LEFT
TFA -6	Male	53	175	99.2	RIGHT
TFA -7	Male	66	170	84.5	LEFT
TFA -8	Male	58	165	73	RIGHT
TFA -9	Male	57	187	85	LEFT
TFA -10	Male	70	160	70	LEFT
TFA -11	Male	40	180	103	RIGHT
Mean (SD)		55 (8)	170.9 (7.9)	78 (15.3)	

Table B.3: Details of TFA.

Subject	Type of Prosthetic Knee	Type of Prosthetic Foot	Amputation reason	Year of Amputation
TFA -1	Mechanically Passive	SACH	War Field	1985
TFA -2	Mechanically Passive	SACH	War Field	1985
TFA -3	Mechanically Passive	SACH	War Field	1986
TFA -4	Mechanically Passive	SACH	War Field	1988
TFA -5	Mechanically Passive	SACH	Trauma (Road Traffic Accident)	1970
TFA -6	Mechanically Passive	SACH	Trauma (Road Traffic Accident)	1978
TFA -7	Mechanically Passive	SACH	Trauma (Road Traffic Accident)	1978
TFA -8	Mechanically Passive	SACH	War Field	1980
TFA -9	Mechanically Passive	SACH	Trauma (Road Traffic Accident)	1987
TFA -10	Mechanically Passive	SACH	Trauma (Road Traffic Accident)	1971
TFA -11	Mechanically Passive	SACH	Trauma (Road Traffic Accident)	1998

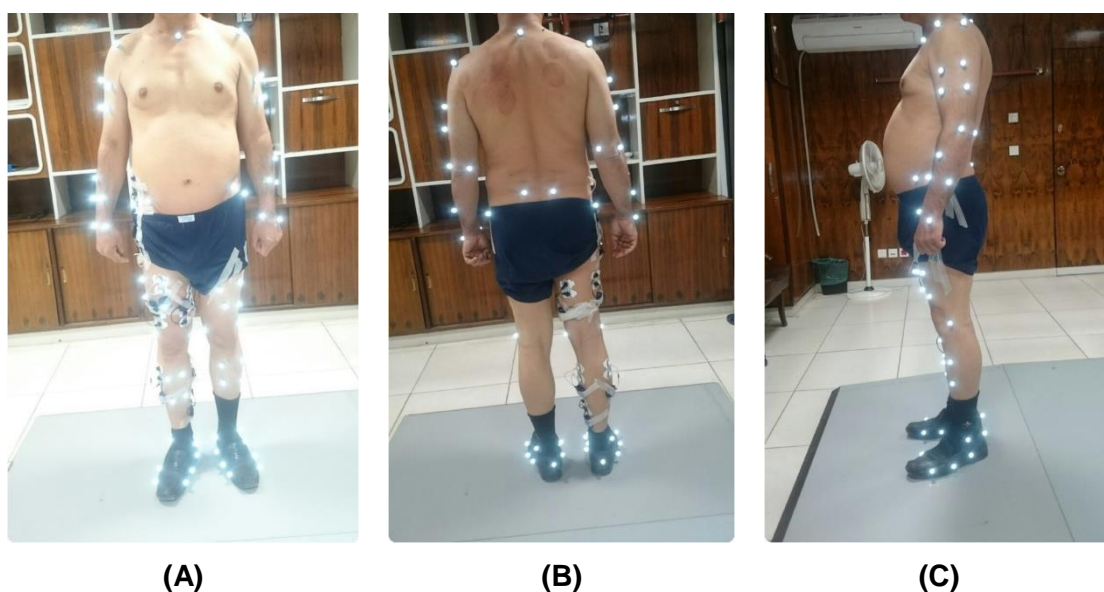


Figure B.1: EMG and reflective markers attachments on one of the HS. (A) front dominant leg, (B) back dominant leg, and (C) side non-dominant leg.

Figure B.2: An example of HS EMG data process during one trial. The first, second, third and fourth rows show raw, bandpass filter (4th order Butterworth HPF 20Hz, LPF 500Hz), rectified and linear envelope (2nd order Butterworth LPF with the cut of frequency of 6 Hz) data during transient-state gait, respectively.

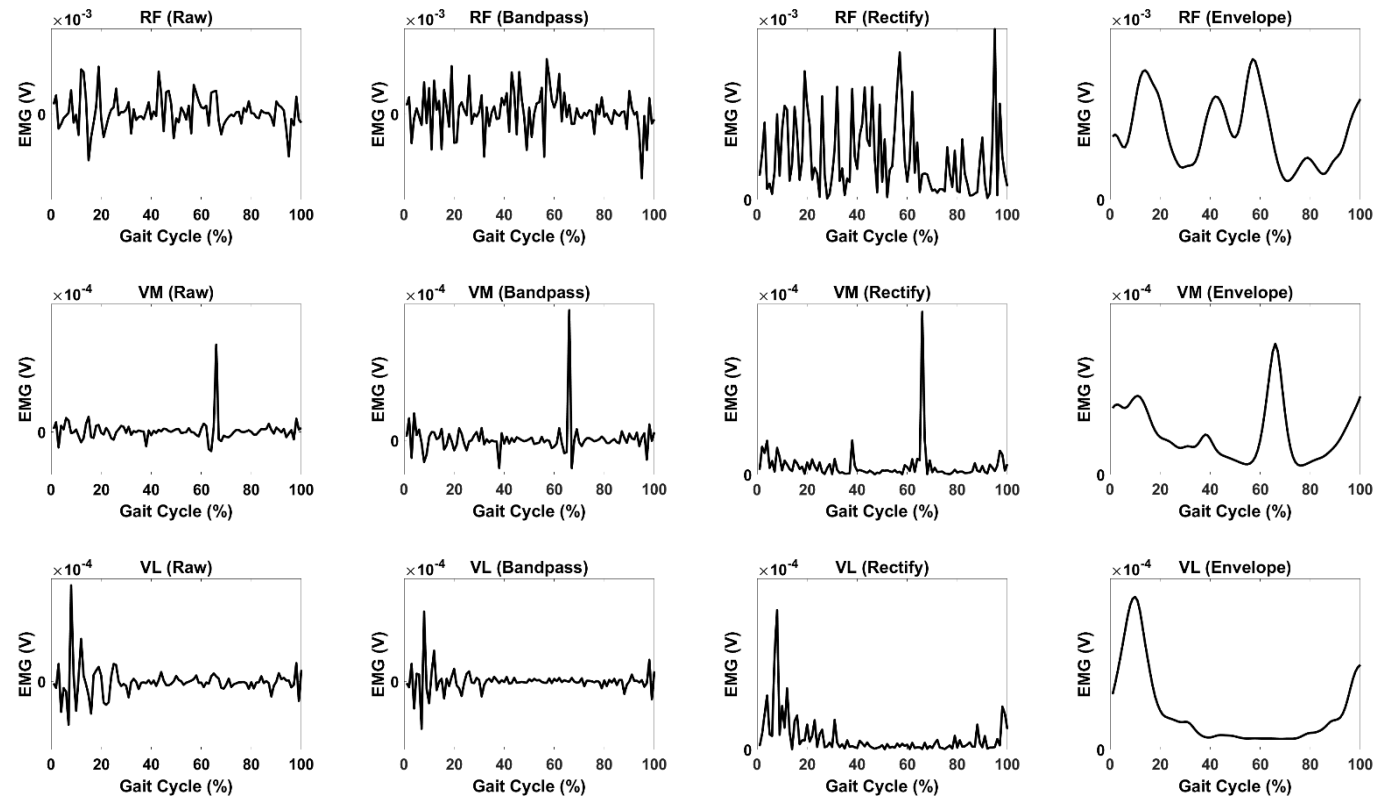


Figure B.2: An example of HS EMG data process during one trial. The first, second, third and fourth rows show raw, bandpass filter (4th order Butterworth HPF 20Hz, LPF 500Hz), rectified and linear envelope (2nd order Butterworth LPF with the cut of frequency of 6 Hz) data during transient-state gait, respectively.

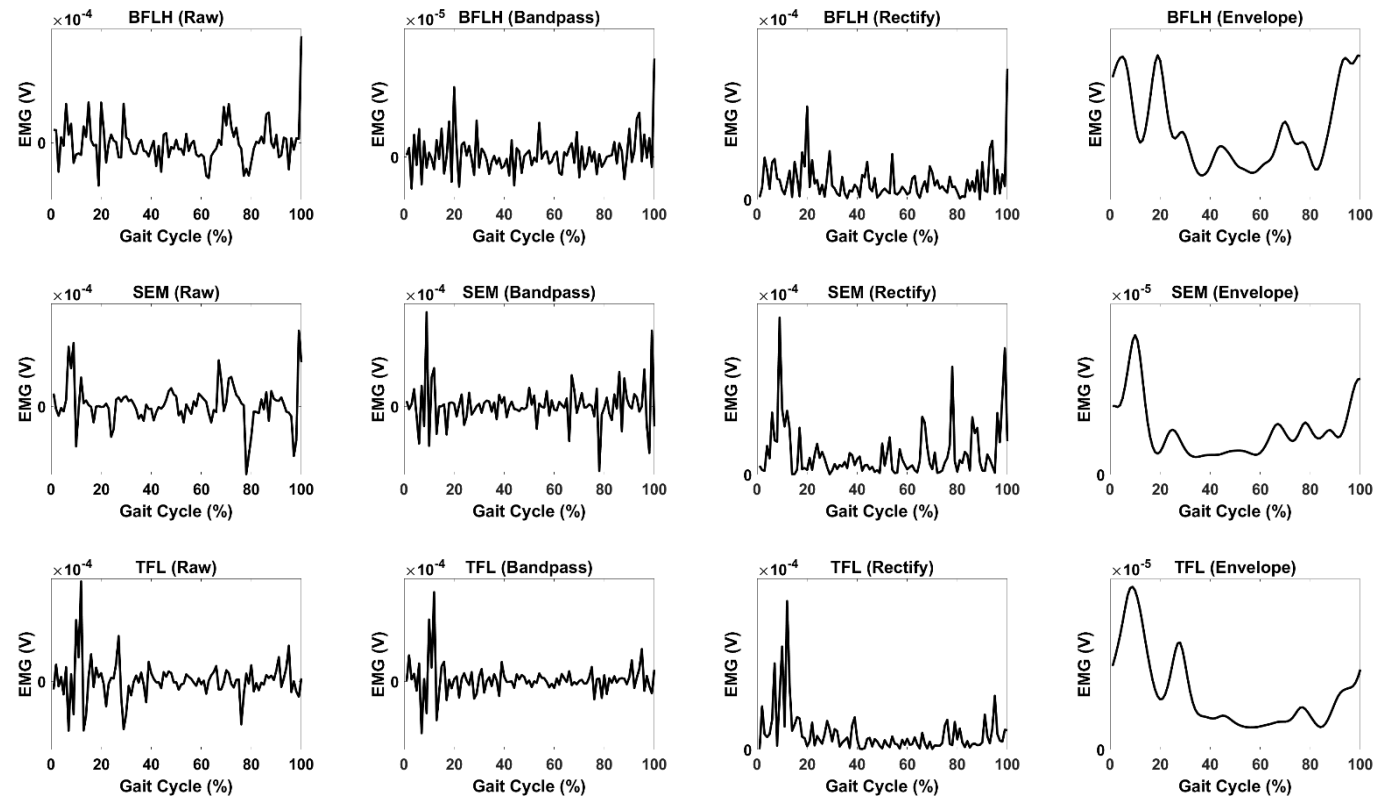


Figure B.2: An example of HS EMG data process during one trial. The first, second, third and fourth rows show raw, bandpass filter (4th order Butterworth HPF 20Hz, LPF 500Hz), rectified and linear envelope (2nd order Butterworth LPF with the cut of frequency of 6 Hz) data during transient-state gait, respectively.

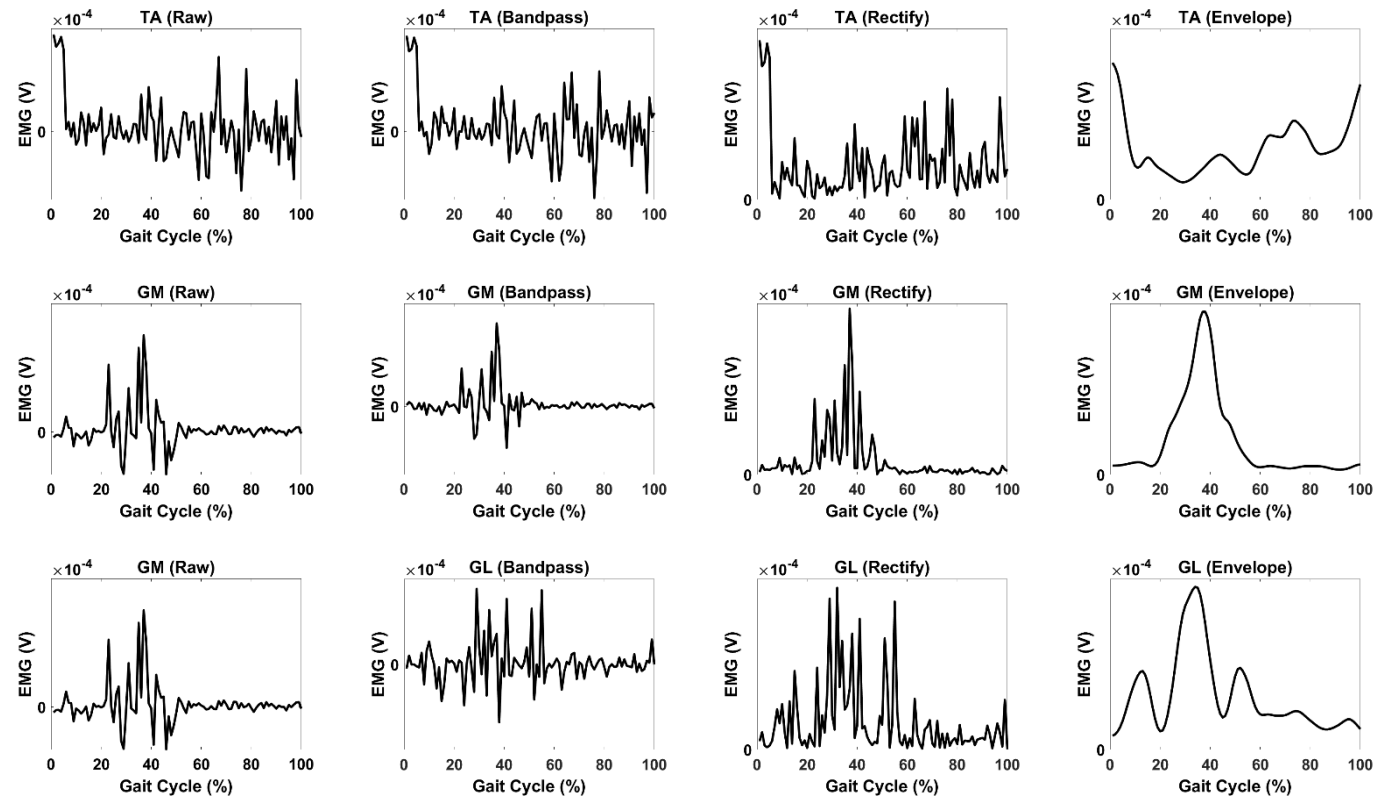
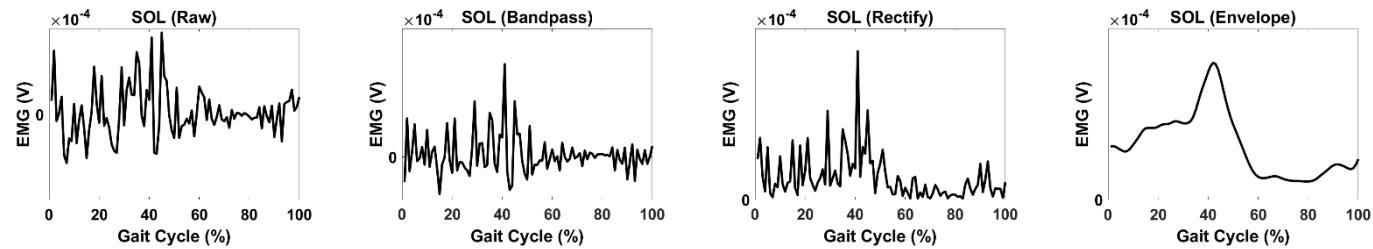


Figure B.2: An example of HS EMG data process during one trial. The first, second, third and fourth rows show raw, bandpass filter (4th order Butterworth HPF 20Hz, LPF 500Hz), rectified and linear envelope (2nd order Butterworth LPF with the cut of frequency of 6 Hz) data during transient-state gait, respectively.



Appendix C

Chapter 5 Supplements

Table C.1: Demographic data of HS during steady-state walking.

Subject	Gender	Age	Height (cm)	Weight (Kg)	Health Status
HS-01	Male	22	167.8	63.3	Good
HS-02	Male	21	175	72.3	Good
HS-03	Male	21	184.6	80.0	Good
HS-04	Male	21	175.2	73.1	Good

Table C.2: Demographic data of TTA during steady-state walking.

Subject	Gender	Age	Height (cm)	Weight (Kg)	Amputati on side (L/R)
TTA	Male	76	185.1	69.3	L

Table C.3: Details of TTA.

Subject	Type of Prosthetic Knee	Type of Prosthetic Foot	Amputation reason	Year of Amputation
TTA	NA	Panthera CF I Medi	Trauma (Road Traffic Accident)	2004

Appendix D

Ethical Approval

Performance, Governance and Operations
 Research & Innovation Service
 Charles Thackrah Building
 101 Clarendon Road
 Leeds LS2 9LJ Tel: 0113 343 4673
 Email: ResearchEthics@leeds.ac.uk



UNIVERSITY OF LEEDS

Hafiz Farhan Maqbool & Pouyan Mehryar
 Room 536c
 School of Mechanical Engineering
 University of Leeds
 Leeds, LS2 9JT

MaPS and Engineering joint Faculty Research Ethics Committee (MEEC FREC)
 University of Leeds

28 November 2014

Dear Hafiz and Pouyan

Title of study **A Smart Biomimetic, Self-Tuning, and Fully Adaptable
 Lower Limb Prosthetics with Energy Recovery (Smart
 BioLeg)**
Ethics reference **MEEC 14-011**

I am pleased to inform you that the application listed above has been reviewed by the MaPS and Engineering joint Faculty Research Ethics Committee (MEEC FREC) and following receipt of your response to the Committee's initial comments, I can confirm a favourable ethical opinion as of the date of this letter. The following documentation was considered:

Document	Version	Date
MEEC 14-011 Final Version- Ethical Review Form Smart_BioLeg.pdf	1	28/10/14
MEEC 14-011 Answers_Final.docx	1	12/11/14
MEEC 14-011 Advertisement.docx	1	12/11/14

Committee members made the following comment about your response:

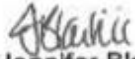
The information sheet should give more details of exactly what is involved in obtaining the measurements - that it will be necessary to remove clothing, down to shorts and sports bra (for women), and as skin contact is required, this may mean "sanding down"... or whatever. This is especially needed as the sessions could be videoed, and participants should be made aware before giving their final consent.

Please notify the committee if you intend to make any amendments to the original research as submitted at date of this approval, including changes to recruitment methodology. All changes must receive ethical approval prior to implementation. The amendment form is available at <http://ris.leeds.ac.uk/EthicsAmendment>.

Please note: You are expected to keep a record of all your approved documentation, as well as documents such as sample consent forms, and other documents relating to the study. This should be kept in your study file, which should be readily available for audit purposes. You will be given a two week notice period if your project is to be audited. There is a checklist listing examples of documents to be kept which is available at <http://ris.leeds.ac.uk/EthicsAudits>.

We welcome feedback on your experience of the ethical review process and suggestions for improvement. Please email any comments to ResearchEthics@leeds.ac.uk.

Yours sincerely



Jennifer Blaikie

Senior Research Ethics Administrator, Research & Innovation Service
On behalf of Professor Gary Williamson, Chair, [MEEC FREC](#)

CC: Student's supervisor(s)

Research & Innovation Service
 Level 11, Worsley Building
 University of Leeds
 Leeds, LS2 9NL
 Tel: 0113 343 4873
 Email: ResearchEthics@leeds.ac.uk



UNIVERSITY OF LEEDS

Pouyan Mehryar
 School of Mechanical Engineering
 University of Leeds
 Leeds, LS2 9JT

**MaPS and Engineering joint Faculty Research Ethics Committee (MEEC FREC)
 University of Leeds**

11 May 2018

Dear Pouyan

Title of study **A Smart Biomimetic, Self-Tuning, and Fully Adaptable
 Lower Limb Prosthetics with Energy Recovery (Smart
 BioLeg)**
Ethics reference **MEEC 14-011 amendment Aug 2017**

I am pleased to inform you that the amendment to the application listed above has been reviewed by the Deputy Chair of the MaPS and Engineering joint Faculty Research Ethics Committee (MEEC FREC) and I can confirm a favourable ethical opinion as of the date of this letter. The following documentation was considered:

Document	Version	Date
MEEC 14-011 amendment Aug 2017 ethical_review_amendment.pdf	1	15/08/17
MEEC 14-011 amendment Aug 2017 supporting_documents.pdf	1	15/08/17
MEEC 14-011 Final Version- Ethical Review Form Smart_BioLeg.pdf	1	28/10/14
MEEC 14-011 Answers_Final.docx	1	12/11/14
MEEC 14-011 Advertisement.docx	1	12/11/14

Please notify the committee if you intend to make any further amendments to the original research as submitted at date of this approval, including changes to recruitment methodology. All changes must receive ethical approval prior to implementation. The amendment form is available at <http://ris.leeds.ac.uk/EthicsAmendment>.

Please note: You are expected to keep a record of all your approved documentation, as well as documents such as sample consent forms, and other documents relating to the study. This should be kept in your study file, which should be readily available for audit purposes. You will be given a two week notice period if your project is to be audited. There is a checklist listing examples of documents to be kept which is available at <http://ris.leeds.ac.uk/EthicsAudits>.

We welcome feedback on your experience of the ethical review process and suggestions for improvement. Please email any comments to ResearchEthics@leeds.ac.uk.

Yours sincerely

Jennifer Blaikie
Senior Research Ethics Administrator, the Secretariat
On behalf of Dr Dawn Groves, Chair, [MEEC FREC](#)

CC: Student's supervisor(s)



مرکز تحقیقات فناوری های توان بخشی عصبی هوشمند جواد موفقیان



Djavad Mowafaghian Research Center for Intelligent NeuroRehabilitation Technologies

Dr Neil Messenger
School of Biomedical Sciences
University of Leeds
LS2 9JT

9 October 2016

Subject: Approval of the study "Balance and lower back pain in lower limb amputees" by the Ethics Committee

Dear Dr Messenger

I am glad to inform you that the above research application has been reviewed by the Ethics Committee of the Djavad Mowafaghian Research Center for Intelligent Neuro-Rehabilitation Technologies. The committee considered sample informed consent forms for non-amputee and amputee subjects in addition to protocol of the tests in Persian Language which are translation of the approved English version by the Faculty of Biological Sciences Research Ethics Committee in University of Leeds. The committee approved the trials to be conducted in the presented form in the Gait Lab of the Djavad Mowafaghian Research Center for Intelligent Neuro-Rehabilitation Technologies.

Farzam Farahmand
Yours sincerely
Farzam Farahmand

Appendix E

List of Publications and Awards

E.1 Publications from this Thesis (P. Mehryar, main author)

1. **Mehryar, P.**, Rezaeian, T., Shourijeh, M.S., Raveendranathan, V., Messenger, N., O'Connor, R. and Dehghani-Sanij, A., 2017. Changes in knee joint kinetics of transfemoral amputee's intact leg: An osteoarthritis indication?. *Gait and Posture*.
2. **Mehryar, P.**, Shourijeh, M.S., Rezaeian, T., Crisp, C., Messenger, N., and Dehghani-Sanij, A.A., 2017, September. Do activation & synergy of above knee amputees' intact leg change?. *School and Symposium on Advanced Neurorehabilitation, 2017 SSNR-2017. Baiona, Spain*.
3. **Mehryar, P.**, Shourijeh, M.S., Rezaeian, T., Iqbal, N., Messenger, N., and Dehghani-Sanij, A.A., 2017, August. Changes in synergy of transtibial amputee during gait: A pilot study. In *Engineering in Medicine and Biology Society (EMBC), 2017 IEEE BHI-2017 Internation Conference on Biomedical and Health Informatics*. IEEE.
4. **Mehryar, P.**, Shourijeh, M.S., and Dehghani-Sanij, A.A., 2016, October. Muscle synergy analysis in transtibial amputee during ramp descending activity. In *Internation Conference on neurorehabilitation 2016. Segovia, Spain: Springer*.
5. **Mehryar, P.**, Shourijeh, M.S., Maqbool, H.F., Torabi, M. and Dehghani-Sanij, A.A., 2016, August. Muscle synergy analysis in transtibial amputee during ramp ascending activity. In *Engineering in Medicine and Biology Society (EMBC), 2016 IEEE 38th Annual International Conference of the* (pp. 1676-1679). IEEE.
6. **Mehryar, P.**, Raveendranathan, V., Shourijeh, M.S., and Dehghani-Sanij, A.A., 2016, August. How does disuse of plantar flexors affect upper knee kinetic?. In *Engineering in Medicine and Biology Society (EMBC), 2016 IEEE 38th Annual International Conference of the*. IEEE.
7. **Mehryar, P.**, Maqbool, H.F., Awad, M.I., Abouhossein, A. and Dehghani-Sanij, A.A., 2015, June. Investigation of thigh muscles for events/phases detection using surface electromyography. In *Conference MELbioEng. Leeds*.

E.2 Related Publications (P. Mehryar, co-author)

1. Zakiria, M., Maqbool, H.F., Hussain, T., Awad, M. I., **Mehryar, P.**, Iqbal, N., and Dehghani-Sanij, A.A., 2017, August. Heuristic Based Gait Event Detection for Human Lower Limb Movement. In *Engineering in Medicine and Biology Society (EMBC), 2017 IEEE BHI-2017 Internation Conference on Biomedical and Health Informatics*. IEEE.
2. Maqbool, H.F., Husman, M.A.B., Awad, M.I., Abouhossein, A., **Mehryar, P.**, Iqbal, N. and Dehghani-Sanij, A.A., 2016, August. Real-time gait event detection for lower limb amputees using a single wearable sensor. In *Engineering in Medicine and Biology Society (EMBC), 2016 IEEE 38th Annual International Conference of the* (pp. 5067-5070). IEEE.
3. Maqbool, H.F., **Mehryar, P.**, Husman, M.A.B., Awad, M.I., Abouhossein, A. and Dehghani-Sanij, A.A., 2015, September. Towards Intelligent Lower Limb Prostheses with Activity Recognition. In *Conference Towards Autonomous Robotic Systems* (pp. 180-185). Springer International Publishing.

E.3 Awards

1. Winning the second prize in a poster competition for “Investigation of above knee muscles for event detection using surface electromyography.” MEIbioeng, 2015.
2. Winning the PhD poster prize for post graduate researcher competition., University of Leeds, 2015.